New therapeutic approaches for achondroplasia

Davide Selom Komi Komla-Ebri

Thèse de l'Université Paris Descartes

Ecole Doctorale BioSPC

Spécialité : GENETIQUE

Auteur :

Davide Selom Komi KOMLA-EBRI

Titre :

Nouvelles approches thérapeutiques pour l'achondroplasie

New therapeutic approaches for achondroplasia

Soutenue le 04 juillet 2016

Jury
Pr Jeanne AMIEL Président
Dr Laurence LEGEAI-MALLET Directeur de thèse
Dr Laurent BECK Rapporteur
Dr Frédéric MALLEIN-GERIN Rapporteur
Dr Patricia BUSCA Examinateur
Dr Hervé KEMPF Examinateur

Remerciements

Je remercie tout d'abord le jury de thèse, Jeanne Amiel, Laurent Beck, Patricia Busca, Hervé Kempf et Frédéric Mallein-Gerin, pour avoir accepté de juger ce travail et de m'avoir fait l'honneur de présider à cet événement pour moi si important.

J'adresse tous mes meilleurs remerciements à Laurence Legeai-Mallet, ma directrice de thèse. Elle m'a accueilli au sein de son équipe il y a plus que 5 ans quand j'étais à la recherche d'un stage M2. Cela me rappelle combien le temps passe vite. Elle m'a aidé, poussé, fait confiance, reprit, félicité, suivi tout au long de mon parcours. A bien voir elle a bien mérité le titre de "maman" du labo !

Je remercie Pr Alain Fischer et le comité de direction de l'Institut Imagine pour m'avoir accordé une bourse de 4 mois pour ma 4ème année de thèse. Je remercie également le comité de la Fondation pour la Recherche Médicale pour m'avoir assigné un financement de 6 mois de 4ème année de thèse.

Je remercie les DURs pour avoir fait partie de mon aventure et de l'avoir rendue si agréable !

Catherine pour la bonne humeur, le soutien, pour m'avoir appris la culture cellulaires, les western blots, et pour la blague de la lamelle de la malassez cassée (je l'oublierai jamais !).

Nabil pour m'avoir appris tout ce que je connais de la souris, pour ses conseils, les perles de sagesse et sa passion cachée pour la danse et la fête.

Emilie pour m'avoir appris plein de techniques pendant mon M2 pour ensuite se les faire réexpliquer à son retour comme postdoc ! Je te souhaite plein de succès avec les petits poissons !

Ludovic, mon roi des cils et de Nantes. PREGO !

Maxence pour son humour parfois un peu décalé, la cinéphilie et Les boloss des belles lettres. LOL !

Valentin pour ton professionnalisme et tes blagues. Allez viens !

Léa pour ne pas avoir pris soin de mon alcoolisme de mèche avec Marko (que je remercie en passant).

Martin pour ses avis, le travail sur les mandibules et pour m'avoir conseillé Searching for Sugarman.

Federico et son travail sur le crâne des souris et pour m'avoir fait connaître les synchondroses.

Cindy toujours là loin en Calédonie. Je te rassure, je n'ai toujours pas goûté la BSA !

Les espagnols Mariluz et Salva, j'espère qu'on se rencontrera sous le soleil de l'Espagne.

Je remercie les VCD Valérie, Carine, Céline, Mathilde, Quentin, Norine, Laure (pour m'avoir nourri !)

Merci à tous les « vieux » qu'on fait partie de l'ancienne U781 d'Arnold Munnich et aux « nouveaux » rencontrés à l'Institut Imagine.

Merci à ma famille qui m'a toujours soutenu. Sachiez que même si je ne donne jamais de mes nouvelles vous êtes toujours dans mes pensées.

Merci Aliénor pour m'avoir supporté pendant la rédaction de cette thèse, pour vivre avec moi et pour m'avoir appris que « quand y en a plus y en a encore ! ». Je ne t'ai pas laissée tomber comme une vieille chaussette !

Merci Milène, Léa (les super-colocs), Miccols, (Bella !)Valoz, Fox, (Hola !) Norex, (Ohi zi) Cami "Pede"-rsen, Scianna, Quentin, Matty, David (Mamma mia !), Andrea Angiuli (à lire avec la voix de la boite vocale), Marco, Alice, Dorian Gamba, Mejdou, Flà, Giselita, Sarah, Juliette, Danilo, Victor, Filo, Bozzi, May, Will, bref les “Tous chez Nora”.

Je remercie les amis connus à Paris, en Italie, les amis de toujours et les amitiés plus récentes.

Table of Contents

Abbreviations

AB = Acidic box

ACH = Achondroplasia

BMP = Bone Morphogenetic Protein

CAN = Crouzon with Acanthosis Nigricans syndrome

CATSHL = CAmpodactyly, Tall Stature, and Hearing Loss syndrome

CNP = C-type Natriuretic Peptide

COL = Collagen

EGF = Epidermal growth factor

ERK = Extracellular signal-Regulated Kinase

FGF = Fibroblast Growth Factor

FGFR = Fibroblast Growth Factor Receptor

HBS = Heparin Binding Site

HCH = Hypochondroplasia

HS = Heparan sulfate

IGF = Insuline Growth Factor

IHH = Indian HedgeHog

IVD = InterVertebral Disc

MAPK = mitogen activated protein kinase

MMP = Matrix MetalloProteinases

MS = Muenke Syndrome

NP = Nucleus Pulposus

PP2a = Protein Phosphatase 2a

PI3K = Phosphatidyl Inositol-3-Kinase

PLCγ = Phospholipase C-Gamma

PTH = Parathyroid Hormone

PTH1R = Parathyroid Hormone 1 Receptor

PTHrP = Paratyroid Hormone-Related Peptide

RANK = Receptor activator of nuclear factor κB

RANKL = Receptor activator of nuclear factor κB Ligand

SADDAN = Severe Achondroplasia with Developmental Delay and Acanthosis Nigricans

SNAIL = Zinc finger protein SNAI1

STAT = Signal Transducer and Activator of Transcription

SOX = Sry bOX containing

TD = Thanatophoric Dysplasia

TGFβ = Transforming Growth Factor β

TK = Tyrosine Kinase domain

TKI= Tyrosine Kinase Inhibitor

TM = TransMembrane domain

VEGF = Vascular Endothelial Growth Factor

WNT = Wingless-related integration site

Introduction

1. FGFs and FGFRs

1.1 Fibroblast Growth Factors (FGFs)

The fibroblast growth factor (FGF) family consists of a large group of structurally and evolutionarily related polypeptides. In human and mouse, 22 FGF genes exist (FGF1-FGF23) it being understood that the human and mouse FGF families do not include FGF15 and FGF19 respectively, as they are orthologs (1).

The first two FGFs discovered, FGF1 and FGF2, were named acidic and basic FGF (aFGF and bFGF) based on their activity to stimulate fibroblast proliferation and their isoelectric point (2, 3). It was later found that the name “fibroblast growth factor” was not the best name to describe the diverse functions of the family members and their receptors since many FGFs do not even have receptors expressed in fibroblasts and elicit no activity in fibroblasts (4). However the name “fibroblast growth factor” followed by a number (FGF1, 2, 3, 4…) has been preserved.

FGFs are usually classified in 3 different sets (Figure 1). 15 out of 22 FGFs (FGF1-10, 16-18, 20, 22) are paracrine factors belonging to the canonical FGFs group. These growth factors are able to stimulate Fibroblast Growth Factor Receptors (FGFRs) assisted by heparin or heparan sulfate. 3 polypeptides (endocrine FGFs: FGF15/19, 21, 23) are hormone-like factors that need the presence of co-factors belonging to the Klotho family of proteins to perform their action. The 4 lasts FGFs (intracellular FGFs: FGF11-14) are intracellular proteins lacking the capacity to bind FGF receptors at the cell surface. Those FGFs (also known as iFGFs) interact with the cytosolic carboxy terminal tail of voltage gated sodium (Nav) channels.

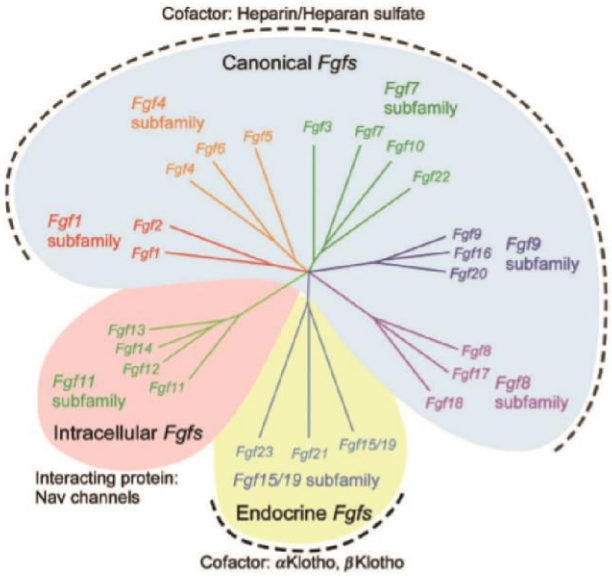

Figure 1. FGFs and their subfamilies. Phylogenetic analysis suggests that 22 *Fgf* genes can be arranged into seven subfamilies containing two to four members each. FGFs can also be regrouped in three classes based on their biological action: Canonical FGFs, Endocrine FGFs and Intracellular FGFs (1).

FGFs control a variety of physiological responses during embryonic development and in adult organisms. During development FGFs play key roles in patterning and morphogenesis by controlling cell proliferation, survival, migration and differentiation. In adult organisms, they are involved in tissue repair, response to injury, as well as energy, bile acid, mineral ion and metabolic homeostasis. The identification of the roles of most FGFs was made possible by the use of knock-out mouse models for one or more of these factors (Table 1).

Table 1. Phenotypes of germline and conditional loss-of-function Fgf mutations in mice. (Ornitz & Itoh 2015).

Gene Name	Viability /Age at Death of Null Mutant	Null Phenotype (Organ, Structure, or Cell Type Affected)	Tissue-Specific (Conditional) Phenotypes, Redundant Phenotypes, Phenotypes Induced by Physiological Challenge
Fgf1	Viable	No apparent phenotype	An aggressive diabetic phenotype with white adipocyte remodeling on high-fat diet
Fgf2	Viable	Cortical neuron, vascular smooth muscle, blood pressure, skeletal development, and wound healing	Decreased cardiac hypertrophy induced by ischemic injury and delayed wound healing; Increased bone mineralization in high molecular weight isoform knockout
Fgf3	Viable	Inner ear and skeletal development	Heart development (redundant with *Fgf10*)
Fgf4	E4-5	Blastocyst inner cell mass	Limb bud development (redundant with *Fgf8*)
Fgf5	Viable	Hair follicle development	
Fgf6	Viable	Muscle development	Muscle regeneration
Fgf7	Viable	Hair follicle and ureteric bud development and synaptogenesis	Thymus regeneration (radiation injury) and wound healing
Fgf8	E7	Gastrulation	Heart field, limb, somitogenesis, kidney, CNS, inner ear development, spermatogenesis
Fgf9	P0	Lung, heart, skeletal, gonad, inner ear, and intestine development	Migration of cerebellar granule neurons and kidney agenesis (redundant with *Fgf20*)
Fgf10	P0	Limb bud, lung bud, trachea, thymus, pancreas, pituitary, palate, tongue epithelium, cecum, kidney, submandibular, salivary, lacrimal, and mammary gland, heart, stomach, and white adipose tissue	Lung branching morphogenesis and inner ear development (redundant with *Fgf3*)
Fgf11	Viable	No identified phenotype	
Fgf12	Viable	No identified phenotype	Severe ataxia and motor weakness (redundant with *Fgf14*)
Fgf13	Viable	Neuronal migration, learning and memory deficits, and microtubule binding	
Fgf14	Viable	Ataxia, motor weakness, learning and memory deficits, and impaired neuronal excitability	Severe ataxia and motor weakness (redundant with *Fgf12*)
Fgf15	E13.5-P7	Cardiac outflow tract development, neurogenesis, and bile acid metabolism	Liver regeneration
Fgf16	Viable	Heart development	Promotes cardiac remodeling induced by angiotensin II
Fgf17	Viable	Cerebellum and frontal cortex development	
Fgf18	P0	CNS, skeletal, palate, and lung development	
Fgf20	Viable	Guards hair, teeth, cochlea, and kidney development	Kidney agenesis (redundant with *Fgf9*)
Fgf21	Viable	Energy/lipid metabolism	
Fgf22	Viable	Synaptogenesis	Decreased skin papillomas formation following carcinogenesis challenge
Fgf23	PW4-13	Phosphate and vitamin D homeostasis, deafness, middle ear development	

1.2 Fibroblast Growth Factor Receptors (FGFRs)

The FGFR family is composed by 5 proteins: FGFR1, 2, 3, 4 and L1. The FGFR1, 2, 3, 4 are single chain transmembrane tyrosine kinases that consist of a ligand binding extracellular domain, a single transmembrane domain (TM), and an intracellular tyrosine kinase domain that is separated into two parts by an insertion domain. FGFRL1 (also recently called FGFR5) is an exception to this scheme since it has a short intracellular tail with no tyrosine kinase domain (Figure 2). The FGFR extracellular domain contains two or three immunoglobulin (Ig)-like loops (D1, D2, D3). D1 loop and the D1-D2 link, also known as acidic box (AB) due to the presence of acidic residues, are involved in receptor autoinhibition (5) and they're not necessary for FGF binding (6). FGFR portion responsible for the ligand binding is composed by D2 and D3, with the first loop presenting the heparin binding site (HBS). While FGFR4 and L1 present only one splice isoform, the other three FGFRs have been found to naturally encode different variants. In fact in FGFR1–FGFR3, two alternative exons (IIIb and IIIc) code for the second half of D3 and are spliced to the common exon IIIa (encoding the first half of D3) (Figure 2). These alternative splicing events occur in a tissue specific fashion, resulting in mesenchymal "c" and epithelial "b" isoforms and this variation defines ligand-binding affinity and specificity of FGFR1-3.

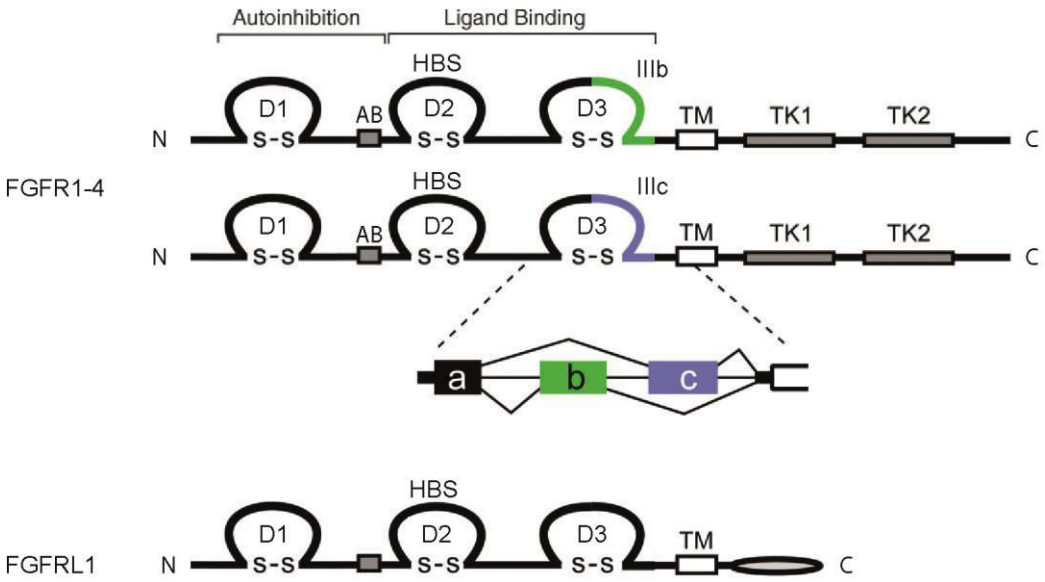

Figure 2. FGFRs structures and isoforms. (N: N-terminus; D1-3: immunoglobulin (Ig)-like loops; AB: Acidic Box; HBS: Heparin Binding Site; TM: Transmembrane domain; TK1-2: Tyrosine kinase domain; C: C-terminus; a,b,c: exons participating to splicing events) (1, 6).

FGFRs role has been evaluated through the use of null or conditional loss-of-function transgenic mice (Table 2). $Fgfr1^{-/-}$ mice do not survive early embryonic phases while, using conditional inactivation of Fgfr1 in osteo-chondrocyte progenitor cells and in differentiated osteoblasts, it has been shown that FGFR1 signalling is important in limb establishment and bone formation (7, 8). Mice lacking Fgfr2 survive until embryonic day 10–11. These embryos fail to form a functional placenta and do not form limb buds (9). The conditional inactivation of Fgfr2 showed osteoprogenitors proliferation defects and mice presented dwarfism (10). Fgfr3-null mice are viable and present a skeletal overgrowth and other defects. Mice lacking Fgfr4 are viable, and they present minor liver-related defects (11). Finally $Fgfrl1^{-/-}$ mice present diaphragm hypoplasia, heart and skeletal anomalies (12, 13). The involvement and role of FGFRs in skeletal development will be later discussed.

Table 2. Phenotypes of germline and conditional loss-of-function Fgfr mutations in mice. (1)

Gene Name	Viability /Age at Death of Null Mutant	Null Phenotype (Organ, Structure, or Cell Type Affected)	Tissue-Specific (Conditional) Phenotypes, Redundant Phenotypes, Phenotypes Induced by Physiological Challenge
Fgfr1	E7.5-9.5	Gastrulation, Blastocyst inner cell mass	Hematopoietic cell engraftment
			Osteoblast maturation
			Limb bud development
			Hippocampal progenitor cell proliferation Inner ear sensory epithelium
			Deletion of Ig domain 1 (defect in node regression)
			Adipocyte metabolism
			Endothelial *Tgfβ* expression and endothelial-mesenchymal transition; Endothelial regulation of CXCR4 in liver regeneration and fibrosis
			Spermatogenesis
Fgfr2	E10-11	Placenta, no limb buds	Skeletal, lung, limb bud, CNS, GI tract, skin, and adrenal cortex development in *Fgfr2b* null mice
Fgfr1/2			Myelin sheath thickness in oligodendrocyte
			Kidney, metanephric mesenchyme, ureteric bud, ocular gland development
			Angiogenesis, vascular integrity
			Hepato-cytoprotective through regulation of cytochrome P450 enzymes
Fgfr3	Viable	Skeletal overgrowth, inner ear, brain, articular cartilage, oligodendrocyte differentiation, pancreatic growth, intestinal crypt cell growth arrest	Alveolar septation and elastogenesis (redundant with *Fgfr4*)
Fgfr4	Viable	Cholesterol metabolism and bile acid synthesis	Increased liver injury and fibrosis induced by carbon tetrachloride
			Alveolar septation and elastogenesis (redundant with *Fgfr3*)
			Vitamin D homeostasis (redundant with *Fgfr3*)
			Phosphate homeostasis (redundant with *Fgfr1*)
Fgfrl1	P0	Kidney, diaphragm, skeleton	

Ligand binding specificity of the 18 secreted (canonical and endocrine) FGFs have been compared using various mitogenic assays and by directly measuring affinity for FGFRs (Zhang 2006). Each FGFR isoform react to specific FGFs (Table 3). These FGFs bind FGFRs in dimers in concert with heparan sulfate proteoglycan (HS). Complex FGF-HS-FGFR dimers stimulate the tyrosine kinase activity through a process of trans-autophosphorylation that triggers the transduction signalling that will end in the activation of the targeted genes. In fact the activated receptor is able to bind and phosphorylate other proteins that will lead to the transduction of the signalling through different pathways.

FGFR dimerization is needed to transduce biochemical signalling, but the widely believed role of FGFs in producing FGFR dimerization (14) is a current object of debate since a recent study shows the presence of FGFR dimers in FGFs absence (15). The same study indicates the presence of FGFR phosphorylation in unlinganded dimers, however the FGF binding still determines a more consistent phosphorylation of the FGFR dimers.

Table 3. Receptor specificity of canonical and endocrine FGFs. (1)

FGF subfamily	FGF	Cofactor	Receptor specificity
FGF1 subfamily	FGF1		All FGFRs
	FGF2		FGFR 1c, 3c > 2c, 1b, 4Δ
FGF4 subfamily	FGF4		FGFR 1c, 2c > 3c, 4Δ
	FGF5		
	FGF6		
FGF7 subfamily	FGF3	+ Heparin or Heparan sulfate	FGFR 2b > 1b
	FGF7		
	FGF10		
	FGF22		
FGF8 subfamily	FGF8		FGFR 3c > 4Δ > 2c > 1c >> 3b
	FGF17		
	FGF18		
FGF9 subfamily	FGF9		FGFR 3c > 2c > 1c, 3b >> 4Δ
	FGF16		
	FGF20		
FGF15/19 subfamily	FGF15/19	+βKlotho	FGFR 1c, 2c, 3c, 4Δ
	FGF21		FGFR 1c, 3c
	FGF23	+αKlotho	FGFR 1c, 3c, 4

2. FGFR-related diseases

Mutations in FGFRs have been found responsible for several pathological syndromes. Here we will detail the FGFR-related diseases with a special focus on pathologies du to FGFR3 mutations.

2.1 FGFR1 and FGFR2-related diseases

Fgfr1 is located on 8p11.23 and spans 58 kb whereas Fgfr2 is located on 10q26.13 spanning 120 kb. Both Fgfr1 and Fgfr2 transcripts are composed of 18 exons (17 coding exons), their expression is limited to bone and cartilage (16). Most of the activating mutations in Fgfr1 or Fgfr2 have been detected in cranyosinostosis syndromes that are briefly describe in Table 4. Craniosynostosis occurs in approximately 1 in 2 100 to 1 in 2 500 live births (17, 18), and is characterized by the premature fusion of one or more cranial sutures resulting in malformation of the skull. Potential consequences of abnormal skull growth include increased intracranial pressure, problems with hearing and vision, impaired blood flow in the cerebrum, and developmental delay (19).

Table 4. FGFR1 and FGFR2 related craniosynostoses.

	Pfeiffer syndrome type 1	Pfeiffer syndrome type 2	Pfeiffer syndrome type 3	Apert syndrome	Crouzon syndrome	Jackson-Weiss syndrome	Beare-Stevenson syndrome	Isolated coronal synostosis
Gene involved	FGFR1 (5%) FGFR2 (95%)	FGFR2	FGFR2	FGFR2	FGFR2	FGFR2	FGFR2	FGFR2
Craniofacial defects	Midface hypoplasia	Cloverleaf skull, proptosis	Turribrachycephalic skull, proptosis	Turribrachycephalic skull, midface hypoplasia	Proptosis, strabismus, mandibular prognathism	Mandibular prognathism	Midface hypoplasia, abnormal ears, natal teeth	Unilateral coronal synostosis
Intellect	Normal	Developmental delay, intellectual disability	Developmental delay, intellectual disability	Developmental delay, intellectual disability	Normal	Normal	Intellectual disability	Normal
Other	Hydrocephalus, hearing loss	Cleft palate, hydrocephalus, seizures	Cleft palate, hydrocephalus, seizures	Fused cervical vertebrae (70%)	Hydrocephalus (30%)	Extremities anomalies	Cutis gyrata, acanthosis nigricans, genital anomalies	None

2.2 FGFR3-related diseases

Fgfr3 is located on 4p16.3 and spans 16.5 kb. Its transcript is composed of 19 exons which only 2 to 18 are coding exons. The gene expression has been demonstrated in brain (astrocytes and glial cells), growth plate cartilage, intestine, pancreas, testis, cochlea and crystalline lens (20). Mutations in FGR3 are responsible for bone disorders (chondrodysplasias and craniosynostoses) and for various forms of cancer. Fgfr3 harbors almost exclusively dominant mutations leading to a gain of function in almost all cases. Only in the very rare case of Camptodactyly, tall stature, and hearing loss (CATSHL) syndrome it has been proposed a dominant negative mechanism. In any case Fgfr3 is not a haplo-insufficient gene: it means that removing one of the two copies of the gene doesn't lead to mutant phenotype. In this chapter we explore the FGFR3-related pathologies highlighting their clinical features and the mutations underlying their etiology.

2.2.1 Osteochondral disorders

2.2.1.1 Chondrodysplasias

Chondrodysplasias is a family of genetic diseases characterized by a disturbance in the development of the cartilage of the long bones, especially of the epiphysial plates, resulting in arrested growth and dwarfism. Here we present chondrodysplasias due to point mutations in FGFR3 gene.

2.2.1.1.1 Achondroplasia (ACH)

The term 'achondroplasia' was first used by Jules Parrot in 1878, and in 1900 Pierre Marie described the main features in children and adults. As ACH (OMIM#100800) is the most common disorder associated and with its disproportionate short stature is probably one of the best-known and -defined chondrodysplasias (Figure 3). This condition is estimated to occur in between 1 in 10 000 and 1 in 30 000 live births (21, 22). ACH patients present a rhizomelic dwarfism associated with macrocephaly, midface hypoplasia, prognatism (23), kyphoscoliosis (24), cervicomedullary compression, spinal stenosis and loss of synchondroses (25). ACH is an autosomal dominant disorder, frequently de novo and associated with

advanced paternal age due to an increased presence of FGFR3 mutations during spermatogenesis in men over 35 (26). The cause of this disease has been identified in a point gain-of-function heterozygous mutation in FGFR3 (27, 28). The most recurrent mutation (over 95% of cases (21)) is Gly380Arg localized in the TM domain of the receptor (Figure 9). In adulthood affected patients reach an average of 130 cm for males and 125 cm for females (29) due to an abnormal development that can be diagnosed in utero through medical ultrasound since the beginning of the third trimester (30, 31). ACH patients face higher rates of deaths compared to the unaffected population (basically due to sudden death, heart diseases end neurological diseases) (32) and present severe medical complications (spinal stenosis, tibial bowing, obstructive apnea).

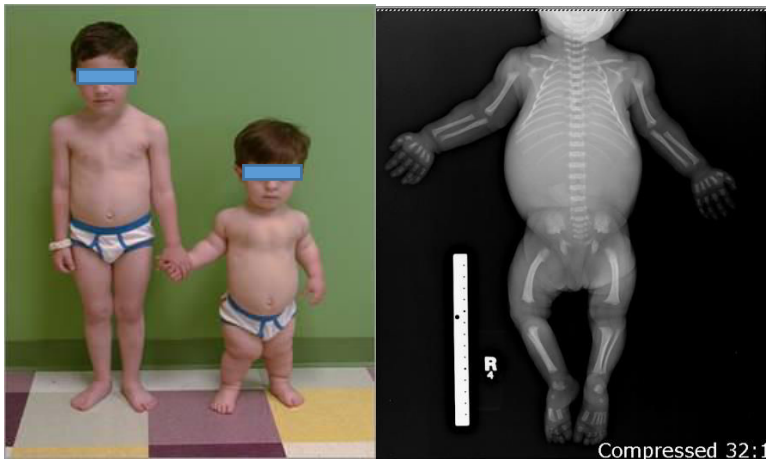

Figure 3. ACH phenotype. In the left picture a couple of twins, the right one is affected by ACH. In the Right picture X-rays of ACH patient.

2.2.1.1.2 Hypochondroplasia (HCH)

HCH (OMIM#146000) (1 / 30 000 live births) is a skeletal dysplasia, characterized by short stature, disproportionately short arms and legs; broad, short hands and feet; mild joint laxity; and macrocephaly (33). The skeletal features are very similar to those seen in ACH but tend to be milder. Medical complications common to ACH (spinal stenosis, tibial bowing and obstructive apnea) occur less frequently in HCH, but intellectual disability and epilepsy may be more prevalent. The diagnosis is difficult to make in children under the age of three years, as skeletal disproportion tends to be mild and many of the radiographic features are subtle during infancy. DNA-based testing is possible and about 70% of affected individuals

are heterozygous for a mutation in FGFR3. However, there is evidence that locus heterogeneity exists, implying that mutations in other as-yet unidentified genes may result in similar, if not identical, phenotypes. The adult height for men with this condition ranges from 138 centimeters to 165 centimeters while the height range for adult women is 128 centimeters to 151 centimeters. Missense, gain-of-function, mutations responsible for this disease are localized in different FGFR3 domains: extracellular, transmembrane and tyrosine kinase with N540K as the most recurrent mutation.

Figure 4. Patients affected by HCH. These sufferers show a rhizomelic dwarfism less severe compared to ACH patients.

2.2.1.1.3 Thanatophoric Dysplasia (TD) and Severe Achondroplasia with Developmental Delay and Acanthosis Nigricans (SADDAN)

TD and SADDAN are the more severe diseases related to gain-of-function mutations in FGFR3. TD (1 / 20 000 to 1 / 50 000 live births) is a lethal skeletal dysplasia due to heterozygous mutations in FGFR3. This pathology was firstly described in 1967 (34). Two types of TD are clinically diagnosed based on ultrasound and radiographic findings. TD type 1 (OMIM#187600) patients have prominently curved femurs, while TD type 2 (OMIM#187601) patients typically have straight femurs, a severe form of craniosynostosis (often referred to as a cloverleaf skull) and a small chest (35). Several different gain-of-function mutations in FGFR3 cause TD type 1. Mutations R248C, S249C, S371C, and Y373C create novel cysteine residues in the extracellular and intramembranous domains, while other mutations causing TD

type 1, such as X807R, X807C, X807E, X807S, and X807W, obliterate the stop codon resulting in extension of the intracellular domain by an additional 141 amino acids. TD type 2 is caused by the FGFR3 mutation K650E. SADDAN Severe achondroplasia, developmental delay and acanthosis nigricans (OMIM#616482) was first discovered in 1999 (36) and it is caused by a K650M mutation in FGFR3. Most of the patients develops extensive areas of acanthosis nigricans in early childhood, suffers from severe neurological impairments, and survives without prolonged life-support measures (37). However the differences between TD and SADDAN phenotypes are not always evident (38). The substitution of a methionine residue at position 650 differentiates SADDAN from type 2 thanatophoric dysplasia, which arises from a glutamic acid substitution at the same position. Interestingly mutations at the same residue K650N, K650Q (39) and K650T (40) are responsible for the less severe hypochondroplasia. The SADDAN amino acid change induces a FGFR3 phosphorylation that is threefold greater than normal.

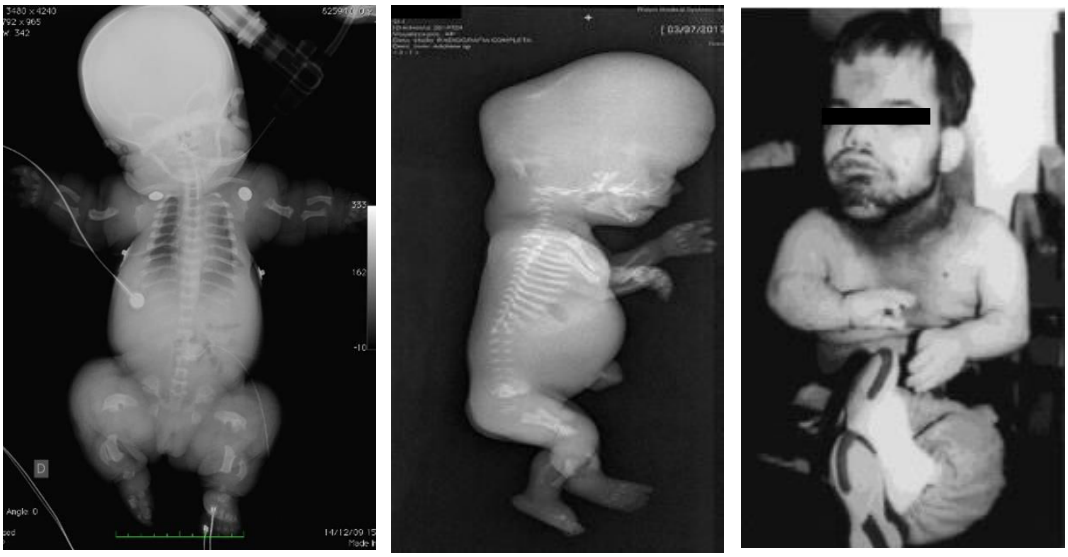

Figure 5. From left to right examples of TD type 1, TD type 2 and SADDAN. TD type 1 patients present femurs with a “telephone receiver" appearance. TD type 2 affected individuals are recognized by straight femurs and presence of cloverleaf craniosynostosis. SADDAN patients suffer of a severe dwarfism and feature the skin lesion acanthosis nigricans.

2.2.1.2 Craniosynostoses

As previously defined for FGFR1 and FGFR2 related craniosynostoses, these pathologies arise from the premature fusion of skull sutures. Also mutations in FGFR3 can lead to craniosynostosis: until now this gene contributes to craniosynostoses family with two syndromes.

2.2.1.2.1 Muenke Syndrome (MS)

MS (OMIM#602849) constitutes the most common syndromic form of craniosynostosis, with an incidence of 1 in 30 000 births. Of all patients with craniosynostosis, 8% have MS (17, 18). Both sporadic and familial cases have been reported. MS displays incomplete penetrance and a variable phenotype even within families (41). Characteristics include bi- or unicoronal synostosis, midfacial hypoplasia, macrocephaly, and downslanting palpebral fissures. Some affected individuals have additional features that may include sensorineural hearing loss, developmental delay, brachydactyly, and coned epiphyses in the hands and feet. MS craniosynostosis is a result of a specific heterozygous gain-of-function mutation, P250R, found in the linker region between domains D2 and D3 of FGFR3 (42). Increasing paternal age is a contributing factor for de novo mutations (43).

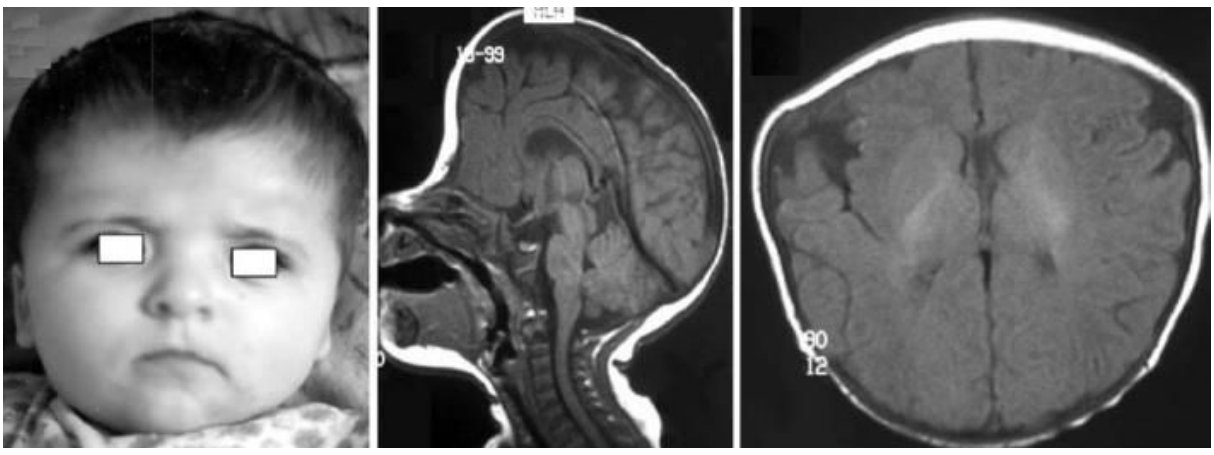

Figure 6. 4 month child affected by MS. The MR images in sagittal and axial views show the severity of the brachycephaly.

2.2.1.2.2 Crouzon with Acanthosis Nigricans syndrome (CAN)

Patients with CAN (OMIM#612247) have multiple sagittal or coronal fusions causing brachycephaly, trigonocephaly, and rare reports of cloverleaf skull malformation. Attributes typically include hypertelorism, a small midface, beaked nose and protrusion of the eyes. CAN has an estimated prevalence of 1 / 1 000 000 newborns and most cases are sporadic and associated with paternal aging, although familial cases consistent with autosomal dominant inheritance have been reported. Characteristic of this disease is the presence of hyperpigmentation of the skin (acanthosis nigricans), hyperkeratosis, and other skin findings. A specific FGFR3 heterozygous gain-of-function mutation A391E, responsible for the syndrome, is located in TM (44, 45).

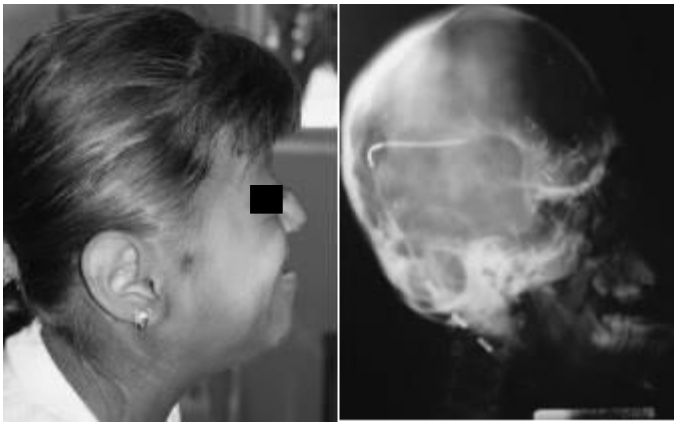

Figure 7. Manifestation of CAN syndrome. Lateral close up and radiograph.

2.2.1.3 Other FGFR3-disorders

Camptodactyly, tall stature, and hearing loss (CATSHL) syndrome

Dominantly inherited, camptodactyly, tall stature, scoliosis, and hearing loss syndrome (CATSHL; OMIM#610474) is caused by a FGFR3 heterozygous missense mutation, R621H, residing within the tyrosine kinase domain generating a loss-of-function that promotes endochondral bone growth (46). For several reasons, it is unlikely that the loss of function caused by p.R621H results from haploinsufficiency. In fact, mice heterozygous for an Fgfr3 null allele are phenotypically normal and the

fibroblasts of individuals affected with CATSHL syndrome express both wild-type and mutant FGFR3 RNA in nearly equal proportions, and the expression levels of all five FGFRs in patients are similar to those of normal individuals. Furthermore, both mutant and wild-type FGFR3 localize to their normal position in the cell membrane (46). These observations suggest that p.R621H might, instead, cause loss of FGFR3 function by a dominant negative mechanism. Recently, a novel homozygous mutation T546K has been described as also causing skeletal overgrowth (47).

Figure 8. Patient affected by CATSHL syndrome. The disorder is characterized by tall stature and scoliosis.

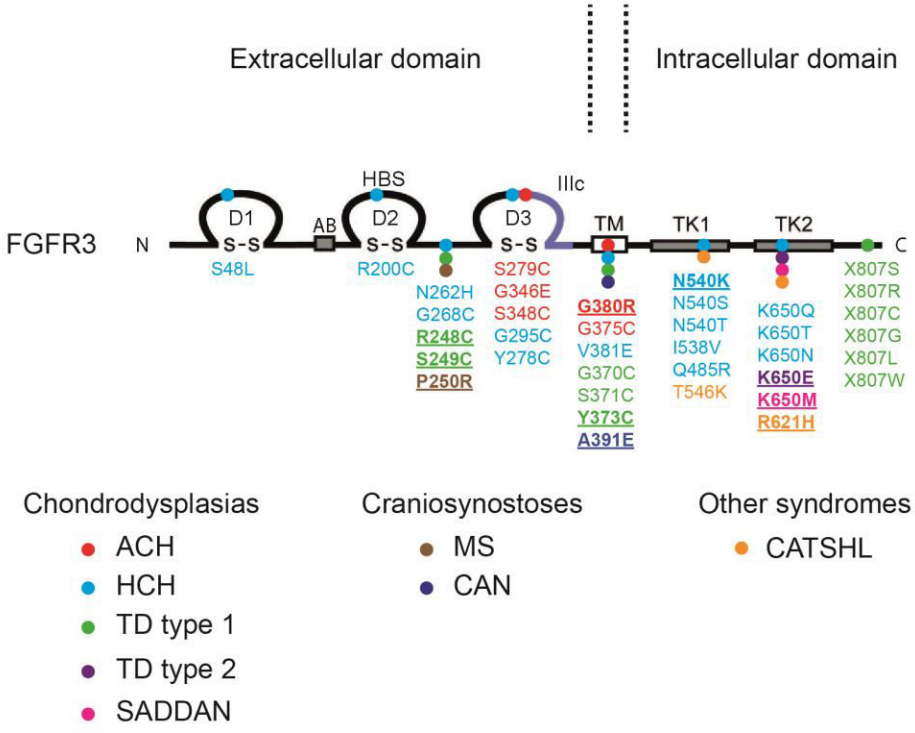

Figure 9. FGFR3 mutations in osteochondro-related disorders. Most common mutations for each disease are underlined.

2.2.2 Cancer

As already shown, germline mutations in FGFR3 cause skeletal disorders. The same point mutations have been identified to cause cancer (48). In literature we can find various examples of FGFR3 constitutive activation in the cancer field. In fact somatic mutations in this gene can induce the cancer progenitors to fulfill their maturation, meaning that FGFR3 mutations are tumorigenic thus FGFR3 is an oncogene. FGFR3 have been reported to play a role in multiple myeloma (49) where a translocation t(4;14)(p16.3;q32) causes the overexpression of the gene. This translocation links FGFR3 to the immunoglobulin heavy chain ICH locus. These translocations are intergenic, with the breakpoints occurring ~70 kb upstream of FGFR3, and bring FGFR3 under the control of the highly active IGH promoter. It is important to note that the translocations involving FGFR3 in multiple myeloma also involve the adjacent multiple myeloma SET domain-containing (MMSET) gene, and the relative contributions of FGFR3 and MMSET to oncogenesis are subject to ongoing debate. The ultimate effect of the translocation is to overexpress FGFR3 out of context, which might result in aberrant ligand-dependent signalling or ligand-independent signalling. In a small proportion of t(4;14) multiple myeloma, FGFR3 is also mutated (~5% translocated cases), presumably further reinforcing FGFR3 signalling.

FGFR3 is also implied in bladder cancer, the fourth most common tumor among males. More than 90% of bladder cancers are urothelial cell carcinoma and about 5% are squamous cell carcinoma. The gender ratio of male to female is 3 to 1 and the best known environmental risk factor is smoking. Urothelial cell carcinoma patients are classified by pathologic stage. The stage classification differentiates between non-muscle invasive (NMI; Tis, Ta, and T1) and muscle-invasive (T2, T3, and T4) tumors according to the invasion depth. Ta tumors are restricted to the urothelium, T1 tumors present invasion of the lamina propria, T2 of the superficial muscle, T3 of the perivesical fat and T4 of surrounding organs. Tis is poorly understood and believed to be a precursor of muscle-invasive tumors. Most of the patients (70%) initially present NMI tumors and after treatment up to 70% of these patients will develop one or several local recurrences. About 25% of NMI patients progress to muscle-invasive tumors disease that can potentially lead to metastasis.

About 50% of all patients present an FGFR3 mutation and the most recurrent is S249C (50–52).

Somatic mutations were found also in other cancers: prostate cancer (53) with 2 missense mutations (S249C and A393E), spermatocytic cancer (54) with the K650E mutation and in cervix cancer as well (55, 56) with the only S249C missense mutation.

2.2.3 Skin lesions

FGFR3 mutations are also associated with particular skin lesions. In the case of SADDAN we have already discussed the appearance of the skin lesion acanthosis nigricans, a velvety hyperpigmentation of the skin. Somatic FGFR3 mutations were also identified in benign skin tumors. Analysis of human seborrheic keratoses revealed somatic FGFR3 mutations in 40% of the benign tumors. The prevalence of FGFR3 mutations was even higher (85 %) in adenoid seborrheic keratoses, a particular histological subtype of seborrheic keratosis (57). FGFR3 mutations in human skin can cause common non-organoid epidermal nevi (58). In that study normal skin adjacent to the epidermal nevus did not show the presence of FGFR3 mutations. Finally other studies showed the presence of FGFR3 mutations in solar lentigo, in 5 out 30 patients, (59) and in lichenoid keratosis, in 6 out of 52 patients (60).

2.2.4 Consequences of different mutations on receptor activity

FGFR3 mutations implied in chondrodysplasias are localised in different receptor domains (Figure 9). FGFR3 gain-of-function mutations are characterized by an abnormal phosphorylation of the receptor. However the phosphorylation level varies depending on the FGFR3 harboured mutation. FGFR3 studies *in vitro* have highlighted higher phosphorylation levels for the mutation K650M (SADDAN) and K650E (TD type 2) (61), with the K650M mutation presenting the higher phosphorylation level (62). This elevated FGFR3 phosphorylation will be transduced to the downstream signalling pathway activating its function disproportionately. We can imagine that mutations in TK1 and TK2 determine protein conformational

modification that increase the transphosphorylation between the receptors that make up the dimer (39). Even if other mutations are not localised in TK1 and TK2 as G380R (ACH), Y373C (TD Type 1) or A391E (CAN) the higher phosphorylation level compared to FGFR3 wild-type could be explained. In fact these mutations localised in TM domain could lead to an over-stabilization of the dimer causing an increase of the transmitted signals (63, 64). Other studies have also suggested that these mutations disrupt c-Cbl-mediated ubiquitination that serves as a targeting signal for lysosomal degradation and termination of receptor signalling. This defect would distance actively signalling receptors from lysosomes prolonging their survival and signalling capacity (65).

3. Skeletogenesis

Skeletogenesis it is a hard task that consists in elaborating an edifice of more than 200 pieces of bone and cartilage. Each skeletal piece is modeled at a distinct location in the body, is articulated with others, and reaches specific sizes, shapes, and tissue compositions according to both species instructions and role. Here we will explore the main stages of this process with a special focus on FGFR role in the phenomenon.

3.1 Early embryo development

The first step in skeletogenesis consists in generating osteochondral progenitor cells. The origin of these cells is linked with the early stages of embryo development, when the vertebrate embryo is composed of three germ layers: ectoderm, mesoderm, and endoderm (Figure 10). From the neural crest several throat and craniofacial skeletal elements arise; the lateral plate mesoderm gives rise to other craniofacial skeletal structures, the limb skeletal elements (appendicular skeleton), the sternum (part of the axial skeleton); finally the paraxial mesoderm gives rise to somites, which develop into sclerotomes (ribs and vertebrae). The vertebrae, developing around the notochord, will force the notochord cells to change phenotype, migrate to the intervertebral spaces, and develop the nuclei pulposi (NP) of Intervertebral Discs (IVDs) (Lefebvre and Bhattaram, 2010).

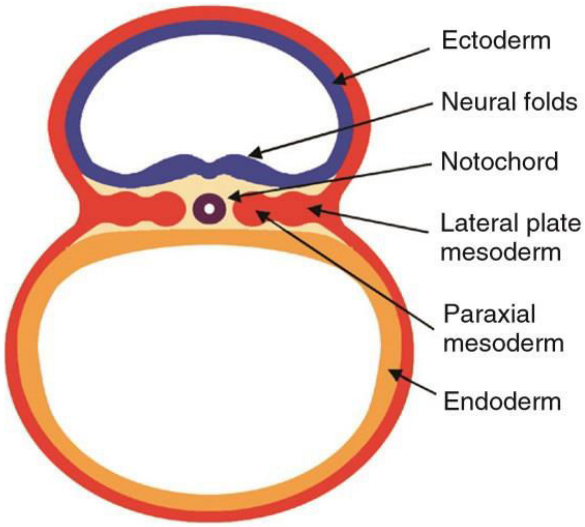

Figure 10. Origin of osteochondro-progenitor cells in the vertebrate embryo. Scheme of a cross-section of mouse embryo after gastrulation at day 8 of development (equivalent to day 17 in humans). The three germ layers are shown: ectoderm, endoderm, and mesoderm (66)

These neural crest and mesoderm cells will reach their skeletal sites through the expression of specific factors as the Homeobox (Hox) genes (67). Before reaching their skeletal sites, neural crest- and mesoderm-derived cells produce a matrix rich in collagen-1, fibronectin, and hyaluronan, and they proliferate or die in a tightly controlled spatial and temporal manner (68). They thereby establish mesenchymal structures that prefigure the future skeletal elements. These cells are called osteochondro-progenitors because most of them give rise to osteoblasts and chondrocytes.

Development of the vertebrate skeleton occurs through the processes of endochondral and intramembranous bone formation. Endochondral-derived bones comprise the appendicular skeleton, facial bones, vertebrae, and medial clavicles, while intramembranous bones comprise the cranium and lateral clavicles. Endochondral ossification initiates with the condensation of mesenchyme, followed by the formation of a cartilaginous template that patterns the developing skeleton and the segmentation of this template into cartilaginous joints. Intramembranous bone forms from a mesenchymal condensation that directly gives rise to bone.

3.2 Chondrogenesis

Mesenchymal condensation is characterized by the aggregation of loose mesenchymal cells and the expression of extracellular matrix proteins and cell adhesion molecules (type I collagen (Col I), hyaluronan, N-cadherin, tenascin-C). The transcription factor Sry box containing 9 (Sox9), that acts in concert with Sox5 and Sox6, is necessary for the beginning of the chondrogenesis as well as the bone morphogenetic protein (BMP) receptors 1a and 1b (69). Proliferating cells within the mesenchymal condensation begin to express type II collagen (Col II) (chondroprogenitors) while cells on the borders of the structure express Col I (osteoprogenitors) (70). Proliferating chondrocytes form columns that are oriented along the longitudinal axis of the developing bone to define the future growth plate (Figure 11).

At the center of the developing bone chondrocytes expressing specific markers (type X collagen (Col X), Indian Hedgehog (IHH), ParaThyroid Hormone (PTH) 1 Receptor (PTH1R)) differentiate into prehypertrophic chondrocytes increasing their volume and arresting their proliferation. The down-regulation of Sox9 is necessary to allow this chondrocyte maturation, however a level of expression of this transcriptor factor is a requirement for the chondrocyte identity (71, 72). Runt-related protein 2 (Runx2) and Runx3 are required for chondrocyte differentiation, with Runx2 determining chondrocyte proliferation through Ihh expression (73). Several signalling pathways (IHH, PTH, FGF, BMP and Wnt) regulate the equilibrium between proliferating and hypertrophic chondrocytes (74). Wnt and PTH-related peptide (PTHrP) signals modulates the calcium/calmodulin-dependent protein kinase II (CAMK2) level, which induces chondrocyte hypertrophy increasing RUNX2 and β-catenin activity (75). Hypertrophic chondrocytes, pushed by the proliferative chondrocytes along the axis, in their late phase secrete vesicles containing enzymes that degrade the cartilage matrix and mineralize their surroundings (76). Finally those chondrocytes commit apoptosis or differentiate into osteoblasts (77, 78).

3.3 Endochondral ossification

The formation of a primary ossification center and bone collar that starts prenatally (79) is characterized by the differentiation of Col I-producing osteoblasts on the border of the hypertrophic chondrocyte zone and determines the origin of mineralized bone. Osteoprogenitor cells (belonging to the Osterix lineage) localized in the perichondrium and in the periosteum differentiate into osteoblasts responsible of the trabecuale formation. The osteoblasts derived from the late hypertrophic cells (belonging to the Col I lineage) will be responsible of the cortical bone (80). The expression of Vascular Endothelial Growth Factor (VEGF-A) in hypertrophic chondrocytes determines the beginning of the vascularization leading to the recruitment of endothelial cells, osteoprogenitor cells, and osteoclasts that will later participate in the bone remodeling process (81). The cartilaginous matrix left behind by the hypertrophic chondrocytes will work like a mold for the osteoblastic progenitors that they will fulfill with mineralized matrix giving rise to the primary ossification center. The primary ossification center will progressively elongate following the same longitudinal axis primarily determined by the columnar chondrocytes. The late hypertrophic chondrocytes, osteoblasts and osteoclasts will take the charge of dismantling the remains of the cartilage matrix through Matrix metalloproteinases (MMP) expression (82). With the postnatal formation of a secondary ossification center at the epiphysis we observe the classic growth plate with well-demarcated zones of cells presenting vascular elements in the primary bone (Figure 12). Finally osteoclasts bone remodeling abilities will be applied in the definition of the bone marrow cavity in the diaphysis that presents an intricate network of vessels compared to the growth plate.

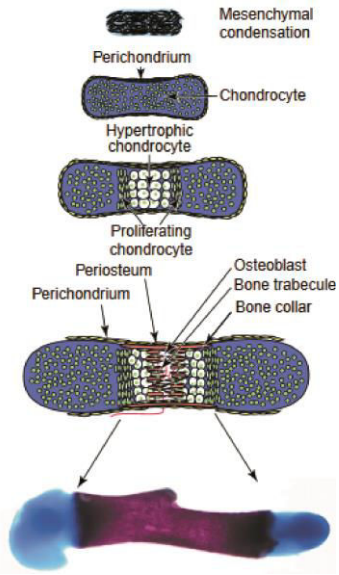

Figure 11. Endochondral ossification. Long bones are formed by endochondral ossification (83).

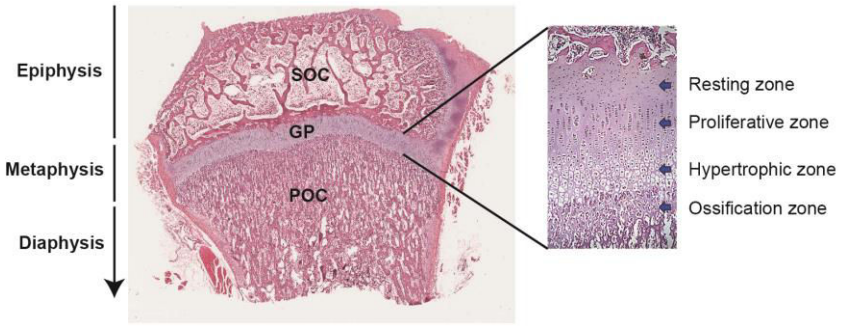

Figure 12. Long bone and growth plate structure. Primary Ossification Center (POC), Growth Plate (GP) and Secondary Ossification Center (SOC).

3.4 Intramembranous ossification

In the structure that will give rise to the skull, at the beginning of intramembranous ossification (Figure 13) mesenchymal cells condensate and differentiate primarily into osteoprogenitor cells and secondly into osteoblasts, in total absence of cartilage and chondrocytes. These osteoblasts directly derived from osteoprogenitor give rise to ossification centers where they will produce mineralized (84). These ossification centers are responsible for the development of the skull bone, but their osteogenic

fronts will never merge determining the appearance of the sutures (85). An abnormal fusion of the sutures (synostosys) would impair the skull growth. Mesenchymal cells surround the suture and part of them differentiate into osteoprogenitors and then into osteoblasts lining the developing bone. When the bone is formed osteoblasts finally die by apoptosis or become embedded in the bone matrix as osteocytes, which then also eventually undergo apoptosis (86). The expression of Runx2 is responsible for the differentiation of mesenchymal stem cells into osteoblasts (opposed to Sox9 responsible for the differentiation of the same cells into chondrocytes). Runx2 is a fundamental transcription factor that regulates several genes in osteoblasts, such as Col I, bone sialoprotein (BSP), osteopontin (OP), alkaline phosphatase (ALP), transforming growth factor (TGFβ), and osteocalcin (OC) (87, 88). Transcription factors, such as Msh homeobox 2 (MSX2) and Distal-less homeobox 5 (DLX5), play important roles in osteoblast differentiation during cranial bone formation in part by interacting with RUNX2 (89). Several factors (as TGFβs, BMPs, FGFs, and Wnt signalling) are responsible for the regulation of differentiation and survival of the cells participating to the bone formation process (85, 89).

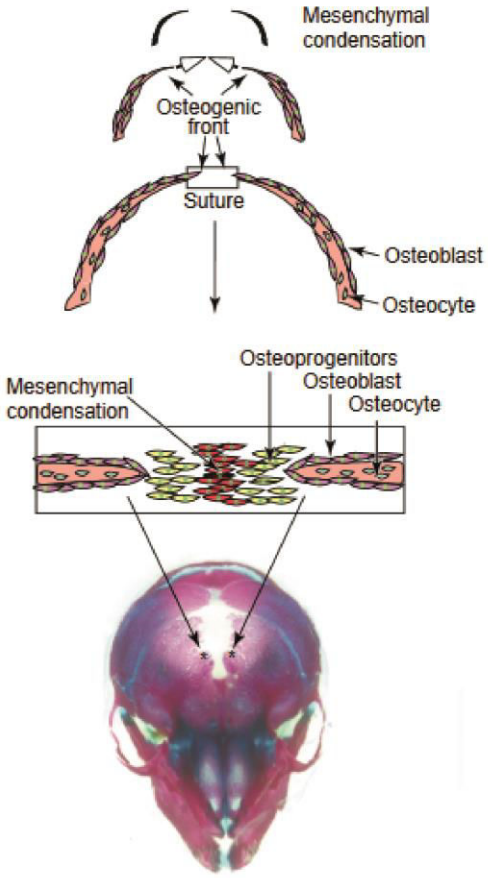

Figure 13. Intramembranous ossification. Craniofacial bones are formed directly from condensations of mesenchymal cells without the formation of a cartilage intermediate. (83).

3.5 FGFR signalling and early skeletal development

FGFs and FGFRs will participate in all the skeletal development stages. We can observe the first FGFR expression even before the mesenchymal cells condensation. The origin of the appendicular skeletal is recognizable in the embryonic mesenchymal limb bud formation (Figure 14). Different mechanisms have been proposed to determine the limb bud development process (90) and in all of them FGFRs and FGFs play an essential role. In fact the distal limb bud mesenchyme expresses both FGFR1 and FGFR2 (91, 92). FGFR3 and FGFR4 are not expressed, so they do not take part to the process (92). At the bottom of the limb bud the apical ectodermal ridge (AER) produces FGFs called AER-FGFs. AER-FGFs (FGF4 and FGF8) bind FGFR1 and FGFR2 stimulating the limb growth (90) (Figure 14). FGFR1 and FGFR2 are redundant in this tissue (93). Conditional inactivation mice have been used to determine the function of FGFR1 and FGFR2 in the mesenchymal limb bud. The conditional knockout in mesenchymal cells of both Fgfr1 and Fgfr2 or the knockout of Fgfr1 lead to severe skeletal hypoplasia highlighting the major role of the receptors in mesenchymal tissue (8, 94). On the other hand the knockout Fgfr1 or Fgfr2 in distal limb bud mesenchyme resulted in milder skeletal phenotypes (95, 96), thus FGFR1 and FGFR2 are redundant in distal limb bud.

At the beginning of endochondral ossification an increase of FGFR2 and Sox 9 expression is observed in condensing mesenchymal cells compared to the surrounding cells of the mesenchyme (92, 97) (Figure 15). At the borders of the mesenchymal condensation both FGFR1 and FGFR2 expressing-cells are present and they will constitute the perichondrium and periosteum (97) (Figure 15). With the differentiation of mesenchymal cells into chondrocytes there is an expression of FGFR3, Sox9 and Col II while FGFR2 expression is decreased (98). The expression of these markers indicate the appearance of proliferative chondrocytes. In hypertrophic chondrocytes FGFR3 expression is decreased whereas FGFR1 expression is increased (7, 99) (Figure 15). The mesenchymal condensation and the differentiation of its cells in chondrocytes is modulated by the FGFRs (94, 100). In fact in chondroprogenitor cells and in primary chondrocytes the FGF signalling is responsible for an increase of Sox9 expression and Extracellular Signal-Regulated Kinase 1/2 (ERK1/2) activation (101, 102). FGFR3 expression in proliferating

chondrocytes requires Sox9 expression, and Sox9 regulatory binding sites have been found in the Fgfr3 gene (103). FGFR3 is activated by FGF9 and FGF18 expressed in mesenchyme stimulating chondrocyte proliferation (104, 105). In the forming perichondrium, bonecollar, and trabecular bone the expression of FGFR1 in mesenchymal progenitors and FGFR2 in differentiating osteoblasts are detected (7, 106). Moreover FGFR1 and FGFR3 are co-expressed in mouse and human articular chondrocytes (107, 108). Difference in FGFRs expression has been observed between immature cultured osteoblasts and mature osteoblasts *in vitro*: the first express relatively higher levels of FGFR1, the second of FGFR2 (109)

FGFs (FGF2, FGF4, FGF9, FGF18) and FGFRs (FGFR1, FGFR2, and FGFR3) are also determinant for the early stages of intramembranous ossification (110, 111). FGFR2 is expressed in early mesenchymal condensations and then in sites of intramembranous ossification, where it interacts with FGF18 (97). At later stages during cranial bone development, FGF8 is expressed in mesenchymal cells and differentiating osteoblasts (110, 112). FGF9 is expressed throughout calvarial mesenchyme during mid to late stages of embryonic development (113). Mice lacking both FGF9 and FGF18 have severe defects in skull bone formation (114). FGFR1 and FGFR2, which are expressed in preosteoblasts and osteoblasts (109), are likely receptors for FGF9 and FGF18 in developing membranous bone (115).

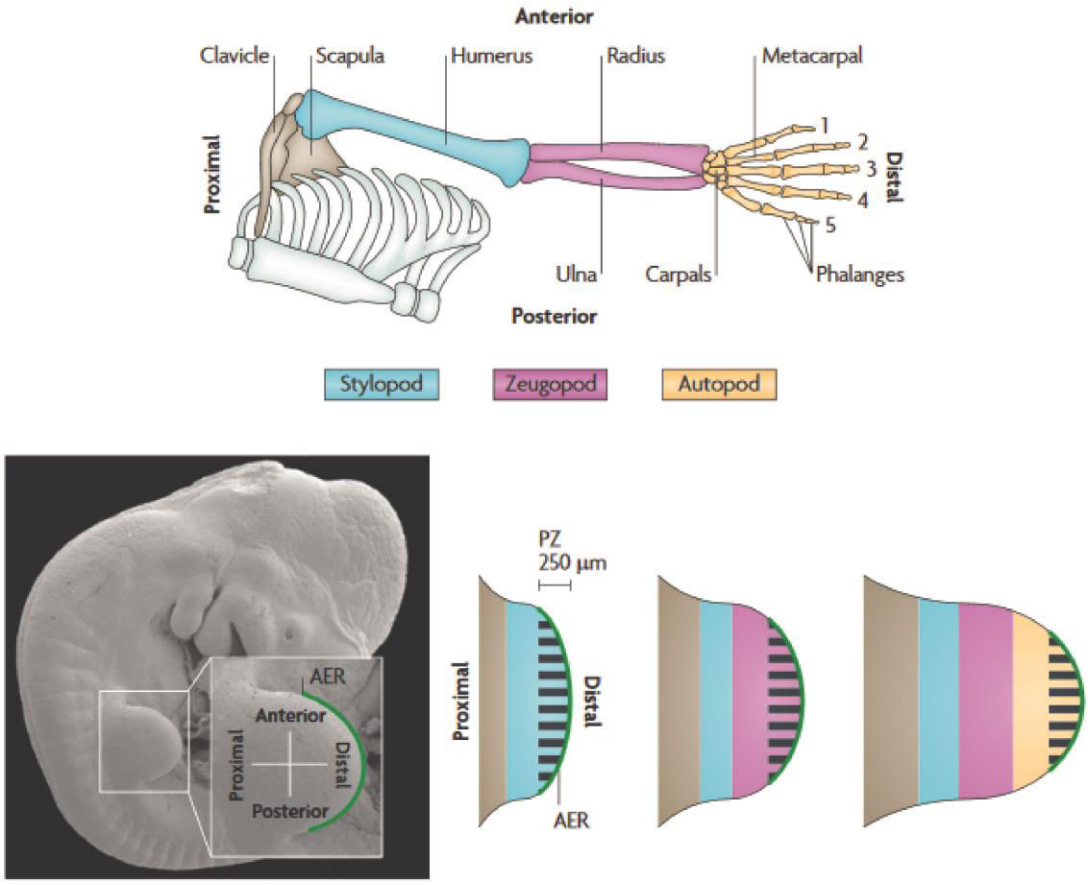

Figure 14. Proximodistal limb bud axis development. The limb skeletal elements (stylopod, zeugopod, autopod) are determined early in embryo development. The origin of limb development is in the limb bud, however different models of this mechanism have been formulated. In all of them the role of AER and AER-FGFs is essential. Here it is presented the progress zone (PZ) model: the mesenchyme that underlies the AER contains mesenchymal cells regulated by AER signals. As limb bud growth progresses distally, proximal cells are too far to be influenced by AER-FGFs. The first cells to lack their influence will give rise to stylopod, the second the zeugopod and finally the autopod.(90).

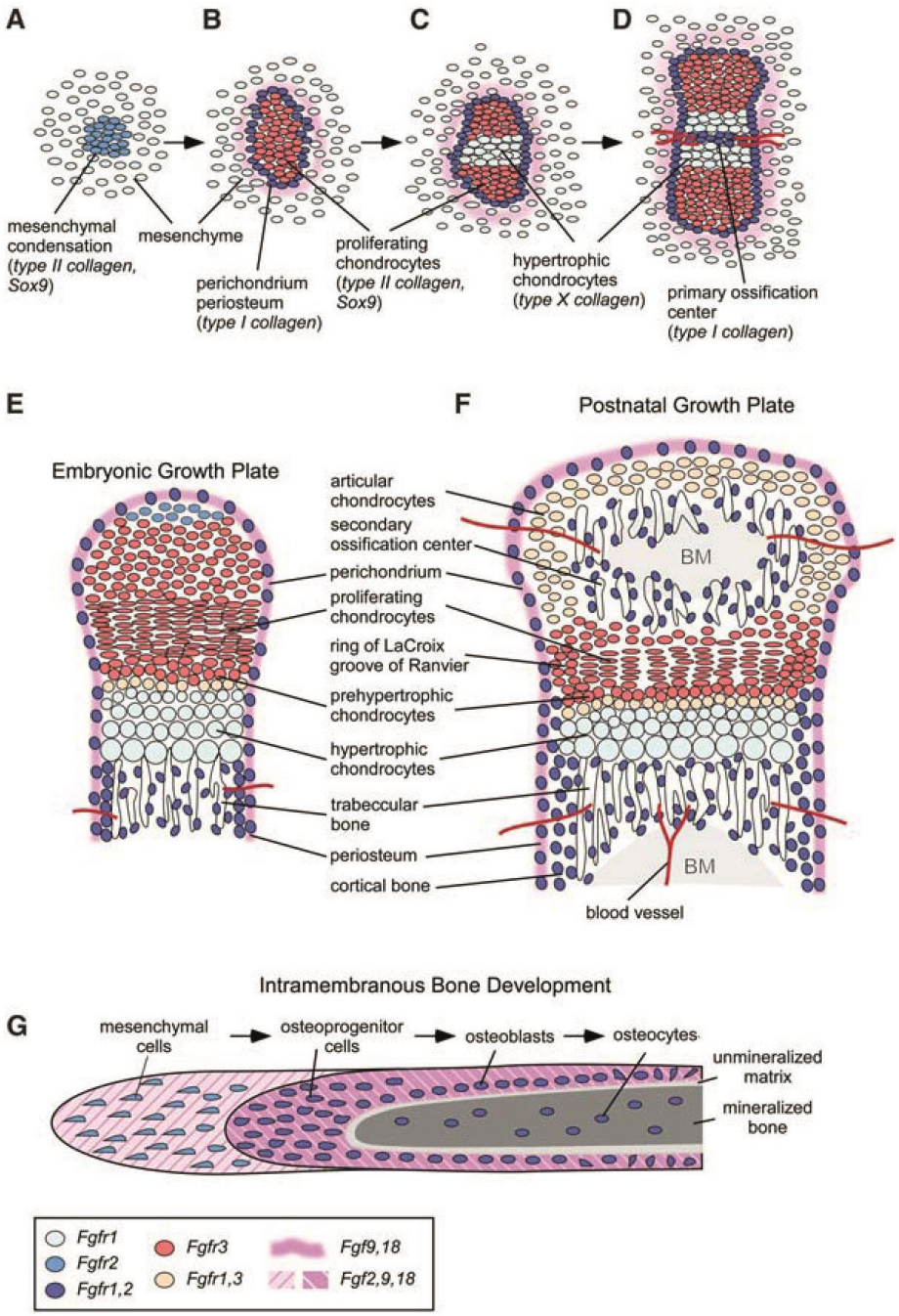

Figure 15. FGF and FGFR expression during endochondral and intramembranous ossifications. (A–D) From chondrogenesis to the primary ossification center. (E) Embryonic growth plate. (F) Postnatal growth plate after formation of the secondary ossification center. (G) Intramembranous ossification. Cells and tissues are color-coded for expression domains of FGFs and FGFRs. (BM) Bone marrow. (93).

3.6 FGFR signalling in growth plate

Chondrocytes FGFRs expression is different within the growth plate (Figure 15). Briefly, there are low levels of FGFR2 in the resting zone, high levels of FGFR3 in the proliferating and prehypertrophic zone, and high levels of FGFR1 in hypertrophic chondrocytes (99, 116). We will now investigate the role of the FGFRs and their signaling pathways in this tissue.

Conditional inactivation experiments in mice shed light on FGFR2 function in resting chondrocytes. The conditional knockout in limb bud mesenchyme (10) leads to a reduced growth in mice. This data could suggest a role in skeletal development, but at the analysis of the growth plate no anomalies were detected in proliferative chondrocytes. The phenotype is probably linked to an effect on osteoblasts rather than on chondrocytes, or on an indirect increase of osteoclastic activity (10). Thus FGFR2 has more a redundant function in resting or proliferating chondrocytes.

In early embryonic stages of skeletal development, during the growth plate formation, FGFR3 stimulates the chondrocyte proliferative activity (62, 104). By cons, during postnatal skeletal growth, FGFR3 signalling inhibits chondrogenesis, leading the proliferating chondrocytes to their differentiation into prehypertrophic and hypertrophic chondrocytes (117, 118). This paradoxical activity of FGFR3 is the reason why chondrodysplastic disorders due to gain-of-function mutations in FGFR3 (that we have already discussed in chapter 2) have a decreased proliferation and differentiation of proliferating chondrocytes during pre-pubertal skeletal growth (119, 120).

FGFR3 downstream signalling pathways in growth plate chondrocytes involve several factors: Signal Transducer and Activator of Transcription 1 (STAT1), ERK1/2, p38, Snail1 (Zinc finger protein SNAI1), AKT, protein phosphatase 2a (PP2a), p107 and p130 (Figure 16) (121, 122). The chondrocyte proliferation arrest resulted from FGFR3 activation is effected through increased expression of the cell cycle inhibitor p21Waf1/Cip1 and activation of p107 and p130 (121, 123). Snail1 expression is induced by FGFR3 and is expressed at high levels in human thanatophoric dysplasia bone tissue. Ectopic activation of SNAIL1 in mice resulted in an ACH phenotype with decreased chondrocyte proliferation and shortened bones at late embryonic stages (124). Interestingly SNAIL1 acts activating both STAT1 and MAPK branches of the

FGFR3 signalling pathway, as the ectopic activation of the protein resulted in nuclear translocation of STAT1 and increased phosphorylation of ERK1/2 (124). The mechanism behind SNAIL1 regulation of STAT1 and MAPK pathways is still poorly understood. However it has been proposed, analyzing breast cancer cells, that SNAIL1 may regulate the nuclear localization of p-ERK (125). In the same cells it has also been shown that activated ERK2 directly phosphorylates SNAIL1, leading to its nuclear accumulation (126). In support of a requirement for SNAIL proteins in regulating chondrogenesis, conditional inactivation of both Snail1 and Snail2 resulted in increased p21Waf1/Cip1 and decreased chondrocyte proliferation (127). The bone growth anomalies lead by activating mutations in FGFR3 are due to decreased chondrocyte proliferation and differentiation. Experiments have led us to consider that these chondrocyte defects are diverse and regulated by different members of the FGFR3 signalling pathway. It has been proven that STAT1 regulates chondrocyte proliferation through *in vivo* experiments when proliferative defects in growth plate of mice with activating mutations in FGFR3 were rescued by the full inactivation of Stat1 (128). However, in this model, inactivation of Stat1 still does not rescue the overall ACH phenotype considering that chondrocyte differentiation to hypertrophy was not corrected: in FGFR3-related disorders impaired chondrocyte hypertrophy, and not only the defective proliferation, is responsible for the decreased bone growth. The same studies proved also that the activation of MAPK signalling suppressed chondrocyte hypertrophy, resulting in skeletal dwarfism (128).The mechanism may involve the suppression of SOX9 down-regulation in prehypertrophic chondrocytes by activated FGFR3 signalling (102, 129). Additionally, activation of the PP2A–B55α holoenzyme by FGFR3, which dephosphorylates and activates p107, could contribute to decreased chondrocyte hypertrophy (121, 122). In support of the model, previously presented, according to which STAT1 activation arrests chondrocyte proliferation and MAPK signalling is responsible for chondrocyte differentiation, there are the studies performed on the C-type natriuretic peptide (CNP) signalling pathway and its interaction with the FGFR3 pathway (130). In fact CNP expression was found to attenuate the phenotype of ACH mice through inhibition of MAPK signalling, which restored matrix production and hypertrophic differentiation. The activity of CNP was independent of the STAT1 one and did not modify chondrocyte proliferation. However that the functions of the STAT1 and MAPK pathways are completely distinct is still unsure. In fact it has been shown that in cultured chondrocyte the suppression

of proliferation required MAPK signalling and was independent of STAT signalling (131, 132). In support of these studies, mice lacking ERK1 and conditionally lacking ERK2 in chondrocytes showed an increase in chondrocyte proliferation at late embryonic stages (133, 134). Still we have to consider some variables that could have produced these results: the variability in the experiments may be due to *in vitro* culture conditions or by the developmental stage being examined. In fact it is really common to observe differences between the embryonic and postnatal signallings.

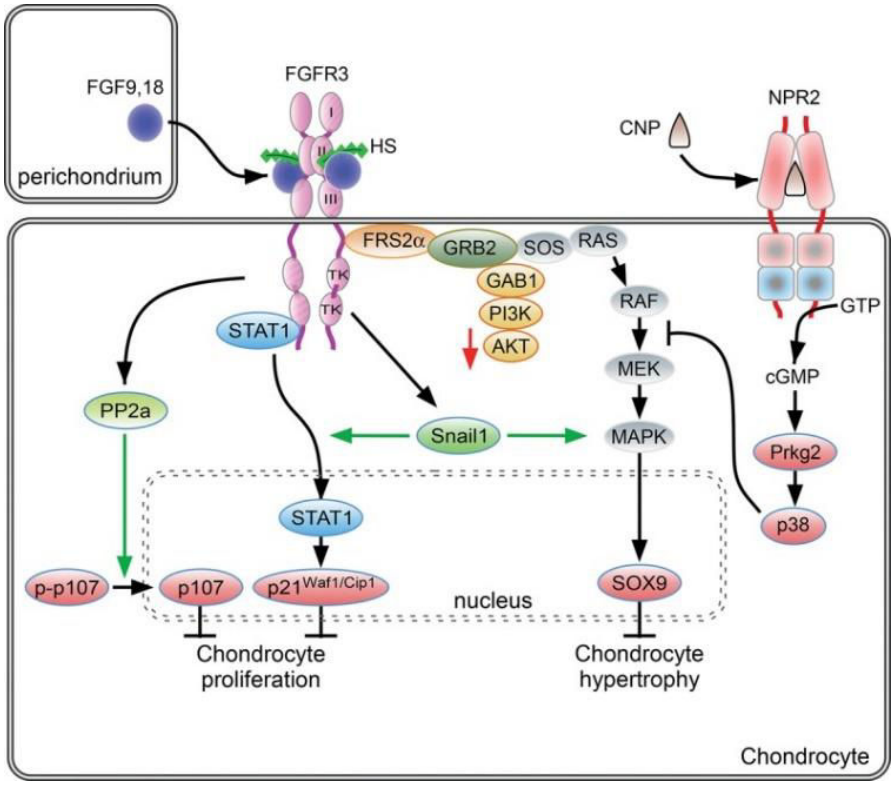

Figure 16. FGF/FGFR signalling pathways involved in proliferating chondrocytes. (93)

Other mechanisms by which FGFR3 signalling may indirectly regulate growth plate development include the regulation of BMP, Wnt, IHH, and PTHrP/PTH1R expression and activity (Figure 17). Comparisons of activating mutations in Fgfr3 and mice lacking Fgfr3 show that FGFR3 signalling suppresses expression of Bmp4, BMPR1a (BMP-receptor type 1A), Ihh, and PTH1R in postnatal growth plate chondrocytes (120, 135, 136). Additionally, in a chondrocyte cell line, overexpression of FGFR3 suppresses expression of both PTHrP and its receptor, PTH1R (137), and, in chondrocyte cell lines and micromass cultures, FGF signalling activates Wnt/β-catenin signalling through phosphorylation of LRP6 (Low-density lipoprotein receptor-related protein 6) and functions to suppress hypertrophic differentiation (138, 139).

PTHrP may also regulate FGFR3 expression. Analyses of the Fgfr3 promoter identified a transcriptional regulatory element, CSRh, which was repressed by PTH through a cAMP and protein kinase A (PKA)-dependent mechanism (140).

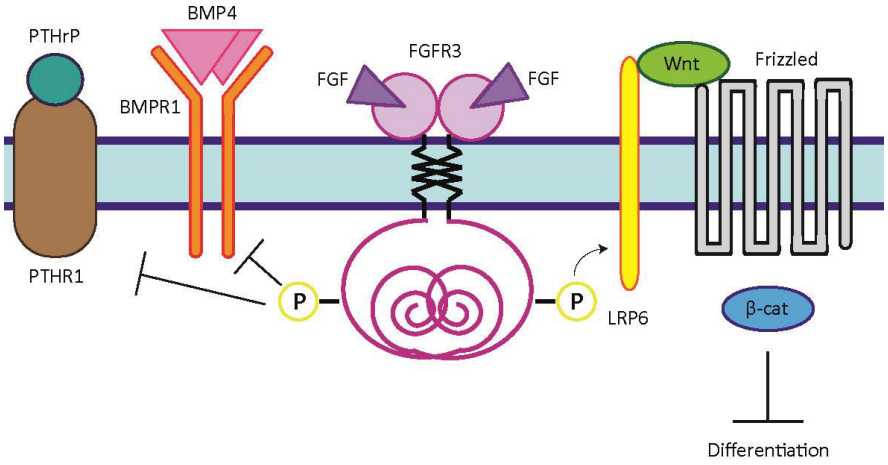

Figure 17. Alternative pathways regulated by FGFR3.

FGFR1 is prominently expressed in prehypertrophic and hypertrophic chondrocytes and overlaps with FGFR3 in the latters (Figure 15). To understand the role of FGFR1 signalling experiments have been performed in mice through the targeted inactivation of FGFR1. At early stages of development, Fgfr1 conditional knockout mouse shows impaired chondrocyte hypertrophy (105) on the other hand the Fgfr1 conditional knock-out mouse for later stages presents an increased hypertrophic zone (7).

FGF9 and FGF18, FGFR3 ligands, are expressed in the perichondrium and are fundamental for growth plate organization (105, 112) (Figure 15). Mice lacking Fgf9, present rhizomelic shortening of the limbs. At early embryonic stages chondrocyte proliferation and differentiation are impaired in Fgf9 null mice (105). Mice lacking Fgf18 also showed decreased chondrocyte proliferation, but in the more distal part of the limb (141). These defects are related with FGF9 and FGF18 signalling to FGFR3 and the proliferative-inducing activity FGFR3 in embryonic chondrocytes (62, 105). In fact the inactivation of FGF9 and FGF18 at later stages leads to an expansion of the hypertrophic chondrocyte zone, thus confirming that in mature growth plate FGFR3 suppresses chondrocyte proliferation and differentiation (105, 110).

3.7 Bone modeling

Bone remodeling is required to repair old the bone and to prevent the aging effects and its consequences. This process requires balance between bone formation and bone resorption and direct communication among different bone cells. Cells of the osteoblast lineage (osteoblasts, osteocytes) and bone-resorbing cells (osteoclasts), together with their precursor cells, are organized in specialized units called bone/basic multicellular units (BMU) (142). We have already detailed the origin of osteoblasts, responsible for bone matrix synthesis and its subsequent mineralization, and osteoblasts-derived osteocytes. On the other hand osteoclasts are large, multinucleated giant cells formed from the fusion of mononuclear progenitors of the monocyte/macrophage in a process termed osteoclastogenesis (143). These cells are the main characters of the remodeling cycle. This process can be analyzed in seven sequential phases: quiescence, activation, resorption, reversal, formation, mineralization, and termination (Figure 18). The bone remodeling process is controlled by various local and systemic factors (Figure 19). The main factors regulating this system are Calcitonin, PTH, vitamin D3 and estrogen. PTH stimulates the proliferation and differentiation of osteoprogenitors to mature osteoblasts via IGF-1 (144), induces RUNX2 expression in osteoblasts (145), increases osteoblast numbers and extends their survival (146). Along with IGF-I, PTH induces Receptor Activator of Nuclear factor κB Ligand (RANKL) and Macrophage Colony-Stimulating Factor (MCSF) from mature osteoblasts to promote osteoclastogenesis (147). PTH elevates cAMP levels and inhibits Mef2-stimulated Sost promoter activity in osteocytes, leading to decreased expression of sclerostin and an elevated bone formation rate (148). Vitamin D3 stimulates osteoblastogenesis via differentiation of mesenchymal stem cells to osteoblasts (149). Calcitonin suppresses bone resorption by inhibiting the activity of osteoclasts (150). Estrogen inhibits bone resorption by directly inducing apoptosis of the bone-resorbing osteoclasts (151). Androgens can also indirectly inhibit osteoclast activity and bone resorption via effects on osteoblasts/osteocytes and the RANKL/RANK/OPG (OPG: Osteoprotegerin) system (152, 153). In addition to systemic hormonal regulation, it is known that growth factors such as Insuline Growth Factors (IGFs), TGF-β, FGFs, Epidermal growth factor (EGF), WNTs, and BMPs play significant roles in regulation of physiological bone remodeling (143).

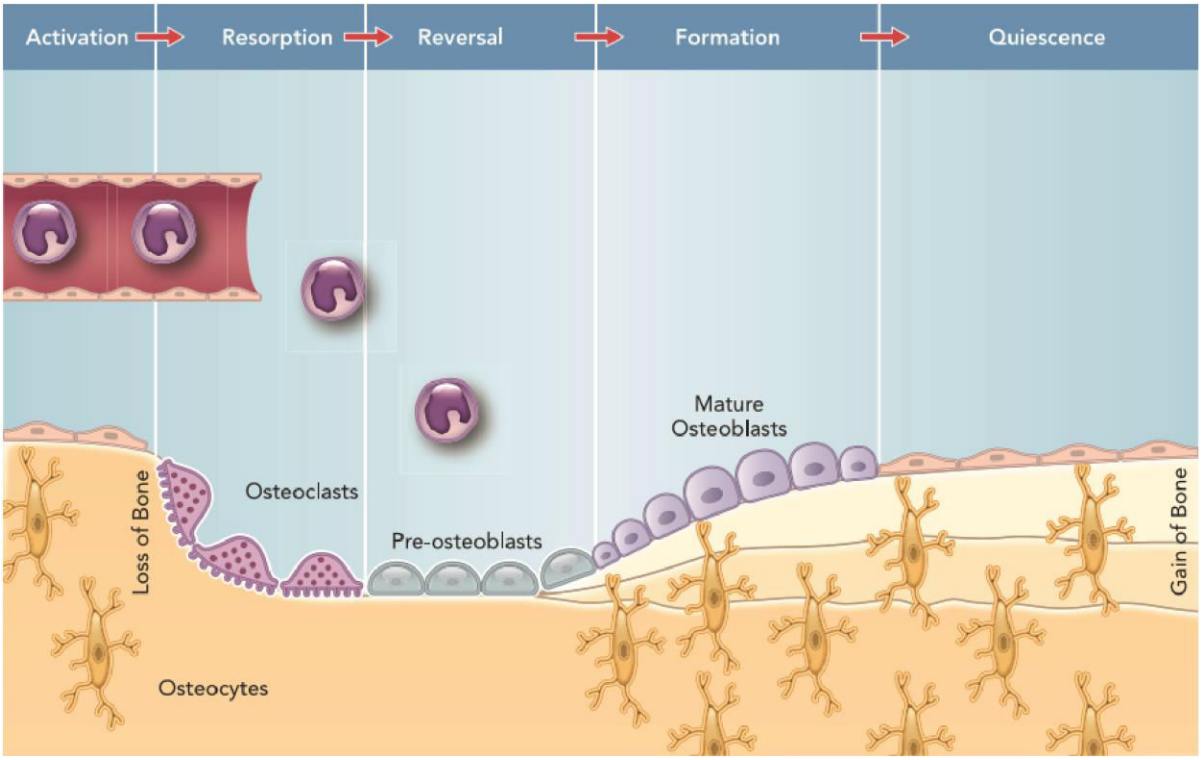

Figure 18. Bone remodeling sequencial phases. The first stage of bone remodeling involves detection of an initiating remodeling signal, which has usually been described as resorption by osteoclasts. In the resorption phase, osteoblasts respond to signals generated by osteocytes or direct endocrine activation signals, recruiting osteoclast precursors to the remodeling site. It is followed by the reversal phase that is characterized by disappearance of almost all osteoclasts. The formation phase is distinct by complete replacement of osteoclastic cells with osteoblastic cells. The termination signals of bone remodeling include the terminal differentiation of the osteoblast. The resting bone surface environment is maintained until the next wave of remodeling is initiated. (143).

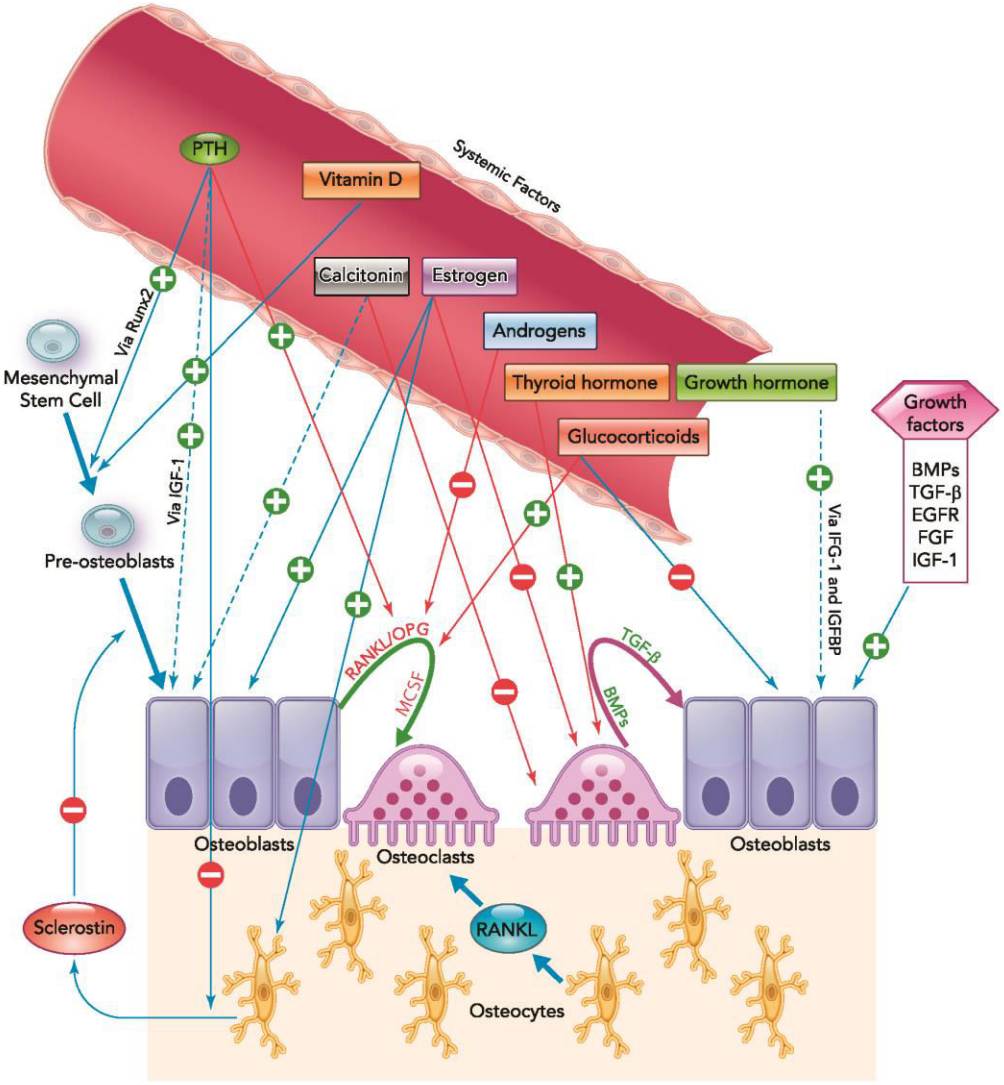

Figure 19. Regulation of bone remodeling. (143).

4. Therapeutic strategies

Skeletal anomalies due to aberrant FGFR signalling require several surgical treatments to extend and improve the life of affected patients. For ACH, life threatening features as cervicomedullary compression, hydrocephalus and lumbar spinal stenosis are solved by surgical interventions (154, 155). Moreover affected individuals attain adult heights that are well below the fifth percentile and undergo long, painful and costly limb lengthening surgical treatments (156).Other surgical interventions are required for other FGFR-related pathologies, notably for craniosynostoses where they are necessary to allow a correct brain development (157).

All treatments routinely administrated today to the affected population are surgical. There have been several trials of human growth hormone treatment in children with ACH: although there has been some increase in growth rate reported, especially early in the trials, no clear long-term benefit has been established and most experts do not recommend such treatment for ACH (158). However nowadays several alternative approaches have been proposed to enhance skeletal growth suppressing or counteracting the FGFR signalling pathway. We will now explore pharmacological approaches that have been tested or proposed to treat FGFR-related diseases, focusing on the FGFR3 signalling pathway and ACH treatments.

4.1 FGFR3 signalling targeting strategies

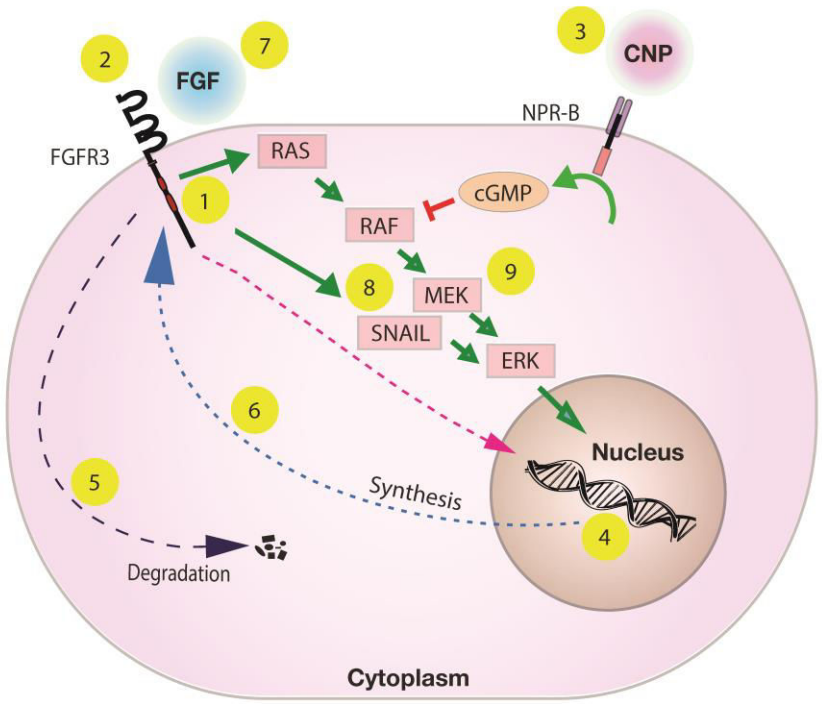

Figure 20. Strategies for therapeutic intervention. (1) chemical inhibitors to reduce fibroblast growth factor receptor 3 (FGFR3) tyrosine kinase activity; (2) antibodies to block receptor activation; (3) exogenous C-type natiuretic peptide (CNP) to enhance CNP-mediated antagonism of downstream signals; (4) RNAi to reduce FGFR3 production; (5) Hsp90 inhibitors to induce degradation of activated receptor; (6) agents to disrupt direct nuclear signalling of FGFR3. (7) Inhibition of FGF ligands that activate FGFR3; (8) chemical inhibitors to reduce SNAIL activity; (9) chemical inhibitors reducing MEK activity (modified from (159)).

4.1.1 FGFR3 tyrosine kinase inhibitors (TKIs) (1)

The rationale for this strategy is that activation and signalling of FGFR3 depend on its kinase activity; consequently, chemical inhibition of its kinase activity should block its inhibitory output and restore bone growth. Several FGFR3 inhibitors have been discovered. CHIR-258, a small molecule inhibitor of receptor tyrosine kinase, inhibits FGFR3. Therapeutic efficacy of CHIR-258 was demonstrated in a xenograft mouse model of FGFR3 multiple myeloma (160). Two others inhibitors of FGFR3, PD173074 and SU5402, inhibit the growth and induce apoptosis of multiple

myeloma cells (161). PD173074 in mice can effectively block angiogenesis induced by either FGF or VEGF with no apparent toxicity and block small cell lung cancer growth (162, 163). A large number of these FGFR tyrosine kinase inhibitors reached the clinical trial phase (164).

However only two FGFR3 selective inhibitors have been reported to have an effect on bone growth. Aviezer and colleagues described synthesis of an oxindole-based TKI selective for FGFR3 (165). The compound stimulated cartilage growth in cultured limb bones from a knock-in *Fgfr3*$^{G369C/+}$ mouse model of ACH (166). Another effective TKI is A31 (167) that leads to the FGFR3 phosphorylation inhibition in cells and restores growth in limb explants of *Fgfr3*$^{Y367C/+}$ mouse embryo, an ACH mouse model (168). However, because the structure of the tyrosine kinases domain is highly conserved among tyrosine kinase receptor subfamilies, kinase inhibitors frequently cross-react with other tyrosine kinase receptors. Such cross-reactivity is not problematic in cancer therapy, because cancer cells frequently depend on multiple tyrosine kinase receptors, but it could be more of a problem in the treatment of children with ACH, which involves only the single receptor. Moreover no TKI has been reported to be able to ameliorate growth *in vivo* (93). Gudernova and colleagues even assert that the use of TKIs *in vivo* show no positive effect on skeletal growth, but rather a toxic effect testing the compound AZD4547 (169). However such statements should be taken with a grain of salt since specificity and properties of chemical compounds as the TKIs vary widely depending on their molecular structure.

4.1.2 FGFR3 antibodies (2)

This strategy involves the use of humanized monoclonal antibodies to the extracellular domain of FGFR3. The binding between the antibody and the receptor constitutes a hindrance to the FGF ligand binding so that the activation of the receptor is no more inducible. These inhibitory antibodies have been developed and successfully applied as potential cancer therapeutics (170, 171). On the other hand a positive effect of these antibodies in an animal model of ACH has never been reported (93). Lack of efficacy for this approach in ACH studies could be linked to the nature of the receptor activation. If the gain of function mutation in the receptor leads

to its activation in absence of ligands, as it has recently been reported (15), the obstructive role of the antibody towards the FGF ligand would loose of importance.

4.1.3 CNP antagonism of FGFR3 signalling (3)

The C-type Natriuretic Peptide (CNP) approach is rooted in the observation that mice lacking CNP presented a severe dwarfism that was rescued when the strain was crossed with mice overexpressing CNP under the promoter Col2A1 (172). Considering the phenotypic similarity of CNP knock-out mice to mouse models of ACH, there was the chance that CNP could overcome the bone growth deficit caused by overactive FGFR3 in ACH. To explore this possibility, mice overexpressing CNP in cartilage were crossed with mice *Fgfr3*^{ach} displaying an ACH phenotype resulting from overexpression of FGFR3 bearing the G380R ACH mutation in cartilage (120, 130). The same Col2A1 promoter was used to drive the expression of both mutant FGFR3 and CNP. The growth deficiency of the ACH mice was corrected by the local overexpression of CNP and a dose effect was demonstrated since bone growth was greater in mice homozygous compared with heterozygous for the CNP transgene insertion. The results suggested that the antagonism was primarily directed at MAPK-mediated FGFR3 signals.

These promising studies lead to the idea that administrating exogenous CNP could ameliorate, if not reverse, the dwarf phenotype. The first experiments exploring this strategy were performed through continuous exogenous CNP intravenous infusion and a significant rescue of the bone growth deficiency was observed after 3 weeks of treatment for the *Fgfr3*^{ach} mice (128). However the study highlighted the limits of using exogenous CNP: since CNP half-life in plasma is estimated to be less than 2 minutes (173, 174) the continuous intravenous infusion was necessary to reach the positive effects on bone growth. It was clear that a similar treatment was not suitable for a pediatric population.

To overcome the obstacle the company BioMarin (Navato, California) designed and produced BMN 111, a 39-amino-acid pharmacological variant of CNP, with the same pharmacological properties and an increased half-life. BMN 111 harbors 17-amino-acid sequence necessary for CNP pharmacological activity and is resistant to neutral endopeptidase that normally digests the native CNP (175).The

compound was able to increase the skeletal growth in *Fgfr3*^{ach} and in *Fgfr3*$^{Y367C/+}$ mice (175, 176) through daily subcutaneous injections. The switch from continuous intravenous infusion to daily subcutaneous injections represents an important milestone if we consider the consistent reduction of the possible adverse effects due to the mode of administration. NPR-B, CNP receptor, it is not exclusively expressed in chondrocytes, but also in other cells in particular in cardyomiocytes (177) so that heart-related side effects due to a consistent CNP-like stimulation couldn't be excluded. For this reason BMN 111 has been tested in juvenile cynomolgus monkeys, to assess hemodynamic and pharmacological effects in larger animals. ECG parameters were unaffected at any dose of BMN 111, and there were no clinical signs of hypotension or distress at any time during the treatment. Moreover monkeys treated with the compound presented an improved growth rate, an increased growth plate cartilage area and an enlarged spinal canal at the vertebral lumbar level (175). All these encouraging preclinical data allowed BioMarin to initiate a phase 1 clinical trial in healthy volunteers (ClinicalTrials.gov NCT01590446). The treatment was well tolerated, and a safe dose for the pediatric population was identified (178). In 2014 a multinational clinical trial for pediatric patients with ACH has started (ClinicalTrials.gov NCT01603095). Objectives of this clinical trial is to verify the tolerability and efficacy of daily administration of BMN 111 to an ACH pediatric population. As of today BioMarin communicated through its press the first results after 1 year of administration of BMN 111 (also called vosoritide). Today, we have entered a new era, and to cure patients with skeletal disorders is not a dream but a way of making dreams become reality. After 12 months of daily dosing at 15 µg/kg/day, patients experienced a 46% or 1.9 cm/year increase in mean annualized growth velocity from baseline without serious adverse events (179). Furthermore the company is planning to initiate a single Phase 3 clinical trial by the end of 2016. It is clear that the most promising therapy thus far for treatment of ACH is the use of BMN 111 (vosoritide).

4.1.4 RNA interference (4)

The idea sustaining this strategy is to silence the expression of FGFR3 using techniques that interfere with translation of its mRNA transcripts. To describe these approaches it is used the term of RNA interference (RNAi) indicating a natural process used by cells to protect themselves from foreign DNA and that can be used to silence endogenous genes (180). RNAi can be triggered by endogenous micro RNAs (miRNAs) that are then reduced into short double stranded RNA. These fragments are incorporated into RNA-induced silencing complexes able to recognize, bind and silence target mRNA transcripts. A near-perfect base pairing of the miRNA to the target mRNA determines the cleavage of that specific transcipt, while an imperfect pairing leads to translational repression and mRNA decay (181). It is known that miRNAs participate in the growth plate development (182) and that targeted deletion of miRNA-140 in mouse leads to a mild short stature phenotype (183). Interestingly it has been shown that the overexpression of miR-100 is able to inhibit the growth of osteosarcoma through the reduction of FGFR3 expression (184). A lower level of FGFR3 could improve the ACH growth plate organization, however there's no proof that miR-100 could be endogenously expressed in this cartilage.

The cellular machinery that generates the endogenous genes silencing can also be activated by artificial RNAs that mimic miRNAs function: the so-called small interfering-RNAs or siRNAs. Because targeting is sequence specific, any genes can theoretically be silenced by designing an appropriate siRNA. It could be possible to cure ACH trough siRNA silencing of the FGFR3 allele harbouring the ACH gain-of-function mutation leaving the wild-type FGFR3 allele to function normally. This approach was successful in a FGFR-related preclinical study concerning a mouse model of Apert syndrome (185). Nowadays there's only one research concerning the use of FGFR3 siRNAs in chondrocytes and it was limited to *in vitro* studies (186). Even if a highly efficient FGFR3 siRNA would be developed there would be always to deal with the concern of the drug delivery that is common among all RNAi therapies.

4.1.5 Hsp90 inhibition and FGFR3 cleavage (5)

The control of chaperone complexes to promote the folding or unfolding of disease-causing proteins has been tested for its therapeutic potential in both *in vitro* and *in vivo* experimental models (187) and the chaperone heat shock protein 90 (Hsp90) protein has been the focus of many of these experiments. Inhibition of Hsp90 leads to the degradation of its "client proteins"; this property has been used to destabilize oncogenes in cancer and to reduce the accumulation of aggregation-prone proteins in neurodegenerative disease animal models. FGFR3 has been identified as a client of the chaperone Hsp90 meaning that its stability is dependent on the function of Hsp90 (188). For this reason Hsp90 inhibitors could be used to act on the FGFR3 folding and thus reducing its growth inhibitory signals in ACH. However since FGFR3 is not the only Hsp90 client it's hard to imagine how an inhibitor of this chaperone could avoid the appearance of undesired side-effects. A large number of clinical trials of Hsp90 inhibitors in cancer have been conducted in last years (189) which ended with very different results (190–192).

4.1.6 Modulating FGFR3 expression cleavage and/or nuclear function (6)

In 2011 it was identified that FGFR3, as other transmembrane signalling receptors, was regulated by intramembrane proteolysis (RIP) in response to ligand stimulation, switching FGFR3 localisation from the membrane to the nucleus (193). The major responsible for this displacement is the enzyme γ-secretase that is able to cleave a cytoplasmic fragment of the receptor from its membrane anchorage. The consequence of RIP on the function of FGFR3 in the growth plate remains unknown. Altering the cleavage events of FGFR3 could allow to modify FGFR3 functions influencing endochondral ossification. A number of drugs have been developed to alter the activity of γ-secretase because of its role in other diseases the most cancer-related. These drugs have potential to modulate FGFR3 RIP and its contribution to ACH. Since γ-secretase influences normal human physiology in many ways, it would be risky to administrate a drug that modifies its function in a pediatric population (194). In addition to influencing the cleavage of FGFR3, the nuclear function and/or potential genes regulated by nuclear FGFR3 might become new drug targets for ACH.

4.1.7 Inhibition of FGF ligands (7)

Since the binding of FGFs leads to an increase in phosphorylation and consequent activation of FGFR3 the strategy of intercept these ligands before their interaction with the receptor is tempting. To achieve this result it has been synthetized a soluble form of the extracellular domain of FGFR3 (sFGFR3) that competes with the endogenous full-form FGFR3 by binding the natural ligands FGF9 and FGF18 (195). Subcutaneous injections of recombinant sFGFR3 in the *Fgfr3*^{Ach} mouse model for ACH (120) was found to decrease mortality and improve skeletal growth (195).This sFGFR3 was also characterized by a long half-life time that is a strong point in the study of a potential new drug as already discussed for the synthesis of BMN 111. An enlarged half-life time could allow to pass from a daily treatment to a once in a week treatment and maybe in an even less frequent treatment. However some issues still need to be addressed before reaching a phase 1 clinical trial. First of all decoy receptors as sFGFR3 have the potential to cause immunogenicity reactions and the emerging antibodies against could also cause toxicity issues if there is any cross-reactivity for related human receptors (196). Another consideration is that BMN-111 is a 39 amino acids long peptide, whereas sFGFR3 is about 700 amino acids long. Since growth plate cartilage is an area difficult to attain even by smaller compounds it's difficult to believe that the sFGFR3 action could be directly play in this tissue. Finally, as already argued for FGFR3 antibodies, recent studies show that the mutant FGFR3 is phosphorylated and activated even in absence of ligand (15). If these findings are correct, the strategy of the inhibition / interception of ligands would lose importance.

4.1.8 SNAIL inhibition (8)

As already detailed in "FGF signalling in growth plate" SNAIL 1 is a protein that regulates and activates STAT1 and MAPK (93, 126). In a transgenic mouse model expressing a chimeric construct in which Snail1 could be activated by tamoxifen gave rise to a short stature phenotype (124). From 2008 a patent was registered for Snail1 activity inhibiting compounds in a chondrodrodystrophia context (WO2008107508A1) however no treatment has been proposed in preclinical studies. Instead it has been proposed by the same group the use of morpholinos against

SNAIL1 to treat renal fibrosis *in vivo* in mice (197). Antisense morpholinos inhibit the interactions of macromolecules with mRNA by base pairing with the targeted mRNA. This prevents the initiation complex read-through or modifies the mRNA splicing (198). Since Snail1 is involved in growth plate homeostasis the use of these morpholinos could produce interesting results for the goal of curing ACH.

4.1.9 MEK direct inhibition (9)

There is no doubt that activation of FGFR3 results in activation of ERK pathway and that this stimulus is more important in pathologies related to gain-of-function mutations (199). As already discussed in the RNAi section, a group of scientists performed experiments to reverse the Apert syndrome phenotype in a mouse model (185). They succeeded in their attempt and to validate their discovery they obtained the same positive results treating the affected mice with U0126, an inhibitor of mitogen-activated protein (MAP) kinase kinase 1 and 2 (MEK1/2) that blocks phosphorylation and activation of ERK1/2. Even if from this data we would be tempted of exploring furtherer the use of such inhibitors we have to remember that ERK1/2 are proteins which functions are not limited to chondrocytes. Also in this approach the lack of a specific drug delivery system is an important obstacle.

4.2 FGFR3-unrelated preclinical studies with effects on bone growth

In this section we will explore preclinical studies of compounds not strictly targeting the FGFR3 pathways previously described. These investigations have produced interesting results on ACH mouse models bone growth.

The first of these researches consider the treatment of TD and ACH mice (*Fgfr3*$^{K644E/+}$; *Fgfr3*$^{369C/+}$ under Ella-Cre promoter). With intermittent PTH injections they partially rescued the lethality and skeletal growth phenotype (200). On the other hand the mechanism leading to these positive effects is difficult to elucidate. In cultured cells, PTH treatment down-regulated FGFR3 expression. This observation could make a pair with the fact that CSRh, transcriptional regulatory element of Fgfr3 promoter, is repressed by PTH through a cAMP and protein kinase A (PKA)-dependent mechanism (140). However it is also reported that PTH treatment

inhibited FGFR3 phosphorylation, suggesting that PTH may function in part through regulation of FGFR3 signalling (200).

Another study highlights the role of statin in ameliorating the skeletal development. In induced pluripotent stem cells (iPSCs) differentiated into chondrodrocytes derived from fibroblasts of TD and ACH patients, the compound lovastatin, belonging to the statin family, was able to reduce FGFR3 expression and MAPK phosphorylation (201). In *Fgfr3*^{Ach} mouse model intraperitoneal injections of another statin, rosuvastatin, were able to induce a growth increase. However it's not clear how the cholesterol lowering drug could produce such effects that are somewhat at odds with prior studies on cholesterol signalling and FGFR3 function in chondrocytes, as well as statin use in patients with osteoarthritis (202).

Finally an investigation showed promising results with the molecule meclozine. This antihistamine, routinely used to reduce motion sickness, was able to suppress as able to stimulate chondrocyte proliferation and differentiation, and inhibit ERK phosphorylation (203). The authors of this study showed that the drug was able to promote bone growth embryonic tibial explants of *Fgfr3*^{Ach} mice. Moreover, oral administration of the drug to *Fgfr3*^{Ach} mice, was able to increase the longitudinal skeletal growth, but failed in enlarging the foramen magnum and the spinal canal (204).

Objectives

In the first part we will evaluate the effects of the TKI NVP-BGJ398 *in vitro*, *ex vivo* and *in vivo.* The *in vitro* investigations, conducted employing cell cultures, will highlight the effects on FGFR3 and its downstream signalling pathways. The *ex vivo* and *in vivo* studies will be performed to assess the potential effects on bone growth. For the *ex vivo* an *in vivo* analyses we will use the ACH mouse model *Fgfr3*$^{Y367C/+}$. TKIs are considered a promising therapeutic strategy for ACH and they have never been tested before in a mouse model of Fgfr3-related disorders. These results have been published (2016 May 2;126(5):1871-84. doi: 10.1172/JCI83926. Epub 2016 Apr 11) on The Journal of Clinical Investigation "Tyrosine kinase inhibitor NVP-BGJ398 functionally improves FGFR3-related dwarfism in mouse model".

In the second part we will explore the mandibular defects in ACH and in our Fgfr3$^{Y367C/+}$ mouse model. This work features experiments with the TKI NVP-BGJ398 useful to understand the mandibular growth and the origin of its pathological aspect. These results brought together in the article "Meckel's and condylar cartilages anomalies in achondroplasia result in defective development and growth of the mandible" that has been recently e-published (Hum Mol Genet. 2016 Jun 3. pii: ddw153).

In the last part we will investigate the three FGFR3 mutations (K650N, K650M, K650E) localised at the same position leading to pathologies with increasing severity depending on the substituting aminoacid. *In silico* studies (from the collaboration with ITODYS lab) will detail the molecular changes of the FGFR3 protein, while biological studies will provide findings on the effects that such mutations produce on the molecular signalling pathways. These results are preliminary data that will be studied furtherer and organized in an article titled "Best understanding of structural and functional impact of FGFR3 mutations at the same position (K650N, K650M, K650E) leading to both mild and lethal dwarfism".

Results

Article 1 - Tyrosine kinase inhibitor NVP-BGJ398 functionally improves FGFR3-related dwarfism in mouse model

Tyrosine kinase inhibitor NVP-BGJ398 functionally improves FGFR3-related dwarfism in mouse model

Davide Komla-Ebri,[1] Emilie Dambroise,[1] Ina Kramer,[2] Catherine Benoist-Lasselin,[1] Nabil Kaci,[1] Cindy Le Gall,[1] Ludovic Martin,[1] Patricia Busca,[3] Florent Barbault,[4] Diana Graus-Porta,[2] Arnold Munnich,[1,5] Michaela Kneissel,[2] Federico Di Rocco,[1] Martin Biosse-Duplan,[1,6] and Laurence Legeai-Mallet[1,5]

[1]INSERM U1163, Université Paris Descartes, Sorbonne Paris Cité, Institut Imagine, Paris, France. [2]Novartis Institutes for BioMedical Research, Basel, Switzerland. [3]University Paris Descartes, UMR 8601 CNRS, Paris, France. [4]University Paris Diderot, Sorbonne Paris Cité, ITODYS, UMR CNRS 7086, Paris, France. [5]Service de Génétique, Hôpital Necker-Enfants Malades, Assistance Publique – Hôpitaux de Paris (AP-HP), Paris, France. [6]France Service d'Odontologie, Hôpital Bretonneau, Hôpitaux Universitaires Paris Nord Val de Seine (HUPNVS), AP-HP, Paris, France.

Achondroplasia (ACH) is the most frequent form of dwarfism and is caused by gain-of-function mutations in the fibroblast growth factor receptor 3–encoding (FGFR3-encoding) gene. Although potential therapeutic strategies for ACH, which aim to reduce excessive FGFR3 activation, have emerged over many years, the use of tyrosine kinase inhibitor (TKI) to counteract FGFR3 hyperactivity has yet to be evaluated. Here, we have reported that the pan-FGFR TKI, NVP-BGJ398, reduces FGFR3 phosphorylation and corrects the abnormal femoral growth plate and calvaria in organ cultures from embryos of the *Fgfr3*$^{Y367C/+}$ mouse model of ACH. Moreover, we demonstrated that a low dose of NVP-BGJ398, injected subcutaneously, was able to penetrate into the growth plate of *Fgfr3*$^{Y367C/+}$ mice and modify its organization. Improvements to the axial and appendicular skeletons were noticeable after 10 days of treatment and were more extensive after 15 days of treatment that started from postnatal day 1. Low-dose NVP-BGJ398 treatment reduced intervertebral disc defects of lumbar vertebrae, loss of synchondroses, and foramen-magnum shape anomalies. NVP-BGJ398 inhibited FGFR3 downstream signaling pathways, including MAPK, SOX9, STAT1, and PLCγ, in the growth plates of *Fgfr3*$^{Y367C/+}$ mice and in cultured chondrocyte models of ACH. Together, our data demonstrate that NVP-BGJ398 corrects pathological hallmarks of ACH and support TKIs as a potential therapeutic approach for ACH.

Introduction

Achondroplasia (ACH) is the most common form of dwarfism, which occurs with an estimated prevalence of between 1/16,000 and 1/25,000 live births (1, 2). ACH patients are characterized by disproportionate short stature, with a long trunk deformed by excessive lordosis. The head is large with frontal bossing and the midface is hypoplastic (2). ACH is an autosomal-dominant disorder, and patients with ACH have been found to have a gain-of-function mutation (p.Gly380Arg) localized in the transmembrane domain of the fibroblast growth factor receptor 3 (*FGFR3*), a member of the receptor tyrosine kinase family (3, 4). The *FGFR3* mutation disturbs the balance of proliferation and differentiation in the growth plate. Several papers reported both decreased and increased proliferation related to stage-specific development (5–8). Chondrocyte differentiation is also impaired (9, 10) and seems to be controlled by SRY-box 9 (*Sox9*) expression in the growth plate (11). The ACH mutation activates the tyrosine kinase activity of the receptor and facilitates the transautophosphorylation of key tyrosine residues in the intracellular domain and activates mainly the downstream canonical MAP pathway. Other signaling pathways have been implicated in addition in ACH, e.g., STAT, Wnt/β-catenin, PI3K/AKT, and PLCγ pathways (9, 12, 13).

Potential therapeutic strategies have emerged for ACH over the last 5 years; these have aimed at reducing excessive activation of FGFR3 and its signaling pathways to stimulate linear bone growth. Our group conducted preclinical studies on a C-natriuretic peptide (CNP) analog (14), BMN111, and we showed that this treatment led to a substantial improvement of skeletal parameters in the *Fgfr3*$^{Y367C/+}$ mouse, which is a preclinical model of ACH (15). BMN111 (vosoritide) is currently in a (phase 2) clinical trial in pediatric patients with ACH (ClinicalTrials.gov NCT02055157). Other preclinical studies using different strategies and various compounds, such as parathyroid hormone (PTH) (16), soluble FGFR3 (17), statin (18), and meclozine (19), reported changes in the dwarf *Fgfr3*^{ach} mouse phenotype (7). For most of these strategies, the mechanism of action in the growth plate needs to be elucidated. However, the most direct therapeutic strategy would be to counteract the hyperactivity of FGFR3 using a tyrosine kinase inhibitor (TKI). NVP-BGJ398 was identified as a panspecific FGFR inhibitor that was equally active against FGFR1, FGFR2, and FGFR3 and less active against FGFR4 (20). Recently, cell-free kinase assays showed that NVP-BGJ398 was more selective for FGFR3 than the other FGFRs (21). This TKI is effective in reducing FGFR3 activation and has been used in preclinical murine models for the treatment of several FGFR-related pathological conditions, such as hypophosphatemic rickets (22), malignant rhabdoid tumors (23), and hepatocellular carcinoma (24). We therefore decided to investigate whether NVP-BGJ398 could penetrate into the car-

Conflict of interest: I. Kramer, D. Graus-Porta, and M. Kneissel work for Novartis.
Submitted: July 24, 2015; **Accepted:** February 25, 2016.
Reference information: *J Clin Invest*. 2016;126(5):1871–1884. doi:10.1172/JCI83926.

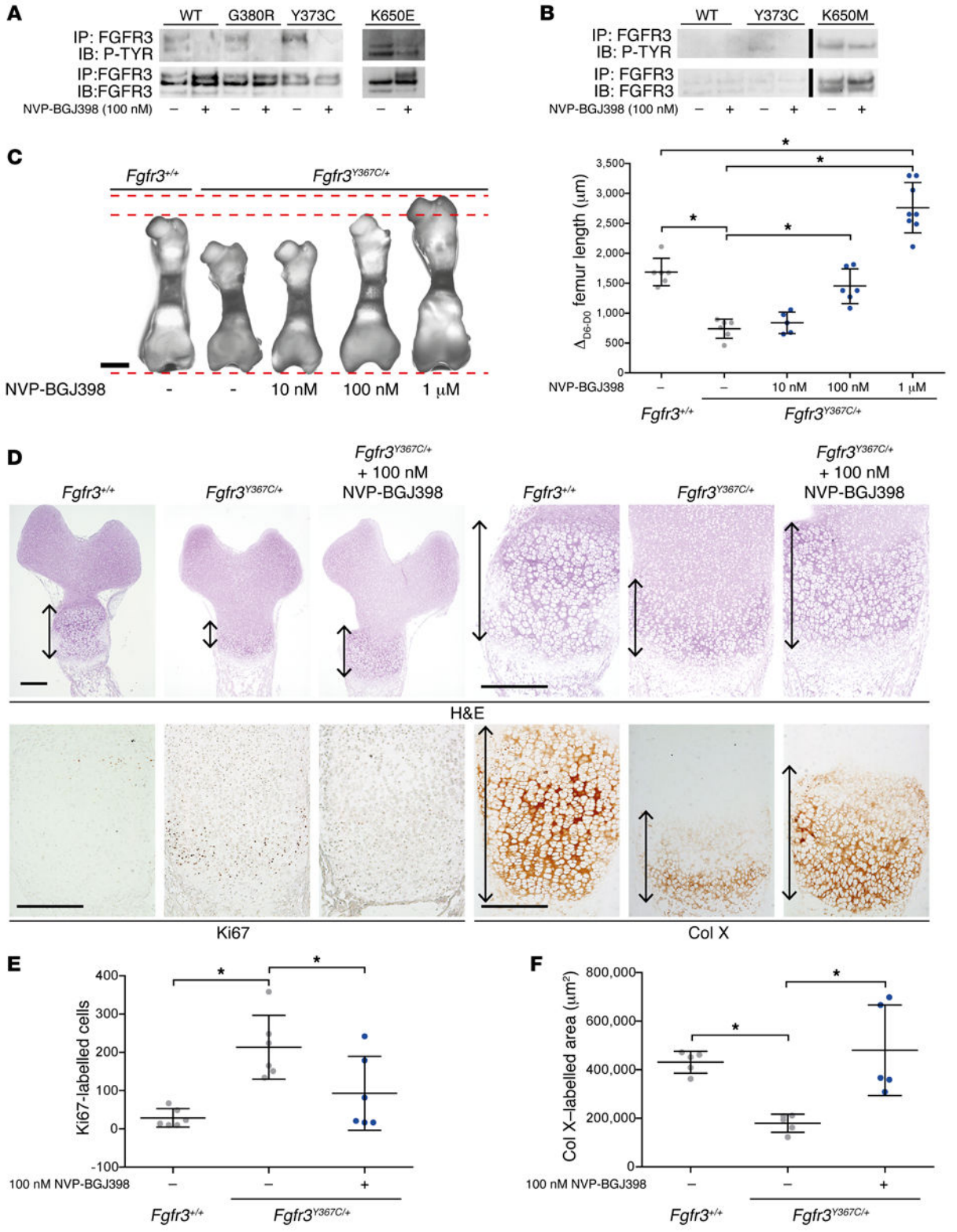

Figure 1. NVP-BGJ398 inhibits the activation of FGFR3 and rescues ex vivo bone growth of *Fgfr3*$^{Y367C/+}$ mouse embryo femurs. (**A**) Phosphorylated FGFR3 expression in transfected human chondrocytes with FGFR3 (WT), FGFR3^{G380R} (ACH), FGFR3^{Y373C} (TDI), and FGFR3^{K650E} (TDII) constructs. (**B**) Phosphorylated FGFR3 expression in transfected HEK293-Vnr cells with FGFR3 (WT), FGFR3^{Y373C} (TDI), and FGFR3^{K650M} (SADDAN) constructs. Lanes were run on the same gel, but were noncontiguous. (**C**) Gain of length of E16.5 femurs in culture for 6 days ($\Delta_{D6\text{-}D0}$) with or without treatment (*Fgfr3*$^{+/+}$, $n = 6$; untreated *Fgfr3*$^{Y367C/+}$, $n = 6$; 10 nM *Fgfr3*$^{Y367C/+}$, $n = 5$; 100 nM *Fgfr3*$^{Y367C/+}$, $n = 6$; *Fgfr3*$^{Y367C/+}$, $n = 8$. *$P < 0.05$, 1-way ANOVA. Scale bar: 1 mm. (**D**) H&E staining and immunohistochemistry for Col X and Ki67 on embryonic distal femur following 6 days of culture with or without treatment. Arrows indicate hypertrophic area. Scale bars: 200 μm. (**E**) Number of Ki67-labeled cells in treated and untreated *Fgfr3*$^{Y367C/+}$ compared with *Fgfr3*$^{+/+}$ embryonic femur ($n = 6$ per group). *$P < 0.05$, 1-way ANOVA. (**F**) Col X–labeled growth plate area in *Fgfr3*$^{+/+}$ and *Fgfr3*$^{Y367C/+}$ treated and untreated embryonic femur ($n = 5$ per group). *$P < 0.05$, 1-way ANOVA. Western blots are representative of 3 independent experiments. Data are expressed as mean ± SD.

Table 1. Improvement of femur lengths after NVP-BGJ398 treatment

Fgfr3$^{+/+}$	*Fgfr3*$^{Y367C/+}$	*Fgfr3*$^{Y367C/+}$+NVP-BGJ398, 10 nM	*Fgfr3*$^{Y367C/+}$+NVP-BGJ398, 100 nM	*Fgfr3*$^{Y367C/+}$+NVP-BGJ398, 1 μM
5,604 ± 144 μm	4,667 ± 104 μm	4,659 ± 61 μm	5,311 ± 127 μm	6,702 ± 151 μm

Size of femurs after 6 days of culture with NVP-BGJ398. Data are expressed as mean ± SD.

tilage and bone and improve the skeletal phenotype in ACH via its inhibitory action on FGFR3 and downstream signaling pathways. In our study, NVP-BGJ398 inhibited the hyperactivity of FGFR3 and the canonical MAPK in ACH human cartilage cells. NVP-BGJ398 rescued the anomalies of fetal calvaria and femur in organ cultures of tissue taken from the *Fgfr3*$^{Y367C/+}$ mouse model of ACH. Moreover, NVP-BGJ398 treatment of *Fgfr3*$^{Y367C/+}$ mice was able to correct the dwarf phenotype. The reduction in the activity of FGFR3 improved all pathological hallmarks of ACH in long bones, skull base, calvaria, intervertebral disc (IVD), and vertebrae. The timing and type of the treatment were 2 important criteria for the improvement of bone growth in *Fgfr3*$^{Y367C/+}$ mice. At cellular and tissue levels, chondrocyte proliferation was restored, as demonstrated by STAT pathway downregulation, and chondrocyte differentiation was improved, as demonstrated by SOX9 and MAPK downregulation. Our data suggest that TKIs may represent a pharmacological approach for the treatment of FGFR3 hyperactivation-related disorders.

Results

NVP-BGJ398 inhibits FGFR3 phosphorylation. We evaluated the ability of NVP-BGJ398 to inhibit FGFR3 phosphorylation in transiently transfected human control chondrocyte lines (Figure 1A) and HEK293-Vnr cells (Figure 1B). Cells were transfected with constructs expressing *FGFR3*^{WT} and *FGFR3* gain-of-function mutations localized in different domains of FGFR3 responsible for chondrodysplasias (*FGFR3*^{G380R} [transmembrane domain; ACH], *FGFR3*^{Y373C} [extracellular domain; thanatophoric dysplasia type 1 [TDI], *FGFR3*^{K650E} intracellular domain; thanatophoric dysplasia type 2 [TDII]) (25, 26). Twenty-four hours after transfection, phosphorylated FGFR3 was detected for each mutant (Figure 1, A and B). For all transfected cells expressing FGFR3 with activating mutations, NVP-BGJ398 reduced FGFR3 phosphorylation (Figure 1, A and B). No phosphorylated *FGFR3*^{WT} was detected in HEK293-Vnr cells (Figure 1B).

NVP-BGJ398 restores bone growth in Fgfr3$^{Y367C/+}$ *embryonic femurs*. In ACH, FGFR3-activating mutations disturb endochondral and membranous ossifications (27, 28). Our in vitro findings therefore prompted us to test the impact of NVP-BGJ398 on long bone and skull growth. To investigate the effect on endochondral ossification, we used ex vivo cultures of embryonic femurs isolated from *Fgfr3*$^{Y367C/+}$ mice (E16.5) with various concentrations of NVP-BGJ398. At day 6, untreated *Fgfr3*$^{Y367C/+}$ femurs exhibited a reduction of length (–16.7%) compared with WT femurs (Figure 1C and Table 1). Six days of ex vivo culture with 10 nM NVP-BGJ398 did not affect bone growth of WT femurs, whereas 100 nM NVP-BGJ398 rescued completely the bone growth defect of *Fgfr3*$^{Y367C/+}$ femurs (Figure 1C and Table 1). At 1 μM, NVP-BGJ398 induced bone overgrowth of *Fgfr3*$^{Y367C/+}$ femurs (+19.6% compared with WT femurs, +43.6% compared with untreated *Fgfr3*$^{Y367C/+}$ femurs). These data show that the induced femoral elongation by NVP-BGJ398 was dose dependent, confirming the role of FGFR3 as a negative regulator of bone growth (5).

In *Fgfr3*$^{Y367C/+}$ mice, the coordinated proliferation and differentiation of chondrocytes that ensure the continuous elongation of the growth plate are defective (29). We observed that in *Fgfr3*$^{Y367C/+}$ explants cultured for 6 days, chondrocyte proliferation (i.e., Ki67 expression) was increased (7 times more than WT) as previously reported (ref. 26 and Figure 1, D and E). NVP-BGJ398 significantly reduced chondrocyte proliferation at 100 nM (–56.4% compared with untreated). Differentiated chondrocytes in the growth plate were assessed using an antibody against collagen X (Col X), and we observed that the growth-plate hypertrophic zone was reduced in *Fgfr3*$^{Y367C/+}$ explants (–58.4% compared with WT) as previously reported (refs. 15, 30, and Figure 1, D and F). The area of the hypertrophic zone was increased (+167.6%) with NVP-BGJ398 treatment compared with vehicle alone, indicating that the defective differentiation of the chondrocytes was ameliorated (Figure 1, D and F).

To analyze the membranous ossification defect in the *Fgfr3*$^{Y367C/+}$ skull vault, we used ex vivo cultures of embryonic mouse calvaria. Previously, we reported a calvarial defect in ACH and *Fgfr3*$^{Y367C/+}$ mice, indicating a role of FGFR3 in skull bone growth (28). This defect gradually disappears during skull growth, as it does in mouse calvaria cultures. We observed that the calvarial defect, corresponding to a bone ossification delay, resolved faster and more completely in NVP-BGJ398–treated cultures (100 nM) compared with untreated *Fgfr3*$^{Y367C/+}$ calvaria from culture day 4 (+20.1%) to culture day 14 (+46.1%) (Figure 2, A and B). These data confirm that the calvaria-formation defect is directly related to the overactivation of FGFR3.

Together, these results indicate that in ex vivo bone models of ACH, NVP-BGJ398 can rescue chondrocyte proliferation and differentiation defects and can reduce the bone-growth anomalies of the growth plate and the skull vault, thus modifying both chondrogenesis and osteogenesis during embryonic bone development.

NVP-BGJ398 improves growth of the appendicular skeleton in Fgfr3$^{Y367C/+}$ *mice*. On the basis of those encouraging in vitro and ex vivo data, we treated *Fgfr3*$^{Y367C/+}$ newborn mice (P1) daily with subcutaneous injections of NVP-BGJ398 (2 mg per kg body weight per day) for 15 days (protocol 1). The *Fgfr3*$^{Y367C/+}$ mouse phenotype mimics human ACH in several respects; short stature, macrocephaly, prognatism, fused synchondroses, and foramen magnum (FM) stenosis (28, 29). Our objective was to evaluate whether and how NVP-BGJ398 inhibition of the overactivity of FGFR3 would affect bone growth in vivo. The treatment was well tolerated by *Fgfr3*$^{Y367C/+}$ and *Fgfr3*$^{+/+}$ mice without noticeable modification of behavior.

X-ray analyses of the forelimbs (Figure 3A) and hind limbs (Figure 3B) showed in NVP-BGJ398–treated *Fgfr3*$^{Y367C/+}$ mice a

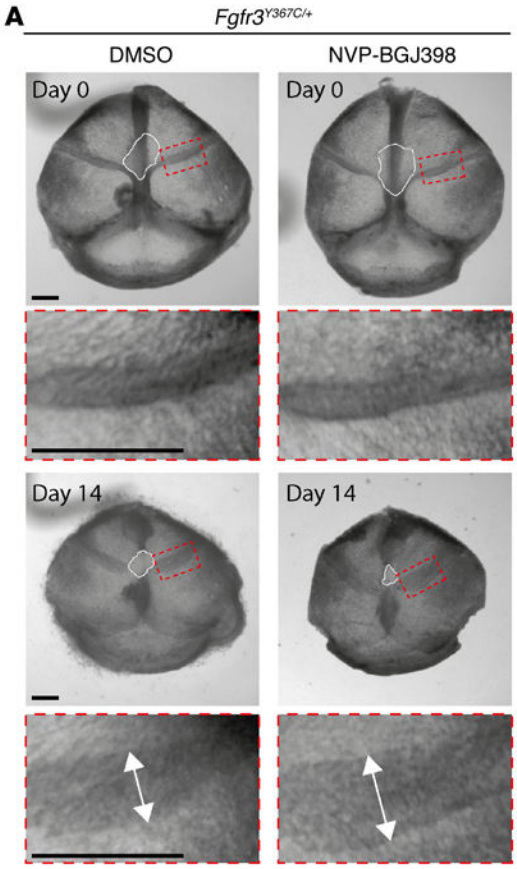

Figure 2. NVP-BGJ398 reduces the ossification gap of *Fgfr3*$^{Y367C/+}$ mouse embryo calvariae ex vivo. (**A**) Fetal calvaria gaps of *Fgfr3*$^{Y367C/+}$ mice with or without treatment are indicated by white lines. Magnified images show the effects on suture. (**B**) The modifications of calvaria gap size of the *Fgfr3*$^{Y367C/+}$ treated mice (n = 11) compared with the untreated *Fgfr3*$^{Y367C/+}$ mice (n = 5) are indicated in the graph. *P < 0.05, Mann-Whitney U test. Scale bars: 1 mm. Data are expressed as mean ± SD.

distinct increase in size of these limbs compared with those of control *Fgfr3*$^{Y367C/+}$ littermates. At necropsy, long bones of treated *Fgfr3*$^{Y367C/+}$ mice (NVP-BGJ398 and vehicle) and their *Fgfr3*$^{+/+}$ control littermates were measured. In *Fgfr3*$^{Y367C/+}$ mice, the lengths of proximal and distal long bones were significantly higher with NVP-BGJ398 treatment than control treatment (femur +20.9%, humerus +11.9%, tibia +32.6%, ulna 22.3%, and radius +24.1%) (Figure 3C and Supplemental Figure 1A; supplemental material available online with this article; doi:10.1172/JCI83926DS1). μCT imaging confirmed these data and also showed that NVP-BGJ398 treatment expanded the total cross-sectional tissue area of *Fgfr3*$^{Y367C/+}$ mouse distal femur metaphysis (+30% vs vehicle) (Figure 3, D–F). The long-bone growth of *Fgfr3*$^{+/+}$ mice treated with NVP-BGJ398 was not affected (data not shown), and no premature death was observed, confirming the mild or null effect of the inhibitor on *Fgfr3*$^{+/+}$ mice.

Histological analyses of the epiphyseal growth plate of long bones showed that NVP-BGJ398 improved growth-plate cartilage homeostasis in both distal and proximal femurs (Figure 4A) and tibias (Supplemental Figure 1B).

Chondrocyte proliferation was lower in *Fgfr3*$^{Y367C/+}$ untreated mice (–59.9%) compared with *Fgfr3*$^{+/+}$ mice, as measured with BrdU incorporation into the growth plate. By contrast, chondrocyte proliferation was significantly higher with NVP-BGJ398 treatment than control treatment in *Fgfr3*$^{Y367C/+}$ mice (+162.1%) (Figure 4B).

Likewise, the impaired differentiation of hypertrophic chondrocytes in femurs and tibias of *Fgfr3*$^{Y367C/+}$ mice was rescued by NVP-BGJ398 treatment, as demonstrated by Col X immunostaining (Figure 4C and Supplemental Figure 1B). In these treated mice, the expression of Col X was observed in the calcified cartilage, showing an active process of bone growth at the subtrabecular bone level (Figure 4C and Supplemental Figure 1B). Previously, we reported that angiogenesis was disturbed in *Fgfr3*$^{Y367C/+}$ mice (29). We hypothesized that the action of NVP-BGJ398 on cartilage could affect angiogenesis in the growth plate and thus activate mineralization reflected by the altered size of the secondary ossification center (Figure 4A, and Supplemental Figure 1B). In support of this hypothesis, CD34, a marker of immature endothelial cells, was higher in the chondroosseous junctions of *Fgfr3*$^{Y367C/+}$ mice with the NVP-BGJ398 treatment in comparison with the control treatment (Supplemental Figure 1C). These data suggest that NVP-BGJ398 treatment increased formation of endothelial sprouts and initiation of angiogenesis in *Fgfr3*$^{Y367C/+}$ mice.

NVP-BGJ398 improves growth of the axial skeleton in Fgfr3$^{Y367C/+}$ *mice*. Most ACH patients exhibit kyphosis, lordosis, platyspondyly, spinal stenosis, and short pedicles, indicating that the axial skeleton is also affected (1). For this reason, we investigated the spine of *Fgfr3*$^{Y367C/+}$ mice. The rate of tail-length growth in *Fgfr3*$^{Y367C/+}$ mice was increased with NVP-BGJ398 treatment from day 9 until the end of the treatment in comparison with the control treatment (+14.9% at day 9, +26.5%, at day 16) (Figure 5A).

Coronal and sagittal x-ray analyses of the axial skeleton did not reveal obvious scoliosis and kyphosis in *Fgfr3*$^{Y367C/+}$ mice at 2 weeks of age. In order to assess differences in the size of the axial skeleton, we decided to study lumbar vertebral bodies, which are usually affected in ACH. On x-rays and μCT, we observed that lum-

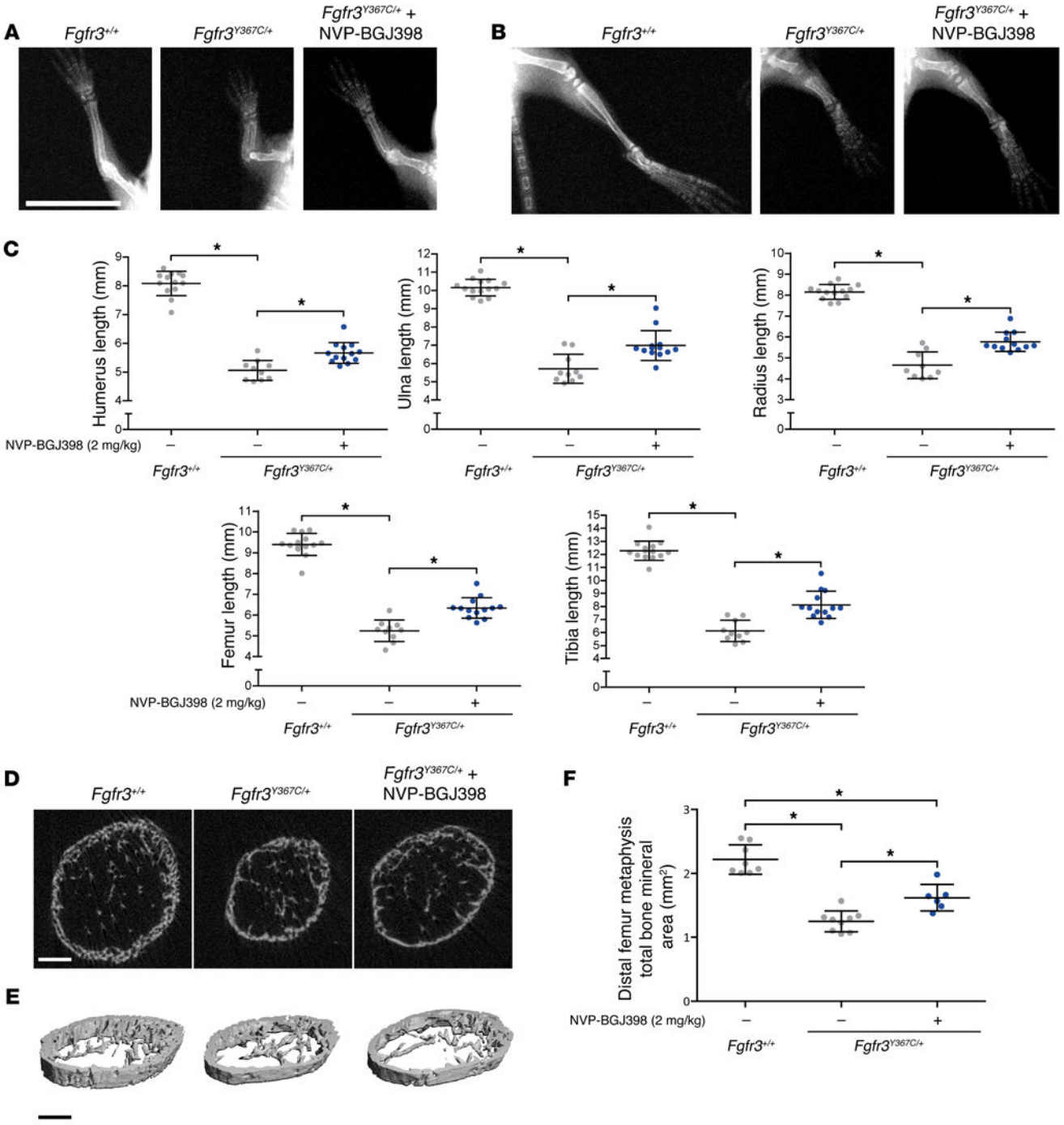

Figure 3. NVP-BGJ398 improves growth of the appendicular skeleton in *Fgfr3*$^{Y367C/+}$ mice. (**A**) Radiograph of *Fgfr3*$^{+/+}$ and treated and untreated *Fgfr3*$^{Y367C/+}$ forelimbs. Scale bar: 1 cm. (**B**) Radiograph of *Fgfr3*$^{+/+}$ and treated and untreated *Fgfr3*$^{Y367C/+}$ hind limbs. (**C**) Lengths of femur, tibia, humerus, ulna, and radius (*Fgfr3*$^{+/+}$, n = 13–14; untreated *Fgfr3*$^{Y367C/+}$, n = 9–10; treated *Fgfr3*$^{Y367C/+}$, n = 12–13). *P < 0.05, 1-way ANOVA. (**D**) 2D μCT of the distal femur metaphysis cross-sectional area. Scale bar: 400 μm. (**E**) 3D μCT of the distal femur metaphysis cross-sectional area. Scale bar: 400 μm. (**F**) Total bone mineral area in the distal femur metaphysis (*Fgfr3*$^{+/+}$, n = 8; untreated *Fgfr3*$^{Y367C/+}$, n = 8; treated *Fgfr3*$^{Y367C/+}$, n = 6). *P < 0.05, 1-way ANOVA. All data are from animals treated with protocol 1 (16 days old). Data are expressed as mean ± SD.

bar pedicles were shorter (–62.4%) in *Fgfr3*$^{Y367C/+}$ mice compared with *Fgfr3*$^{+/+}$ mice. After treatment with NVP-BGJ398 in *Fgfr3*$^{Y367C/+}$ mice, the lumbar pedicles were greater in size than with the control treatment (+21.8%) (Figure 5, B and C, and Supplemental Figure 2A). We noted a lower size of the L4–L6 segment in *Fgfr3*$^{Y367C/+}$ compared with *Fgfr3*$^{+/+}$ mice (–29%), and after 15 days of treatment with NVP-BGJ398, the size was greater than with the control treatment (+12.1%) (Figure 5D and Supplemental Figure 2A).

To complete these analyses, we focused on IVDs, where FGFR3 is expressed (Supplemental Figure 2B). The IVD contains the cartilage endplate (CEP) and fibrocartilaginous tissues, including the annulus fibrosus (AF) and the nucleus pulposus

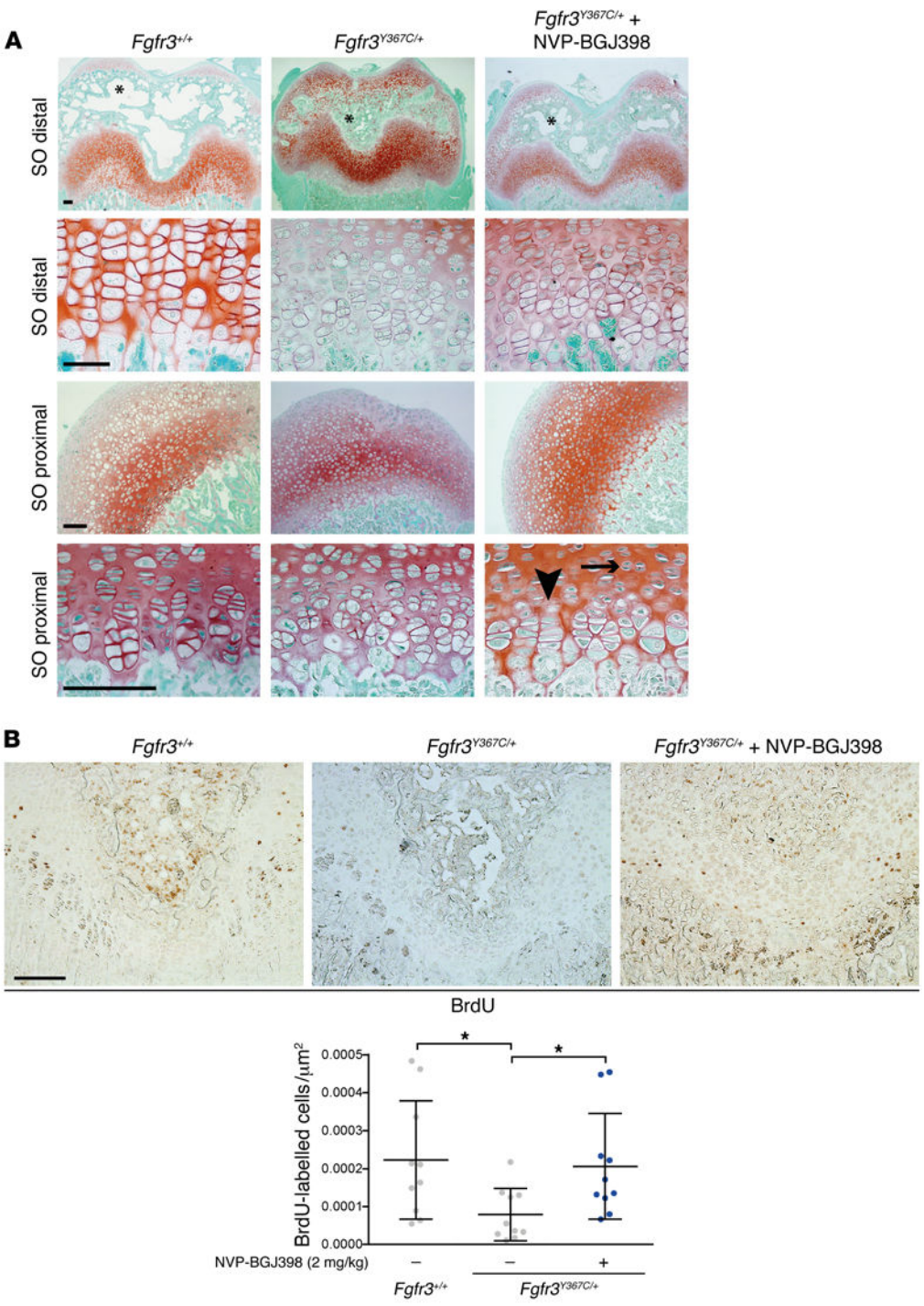

Figure 4. NVP-BGJ398 improves chondrocyte differentiation and proliferation in growth plate. (**A**) Safranin O (SO) staining on femur from *Fgfr3*$^{+/+}$ and untreated or treated *Fgfr3*$^{Y367C/+}$ mice. Scale bars: 100 μm. Asterisks show secondary ossification centers (*Fgfr3*$^{+/+}$ and treated *Fgfr3*$^{Y367C/+}$ have these centers more developed compared with *Fgfr3*$^{Y367C/+}$ vehicle). Arrowhead highlights appearance of columnar hypertrophic chondrocytes, while arrow indicates flattening of prehypertrophic cells in *Fgfr3*$^{Y367C/+}$ treated mice. (**B**) BrdU immunohistology on distal femur growth plates from *Fgfr3*$^{+/+}$ and untreated or treated *Fgfr3*$^{Y367C/+}$. Quantification of cell proliferation (BrdU-labeled cells/μm^2) (n = 10 per group). *$P < 0.05$, 1-way ANOVA. Scale bar: 100 μm. (**C**) Immunohistochemistry for Col X on femur from *Fgfr3*$^{+/+}$ and untreated or treated *Fgfr3*$^{Y367C/+}$. Scale bar: 100 μm. Images shown are representative of n = 6 animals per group. All data are from animals treated with protocol 1 (16 days old). Data are expressed as mean ± SD.

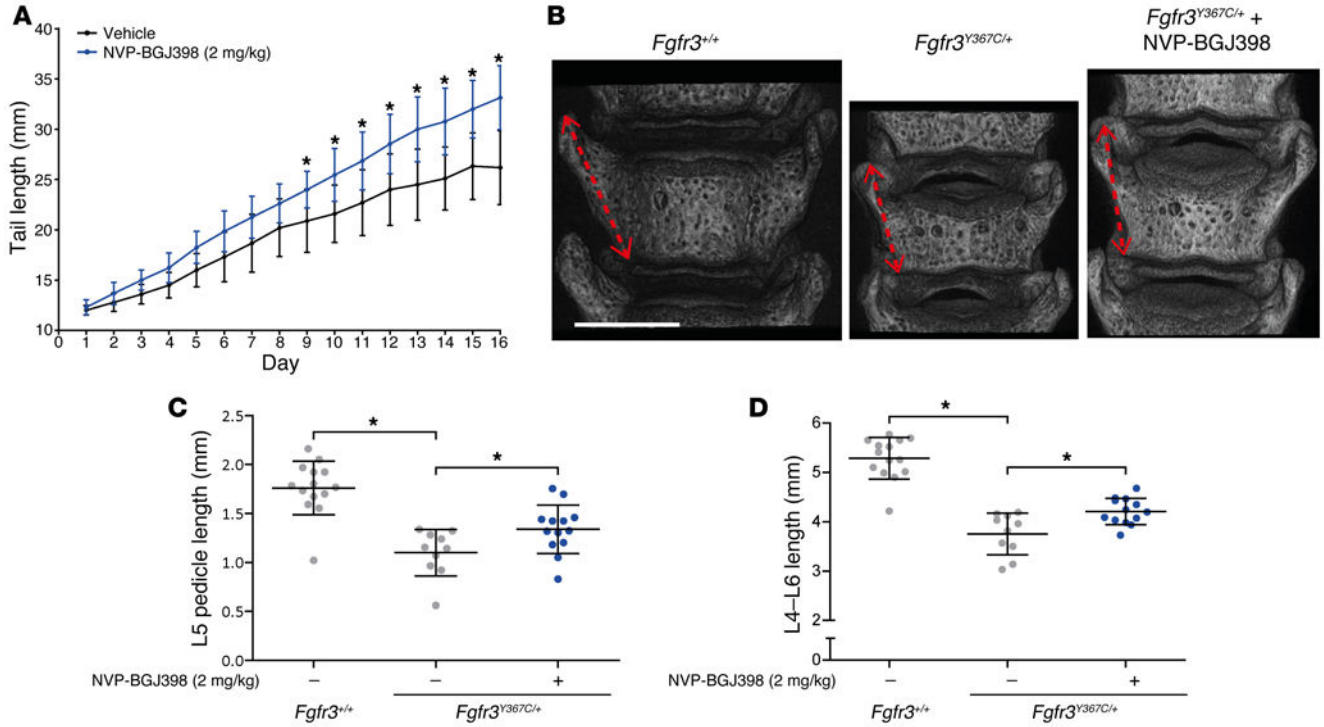

Figure 5. NVP-BGJ398 improves axial skeleton defect of *Fgfr3*$^{Y367C/+}$ mice. (**A**) Tail length from P1 to P16 of *Fgfr3*$^{Y367C/+}$ untreated or treated mice (untreated *Fgfr3*$^{Y367C/+}$, $n = 9$; treated *Fgfr3*$^{Y367C/+}$, $n = 12$). *$P < 0.05$, Mann-Whitney *U* test. (**B**) 3D μCT scan of *Fgfr3*$^{+/+}$ and treated and untreated *Fgfr3*$^{Y367C/+}$ mice. Red arrows show landmarks used to measure L5 pedicle lengths. Scale bar: 1 mm (frontal view). (**C**) L5 pedicle length of *Fgfr3*$^{+/+}$ and treated and untreated *Fgfr3*$^{Y367C/+}$ mice (*Fgfr3*$^{+/+}$, $n = 14$; untreated *Fgfr3*$^{Y367C/+}$, $n = 10$; treated *Fgfr3*$^{Y367C/+}$, $n = 13$). *$P < 0.05$, 1-way ANOVA. (**D**) Spine length L4 to L6. *Fgfr3*$^{+/+}$ and treated and untreated *Fgfr3*$^{Y367C/+}$ mice (*Fgfr3*$^{+/+}$, $n = 14$; untreated *Fgfr3*$^{Y367C/+}$, $n = 10$; treated *Fgfr3*$^{Y367C/+}$, $n = 13$). *$P < 0.05$, 1-way ANOVA. All data are from animals treated with protocol 1 (16 days old). Data are expressed as mean ± SD.

(NP) (31). The NP is a gelatinous tissue located in the center of the IVD surrounded by the lamellar structured AF. First of all, we observed a lower width (–52.6%) and a greater length (+54.2%) of the NP in *Fgfr3*$^{Y367C/+}$ mice compared with *Fgfr3*$^{+/+}$ mice at 16 days (Figure 6, A and B). These defects were significantly ameliorated by NVP-BGJ398 treatment compared with control treatment for both the width (+73.3%) and length (–17.1%) in *Fgfr3*$^{Y367C/+}$ mice. In order to analyze the AF extracellular matrix (ECM), we studied Col I and II expression. The cartilaginous area (Col II) corresponds to the inner AF (IAF), and the fibrous area (Col I) forms the outer AF (OAF) (31). Interestingly, we observed for what we believe is the first time that the length of the IAF was higher in *Fgfr3*$^{Y367C/+}$ mice (+72.4%) than in *Fgfr3*$^{+/+}$ mice (Figure 6C and Supplemental Figure 2B). This IAF phenotype was significantly ameliorated by NVP-BGJ398 treatment compared with control treatment (–60%). As a consequence, the IAF/OAF ratio was also modified with the treatment.

In addition, we observed that the size of the CEP was lower in *Fgfr3*$^{Y367C/+}$ mice (–18%) compared with *Fgfr3*$^{+/+}$ mice, probably due to defective hypertrophic-chondrocyte differentiation (Supplemental Figure 3, A and B). This CEP phenotype was significantly ameliorated by NVP-BGJ398 treatment compared with control treatment (+29.3%) (Supplemental Figure 3, A and B).

Taking these data together, we demonstrate here that 15 days of NVP-BGJ398 treatment corrected the size of L4–L6 and pedicles and modified collagen expression in the IVD. These data suggest a possible improvement of the ACH spinal stenosis phenotype with treatment.

NVP-BGJ398 improves the growth of the craniofacial skeleton in Fgfr3$^{Y367C/+}$ *mice*. The cranial base is severely affected in humans with ACH and in *Fgfr3*$^{Y367C/+}$ mice and hence contributes greatly to the craniofacial phenotype (28).

Therefore, we assessed whether early treatment with NVP-BGJ398 could correct the cartilage defects of the skull base and thus prevent the premature loss of synchondroses. Imaging of the skull using μCT revealed that after 2 weeks of NVP-BGJ398 treatment compared with control treatment, the brachycephalic appearance of *Fgfr3*$^{Y367C/+}$ mice was less obvious because the anterior-posterior length of the skull was greater (+5.9%) (Figure 7A). In addition, we observed that the size of nasal-bone length was lower in *Fgfr3*$^{Y367C/+}$ mice (–33.8%) than in *Fgfr3*$^{+/+}$ mice. This nasal-bone phenotype was significantly ameliorated by NVP-BGJ398 treatment compared with control treatment (+20.45%) (Figure 7A). NVP-BGJ398 treatment partially prevented the loss of 4 synchondroses: the sphenoccipital synchondrosis (SOS), the intersphenoidal synchondrosis (ISS), and the 2 interoccipital synchondroses (IOSs) in *Fgfr3*$^{Y367C/+}$ mice (Figure 7, A and B). The efficacy of the NVP-BGJ398 treatment was more prominent on the IOSs (all treated mice had at least one IOS active) than on the SOS and ISS (Table 2).

The size of the FM is much smaller in ACH patients and *Fgfr3*$^{Y367C/+}$ mice, causing cervicomedullary compression (28). In *Fgfr3*$^{Y367C/+}$ mice, the size of the FM was significantly higher after

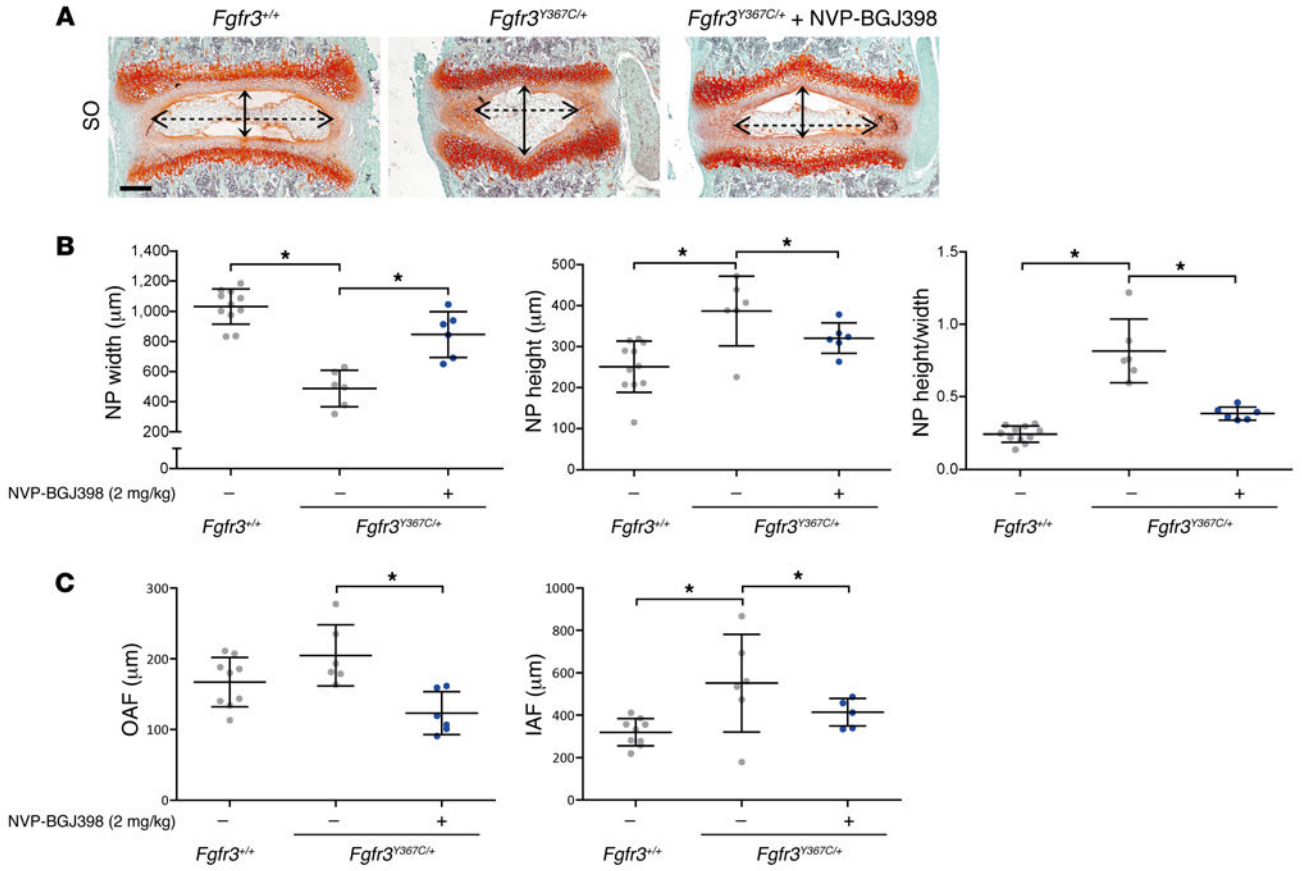

Figure 6. NVP-BGJ398 reduces IVD defects of *Fgfr3*$^{Y367C/+}$ mice. (**A**) Safranin O staining on lumbar IVD. Dashed arrow shows NP width; arrow indicates NP height. Scale bar: 200 μm. (**B**) NP width (*Fgfr3*$^{+/+}$, *n* = 11; untreated *Fgfr3*$^{Y367C/+}$, *n* = 6; treated *Fgfr3*$^{Y367C/+}$, *n* = 6). Height and ratio between height and width (*Fgfr3*$^{+/+}$, *n* = 11; untreated *Fgfr3*$^{Y367C/+}$, *n* = 6; treated *Fgfr3*$^{Y367C/+}$, *n* = 6). **P* < 0.05, 1-way ANOVA test. (**C**) IAF and OAF lengths (*Fgfr3*$^{+/+}$, *n* = 9; untreated *Fgfr3*$^{Y367C/+}$, *n* = 6; treated *Fgfr3*$^{Y367C/+}$, *n* = 6). **P* < 0.05, 1-way ANOVA. All data are from animals treated with protocol 1 (16 days old). Data are expressed as mean ± SD.

NVP-BGJ398 treatment (area, +16.8%; transversal length, +15.8%; and sagittal length, +7.6% as assessed by μCT) (Figure 8, A and B). The rescue of the synchondroses phenotype presumably played a role in the amelioration of the FM phenotype.

These data indicate an impact of FGFR3 on both mesenchymal (synchondroses) and neural crest–derived osteoblasts (nasal bone) and suggest an important role of FGFR3 on both intramembranous and endochondral ossification processes.

NVP-BGJ398 rescues defective FGFR3 signaling. FGFR3 is expressed in proliferative and prehypertrophic zones of the growth plate and modulates both proliferation and differentiation of the chondrocytes (32). The activating mutation stabilizes the receptor in cells, as demonstrated by the high expression of the receptor in the growth plate. The treatment of NVP-BGJ398 had a beneficial effect on the turnover of the receptor and lowered its expression in chondrocytes (Supplemental Figure 4A). In our *Fgfr3*$^{Y367C/+}$ mice, as expected, another tyrosine kinase, FGFR1, was expressed in the hypertrophic zone of the growth plate, and its expression was not modified with NVP-BGJ398 treatment (Supplemental Figure 4B).

FGFR3 negatively regulates chondrocyte proliferation and differentiation via several signaling pathways. The 2 principal signaling pathways are the MAPK pathway, which regulates matrix production and chondrocyte differentiation, and the STAT1 pathway, which controls proliferation (32). The FGFR3 canonical downstream MAPK signaling pathway is more active in FGFR3-related disorders (33, 34). Consistent with decreased FGFR3 phosphorylation, the activation of MAPK and PLCγ pathways was reduced with NVP-BGJ398 dosing in HEK293-Vnr cells and human chondrocytes transiently transfected with constructs encoding activation mutants of FGFR3 (Supplemental Figure 5, A and B). These results were confirmed using human immortalized ACH (p.Gly380Arg/+) and TD (p.Ser249Cys/+) chondrocytes (ref. 25 and Supplemental Figure 5C) and using human (ACH, control) and mouse primary chondrocytes (Figure 9, A and B). With these cell cultures, we also observed a NVP-BGJ398 dose-dependent decrease in the level of phosphorylated ERK1/2 (Supplemental Figure 5C).

High levels of phosphorylated ERK1/2 were observed in *Fgfr3*$^{Y367C/+}$ chondrocyte cultures and in the growth plate of *Fgfr3*$^{Y367C/+}$ mice in vivo, thus confirming the constitutive activation of the MAPK pathway in those mice (Figure 9C). Interestingly, ERK1/2 phosphorylation was undetectable in NVP-BGJ398–treated chondrocyte cultures, and ERK1/2 phosphorylation was lower in growth-plate cartilage after NVP-BGJ398 treatment compared with control treatment in *Fgfr3*$^{Y367C/+}$ mice (Figure 9, A–C, and Supplemental Figure 5, A–C). These data show that NVP-BGJ398 inhibited FGFR3 activity in a RAS-ERK–dependent fashion.

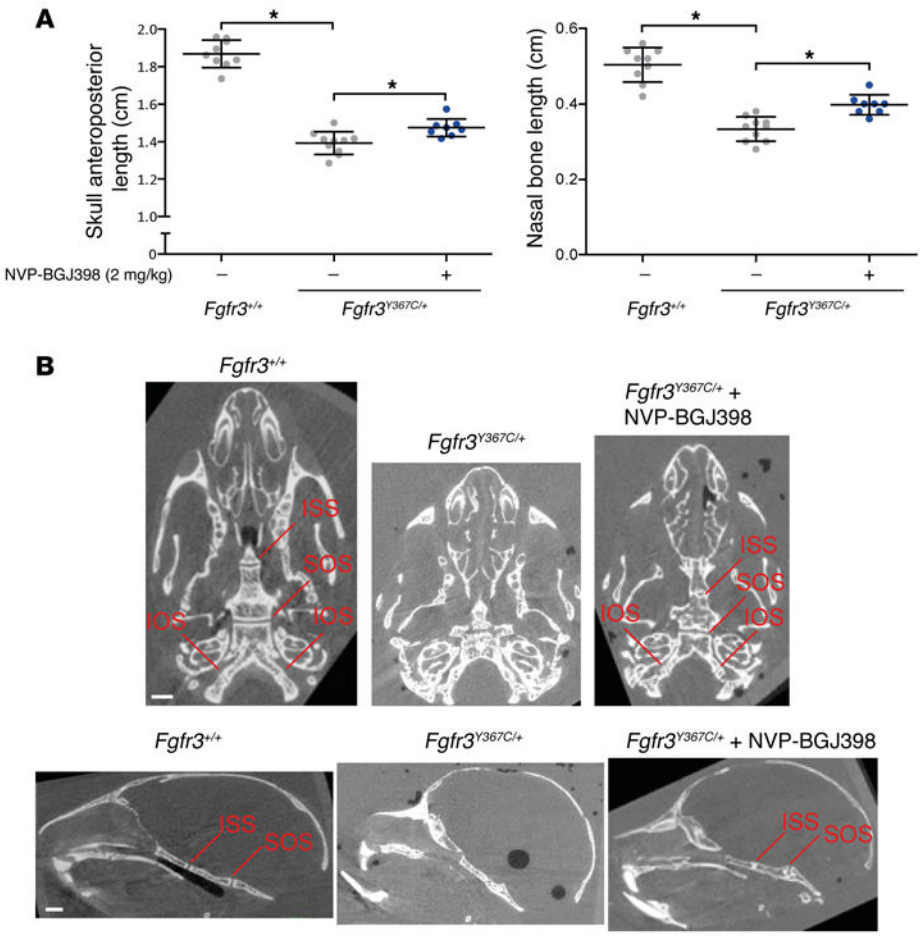

Figure 7. NVP-BGJ398 improves growth of the craniofacial skeleton in *Fgfr3*$^{Y367C/+}$ mice. (**A**) Skull anteroposterior length and nasal bone length (*Fgfr3*$^{+/+}$, $n = 9$; untreated *Fgfr3*$^{Y367C/+}$, $n = 8$; treated *Fgfr3*$^{Y367C/+}$, $n = 10$). $^*P < 0.05$, 1-way ANOVA. Data are expressed as mean ± SD. (**B**) 2D μCT scan of *Fgfr3*$^{+/+}$ and treated and untreated *Fgfr3*$^{Y367C/+}$ mouse skulls shows the presence and loss of synchondroses. Scale bar: 1 mm. All data are from animals treated with protocol 1 (16 days old).

The role of the transcription factor SOX9 in chondrogenic differentiation is well recognized (35, 36). Previously, it was reported that activated FGFR3 prevents the downregulation of transcription factor SOX9 in differentiated chondrocytes (11). This mechanism was also observed in *Fgfr3*$^{Y367C/+}$ mice where the high expression of SOX9 in the prehypertrophic chondrocytes was lowered with NVP-BGJ398 treatment (Figure 9D). Also, the downregulation of SOX9 correlated with the modification of the size and the shape of hypertrophic chondrocytes (Figure 4, A and C).

In FGFR3-related disorders, it has been demonstrated that the STAT1 pathway regulates chondrocyte proliferation (37, 38). In the *Fgfr3*$^{Y367C/+}$ growth plate, the level of phosphorylated STAT1 is higher than in *Fgfr3*$^{+/+}$ mice, and the level of phosphorylated STAT1 is lowered by NVP-BGJ398 treatment (Supplemental Figure 5D). Hence, these data provide an underlying molecular explanation for the higher rate of chondrocyte proliferation with NVP-BGJ398 treatment in *Fgfr3*$^{Y367C/+}$ mice, as shown with BrdU data (Figure 4B).

Overall, the data suggest that NVP-BGJ398 treatment in *Fgfr3*$^{Y367C/+}$ mice restores the activity of FGFR3 downstream-signaling pathways to that of levels observed in *Fgfr3*$^{+/+}$ mice.

Effect of timing and type of treatment on the improvement of bone growth. Bone elongation relies on an active process controlled by proliferation and differentiation of chondrocytes within the growth plate. In humans, this process comes to a halt at puberty and corresponds to the disappearance of the growth plate. Therefore, in ACH patients, treatment effectiveness may be better if the treatment commences before puberty. For this reason, we chose to treat *Fgfr3*$^{Y367C/+}$ mice from day 1 for 15 days (protocol 1). However, in order to compare the efficacy of NVP-BGJ398 with that shown in previously published data, we also tested a second protocol (protocol 2), similar to the one used for BMN111 (start at day 7 for 10 days) (15). The gain of growth of femurs and tibias was 50% higher in animals treated earlier and longer with NVP-BGJ398 (from day 1) than those treated from day 7 (Supplemental Figure 6 and Table 3). When NVP-BGJ398 treatment was compared with BMN111 treatment in *Fgfr3*$^{Y367C/+}$ mice using protocol 2, we observed a greater amelioration of several aspects of the dwarfism pheno-

Table 2. Active synchondroses

	Fgfr3$^{+/+}$	*Fgfr3*$^{Y367C/+}$	*Fgfr3*$^{Y367C/+}$ + NVP-BGJ398
ISS	100% (9/9)	0% (0/10)	37.5 % (3/8)
SOS	100% (9/9)	0% (0/10)	25% (2/8)
Both IOSs	100% (9/9)	0% (0/10)	75% (6/8)
1 IOS only	–	0% (0/10)	25% (2/8)

Percentage of active synchondroses. All data are from animals treated with protocol 1 (16 days old).

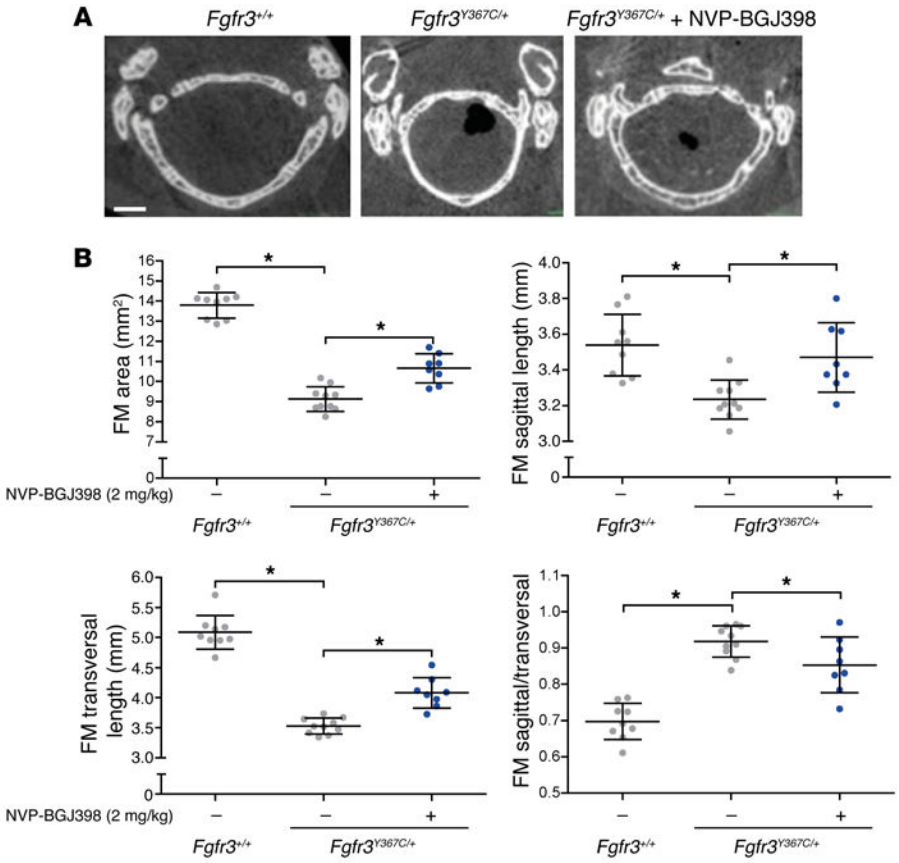

Figure 8. NVP-BGJ398 reduces FM defects in *Fgfr3*$^{Y367C/+}$ mice. (**A**) FM μCT images. Scale bar: 1 mm. (**B**) FM area, transversal and sagittal length, ratio between FM sagittal and transversal length (*Fgfr3*$^{+/+}$, $n = 9$; untreated *Fgfr3*$^{Y367C/+}$, $n = 8$; treated *Fgfr3*$^{Y367C/+}$, $n = 10$). $^*P < 0.05$, 1-way ANOVA test. All data are from animals treated with protocol 1 (16 days old). Data are expressed as mean ± SD.

type with NVP-BGJ398 than with BMN111 (femur, tibia, tail, L4–L6) (Supplemental Figure 6, Table 3, and ref. 15). In conclusion, NVP-BGJ398 treatment of *Fgfr3*$^{Y367C/+}$ mice appeared more effective when administered earlier postnatally and for a longer period. NVP-BGJ398 treatment also appeared more effective than BMN111 treatment, suggesting that directly targeting FGFR3 with a TKI represents a better approach than targeting FGFR3 downstream-signaling pathways.

Discussion

Elevated kinase activity of the FGFR3 receptor due to germinal or somatic mutations disrupts several biological functions, as demonstrated in FGFR3-related disorders (ACH, TD, hypochondroplasia, Muenke syndrome) (1, 2, 39) and numerous cancers (bladder cancers and multiple myeloma) (40–42). Hyperactive FGFR3 signaling causes dwarfism, including ACH, which is characterized by anomalies in bone development, and the gain-of-function *Fgfr3*$^{Y367C/+}$ mutation can be used to model ACH in mice (6, 28, 29, 43). Conversely, a total impairment of the FGFR3 signaling pathway can cause bone overgrowth, confirming that FGFR3 is a negative regulator of bone growth (5). On a functional level, FGFR activation affects various cell behaviors via the downstream activation of the MAPK intracellular signaling cascade. The MAPK pathway plays an important role in bone development, as demonstrated in MEK1 gain-of-function mice (12) and ERK1 and ERK2 null mice (44), leading to a dwarf or skeletal overgrowth phenotype, respectively. The underlying mechanisms in FGFR3-related disorders suggest that chondrocyte differentiation is regulated by MAPK signaling through the control of SOX9 (32) and chondrocyte proliferation is suppressed by STAT1 activation (12).

One therapeutic strategy to rescue the defective skeletal development caused by *FGFR3* gain-of-function mutations is to reduce or counteract the hyperactivity of FGFR3. Among the putative therapeutic approaches for ACH, the use of TKIs seems the most suitable. Although TKIs have been successfully used in cancer (45–47), TKIs have so far not been applied in skeletal disorders. Here, we demonstrate that NVP-BGJ398, a pan-FGFR inhibitor (20), was able to reduce the increased phosphorylation of FGFR3 and the activation of its downstream signaling pathways in vitro, in human and mouse (*Fgfr3*$^{Y367C/+}$) chondrocyte models of ACH, and to rescue the growth-plate phenotype in vivo in *Fgfr3*$^{Y367C/+}$ mice. We believe the result obtained with NVP-BGJ398 is novel, as previous in vivo experiments using TKIs failed to demonstrate any rescue of the dwarf phenotype (48). Previously, NVP-BGJ398 was tested in animal models for cancers, including hepatocellular carcinoma (24) and malignant rhabdoid tumors (23) as well as FGF23-dependent hypophosphatemic rickets (22). The effective doses administrated in these preclinical studies for cancer were 10 to 100 times higher than the doses used in this present study to correct the dwarfism phenotype. Other therapeutic strategies were explored for ACH, with protocols using soluble FGFR3 (17), statin (18), or meclozine (19) in another mouse model of ACH (*Fgfr3*^{Ach}) in which the *Fgfr3* transgene with the ACH mutation is expressed under the control of *Col2a1* (7). The comparison of those results with the results from our study is made complicated by the differences among the mouse models (genotypes, skeletal

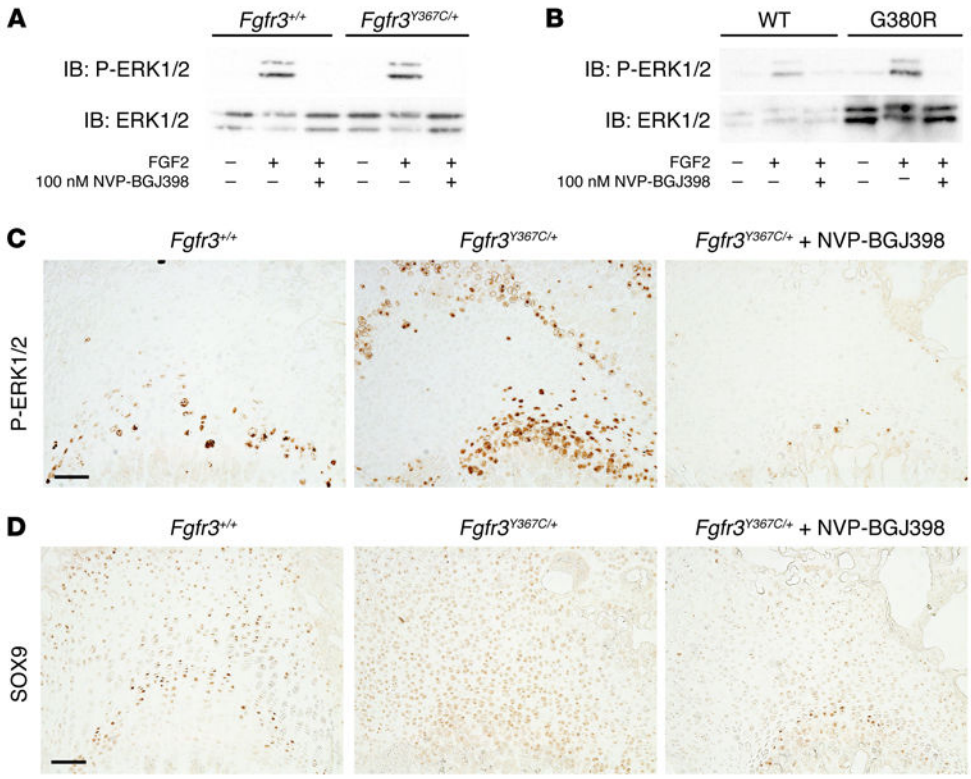

Figure 9. NVP-BGJ398 rescues defective FGFR3 signaling. (**A**) Phosphorylated ERK1/2 expression in mouse primary chondrocytes (*Fgfr3*$^{+/+}$ and *Fgfr3*$^{Y367C/+}$). (**B**) Phosphorylated ERK1/2 expression in human primary chondrocytes expressing FGFR3^{WT} or the heterozygous mutation G380R (ACH). (**C**) Immunohistology for phosphorylated ERK1/2 in femur distal growth plate of protocol 1 mice. Scale bar: 100 μm. Images shown are representative of n = 9 animals per group. (**D**) Immunohistology for SOX9 in femur distal growth plate of protocol 1 mice. Scale bar: 100 μm. Images shown are representative of n = 6 animals per group. All immunohistological data are from animals treated with protocol 1 (16 days old). Western blots are representative of 3 independent experiments.

phenotypes, and FGFR3 expression pattern) (17–19). Interestingly, NVP-BGJ398 treatment for 10 days improved the bone growth 2 to 3 times more than what had been reported for BMN111 (15). NVP-BGJ398 (2 mg/kg) treatment of WT mice did not affect skeletal growth (data not shown), and treatment of *Fgfr3*$^{Y367C/+}$ mice did not modify the expression of FGFR1 in the hypertrophic zone of the growth plate. Thus, in this preclinical study, NVP-BGJ398–mediated effects were mainly due to FGFR3 inhibition, with no other gross side effects being observed.

The rescue of the growth-plate disorganization, the defective chondrocyte proliferation, and the delay of differentiation and secondary ossification were remarkable. The disrupted downstream FGFR3 signaling pathways were corrected with the NVP-BGJ398 treatment, confirming the key role of ERK1/2, SOX9, and STAT1 signaling during skeletal development (32).

Of major importance, NVP-BGJ398, when applied from birth onwards, increased the size of the reduced FM and inhibited the premature fusion of synchondroses. In addition, the size of the neural crest–derived nasal bone was increased, reflecting that intramembranous ossification is also affected in ACH (28). These treatment-related effects on the skull suggested the potential of correcting facial appearance in ACH patients and, most importantly, the potential of reducing the risks related to the cervicomedullary compression and early death that can occur in ACH children (1, 49, 50).

The spine anomalies of children and adults with ACH are kyphosis at the thoracolumbar junction (51) and spinal stenosis (52), eventually leading to leg paralysis and neurogenic claudication (2). Here, we demonstrate that the axial skeleton was affected in *Fgfr3*$^{Y367C/+}$ mice and the size of the lumbar vertebral bodies and pedicles was reduced. In addition, we showed that the 3 components (NF, AF, CEP) of the IVD were affected. One of the findings of this study is that NVP-BGJ398 treatment remarkably corrected the lumbar vertebral body and pedicle size defects and modified the components of the ECM of the IVD. These data demonstrate that overactivation of FGFR3 disturbs cartilage, IVDs, and bone-forming lumbar rachis, thus explaining the spinal stenosis, herniated disc, and kyphoscoliosis phenotypes of ACH patients. The positive impact of NVP-BGJ398 treatment is particularly noteworthy in this context: an improvement of axial skeletal development in ACH could reduce the need for decompressive laminectomy surgery, a procedure required for treating severe spinal stenosis (52).

The duration of the NVP-BGJ398 treatments were probably too short for the amelioration of the defective bone structure of the long bones in *Fgfr3*$^{Y367C/+}$ mice (43). Longer treatments might be necessary to improve the bone architecture, as demonstrated previously with 2 months of PTH injection in an *Fgfr3*-related

Table 3. Effect of timing and type of treatment

Treatment	Tail	Femur	Tibia	L4–L6
NVP-BGJ398 2 mg/kg (protocol 1)	26.5%^{A}	20.9%^{A}	32.6%^{A}	12.1%^{A}
NVP-BGJ398 2 mg/kg (protocol 2)	25.8%^{A}	12.1%^{A}	25.5%^{A}	11.6%^{A}

Gain in length (percentage) for tail, femur, tibia, and L4–L6 of NVP-BGJ398–treated mice compared with vehicle 1. A best improvement is observed with animals treated at day 1 (protocol 1). The dwarfism improvement is more important with NVP-BGJ398 than with BMN111 (protocol 2 compared with data from ref. 15). $^{A}P < 0.05$ by 1-way ANOVA test.

dwarf mouse model (16). Because short-term NVP-BGJ398 treatment improved the chondroosseous junction in the long bones of the growing *Fgfr3*$^{Y367C/+}$ mice, there is potential that longer NVP-BGJ398 treatments could lead to a secondary positive effect on the resulting bone structure.

The different skeletal phenotypes and molecular pathways evaluated in our study provide a wide range of markers that can be monitored for further optimization of dosing schedules of TKI in addition to prolongation, such as reductions in dose quantity or frequency (e.g., intermittent injections every 2 or 3 days).

In summary, we have shown that NVP-BGJ398 inhibits FGFR3 and its downstream signaling pathways, which are overactive in cartilage in ACH. As a consequence, NVP-BGJ398 rescues the endochondral and membranous ossification processes in a mouse model of ACH. Our results provide a rationale for targeting FGFR3 with a specific TKI for the treatment of children with ACH.

Methods

Transient transfections of cDNA FGFR3 constructs. Human control chondrocyte lines (25) and human embryonic kidney (HEK) cells (26) at 80%–90% confluence were transiently transfected with FGFR3 human constructs (FGFR3^{WT,} FGFR3^{G380R}, FGFR3^{Y373C}, FGFR3^{K650E}, FGFR3^{K650M}) obtained as previously reported (26) using JetPrime (Polyplus-transfection) following the manufacturer's instructions. Transfected cells were incubated with NVP-BGJ398 (Novartis Basel, ref. 20) at concentrations of 100 nM, 1 nM, or 10 μM overnight. Transfected cells were lysed in RIPA buffer (50 mM Tris-HCl pH 7.6, 150 mM NaCl, 0.5% NP40, and 0.25% sodium deoxycholate, supplemented with protease and phosphatase inhibitors; Roche). Immunoprecipitations were performed by incubating 3 μl rabbit anti-FGFR3 (Sigma-Aldrich F0425)/500 μg protein with protein A–agarose (Roche).

Primary and immortalized human chondrocytes and mouse chondrocytes cultures. Primary and immortalized mutant cells were obtained as previously described (25). The protocol used for mouse chondrocytes was previously reported (24). Human and mouse cells were incubated with NVP-BGJ398 (1, 10, 50, 100, 250, and 500 nM) overnight.

Immunoblotting. Whole-cell lysates and immunoprecipitated proteins were subjected to NuPAGE 4%–12% bis-tris acrylamide gels (Life Technologies). Blots were probed with antibodies using standard protocols: anti-FGFR3 polyclonal antibody (Sigma-Aldrich F0425; 1:1,000 dilution), anti–phospho-tyrosine P-Tyr-100 monoclonal antibody (Cell Signaling catalog 9411; 1:1,000 dilution), anti–phospho-ERK1/2 monoclonal antibody (Cell Signaling catalog 4370; 1:1,000 dilution), anti-ERK1/2 polyclonal antibody (Sigma-Aldrich M5670; 1:1000 dilution), anti–phospho-PLCγ polyclonal antibody (Cell Signaling catalog 2821; 1:1,000 dilution), and anti-PLCγ polyclonal antibody (Cell Signaling catalog 2822; 1:1,000 dilution).

Mouse model and drug treatment. *Fgfr3*$^{Y367C/+}$ mice were described previously (29). All mice were on a C57BL/6 background. Cartilage and bone analyses were performed in 16-day-old mice. Protocol 1 was as follows: *Fgfr3*$^{Y367C/+}$ mice were 1 day old at treatment initiation and received daily subcutaneous administrations of NVP-BGJ398 for 15 days (2 mg/kg body weight) or vehicle (HCl 3.5 mM, DMSO 5%). Treated and control mice received an intraperitoneal BrdU (Invitrogen) injection (1 ml per 100 g body) 2 hours before sacrifice. Long bones were measured by caliper (VWRi819-0013, VWR International), while vertebrae measures were determined from radiograph with ImageJ (https://imagej.nih.gov/ij/). Protocol 2 was as follows: *Fgfr3*$^{Y367C/+}$ mice were 7 days old at treatment initiation and received daily subcutaneous administrations of NVP-BGJ398 (2 mg/kg body weight) or vehicle (HCl 3.5 mM, DMSO 5%) for 10 days; this protocol is similar to the BMN111 protocol previously described (15).

Genotyping. Genomic DNA was isolated from tail tips by proteinase K digestion and extracted with NucleoSpin Tissue (Macherey-Nagel) according to the manufacturer's instructions. PCR was performed using primers as previously described (29).

Femoral culture system. Ex vivo femur cultures were conducted as described previously (30). Right femur was cultured with NVP-BGJ398 at a concentration of 10–100 nM to 1 μM and compared with the untreated left femur. The bone length was measured at the beginning (before treatment) and at the end of time course. Each experiment was repeated at least 5 times. Images were captured with an Olympus SZX12 stereo microscope. The size of the femur was measured using cellSens software (Olympus).

Calvarial culture system. Ex vivo calvarial cultures were conducted as described previously (28). Calvaria (E18.5) were placed in 24-well plates on top of 250 μl of Matrigel (BD Biosciences) previously placed at the bottom of the well. Calvaria were cultured in α-MEM (Gibco, Life Technologies) supplemented with 10% FBS (Gibco, Life Technologies), 100 μg/ml ascorbic acid (Sigma-Aldrich), and 1% penicillin/streptomycin (Gibco, Life Technologies) and NVP-BGJ398 at 100 nM over 14 days. Images were captured with an Olympus SZX12 stereo microscope. The size of the calvaria defect was measured using ImageJ software.

Histological and immunohistochemical analyses. Fetal femur explants, long bones (femurs, tibias), and L4–L6 vertebrae were fixed in 4% paraformaldehyde, decalcified with EDTA 0.4 M, and embedded in paraffin. Serial sections of 5 μm were stained with H&E and safranin O. For immunohistochemistry, sections were labeled with antibodies against Ki67 (monoclonal antibody, Abcam ab92353; 1:3,000 dilution), Col X (BIOCYC, N.2031501005; 1:50 dilution), CD34 (monoclonal antibody, Abcam ab8158; 1:100 dilution) Col I (polyclonal antibody, Novotec, catalog 20151; 1:1,000 dilution), Col II (polyclonal antibody, Novotec, catalog 20251; 1:1,000 dilution), SOX9 (polyclonal antibody, Santa Cruz Biotechnology Inc., catalog D0609; dilution 1:75), phospho-ERK1/2 (monoclonal antibody, Cell Signaling, catalog 4370; 1:100 dilution), phospho–Stat 1 (polyclonal antibody, Abcam, catalog ab119331; 1:200 dilution), FGFR1 (polyclonal antibody, Abcam, catalog ab63601; 1:75 dilution), and FGFR3 (polyclonal antibody, Sigma-Aldrich, catalog F0425; 1:250 dilution) using the Dako Envision Kit. Proliferation was analyzed with the BrdU Staining Kit (Life Technologies). Images were captured with an Olympus PD70-IX2-UCB microscope and cellSens software. Labeled cells were counted using ImageJ software.

X-rays and CT scanner. The whole skeletons of the mice were radiographed using Faxitron (MX-20). μCT analyses were performed using a μCT40 Scanco vivaCT42 (Scanco Medical) instrument and the following settings: integration time, 300 ms (skull) or 175 ms (femur); 45 E(kVp); 177 μA. For determination of femoral structural parameters, a segmentation threshold of 270 was applied and a Gaussian filter (σ = 0.7, support of 1 voxel) was used to suppress the noise. The evaluated volume was proportional to the femoral length, as measured on plain radiographs using a specimen radiography system (Faxitron LX-60), and corresponded to an average of 142 μm (metaphysis) or

120 μm (diaphysis) for vehicle-treated and 169 μm (metaphysis) or 143 μm (diaphysis) for compound-treated *Fgfr3*$^{Y367C/+}$ mice.

Statistics. Differences between experimental groups were assessed using ANOVA with Tukey's post hoc test or Mann-Whitney *U* test. The significance threshold was set at $P \leq 0.05$. Statistical analyses were performed using GraphPad PRISM (v5.03). All values are shown as mean ± SD.

Study approval. Experimental animal procedures and protocols were approved by the French Animal Care and Use Committee.

Author contributions

DKE, ED, IK, AM, and LLM designed the research. DKE, ED, CBL, NK, CLG, LM, and MBD performed the experiments. DKE, IK, FDR, and MBD analyzed the scanners. PB, FB, and DGP analyzed NVP-BGJ398 activity. DKE prepared the figures. DKE, IK, MK, MBD, and LLM wrote the manuscript.

Acknowledgments

This program received a state subsidy managed by the National Research Agency under the Investments for the Future program bearing the reference ANR-10-IHU-01 and the ANR-ATAK 2013 program. Some of the work presented here was funded by the European Community's Seventh Framework Programme under grant agreement no. 602300 (Sybil). We are grateful to the Association des Personnes de Petites Tailles, the Fondation des Gueules Cassées, the Fondation pour la Recherche Médicale (FDT20150532684), and the Société Française de Biologie des Tissus Minéralisés.

Address correspondence to: Laurence Legeai-Mallet, INSERM U1163, Université Paris Descartes, Sorbonne Paris Cité, Institut Imagine, Paris, France. Phone: 00.33.1.42.75.43.02; E-mail: laurence.legeai-mallet@inserm.fr.

1. Baujat G, Legeai-Mallet L, Finidori G, Cormier-Daire V, Le Merrer M. Achondroplasia. *Best Pract Res Clin Rheumatol*. 2008;22(1):3–18.
2. Horton WA, Hall JG, Hecht JT. Achondroplasia. *Lancet*. 2007;370(9582):162–172.
3. Rousseau F, et al. Mutations in the gene encoding fibroblast growth factor receptor-3 in achondroplasia. *Nature*. 1994;371(6494):252–254.
4. Shiang R, et al. Mutations in the transmembrane domain of FGFR3 cause the most common genetic form of dwarfism, achondroplasia. *Cell*. 1994;78(2):335–342.
5. Colvin JS, Bohne BA, Harding GW, McEwen DG, Ornitz DM. Skeletal overgrowth and deafness in mice lacking fibroblast growth factor receptor 3. *Nat Genet*. 1996;12(4):390–397.
6. Pannier S, et al. Delayed bone age due to a dual effect of FGFR3 mutation in Achondroplasia. *Bone*. 2010;47(5):905–915.
7. Naski MC, Colvin JS, Coffin JD, Ornitz DM. Repression of hedgehog signaling and BMP4 expression in growth plate cartilage by fibroblast growth factor receptor 3. *Development*. 1998;125(24):4977–4988.
8. Iwata T, et al. A neonatal lethal mutation in FGFR3 uncouples proliferation and differentiation of growth plate chondrocytes in embryos. *Hum Mol Genet*. 2000;9(11):1603–1613.
9. Legeai-Mallet L, Benoist-Lasselin C, Munnich A, Bonaventure J. Overexpression of FGFR3, Stat1, Stat5 and p21Cip1 correlates with phenotypic severity and defective chondrocyte differentiation in FGFR3-related chondrodysplasias. *Bone*. 2004;34(1):26–36.
10. Minina E, Kreschel C, Naski MC, Ornitz DM, Vortkamp A. Interaction of FGF, Ihh/Pthlh, and BMP signaling integrates chondrocyte proliferation and hypertrophic differentiation. *Dev Cell*. 2002;3(3):439–449.
11. Zhou ZQ, Ota S, Deng C, Akiyama H, Hurlin PJ. Mutant activated FGFR3 impairs endochondral bone growth by preventing SOX9 downregulation in differentiating chondrocytes. *Hum Mol Genet*. 2015;24(6):1764–1773.
12. Murakami S, et al. Constitutive activation of MEK1 in chondrocytes causes Stat1-independent achondroplasia-like dwarfism and rescues the Fgfr3-deficient mouse phenotype. *Genes Dev*. 2004;18(3):290–305.
13. Nowroozi N, et al. Sustained ERK1/2 but not STAT1 or 3 activation is required for thanatophoric dysplasia phenotypes in PC12 cells. *Hum Mol Genet*. 2005;14(11):1529–1538.
14. Wendt DJ, et al. Neutral endopeptidase-resistant C-type natriuretic peptide variant represents a new therapeutic approach for treatment of fibroblast growth factor receptor 3-related dwarfism. *J Pharmacol Exp Ther*. 2015;353(1):132–149.
15. Lorget F, et al. Evaluation of the therapeutic potential of a CNP analog in a Fgfr3 mouse model recapitulating achondroplasia. *Am J Hum Genet*. 2012;91(6):1108–1114.
16. Xie Y, et al. Intermittent PTH (1-34) injection rescues the retarded skeletal development and postnatal lethality of mice mimicking human achondroplasia and thanatophoric dysplasia. *Hum Mol Genet*. 2012;21(18):3941–3955.
17. Garcia S, et al. Postnatal soluble FGFR3 therapy rescues achondroplasia symptoms and restores bone growth in mice. *Sci Transl Med*. 2013;5(203):203ra124.
18. Yamashita A, et al. Statin treatment rescues FGFR3 skeletal dysplasia phenotypes. *Nature*. 2014;513(7519):507–511.
19. Matsushita M, et al. Meclozine promotes longitudinal skeletal growth in transgenic mice with achondroplasia carrying a gain-of-function mutation in the FGFR3 gene. *Endocrinology*. 2015;156(2):548–554.
20. Guagnano V, et al. Discovery of 3-(2,6-dichloro-3,5-dimethoxy-phenyl)-1-{6-[4-(4-ethyl-piperazin-1-yl)-phenylamino]-pyrimidin-4-yl}-1-methyl-urea (NVP-BGJ398), a potent and selective inhibitor of the fibroblast growth factor receptor family of receptor tyrosine kinase. *J Med Chem*. 2011;54(20):7066–7083.
21. Gudernova I, et al. Multikinase activity of fibroblast growth factor receptor (FGFR) inhibitors SU5402, PD173074, AZD1480, AZD4547 and BGJ398 compromises the use of small chemicals targeting FGFR catalytic activity for therapy of short stature syndromes. *Hum Mol Genet*. 2016;25(1):9–23.
22. Wöhrle S, et al. Pharmacological inhibition of fibroblast growth factor (FGF) receptor signaling ameliorates FGF23-mediated hypophosphatemic rickets. *J Bone Miner Res*. 2013;28(4):899–911.
23. Wöhrle S, et al. Fibroblast growth factor receptors as novel therapeutic targets in SNF5-deleted malignant rhabdoid tumors. *PLoS One*. 2013;8(10):e77652.
24. Scheller T, et al. mTOR inhibition improves fibroblast growth factor receptor targeting in hepatocellular carcinoma. *Br J Cancer*. 2015;112(5):841–850.
25. Benoist-Lasselin C, et al. Human immortalized chondrocytes carrying heterozygous FGFR3 mutations: an in vitro model to study chondrodysplasias. *FEBS Lett*. 2007;581(14):2593–2598.
26. Gibbs L, Legeai-Mallet L. FGFR3 intracellular mutations induce tyrosine phosphorylation in the Golgi and defective glycosylation. *Biochim Biophys Acta*. 2007;1773(4):502–512.
27. Ornitz DM, Marie PJ. FGF signaling pathways in endochondral and intramembranous bone development and human genetic disease. *Genes Dev*. 2002;16(12):1446–1465.
28. Di Rocco F, et al. FGFR3 mutation causes abnormal membranous ossification in achondroplasia. *Hum Mol Genet*. 2014;23(11):2914–2925.
29. Pannier S, et al. Activating Fgfr3 Y367C mutation causes hearing loss and inner ear defect in a mouse model of chondrodysplasia. *Biochim Biophys Acta*. 2009;1792(2):140–147.
30. Jonquoy A, et al. A novel tyrosine kinase inhibitor restores chondrocyte differentiation and promotes bone growth in a gain-of-function Fgfr3 mouse model. *Hum Mol Genet*. 2012;21(4):841–851.
31. Chan WC, Au TY, Tam V, Cheah KS, Chan D. Coming together is a beginning: the making of an intervertebral disc. *Birth Defects Res C Embryo Today*. 2014;102(1):83–100.
32. Ornitz DM, Marie PJ. Fibroblast growth factor signaling in skeletal development and disease. *Genes Dev*. 2015;29(14):1463–1486.
33. Legeai-Mallet L, Benoist-Lasselin C, Delezoide AL, Munnich A, Bonaventure J. Fibroblast growth factor receptor 3 mutations promote apoptosis but do not alter chondrocyte proliferation in thanatophoric dysplasia. *J Biol Chem*. 1998;273(21):13007–13014.
34. Krejci P, et al. Analysis of STAT1 activation by

six FGFR3 mutants associated with skeletal dysplasia undermines dominant role of STAT1 in FGFR3 signaling in cartilage. *PLoS One*. 2008;3(12):e3961.
35. Lefebvre V, Huang W, Harley VR, Goodfellow PN, de Crombrugghe B. SOX9 is a potent activator of the chondrocyte-specific enhancer of the pro alpha1(II) collagen gene. *Mol Cell Biol*. 1997;17(4):2336–2346.
36. Lefebvre V, de Crombrugghe B. Toward understanding SOX9 function in chondrocyte differentiation. *Matrix Biol*. 1998;16(9):529–540.
37. Sahni M, et al. FGF signaling inhibits chondrocyte proliferation and regulates bone development through the STAT-1 pathway. *Genes Dev*. 1999;13(11):1361–1366.
38. Sahni M, Raz R, Coffin JD, Levy D, Basilico C. STAT1 mediates the increased apoptosis and reduced chondrocyte proliferation in mice overexpressing FGF2. *Development*. 2001;128(11):2119–2129.
39. Muenke M, et al. A unique point mutation in the fibroblast growth factor receptor 3 gene (FGFR3) defines a new craniosynostosis syndrome. *Am J Hum Genet*. 1997;60(3):555–564.
40. Cappellen D, et al. Frequent activating mutations of FGFR3 in human bladder and cervix carcinomas. *Nat Genet*. 1999;23(1):18–20.
41. Chesi M, et al. The t(4;14) translocation in myeloma dysregulates both FGFR3 and a novel gene, MMSET, resulting in IgH/MMSET hybrid transcripts. *Blood*. 1998;92(9):3025–3034.
42. Carter EP, Fearon AE, Grose RP. Careless talk costs lives: fibroblast growth factor receptor signalling and the consequences of pathway malfunction. *Trends Cell Biol*. 2015;25(4):221–233.
43. Mugniery E, et al. An activating Fgfr3 mutation affects trabecular bone formation via a paracrine mechanism during growth. *Hum Mol Genet*. 2012;21(11):2503–2513.
44. Sebastian A, et al. Genetic inactivation of ERK1 and ERK2 in chondrocytes promotes bone growth and enlarges the spinal canal. *J Orthop Res*. 2011;29(3):375–379.
45. Trudel S, et al. Inhibition of fibroblast growth factor receptor 3 induces differentiation and apoptosis in t(4;14) myeloma. *Blood*. 2004;103(9):3521–3528.
46. Grand EK, Chase AJ, Heath C, Rahemtulla A, Cross NCP. Targeting FGFR3 in multiple myeloma: inhibition of t(4;14)-positive cells by SU5402 and PD173074. *Leukemia*. 2004;18(5):962–966.
47. De Brito LR, et al. Comparative pre-clinical evaluation of receptor tyrosine kinase inhibitors for the treatment of multiple myeloma. *Leuk Res*. 2011;35(9):1233–1240.
48. Aviezer D, Golembo M, Yayon A. Fibroblast growth factor receptor-3 as a therapeutic target for Achondroplasia — genetic short limbed dwarfism. *Curr Drug Targets*. 2003;4(5):353–365.
49. Reina V, et al. Craniovertebral junction anomalies in achondroplastic children. *Adv Tech Stand Neurosurg*. 2014;40:295–312.
50. Julliand S, et al. Lung function, diagnosis, and treatment of sleep-disordered breathing in children with achondroplasia. *Am J Med Genet A*. 2012;158A(8):1987–1993.
51. Engberts AC, Jacobs WC, Castelijns SJ, Castelein RM, Vleggeert-Lankamp CL. The prevalence of thoracolumbar kyphosis in achondroplasia: a systematic review. *J Child Orthop*. 2012;6(1):69–73.
52. Jeong ST, Song HR, Keny SM, Telang SS, Suh SW, Hong SJ. MRI study of the lumbar spine in achondroplasia. A morphometric analysis for the evaluation of stenosis of the canal. *J Bone Joint Surg Br*. 2006;88(9):1192–1196.

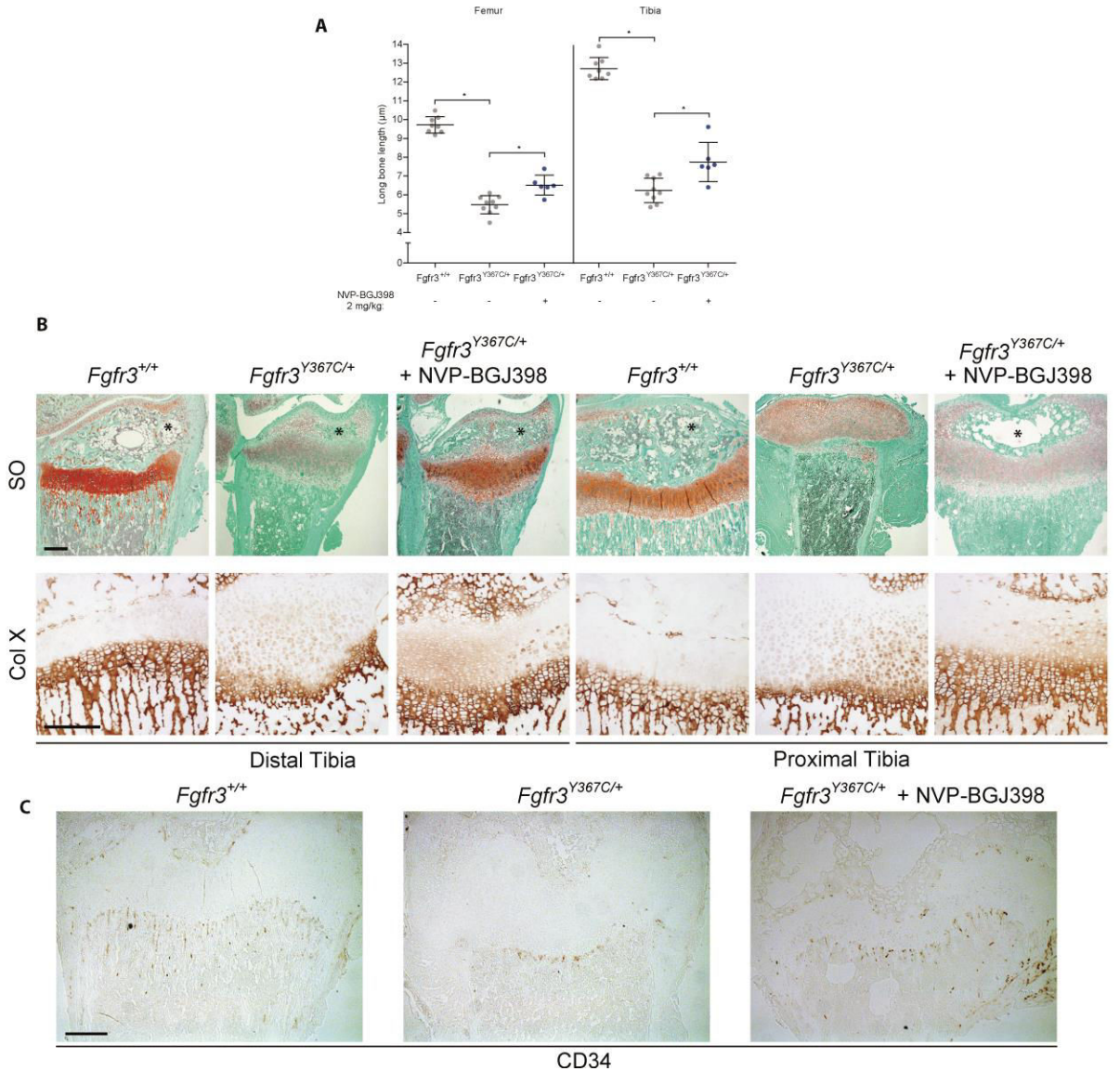

Supplemental Figure 1. NVP-BGJ398 daily injections rescue long bone defect of *Fgfr3*$^{Y367C/+}$ mice. (**A**) Femur and tibia bone length measured with µCT images (*Fgfr3*$^{+/+}$ n = 8, untreated *Fgfr3*$^{Y367C/+}$ n = 9, treated *Fgfr3*$^{Y367C/+}$ n = 6, *P < 0.05 by One-way ANOVA test). Data are expressed as mean ± s.d. (**B**) Safranin-O staining and immunohistochemistry for Col X on histological section of tibia (scale bar = 200 µm). Asterisks show secondary ossification centers. Images shown are representative of n = 5 animals per group. (**C**) Immunohistochemistry for CD34 on histological section of distal tibia (scale bar = 200 µm).

Images shown are representative of n = 5 animals per group. All data concern animals treated with protocol 1 (16 days old).

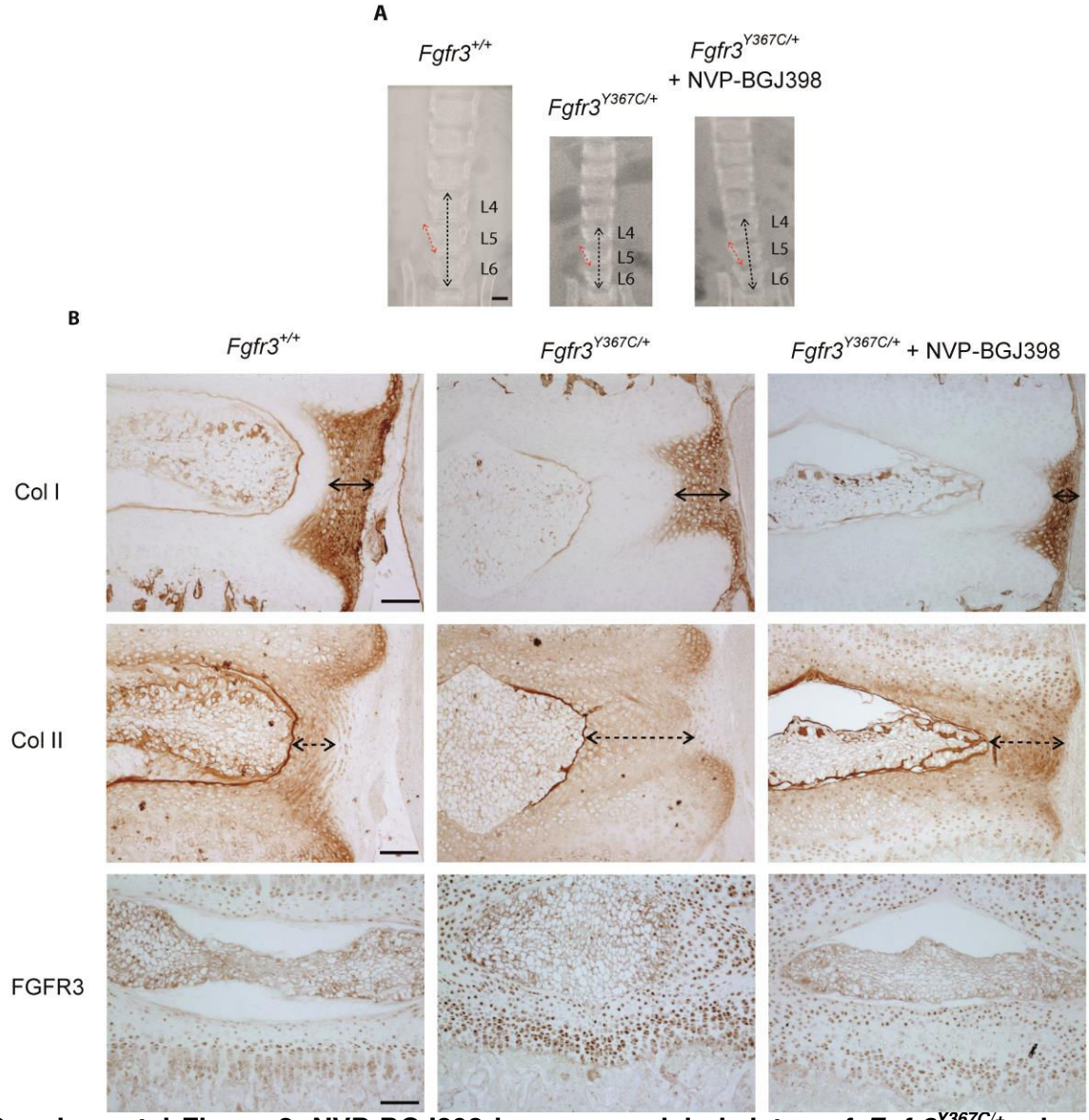

Supplemental Figure 2. NVP-BGJ398 improves axial skeleton of *Fgfr3*$^{Y367C/+}$ mice. (**A**) X-rays of lumbar vertebrae (L4-L6), the black arrows show the L4-L6 segment and red arrow show L5 pedicle landmarks (scale bar = 2 mm). (**B**) Immunohistochemistry for FGFR3, Col I and Col II on lumbar IVD outlying IAF (dashed arrows) and OAF (full arrows) (scale bar = 100 µm). Images shown are representative of n = 6 animals per group. All data concern animals treated with protocol 1 (16 days old).

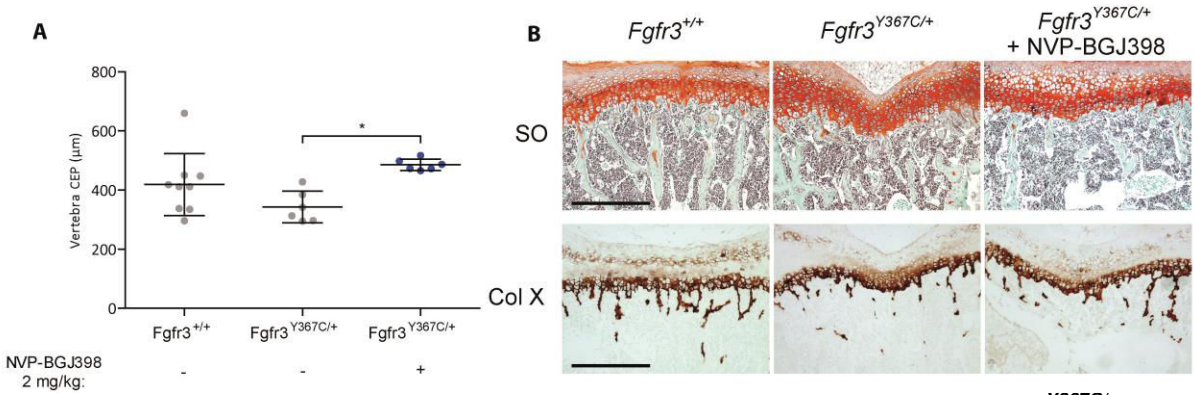

Supplemental Figure 3. NVP-BGJ398 improves cartilage end plate of *Fgfr3*$^{Y367C/+}$ mice. (**A**) Vertebra Cartilage End Plate (CEP) length (*Fgfr3*$^{+/+}$ n = 9, untreated *Fgfr3*$^{Y367C/+}$ n = 6, treated *Fgfr3*$^{Y367C/+}$ n = 6, *P < 0.05 by One-way ANOVA test). (**B**) Safranin-O staining and immunohistochemistry for Col X on histological section of CEP (scale bar = 200 µm). Images shown are representative of n = 6 animals per group. All data concern animals treated with protocol 1 (16 days old). Data are expressed as mean ± s.d.

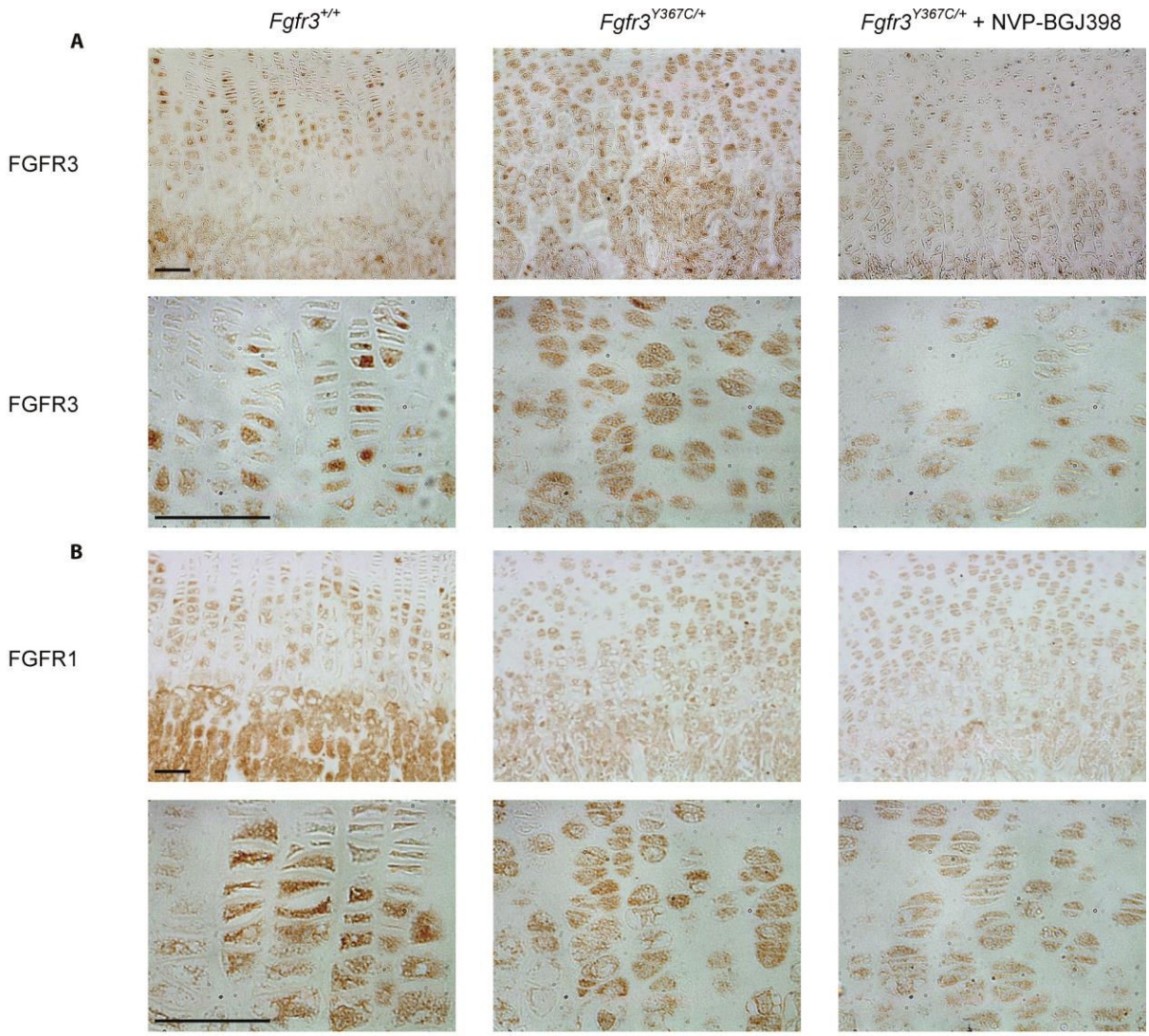

Supplemental Figure 4. FGFR3 and FGFR1 expression in femoral growth plate. (A) Immunohistological analyses of FGFR3 show that the FGFR3 expression is increased in *Fgfr3*$^{Y367C/+}$ mice and decreased after NVP-BGJ398 treatment. **(B)** The expression of FGFR1 revealed by immunohistochemistry is not modified in all conditions. All data concern animals treated with protocol 1 (16 days old) (scale bar = 50 µm). All images shown are representative of n = 6 animals per group. All data concern animals treated with protocol 1 (16 days old).

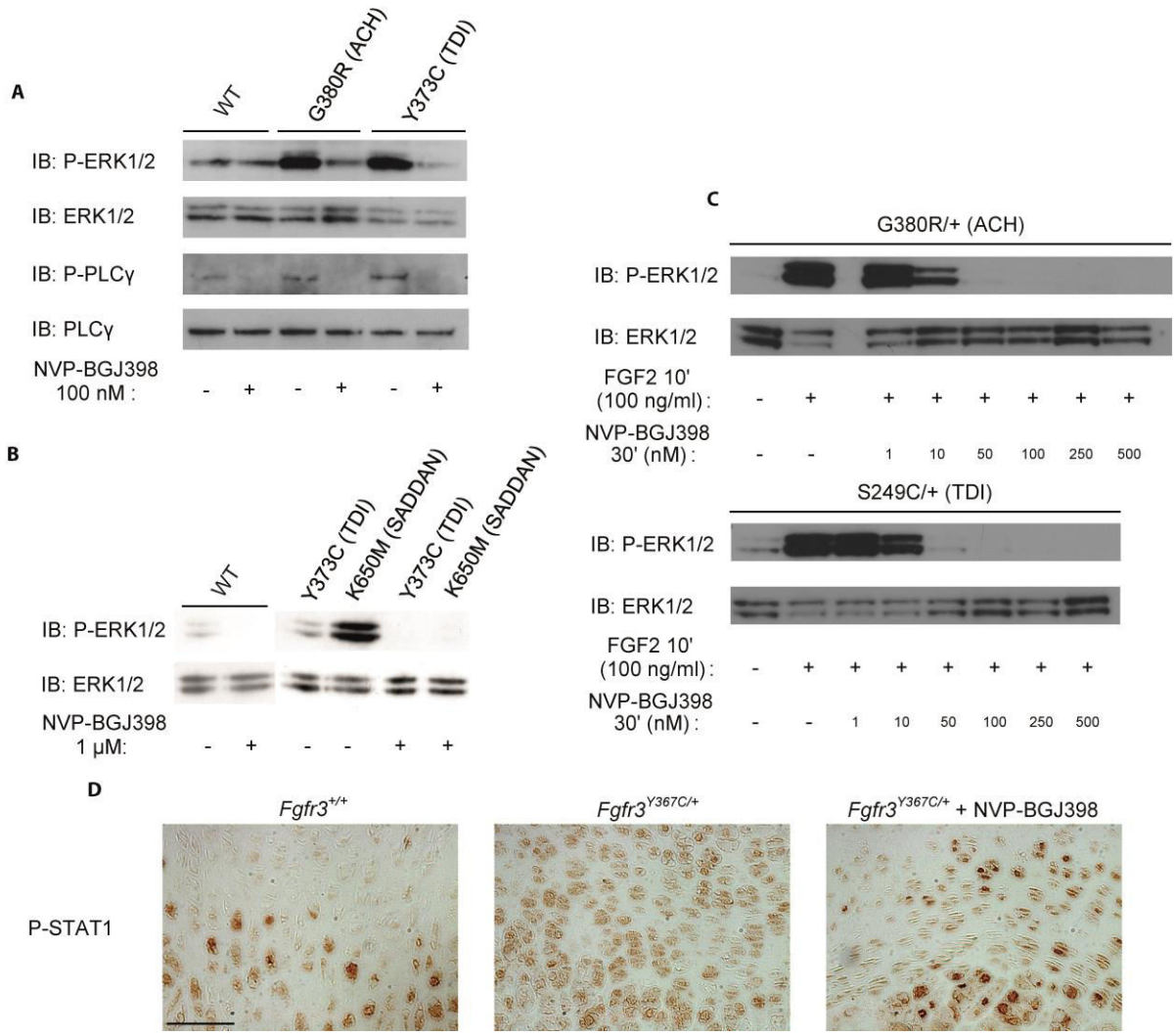

Supplemental Figure 5. NVP-BGJ398 inhibits the FGFR3 downstream signaling pathways. (**A**) Phosphorylated ERK1/2 and PLCγ expression in transfected human chondrocytes with $FGFR3^{WT}$, $FGFR3^{G380R}$ (ACH), $FGFR3^{Y373C}$ (TDI) constructs are reduced with NVP-BGJ398. (**B**) Phosphorylated ERK1/2 expression in transfected HEK293-Vnr cells with $FGFR3^{WT}$, $FGFR3^{Y373C}$ (TDI), $FGFR3^{K650M}$ (SADDAN) constructs are reduced with NVP-BGJ398. (**C**) Dose response effect of NVP-BGJ398 on phosphorylated ERK1/2 in immortalized ACH (G380R/+) and TDI (S249C/+) human chondrocytes. (IP = Immunoprecipitation, IB = Immunoblotting). (**D**) Immunohistological analyses of phosphorylated STAT1 show an increase expression in *Fgfr3*$^{Y367C/+}$ mice and decreased expression after NVP-BGJ398 treatment. Images shown are representative of n = 4 animals per group (scale bar = 50 µm). All data concern animals treated with protocol 1 (16 days old). Western blots are representative of 3 independent experiments.

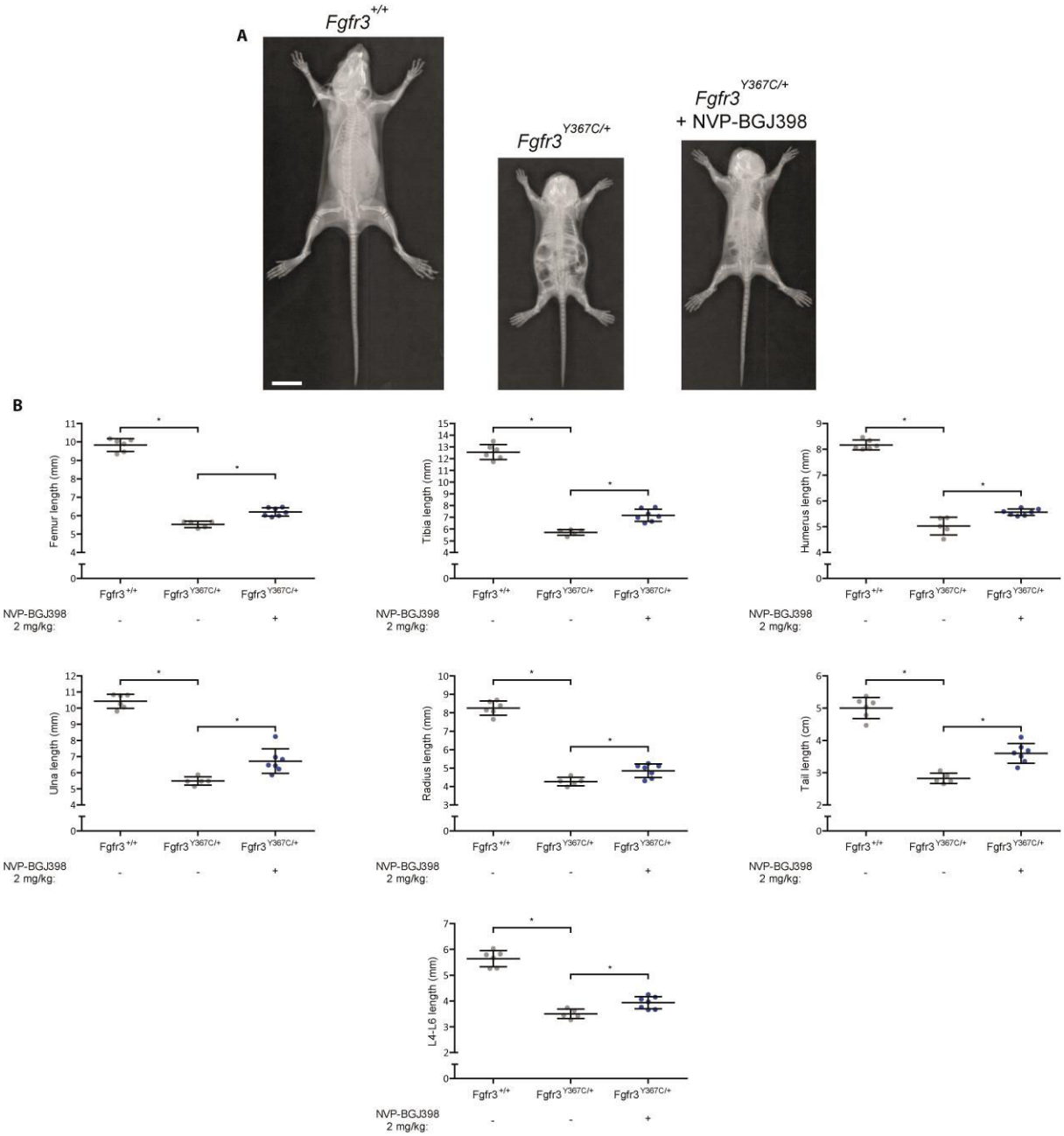

Supplemental Figure 6. NVP-BGJ398 improves growth of the axial and appendicular skeleton in *Fgfr3*$^{Y367C/+}$ mice (protocol 2)

(**A**) Radiographs of *Fgfr3*$^{+/+}$, treated and untreated *Fgfr3*$^{Y367C/+}$ skeletons show the benefit effect of the treatment (scale bar = 1 cm). (**B**) NVP-BGJ398 improvement of the lengths of femur, tibia, humerus, ulna, tail, radius and L4-L6 (*Fgfr3*$^{+/+}$ n = 6, untreated *Fgfr3*$^{Y367C/+}$ n = 5, treated *Fgfr3*$^{Y367C/+}$ n = 7, *P < 0.05 by One-way ANOVA test). Data are expressed as mean ± s.d.

Article 2 - Meckel's and condylar cartilages anomalies in achondroplasia result in defective development and growth of the mandible

HMG Advance Access published June 3, 2016

Meckel's and condylar cartilages anomalies in achondroplasia result in defective development and growth of the mandible

Martin Biosse Duplan[1, 2], Davide Komla-Ebri[1], Yann Heuzé[3], Valentin Estibal[1], Emilie Gaudas[1], Nabil Kaci[1], Catherine Benoist-Lasselin[1], Michel Zerah[4], Ina Kramer[5], Michaela Kneissel[5], Diana Grauss Porta[5], Federico Di Rocco [1, 4$], Laurence Legeai-Mallet [1, 6*]

[1]INSERM U1163, Université Paris Descartes, Sorbonne Paris Cité, Institut Imagine, Paris, France

[2] Service d'Odontologie, Hôpital Bretonneau, HUPNVS, AP-HP, Paris, France

[3]UMR5199 PACEA, Université de Bordeaux, Bordeaux Archaeological Sciences Cluster Of Excellence, Université de Bordeaux, Bordeaux, France

[4]Neurochirurgie Pédiatrique, Unité de chirurgie craniofaciale, Hôpital Necker Enfants malades, AP-HP, Paris, France

[5]Novartis Institutes for BioMedical Research, Basel, Switzerland

[6]Service de Génétique, Hôpital Necker-Enfants Malades, AP-HP, Paris, France

[$]Present address: Neurochirurgie Pédiatrique, Hopital Femme Mère Enfant CHU de Lyon, Université Claude Bernard Lyon 1, Lyon, France

*Corresponding author: laurence.legeai-mallet@inserm.fr

ABSTRACT

Activating FGFR3 mutations in human result in achondroplasia (ACH), the most frequent form of dwarfism, where cartilages are severely disturbed causing long bones, cranial base and vertebrae defects. Since mandibular development and growth rely on cartilages that guide or directly participate to the ossification process, we investigated the impact of FGFR3 mutations on mandibular shape, size and position. By using CT-scan imaging of ACH children and by analyzing *Fgfr3*$^{Y367C/+}$ mice, a model of ACH, we show that *FGFR3* gain-of–function mutations lead to structural anomalies of primary (Meckel's) and secondary (condylar) cartilages of the mandible, resulting in mandibular hypoplasia and dysmorphogenesis. These defects are likely related to a defective chondrocyte proliferation and differentiation and pan-FGFR tyrosine kinase inhibitor NVP-BGJ398 corrects Meckel's and condylar cartilages defects *ex vivo.* Moreover, we show that low dose of NVP-BGJ398 improves *in vivo* condyle growth and corrects dysmorphologies in *Fgfr3*$^{Y367C/+}$ mice, suggesting that postnatal treatment with NVP-BGJ398 mice might offer a new therapeutic strategy to improve mandible anomalies in ACH and others FGFR3-related disorders.

INTRODUCTION

Achondroplasia (ACH) is the most common form of chondrodysplasia and is characterized by a rhizomelic dwarfism with short limbs, macrocephaly, frontal bossing and midface hypoplasia(1)(2)(3). ACH is caused by an activating mutation of *Fibroblast Growth Factor Receptor 3* (*FGFR3*) that affects both endochondral and membranous ossification (3–5). FGFR3 over-activation disturbs the proliferation and differentiation of chondrocytes in the growth plate of long bones (6–8) and synchondroses of the cranial base (3, 9). Other cartilaginous structures are affected in ACH, such as the inner ear (10), vertebral bodies and intervertebral disc (11), and joints (7).

Mandibular growth relies greatly on primary and secondary cartilages, even though their exact roles in the acquisition of the mandible final shape and size are not fully understood (12)(13). Meckel's cartilage (MC) is a rod-shaped primary cartilage that runs through the mandibular process of the first pharyngeal arch and acts as a morphogenic template for the membranous ossification of the mandible body. It is transiently present in the developing mandible and disappears at birth. Secondary cartilages (symphyseal, angular and condylar cartilages) form prenatally and eventually ossify by endochondral ossification during post-natal growth, serving as growth centers (12). The central role of cartilages in mandibular development and growth is exemplified by the mandibular phenotype observed in several chondrodysplasias where mutations in genes involved in chondrocyte function, such as *Collagen II* (responsible for Achondrogenesis type II), *Sox9* (Campomelic dysplasia) or *PTHrP* (Jansen type of metaphyseal chondrodysplasia) result in abnormal mandibular shape, size or position (14–16).

Mutations of *FGFR1*, *FGFR2* and *FGFR3* genes are associated with various aspects of abnormal craniofacial development such as craniosynostoses and maxillary hypoplasia (2, 17, 18). FGFR2 and FGFR3 are expressed in MC (19, 20) and throughout all phases of the chick mandibular development (21). FGFR3 signaling is required for the elongation of chick MC and FGFR2 and FGFR3 play a role during membranous ossification of mandible (22). Mandibular defects have also been observed in $Fgfr1/2^{dcko}$ mice, with a shorter and smaller mandible at birth (20). The deletion in mice of the FGFR3 signaling molecule Snail (23) is associated with a growth retardation of MC and a reduction in mandibular length (24) and mice deficient for the FGFR3 ligand FGF18 display a reduced size of MC and a hypoplastic mandible (25). These data support the role of FGFR signaling in the elongation of MC and morphogenesis of the mandible.

However, it is unknown whether mandibular growth and development are affected in children with ACH and if mandibular cartilages are disturbed by FGFR3 mutations. Analysis of lateral cephalogram from adult ACH patients has shown a prognathic mandible (i.e. anteriorly displaced) (26)(27). It has also been reported that in humans, other skeletal dysplasia caused by activating mutations of *FGFR3* can result in mandibular dysmorphogenesis as seen in thanatophoric dysplasia (TD) (28), and Muenke syndrome (MS) (29).

In this paper, we studied the mandible growth and development in children with ACH and observed an abnormal shape, size and position of the mandible. We compared the human data with those obtained with a mouse model of ACH ($Fgfr3^{Y367C/+}$, (10)), for which we analyzed MC and secondary cartilages of the mandible. We observed proliferation and differentiation defects in chondrocytes of the mandibular cartilages and a delay in the replacement of MC by bone. By targeting the excessive activity of FGFR3 with a tyrosine kinase inhibitor NVP-BGJ398 (30), in organ cultures, we

corrected the modifications of size and shape of the mandibles. Using NVP-BGJ398 in vivo, we observed a strong improvement of the mandibular phenotype. Taken together, these data bring out anomalies of the mandible in ACH and its mouse model and offer new perspective of treatment for ACH.

RESULTS

Achondroplasia results in mandibular hypoplasia and dysmorphogenesis

Although the craniofacial phenotype of patients with ACH has been described (2, 3, 26), no specific analysis of the mandible has been conducted. We took advantage of CT images acquired for assessment of risks for cervicomedullary-junction compression in infants with ACH (n=8, mean age: 21.3 months) and compared these images with those of age-matched controls obtained after traumatic events (n=9, mean age: 24.9 months). The length of the mandible, measured as the distance between condylion (Co) and gnathion (Gn), was significantly and consistently decreased in ACH patients compared to controls (-14%; $p<0.05$; Fig. 1A & 1B). Mandibular body length (Gonion (Go) – Menton (Me)) and mandibular ramus length (Go – Co) were also significantly decreased in ACH children (-16%; $p<0.01$ and -17%; $p<0.05$ respectively).

The analysis of tridimensional coordinates of anatomical landmarks with geometric morphometrics (31) showed differences in mandible shape between ACH patients and controls. Principal components analysis (PCA) of the human mandible shape resulted in the separation of ACH patients and controls along PC1 accounting for 47% of total variance on the basis of shape features represented in Fig. 1C. When compared with controls, mandibles of ACH children were characterized by a defective orientation and size of the ramus with prominent coronoid processes and relatively shorter condyles.

FGFR3 activation in mice results in mandibular hypoplasia and dysmorphogenesis

The role of Fgfr1 and Fgfr2 during mandibular development was demonstrated in mice with a mesenchyme-specific disruption of Fgfr1 and Fgfr2 (20), while, the impact of an activating Fgfr3 mutation on the mandible has not been studied. Here, we compared the mandible size and shape of *Fgfr3*$^{Y367C/+}$ mice that accurately mimic ACH (3, 10, 32) with WT mice at different ages. We sacrificed pregnant mice to collect *Fgfr3*$^{Y367C/+}$ and control littermate embryos at gestational day E16.5 and E18.5. Mice were also sacrificed at postnatal day 0 and 21. The mandibles were dissected and stained with alcian blue for cartilage and alizarin red for mineralized tissue. We observed a significant reduction in the length of the mandible body in the mutant mice at all time-points: -11% $p<0.005$, -9% $p<0.005$, -10% $p<0.005$, -16% $p<0.0001$ compared with WT littermates at E16.5, E18.5, P0 and P21 respectively (Fig. 1D & 1E).

To identify potential dysmorphologies in *Fgfr3*$^{Y367C/+}$ mandibles in addition to the hypoplasia, we measured anatomical landmarks on 3D reconstructed micro CT images of P21 mandibles and analyzed their coordinates with geometric morphometrics. The PCA of the mandible shape resulted in the separation of *Fgfr3*$^{Y367C/+}$ mice and controls littermates along PC1 accounting for 78% of total variance on the basis of shape features (mainly located on the ramus) represented in Fig. 1F. Our results revealed that the shape changes observed in ACH patients and *Fgfr3*$^{Y367C/+}$ mice were relatively similar.

Chondrocytes homeostasis is disturbed in Meckel's cartilage of *Fgfr3*$^{Y367C/+}$ mice

We hypothesized that Fgfr3 activation disturbs chondrocytes homeostasis in MC, as it was shown in other cartilages, such as the growth plate (10), the inner ear (10), the cranial base synchondroses (3) or vertebral bodies (11), and that these defects could be responsible for the mandibular hypoplasia and dysmorphogenesis observed in *Fgfr3*$^{Y367C/+}$ mice. We therefore collected embryos at gestational day E16.5 and E18.5 and

analyzed markers of chondrocyte proliferation and differentiation on histological sections.

At E16.5, MC was readily identifiable on sections stained with safranin'O (Fig. 2A). We focused on the cartilage within the developing mandible. In its central part, chondrocytes are organized into layers (33, 34), as in a growth plate or a synchondrosis. We used several markers to compare the spatial organization of the chondrocytes into distinct zones in WT and mutant embryos and observed that the chondrocyte differentiation was disrupted in mutant embryos. First, immunostaining for Collagen X showed that the size of the hypertrophic chondrocytes zone relative to the total size of the cartilage was reduced (-43% compared to WT, $p<0.05$; Fig. 2A & 2B), as was the size of individual hypertrophic chondrocytes (-51% compared to WT, $p<0.0001$; Fig. 2A & 2C) in *Fgfr3*$^{Y367C/+}$ embryos. Immunostaining of the proliferation marker Ki67 indicated that more cells were proliferating in MC of mutant embryos (+81% compared to WT, $p<0.01$; Fig. 2A & 2D). In WT and *Fgfr3*$^{Y367C/+}$ embryos, the zones of proliferating and hypertrophic cells were clearly delimited and were almost completely mutually exclusive (Fig 2A). We then observed that the number of Fgfr3 positive cells in this cartilage was increased in *Fgfr3*$^{Y367C/+}$ embryos (+151%, $p<0.0001$; Fig. 2A& 2D) as reported in the growth plate of the same mouse model (11, 35) and ACH and TD fetuses (6). FGFR3 exhibits a specific pattern of expression during chondrocyte differentiation (5, 36) and in the growth plate its expression is mostly limited to the resting, proliferating and pre-hypertrophic chondrocytes (37). In WT embryos, Fgfr3 was expressed by proliferative and prehypertrophic chondrocytes (Fig. 2A) whereas in *Fgfr3*$^{Y367C/+}$ embryos, the pattern of expression was less clearly delimited, with an overlapping of Collagen X and Fgfr3 positive cartilage areas.

Differentiation into hypertrophic chondrocytes precedes and contributes to the disappearance of MC and replacement by bone (38)(39). At E18.5 large remnants of cartilage were detected in *Fgfr3*$^{Y367C/+}$ embryos, in contrast with WT embryos where MC was mostly replaced by bone (Fig 2E and 2F) and the size of MC was significantly increased in *Fgfr3*$^{Y367C/+}$ embryos mandible (+129%, $p<0.05$). Similar defects lead to an ossification delay in the growth plate (40).

Overall, these results suggest that Fgfr3 constitutive activation disturbed the chondrocytes proliferation and differentiation and delayed the ossification process in MC.

FGFR3 activation reduces condylar growth in humans and mice

Deviations in the growth of the mandibular condyle can have major functional and aesthetic consequences (41). Although the majority of the mandible is formed by membranous ossification, the upper part of the ramus is formed by endochondral ossification of the condylar cartilage. This process allows the mandible to elongate and grow upward and backward (42). In both humans and mice, endochondral ossification is severely disturbed by *FGFR3* activating mutations and defects in condylar cartilage could contribute to mandibular hypoplasia and dysmorphogenesis. For these reasons, we characterized the condylar process, first in children with ACH, then in *Fgfr3*$^{Y367C/+}$ mice. We observed on sagittal sections from CT images that the length of the condylar neck in children with ACH was reduced compared to age-matched controls (-21%, $p<0.005$; ACH: n= 12, mean age= 32.4 months; controls: n= 14, mean age= 32.4 months) (Fig. 3A and 3B). This reduction was observed in children aged from 1 to 42 months. In *Fgfr3*$^{Y367C/+}$ mice (P21), condylar hypoplasia was also present (Fig. 3C and 3D). In mutant

mice, condyles were significantly reduced in length (-14.2%, p<0.01) and width (-15.8%, p<0.001).

To identify the mechanism that led to this shorter condylar neck, we examined the condylar cartilage on histological sections of E16.5 embryos and P21 mice. In *Fgfr3*$^{Y367C/+}$ mice, the size of the hypertrophic zone in the cartilage was reduced compared to WT littermates as was the average size of individual hypertrophic chondrocytes (E16.5: -48%, p<0.001; P21: -56,3%, p<0.05) (Fig. 3E, 3F, 3G & 3H).

Tyrosine kinase inhibition corrects primary and secondary cartilages defects in *Fgfr3*$^{Y367C/+}$ embryos

To test the hypothesis that the mandibular hypoplasia and dysmorphogenesis observed in children with ACH and *Fgfr3*$^{Y367C/+}$ mice are direct consequences of an overactive FGFR3, we analyzed the effect on mandibular development and growth of pharmacological inhibition of FGFRs using NVP-BGJ398, a pan-specific FGFR inhibitor (30). We first developed an *ex vivo* system of mandible explant cultures, similar to the femur explant cultures we used to test pharmacological approaches of FGFR inhibition (11, 32, 35). We isolated the mandible from WT and *Fgfr3*$^{Y367C/+}$ embryos at E16.5, dissected the mandibles into two hemi-mandibles and cultured those separately for 6 days. One hemi-mandible was treated with NVP-BGJ398, while the other served as control. As expected, the body and condyle of hemi-mandible from *Fgfr3*$^{Y367C/+}$ embryos treated with DMSO were smaller compared to those of WT hemi-mandibles also treated with DMSO (-10,1%, p<0.05; -18%, p<0.05 respectively, Fig. 4A & 4B). Incubation with NVP-BGJ398 of *Fgfr3*$^{Y367C/+}$ hemi-mandibles led to an increase in mandible body (+11%, p<0.05) and condylar neck (+26%, p<0.05) size, reaching the size of cultured WT hemi-mandibles treated with DMSO (Fig. 4A & 4B).

Increases in mandible length with NVP-BGJ398 treatment were associated with the correction of chondrocyte defects observed in primary and secondary mandibular cartilages of *Fgfr3*$^{Y367C/+}$ embryos. While the size of MC hypertrophic zone relative to the size of the cartilage was clearly reduced in *Fgfr3*$^{Y367C/+}$ hemi-mandible treated with DMSO compared to WT (-40.2%, p<0.05), this zone expanded following Fgfr3 inhibition in mutant mandible (+68.3%, p<0.05) (Fig. 4C & 4D). This expansion was associated with an increased size of individual hypertrophic chondrocytes in hemi-mandible from *Fgfr3*$^{Y367C/+}$ embryos treated with NVP-BGJ398 (+165% compared to *Fgfr3*$^{Y367C/+}$ treated with DMSO, p<0.0001) (Fig. 4C & 4E). We noted an increased replacement of MC by bone in the treated mandibles, compared to the untreated *Fgfr3*$^{Y367C/+}$ mandible, rescuing the extinction delay of MC observed in *Fgfr3*$^{Y367C/+}$ mice. The kinase inhibitor also corrected the overexpression of Fgfr3 and the increased proliferation of chondrocytes in MC of *Fgfr3*$^{Y367C/+}$ hemi-mandible (Fig. 4F).

In the condylar cartilage, similar changes were observed. Treatment with NVP-BGJ398 increased the size of the cartilage hypertrophic zone and the size of individual hypertrophic chondrocytes in condyles of *Fgfr3*$^{Y367C/+}$ embryos (+98.4%, p<0.0005 compared to condyles from *Fgfr3*$^{Y367C/+}$ hemi-mandibles treated with DMSO) (Fig 4G & 4H).

Altogether, we observed that the reduction of Fgfr3 activity with NVP-BGJ398 corrected the defective growth and cellular defects observed in the presence of an overactive Fgfr3. As those improvements occurred in the absence of any systemic regulation (*ex vivo* explants), the effect of the inhibitor is likely direct. This reinforces the view that the cartilage defects are responsible for the mandibular hypoplasia.

Tyrosine kinase inhibition improves the mandibular dysmorphogenesis and the size of the condyle in *Fgfr3*$^{Y367C/+}$ mice

Finally, we tested the potential benefit of a pharmacological use of tyrosine kinase inhibitor to correct *in vivo* the mandibular hypoplasia and dysmorphogenesis of *Fgfr3*$^{Y367C/+}$ mice. We performed daily subcutaneous injection of either NVP-BGJ398 (2mg/kg) or vehicle on one-day-old mice from P0 to P15 (11). The mandibles of P16 mice were then imaged by microCT. As in the *ex vivo* experiments, we observed phenotypic changes of the condylar neck in *Fgfr3*$^{Y367C/+}$ mice treated with NVP-BGJ398 compared to *Fgfr3*$^{Y367C/+}$ littermates treated with DMSO. The length (+20.9%, $p<0.005$) and width (+22%, $p<0.005$) of the condylar neck were increased by the reduction of the over-activation of FGFR3 (n=7, n=8 & n=7 for WT vehicle, *Fgfr3*$^{Y367C/+}$ vehicle and *Fgfr3*$^{Y367C/+}$ NVP-BGJ398 respectively) (Fig. 5A and 5B). As expected, the length of mandible body was unchanged since MC had already been replaced by bone at the start of the injections. We confirmed the positive effect of NVP-BGJ398 on condylar cartilage with histological sections of the condyles (Fig. 6A & 6B). The PCA of the Procrustes shape coordinates of the landmarks measured on all mandibles was also run. As for P21 mice, PC1 separated the WT vehicle and the *Fgfr3*$^{Y367C/+}$ vehicle mice (Fig. 5C & 5D). The *Fgfr3*$^{Y367C/+}$ NVP-BGJ398 mice occupied a somewhat intermediate position though they overlap with the *Fgfr3*$^{Y367C/+}$ vehicle mice (Fig. 5C & 5D). P-values from permutation tests (10000 permutation rounds) for Mahalanobis distances among groups showed that the *Fgfr3*$^{Y367C/+}$ NVP-BGJ398 mice were significantly different in the shape of the mandible from either the *Fgfr3*$^{Y367C/+}$ vehicle mice or the WT vehicle. When comparing the centroid size (CS) used as a proxy for overall size of the mandible, WT mice displayed significantly larger mandible than *Fgfr3*$^{Y367C/+}$ mice treated with the vehicle ($t=-6.96$; $p<0.005$) or NVP-BGJ398 ($t=-7.35$; $p<0.005$). *Fgfr3*$^{Y367C/+}$ NVP-BGJ398 mice did not display significantly larger mandible than the *Fgfr3*$^{Y367C/+}$ vehicle mice ($t=-0.0887$; $p=0.931$). These data confirm that the length of the mandible was not corrected by the treatment but that the overall shape of the mandible of *Fgfr3*$^{Y367C/+}$ was improved with NVP-BGJ398.

DISCUSSION

Deviation from normal mandible growth can strongly affect the masticatory and respiratory functions, speech and aesthetic appearance of the face (41)(43) and mandibular cartilages are recognized as critical growth centers for the mandible. Although many cartilages are affected in *FGFR3*-related chondrodysplasias, most strikingly the cartilaginous growth plate in the growing skeleton, mandibular cartilages and their impact on mandible growth had never been investigated in ACH. Our hypothesis was that mandibular cartilages would be affected by *FGFR3* activating mutations, similar to other cartilages, and that these defects would cause modifications in the shape, size and/or position of the mandible.

We first observed differences in the size and shape of the mandible between ACH and control children. The mandible as a whole, or subunits such as the mandibular body and ramus were reduced in size at all ages in children with ACH and morphometric analysis revealed modifications in the shape of the ramus. Comparable changes were present in *Fgfr3*$^{Y367C/+}$ mice, and in both children and mice, the mandibular hypoplasia worsened with age. Our findings illustrate again the similarity of this mouse model with ACH.

In addition to ACH, *FGFR3* activating mutations cause four other types of chondrodysplasia (hypochondroplasia, severe achondroplasia with developmental delay and acanthosis nigricans (SADDAN), and TD type I and II) (1, 2) and two types of craniosynostoses (MS and Crouzon syndrome with acanthosis nigricans) (44). The presence of mandible abnormalities in these diseases has rarely been studied. A report showed mandibular clefting in a case of TD I (28), two cephalometric studies in adult ACH patients reported opposite results concerning the size of the mandible (normal for (26) or decreased for Cardoso et al (27)), while another study showed that MS patients had shorter mandibular body length than controls (29). Several mouse lines carrying *Fgfr3* activating mutations have been generated but a very few comprehensive analysis of the mandible are available. The homozygous *Fgfr3* G380R mouse, a model for ACH, has a reduced mandible length (79% of controls) (45) and the homozygous *Fgfr3* P244R mouse, a model for MS, has a hypomorphic condyle (46).

The *FGFR3* mutations responsible for chondrodysplasias and craniosynostoses were until recently known to primarily affect different ossification processes (endochondral vs membranous), but as observed in ACH (3), FGFR3 over activation can consistently disturbs both ossification processes. The ossification of the mandible relies on these two types, the body being formed by membranous ossification while the ramus is mainly formed by endochondral ossification. If the effect of *FGFR3* mutations responsible for ACH on the ramus is expected, it is intriguing that the same mutations can affect the size of the mandibular body. In order to understand what led to these changes we studied a primary (Meckel's) and a secondary (condylar) cartilage. The exact role of MC is not yet fully understood as it disappears before birth and only marginally participates in the ossification process of the mandible (47). It could play a role in the elongation of the mandible body as exemplified by the severe micrognathia present when MC is strongly perturbed as in the case of *Sox9* haploinsufficiency (48) or deletion of Snai1 and Snai2 (24). Here, we found that Fgfr3 over activation disturbed the differentiation of chondrocytes in MC. The size of the hypertrophic zone was markedly shortened, as was the size of individual hypertrophic chondrocytes. The same defects were observed in the growth plate of ACH patients (6) and *Fgfr3*$^{Y367C/+}$ mice (10, 40). As the chondrocytes differentiate in the growth plate, the volume enlargement to become

hypertrophic determines the size of the growth plate elongation (49, 50)(51). The same mechanism could occur in MC and the disruption of MC chondrocytes differentiation caused by FGFR3 over activation could lead to the shortening of the mandible body. Supporting this view, we observed that reduction of the tyrosine kinase activity of FGFR3 with NVP-BGJ398 corrected not only the hypertrophic chondrocyte phenotype in mandible *ex vivo* cultures but also improved the shortening of the mandible of *Fgfr3*$^{Y367C/+}$ embryos. In contrast, the same molecule had no effect on the mandible body once MC was replaced by bone. We assume this is due to the disappearance of MC before birth and, to us, reinforces the importance of MC in the elongation of the mandible. In mice of this age, ossification of the symphyseal is limited and therefore contributes marginally to the elongation of the mandible body (52).

The activity of FGFR3 must be precisely tuned for normal mandible elongation since the injection of dominant negative (DN) form of FGFR3 in the chick embryo leads to the truncation or shortening of MC (22). In the same study, the DN form reduced the proliferation of the cells in MC, while we observed in our study that it was markedly increased by the activating mutation. Increased chondrocyte proliferation was also observed in the growth plate of embryos carrying either the *Fgfr3* Y367C or K644E mutations (40, 53). In MC, the expression of Fgfr3 was also increased by the Y367C *Fgfr3* mutation. It could be the result of a prolonged half time of the protein, since the mutation of the transmembrane domain could delay the turnover and degradation of the activated receptor (54, 55).

FGFR3 mutations responsible for ACH could also affect the ossification of the mandibular process that was delayed in *Fgfr3*$^{Y367C/+}$ embryos. It could be a consequence of the defective MC homeostasis and subsequent initiation of ossification. Alternatively, mesenchymal cells lateral to MC that directly differentiate into osteoblasts (20) could be independently affected by FGFR3 activation. Further work is needed to determine if this delay affects mandible bone mass acquisition during growth, as reported in long bones (40, 56).

Secondary cartilages are sites of late prenatal and early postnatal growth and eventually ossify. Here we focused on the condylar cartilage. It develops adjacent to the intramembranous bone of the mandible, distinct from MC and in contrast with MC, directly contributes to the formation of the ramus by endochondral ossification and persists postnatally to function as a growth center (42). Genetic defects in chondrogenesis can cause abnormal condylar growth as in Pierre Robin sequence (41), an entity associated with genetic defects of SOX9 (57). We found that children with ACH had shorter condylar neck, a feature also found in *Fgfr3*$^{Y367C/+}$ mice. Histological analysis of the condyle in *Fgfr3*$^{Y367C/+}$ mice, revealed a disturbed cartilage where the hypertrophic chondrocytes were smaller and the hypertrophic zone shortened, as in MC or in the growth plate of the same mice (10). Altered differentiation of chondrocyte is also present in condyles of TD infants (58) and in the hypolpastic condyle of homozygous *Fgfr3* P244R mice (46). Here, cultures of hemi-mandibles and in vivo experiments with partial inhibition of Fgfr3 activity showed that it is likely that the defective chondrocyte differentiation and proliferation directly contributes to the reduced elongation of the condyle. The persistence of the condylar cartilage postnatally allowed us to observe that *in vivo* tyrosine kinase inhibition rescue condylar growth in *Fgfr3*$^{Y367C/+}$ mice, increasing its length by 21% after 15 days of treatment. The same treatment improved the growth of appendicular and axial skeletons with a similar magnitude of change of long bones (11).

Current treatments of maxillofacial deformities and skeletal dysplasia are primarily surgical and can require multiple interventions during childhood (59, 60). Innovative pharmacological treatments of these diseases are needed and reducing the excessive activity of the FGFR3 receptor in *FGFR3*-related chondrodysplasias or craniosynostoses with specific tyrosine kinase inhibitors, such as NVP-BGJ398, is an appealing approach. It potentially targets all downstream signaling pathways of the receptor and in this aspect, NVP-BGJ398 has been shown to normalize *in vitro* and *in vivo* ERK1/2 and PLCγ pathways (11). Our pre-clinical experiments showed here that this inhibitor enters mandibular cartilages and improves cranio-facial growth.

In summary, we showed in this paper that a *FGFR3* gain-of–function mutation disturbs the development and growth of the mandible, via structural anomalies of Meckel's and condylar cartilages. These anomalies are likely related to the defective chondrocyte proliferation and differentiation and the tyrosine kinase inhibitor NVP-BGJ398 corrects these defects and improves condyle growth. This suggests that postnatal treatment with the molecule could be a therapeutic strategy to improve mandible growth in ACH and others FGFR3-related disorders.

MATERIALS AND METHODS

Human subjects

All patients with ACH (n= 12, mean age= 32.4 months) or age-matched controls (n= 14, mean age= 32.4 months) were examined and followed at the Craniofacial Surgery Unit of Necker-Enfants Malades Hospital. Ethics approvals were obtained from the institutional review Board of Necker-Enfants Malades Hospital.

Mouse models

All the experiments were conducted in *Fgfr3*$^{Y367C/+}$ mice, a mouse model that display parts of the clinical hallmarks of ACH (32), or WT littermates, used as controls. WT and *Fgfr3*$^{Y367C/+}$ mice were generated by crossing *Fgfr3*^{neoY367C} mice (10) and *Cmv-Cre* mice (61). The mutant mice express the c.1100A>G (p.Tyr367Cys) mutation corresponding to the c.1118A>G (p.Tyr373Cys) in thanatophoric dysplasia. All mice were on a C57BL/6 background. Mice were genotyped by PCR of tail DNA as described previously (10). Experimental animal procedures and protocols were approved by the French Animal Care and Use Committee.

Computed Tomography (CT) images of human patients and mice

Human patients CT images were produced by a 64-slice CT system (LightSpeed VCT, General Electric Medical Systems, Milwaukee, WI, USA). The images were reconstructed in 3 dimensions (3D) using Carestream PACS v11.0 software (Carestream Health, Rochester, NY, USA). Cephalometric analysis of the mandible was carried on sagittal views of the 3D reconstructions.

Following 15 days of NVP-BGJ398 treatment, *Fgfr3*$^{Y367C/+}$ mice and their control littermates were sacrificed and the whole heads were imaged using a µCT40 Scanco vivaCT42 (Scanco Medical, Bassersdorf, Switzerland). The following settings were used: integration time: 300 ms; 45 E(kVp); 177 µA. The mandible images were reconstructed in 3D using OsiriX 64-bit version software (Pixmeo, Bernex, Switzerland).

Morphometric analysis

The samples consisted of computed tomography (CT) images of patients with ACH and unaffected age-matched individuals, and of high-resolution CT images of 7 P21 *Fgfr3*$^{Y367C/+}$ mice and 7 control littermates. 3D coordinates of 10 landmarks were recorded on the 3D reconstructed mandibles of humans and mice and analyzed with geometric morphometric methods. Standardization for position, scale, and orientation was obtained by Procrustes superimposition (62)(63) and shape information (Procrustes coordinates) and size (centroid size (63)) were extracted. Shape information was subsequently analyzed by principal components analysis (PCA) (for more information on geometric morphometrics applied to craniofacial birth defect see for example (31)). Wireframes are used to visualize the shape differences between positive and negative values of principal component (PC) 1 corresponding to control and ACH mandibles respectively. Geometric morphometric analyses were run with Morpho J (64).

Whole-mount Alcian blue-alizarin red staining

Mandibles of *Fgfr3*$^{Y367C/+}$ mice and their wild type littermates at E16.5, E18.5, P0 and P21 were fixed in 95% ethanol and then stained with Alizarin Red and Alcian Blue, cleared

by KOH treatment, and stored in glycerol according to standard protocols. Size of the mandibles and the condyles were measured on images captured with an Olympus PD70-IX2-UCB using CellSens software (Olympus). Total length of the mandible was measured as well as the length of the condylar and symphyseal cartilages (identified with the alcian blue staining). The length of the body was calculated as the total length minus the condylar and symphyseal cartilages.

Immunohistochemistry

Mandibles of *Fgfr3*$^{Y367C/+}$ and their wild type littermates at E16.5, E18.5, P0 and P21 were fixed in 4% paraformaldehyde at 5°C for 24 hours and decalcified in 0.5 M EDTA (pH 8.0) overnight or up to one week, depending on the age of the mice, and then dehydrated in graded series of ethanol, cleared in xylenes and embedded in paraffin. 5 µm sagittal sections were cut and stained with hematoxylin and eosin (H&E), safranin-O or subjected to immunohistochemical staining using standard protocols using an antibody against Collagen X (1:50 dilution; BIOCYC, Luckenwalde, Germany), FGFR3 (1:250; Sigma-Aldrich Co, St. Louis, MO, USA) or Ki67 (1:3000; Abcam, Cambridge, MA, USA) using the Dako Envision kit (Dako North America, Inc, CA, USA). Images were captured with an Olympus PD70-IX2-UCB microscope (Olympus, Tokyo, Japan) and morphometry was performed with ImageJ software (National Institutes of Health, Bethesda, MD, USA).

Ex vivo experiments

Mandibles from WT and *Fgfr3*$^{Y367C/+}$ E16.5 embryos were dissected and cut at the symphysis to separate the two hemi-mandibles. For each embryo, the two hemi-mandibles were incubated for 5 days in DMEM medium with antibiotics and 0.2% BSA (Sigma), one supplemented with NVP-BGJ398 (100nM) while the other served as control and was supplemented with DMSO (0.1%). The length of the hemi-mandibles was measured at the end of time course, following whole-mount Alcian blue-alizarin red staining.

In vivo experiments

Fgfr3$^{Y367C/+}$ *mice* were 1 day old at treatment initiation and received daily subcutaneous administrations of NVP-BGJ398 at 2mg/kg body weight or vehicle (HCl 3.15 mM, DMSO 2%) for 15 days. Cartilage and bone analyses were thus performed in 16-d-old male and female mice. Experimental animal procedures and protocols were approved by the French Animal Care and Use Committee.

Statistical analysis

Differences between experimental groups were assessed using analysis of variance (ANOVA) or Mann-Whitney test. The significance threshold was set at $p \leq 0.05$. Statistical analyses were performed using GraphPad PRISM (v5) (GraphPad Software Inc., La Jolla, CA, USA). All values are shown as mean ± SD.

ACKNOWLEDGMENT AND FUNDING

We acknowledge the following sources of funding: Comité d'interface INSERM/Odontologie (MBD), YH was partly funded by the French National Agency of Research (ANR) through the program "Investissements d'avenir" (ANR-10-LABX-52). This project received a state subsidy managed by the National Research Agency under the "Investments for the Future" program bearing the reference ANR-10-IHU-01, the European Community's Seventh Framework Programme Under grant agreement no. 602300 (Sybil) and the Fondation des Gueules Cassées. We are grateful to the Association des Personnes de Petites Tailles.

CONFLICT OF INTEREST

IK, DGP and MK work for Novartis. The other authors have declared that no conflict of interest exists.

AUTHORS CONTRIBUTION

MBD, DKE, YH and LLM designed research. MBD, DKE, YH, VE, EG, NK and CBL performed research. IK, MK and DGP contributed new reagents. MZ and FDR contributed human data. MBD, YH and FDR analyzed mouse and human data. MBD, DKE, YH and LLM prepared the figures and wrote the manuscript.

REFERENCES

1. Baujat,G., Legeai-Mallet,L., Finidori,G., Cormier-Daire,V. and Le Merrer,M. (2008) Achondroplasia. *Best Pract. Res. Clin. Rheumatol.*, **22**, 3–18.
2. Horton,W.A., Hall,J.G. and Hecht,J.T. (2007) Achondroplasia. *Lancet*, **370**, 162–172.
3. Di Rocco,F., Biosse Duplan,M., Heuzé,Y., Kaci,N., Komla-Ebri,D., Munnich,A., Mugniery,E., Benoist-Lasselin,C. and Legeai-Mallet,L. (2014) FGFR3 mutation causes abnormal membranous ossification in achondroplasia. *Hum. Mol. Genet.*, **23**, 2914–2925.
4. Rousseau,F., Bonaventure,J., Legeai-Mallet,L., Pelet,A., Rozet,J.M., Maroteaux,P., Le Merrer,M. and Munnich,A. (1994) Mutations in the gene encoding fibroblast growth factor receptor-3 in achondroplasia. *Nature*, **371**, 252–254.
5. Ornitz,D.M. (2005) FGF signaling in the developing endochondral skeleton. *Cytokine Growth Factor Rev.*, **16**, 205–213.
6. Legeai-Mallet,L., Benoist-Lasselin,C., Munnich,A. and Bonaventure,J. (2004) Overexpression of FGFR3, Stat1, Stat5 and p21Cip1 correlates with phenotypic severity and defective chondrocyte differentiation in FGFR3-related chondrodysplasias. *Bone*, **34**, 26–36.
7. Wang,Q., Green,R.P., Zhao,G. and Ornitz,D.M. (2001) Differential regulation of endochondral bone growth and joint development by FGFR1 and FGFR3 tyrosine kinase domains. *Dev. Camb. Engl.*, **128**, 3867–3876.
8. Segev,O., Chumakov,I., Nevo,Z., Givol,D., Madar-Shapiro,L., Sheinin,Y., Weinreb,M. and Yayon,A. (2000) Restrained chondrocyte proliferation and maturation with abnormal growth plate vascularization and ossification in human FGFR-3(G380R) transgenic mice. *Hum. Mol. Genet.*, **9**, 249–258.
9. Matsushita,T., Wilcox,W.R., Chan,Y.Y., Kawanami,A., Bukulmez,H., Balmes,G., Krejci,P., Mekikian,P.B., Otani,K., Yamaura,I., *et al.* (2008) FGFR3 promotes synchondrosis closure and fusion of ossification centers through the MAPK pathway. *Hum. Mol. Genet.*, **18**, 227–240.
10. Pannier,S., Couloigner,V., Messaddeq,N., Elmaleh-Bergès,M., Munnich,A., Romand,R. and Legeai-Mallet,L. (2009) Activating Fgfr3 Y367C mutation causes hearing loss and inner ear defect in a mouse model of chondrodysplasia. *Biochim. Biophys. Acta*, **1792**, 140–147.
11. Komla-Ebri,D., Dambroise,E., Kramer,I., Benoist-Lasselin,C., Kaci,N., Le Gall,C., Martin,L., Busca,P., Barbault,F., Graus-Porta,D., *et al.* (2016) Tyrosine kinase inhibitor NVP-BGJ398 functionally improves FGFR3-related dwarfism in mouse model. *J. Clin. Invest.*, 10.1172/JCI83926.
12. Roberts,W.E. and Hartsfield,J.K. (2004) Bone development and function: genetic and environmental mechanisms. *Semin. Orthod.*, **10**, 100–122.
13. Dixon,A., Hoyte,D. and Rönning,O. (1997) Fundamentals of craniofacial growth Boca Raton : CRC Press.
14. Chen,H., Liu,C.T., Yang,S.S. and Opitz,J.M. (1981) Achondrogenesis: A review with special consideration of achondrogenesis type II (langer-saldino). *Am. J. Med. Genet.*, **10**, 379–394.
15. Mansour,S., Offiah,A.C., McDowall,S., Sim,P., Tolmie,J. and Hall,C. (2002) The phenotype of survivors of campomelic dysplasia. *J. Med. Genet.*, **39**, 597–602.
16. Schipani,E., Langman,C.B., Parfitt,A.M., Jensen,G.S., Kikuchi,S., Kooh,S.W., Cole,W.G. and Jüppner,H. (1996) Constitutively activated receptors for parathyroid hormone and parathyroid hormone-related peptide in Jansen's metaphyseal chondrodysplasia. *N. Engl. J. Med.*, **335**, 708–714.

17. Wilkie,A.O., Slaney,S.F., Oldridge,M., Poole,M.D., Ashworth,G.J., Hockley,A.D., Hayward,R.D., David,D.J., Pulleyn,L.J. and Rutland,P. (1995) Apert syndrome results from localized mutations of FGFR2 and is allelic with Crouzon syndrome. *Nat. Genet.*, **9**, 165–172.
18. Lajeunie,E., El Ghouzzi,V., Le Merrer,M., Munnich,A., Bonaventure,J. and Renier,D. (1999) Sex related expressivity of the phenotype in coronal craniosynostosis caused by the recurrent P250R FGFR3 mutation. *J. Med. Genet.*, **36**, 9–13.
19. Rice,D.P.C., Rice,R. and Thesleff,I. (2003) Fgfr mRNA isoforms in craniofacial bone development. *Bone*, **33**, 14–27.
20. Yu,K., Karuppaiah,K. and Ornitz,D.M. (2015) Mesenchymal fibroblast growth factor receptor signaling regulates palatal shelf elevation during secondary palate formation: Mesenchymal FGFR Regulates Palatal Shelf Elevation. *Dev. Dyn.*, **244**, 1427–1438.
21. Havens,B.A., Rodgers,B. and Mina,M. (2006) Tissue-specific expression of Fgfr2b and Fgfr2c isoforms, Fgf10 and Fgf9 in the developing chick mandible. *Arch. Oral Biol.*, **51**, 134–145.
22. Havens,B.A., Velonis,D., Kronenberg,M.S., Lichtler,A.C., Oliver,B. and Mina,M. (2008) Roles of FGFR3 during morphogenesis of Meckel's cartilage and mandibular bones. *Dev. Biol.*, **316**, 336–349.
23. de Frutos,C.A., Vega,S., Manzanares,M., Flores,J.M., Huertas,H., Martínez-Frías,M.L. and Nieto,M.A. (2007) Snail1 is a transcriptional effector of FGFR3 signaling during chondrogenesis and achondroplasias. *Dev. Cell*, **13**, 872–883.
24. Murray,S.A., Oram,K.F. and Gridley,T. (2007) Multiple functions of Snail family genes during palate development in mice. *Dev. Camb. Engl.*, **134**, 1789–1797.
25. Liu,Z., Lavine,K.J., Hung,I.H. and Ornitz,D.M. (2007) FGF18 is required for early chondrocyte proliferation, hypertrophy and vascular invasion of the growth plate. *Dev. Biol.*, **302**, 80–91.
26. Cohen,M.M., Walker,G.F. and Phillips,C. (1985) A morphometric analysis of the craniofacial configuration in achondroplasia. *J. Craniofac. Genet. Dev. Biol. Suppl.*, **1**, 139–165.
27. Cardoso,R., Ajzen,S., Andriolo,A.R., Oliveira,J.X. de and Andriolo,A. (2012) Analysis of the cephalometric pattern of Brazilian achondroplastic adult subjects. *Dent. Press J. Orthod.*, **17**, 118–129.
28. Tuncer,O., Caksen,H., Kirimi,E., Kayan,M., Ataş,B. and Odabaş,D. (2004) A case of thanatophoric dysplasia type I associated with mandibular clefting. *Genet. Couns. Geneva Switz.*, **15**, 95–97.
29. Ridgway,E.B., Wu,J.K., Sullivan,S.R., Vasudavan,S., Padwa,B.L., Rogers,G.F. and Mulliken,J.B. (2011) Craniofacial growth in patients with FGFR3Pro250Arg mutation after fronto-orbital advancement in infancy. *J. Craniofac. Surg.*, **22**, 455–461.
30. Guagnano,V., Furet,P., Spanka,C., Bordas,V., Le Douget,M., Stamm,C., Brueggen,J., Jensen,M.R., Schnell,C., Schmid,H., *et al.* (2011) Discovery of 3-(2,6-dichloro-3,5-dimethoxy-phenyl)-1-{6-[4-(4-ethyl-piperazin-1-yl)-phenylamino]-pyrimidin-4-yl}-1-methyl-urea (NVP-BGJ398), a potent and selective inhibitor of the fibroblast growth factor receptor family of receptor tyrosine kinase. *J. Med. Chem.*, **54**, 7066–7083.
31. Heuzé,Y., Boyadjiev,S.A., Marsh,J.L., Kane,A.A., Cherkez,E., Boggan,J.E. and Richtsmeier,J.T. (2010) New insights into the relationship between suture closure and craniofacial dysmorphology in sagittal nonsyndromic craniosynostosis. *J. Anat.*, **217**, 85–96.
32. Lorget,F., Kaci,N., Peng,J., Benoist-Lasselin,C., Mugniery,E., Oppeneer,T., Wendt,D.J., Bell,S.M., Bullens,S., Bunting,S., *et al.* (2012) Evaluation of the therapeutic potential of a

CNP analog in a Fgfr3 mouse model recapitulating achondroplasia. *Am. J. Hum. Genet.*, **91**, 1108–1114.
33. Frommer,J. and Margolies,M.R. (1971) Contribution of Meckel's cartilage to ossification of the mandible in mice. *J. Dent. Res.*, **50**, 1260–1267.
34. Shimo,T., Kanyama,M., Wu,C., Sugito,H., Billings,P.C., Abrams,W.R., Rosenbloom,J., Iwamoto,M., Pacifici,M. and Koyama,E. (2004) Expression and roles of connective tissue growth factor in Meckel's cartilage development. *Dev. Dyn. Off. Publ. Am. Assoc. Anat.*, **231**, 136–147.
35. Jonquoy,A., Mugniery,E., Benoist-Lasselin,C., Kaci,N., Le Corre,L., Barbault,F., Girard,A.-L., Le Merrer,Y., Busca,P., Schibler,L., *et al.* (2012) A novel tyrosine kinase inhibitor restores chondrocyte differentiation and promotes bone growth in a gain-of-function Fgfr3 mouse model. *Hum. Mol. Genet.*, **21**, 841–851.
36. Kronenberg,H.M. (2003) Developmental regulation of the growth plate. *Nature*, **423**, 332–336.
37. Delezoide,A.L., Benoist-Lasselin,C., Legeai-Mallet,L., Le Merrer,M., Munnich,A., Vekemans,M. and Bonaventure,J. (1998) Spatio-temporal expression of FGFR 1, 2 and 3 genes during human embryo-fetal ossification. *Mech. Dev.*, **77**, 19–30.
38. Ishizeki,K., Saito,H., Shinagawa,T., Fujiwara,N. and Nawa,T. (1999) Histochemical and immunohistochemical analysis of the mechanism of calcification of Meckel's cartilage during mandible development in rodents. *J. Anat.*, **194 (Pt 2)**, 265–277.
39. Sakakura,Y. (2010) Role of Matrix Metalloproteinases in Extracellular Matrix Disintegration of Meckel's Cartilage in Mice. *J. Oral Biosci.*, **52**, 143–149.
40. Pannier,S., Mugniery,E., Jonquoy,A., Benoist-Lasselin,C., Odent,T., Jais,J.-P., Munnich,A. and Legeai-Mallet,L. (2010) Delayed bone age due to a dual effect of FGFR3 mutation in Achondroplasia. *Bone*, **47**, 905–915.
41. Pirttiniemi,P., Peltomäki,T., Müller,L. and Luder,H.U. (2009) Abnormal mandibular growth and the condylar cartilage. *Eur. J. Orthod.*, **31**, 1–11.
42. Shen,G. and Darendeliler,M.A. (2005) The adaptive remodeling of condylar cartilage--a transition from chondrogenesis to osteogenesis. *J. Dent. Res.*, **84**, 691–699.
43. Obwegeser,H.L. (2001) Mandibular Growth Anomalies Springer Berlin Heidelberg, Berlin, Heidelberg.
44. Vajo,Z., Francomano,C.A. and Wilkin,D.J. (2000) The molecular and genetic basis of fibroblast growth factor receptor 3 disorders: the achondroplasia family of skeletal dysplasias, Muenke craniosynostosis, and Crouzon syndrome with acanthosis nigricans. *Endocr. Rev.*, **21**, 23–39.
45. Naski,M.C., Colvin,J.S., Coffin,J.D. and Ornitz,D.M. (1998) Repression of hedgehog signaling and BMP4 expression in growth plate cartilage by fibroblast growth factor receptor 3. *Dev. Camb. Engl.*, **125**, 4977–4988.
46. Yasuda,T., Nah,H.D., Laurita,J., Kinumatsu,T., Shibukawa,Y., Shibutani,T., Minugh-Purvis,N., Pacifici,M. and Koyama,E. (2012) Muenke syndrome mutation, FgfR3P^{244}R, causes TMJ defects. *J. Dent. Res.*, **91**, 683–689.
47. Harada,Y. and Ishizeki,K. (1998) Evidence for transformation of chondrocytes and site-specific resorption during the degradation of Meckel's cartilage. *Anat. Embryol. (Berl.)*, **197**, 439–450.
48. Bi,W., Huang,W., Whitworth,D.J., Deng,J.M., Zhang,Z., Behringer,R.R. and de Crombrugghe,B. (2001) Haploinsufficiency of Sox9 results in defective cartilage primordia and premature skeletal mineralization. *Proc. Natl. Acad. Sci. U. S. A.*, **98**, 6698–6703.
49. Wang,Y., Spatz,M.K., Kannan,K., Hayk,H., Avivi,A., Gorivodsky,M., Pines,M., Yayon,A.,

Lonai,P. and Givol,D. (1999) A mouse model for achondroplasia produced by targeting fibroblast growth factor receptor 3. *Proc. Natl. Acad. Sci. U. S. A.*, **96**, 4455–4460.
50. Cooper,K.L., Oh,S., Sung,Y., Dasari,R.R., Kirschner,M.W. and Tabin,C.J. (2013) Multiple phases of chondrocyte enlargement underlie differences in skeletal proportions. *Nature*, **495**, 375–378.
51. Wang,Y., Nishida,S., Sakata,T., Elalieh,H.Z., Chang,W., Halloran,B.P., Doty,S.B. and Bikle,D.D. (2006) Insulin-like growth factor-I is essential for embryonic bone development. *Endocrinology*, **147**, 4753–4761.
52. Sugito,H., Shibukawa,Y., Kinumatsu,T., Yasuda,T., Nagayama,M., Yamada,S., Minugh-Purvis,N., Pacifici,M. and Koyama,E. (2011) Ihh signaling regulates mandibular symphysis development and growth. *J. Dent. Res.*, **90**, 625–631.
53. Iwata,T., Chen,L., Li,C., Ovchinnikov,D.A., Behringer,R.R., Francomano,C.A. and Deng,C.X. (2000) A neonatal lethal mutation in FGFR3 uncouples proliferation and differentiation of growth plate chondrocytes in embryos. *Hum. Mol. Genet.*, **9**, 1603–1613.
54. Narayana,J. and Horton,W.A. (2015) FGFR3 biology and skeletal disease. *Connect. Tissue Res.*, **56**, 427–433.
55. Legeai-Mallet,L., Benoist-Lasselin,C., Delezoide,A.L., Munnich,A. and Bonaventure,J. (1998) Fibroblast growth factor receptor 3 mutations promote apoptosis but do not alter chondrocyte proliferation in thanatophoric dysplasia. *J. Biol. Chem.*, **273**, 13007–13014.
56. Mugniery,E., Dacquin,R., Marty,C., Benoist-Lasselin,C., de Vernejoul,M.-C., Jurdic,P., Munnich,A., Geoffroy,V. and Legeai-Mallet,L. (2012) An activating Fgfr3 mutation affects trabecular bone formation via a paracrine mechanism during growth. *Hum. Mol. Genet.*, **21**, 2503–2513.
57. Benko,S., Fantes,J.A., Amiel,J., Kleinjan,D.-J., Thomas,S., Ramsay,J., Jamshidi,N., Essafi,A., Heaney,S., Gordon,C.T., *et al.* (2009) Highly conserved non-coding elements on either side of SOX9 associated with Pierre Robin sequence. *Nat. Genet.*, **41**, 359–364.
58. Berraquero,R., Palacios,J. and Rodríguez,J.I. (1992) The role of the condylar cartilage in mandibular growth. A study in thanatophoric dysplasia. *Am. J. Orthod. Dentofac. Orthop. Off. Publ. Am. Assoc. Orthod. Its Const. Soc. Am. Board Orthod.*, **102**, 220–226.
59. Cottrell,D.A., Edwards,S.P. and Gotcher,J.E. (2012) Surgical correction of maxillofacial skeletal deformities. *J. Oral Maxillofac. Surg. Off. J. Am. Assoc. Oral Maxillofac. Surg.*, **70**, e107–136.
60. Shirley,E.D. and Ain,M.C. (2009) Achondroplasia: manifestations and treatment. *J. Am. Acad. Orthop. Surg.*, **17**, 231–241.
61. Metzger,D., Clifford,J., Chiba,H. and Chambon,P. (1995) Conditional site-specific recombination in mammalian cells using a ligand-dependent chimeric Cre recombinase. *Proc. Natl. Acad. Sci. U. S. A.*, **92**, 6991–6995.
62. Rohlf,F.J. and Slice,D. (1990) Extensions of the Procrustes Method for the Optimal Superimposition of Landmarks. *Syst. Biol.*, **39**, 40–59.
63. Dryden,I. and Mardia,K. (1998) Statistical Shape Analysis Wiley.
64. Klingenberg,C.P. (2011) MorphoJ: an integrated software package for geometric morphometrics. *Mol. Ecol. Resour.*, **11**, 353–357.

LEGENDS

Figure 1. **FGFR3 over activation in humans and mice results in mandibular hypoplasia and dysmorphogenesis.** (A) 3D reconstructed CT images with volume rendering of a control and ACH patient (scale bar = 1cm). (B) Mandible length, measured as the distance between condylion (Co) and gnathion (Gn) on sagittal sections of 3D reconstructed CT images of controls (n= 9, mean age: 24.9 months) or ACH patients (n=8, mean age: 21.3 months) and plotted against the age of the children. (C) Landmarks and associated wireframes measured on the 3D reconstructed human mandibles and corresponding superimposition of the control and ACH wireframes computed on the basis of PC scores along PC1, the PC best separating the two groups and accounting for 47% of total shape variance. (D) & (E) Mandible length of embryos (E16.5 and E18.5), new born and 3 weeks-old WT and *Fgfr3*$^{Y367C/+}$ mice (n≥6 individuals for each age and genotype), measured following alcian blue and alizarin red staining between the condylar and symphyseal ends (marked with *) (scale bar = 1mm). (F) Landmarks and associated wireframes measured on the 3D reconstructed mouse mandibles and corresponding superimposition of the control and *Fgfr3*$^{Y367C/+}$ wireframes computed on the basis of PC scores along PC1, the PC best separating the two groups and accounting for 78% of total shape variance. Data shown as mean with SD; * p<0.05, ***p<0.005.

Figure 2. **Chondrocytes homeostasis is disturbed in Meckel's cartilage of *Fgfr3*$^{Y367C/+}$ mice.** (A) Histological staining (Safranin'O) and immunostaining for Collagen X, Ki67 (proliferation marker) and Fgfr3 of MC of WT and *Fgfr3*$^{Y367C/+}$ E16.5 embryos. An enlargement of the ColX immunostaining (red box) highlights the modification in the size of hypertrophic chondrocytes in *Fgfr3*$^{Y367C/+}$ embryos (scale bar = 200µm). Area delimited with doted lines on the ColX panel corresponds to the hyperthrophic zone. Areas delimited with doted lines on the Ki67 and Fgfr3 panels correspond to immunonegative zones (respectively non-proliferative and Fgfr3-negative). Enlargements of the Ki67 and Fgfr3 immunostainings (red box) highlight the limits of the positive and negative zones. (B) Measurement of the ColX positive zone inside MC of WT and *Fgfr3*$^{Y367C/+}$ E16.5 embryos (n≥7 individuals for each genotype). (C) Mean percentage of hypertrophic chondrocytes for different size categories (expressed in µm^2) inside MC of WT and *Fgfr3*$^{Y367C/+}$ E16.5 embryos (n≥50 cells from n≥6 individuals for each genotype). (D) Mean number of immuno-positive cells for Fgfr3 or Ki67 inside MC of WT and *Fgfr3*$^{Y367C/+}$ E16.5 embryos (n≥7 individuals for each genotype). (E) Histological staining (Safranin'O) of WT and *Fgfr3*$^{Y367C/+}$ E18.5 embryos (scale bar = 200µm). (F) Mean cartilage area, measured on sagittal sections of MC in WT and *Fgfr3*$^{Y367C/+}$ E16.5 and E18.5 embryos (n≥7 individuals for each age and genotype). Data shown as mean with SD; *p<0.05, **p<0.01, ***p<0.005.

Figure 3. **FGFR3 over activation in humans and mice results in condyle hypoplasia.** (A) Representative sagittal sections of a control and ACH child, both 17 months of age, generated from the CT scans (scale bar = 1cm). (B) Condylar neck length, measured on CT scans sagittal sections of controls (n= 14, mean age= 32.4 months) or ACH patients (n= 12, mean age= 32.4 months) and plotted against the age of the children. (C) Representative macroscopic views of condyles of 3 weeks old WT and *Fgfr3*$^{Y367C/+}$ mice, following alcian blue and alizarin red staining (scale bars = 2mm and 1mm). (D) Condylar neck length of 3 weeks-old WT and *Fgfr3*$^{Y367C/+}$ mice, measured following alcian blue and alizarin red staining (n≥6 individuals for each genotype) (E) & (F)

Histological staining (Safranin'O) and immunostaining for Collagen X of the condylar cartilage of WT and *Fgfr3*$^{Y367C/+}$ E16.5 embryos (E) and 3 weeks old mice (F) (scale bar = 100μm). An enlargement of the ColX immunostaining (black box) highlights the modification in the size of hypertrophic chondrocytes in *Fgfr3*$^{Y367C/+}$ embryos and P21 mice. (G) & (H) Mean percentage of hypertrophic chondrocytes for different size categories (expressed in μm^2) inside the condylar cartilage of WT and *Fgfr3*$^{Y367C/+}$ E16.5 embryos (G) and 3 weeks old mice (H) (n≥ 50 cells from n≥6 individuals for each age and genotype). Data shown as mean with SD; **p<0.01, ***p<0.005.

Figure 4. **NVP-BGJ398 corrects primary and secondary cartilages defects in *ex vivo* cultures of mandibles from *Fgfr3*$^{Y367C/+}$ embryos.** (A) Representative macroscopic views of hemi mandibles from E16.5 WT or *Fgfr3*$^{Y367C/+}$ embryos, treated with DMSO or NVP-BGJ398 and cultured for 6 days, following alcian blue and alizarin red staining. Symphyseal (s), condylar (c) and Meckel's (m) cartilages are indicated. (B) Mandibular body and condylar neck length of cultured hemi mandibles (n≥5 individuals for each genotype and treatment). Total length of the hemi-mandible was measured as well as the length of the condylar and symphyseal cartilages (identified with the alcian blue staining). The length of the body was calculated as the total length minus the condylar and symphyseal cartilages. (C) Histological staining (Safranin'O) and immunostaining for ColX of cultured hemi mandibles. An enlargement of the ColX immunostaining highlights the modification in the size of hypertrophic chondrocytes in MC of *Fgfr3*$^{Y367C/+}$ embryos and the correction of the defect with NVP-BGJ398 (scale bar = 200μm). (D) Measurement of the ColX positive zone inside MC of cultured hemi mandibles (n≥6 individuals for each genotype and treatment). (E) Mean percentage of hypertrophic chondrocytes for different size categories (expressed in μm^2) inside MC of cultured hemi mandibles (n≥50 cells from n≥5 individuals for each genotype and treatment). (F) Mean number of immune positive cells for Fgfr3 or Ki67 inside MC of WT, *Fgfr3*$^{Y367C/+}$ DMSO and *Fgfr3*$^{Y367C/+}$ NVP-BGJ398 E16.5 embryos (n≥5 individuals for each genotype). (G) Histological staining (Safranin'O) and immunostaining for Collagen X of cultured hemi mandibles condylar cartilage (scale bar = 100μm). Meckel's cartilage (m) is indicated. (H) Mean percentage of hypertrophic chondrocytes for different size categories (expressed in μm^2) inside condylar cartilage of cultured hemi mandibles (n≥50 cells from n≥5 individuals for each genotype and treatment). Data shown as mean with SD; *p<0.05, **p<0.01.

Figure 5. **NVP-BGJ398 improves *in vivo* condyle growth of *Fgfr3*$^{Y367C/+}$ mice.** (A) Representative 3D reconstructions of 16 days old WT and *Fgfr3*$^{Y367C/+}$ mice treated with DMSO or NVP-BGJ398 for 15 days since P01 (scale bar = 1mm). (B) Measurement of the mandible body and the condyle length and width of WT and *Fgfr3*$^{Y367C/+}$ mice treated with DMSO or NVP-BGJ398 (n≥6 individuals for each genotype and treatment). Total length of the mandible was measured as well as the length of the condyle. The length of the body was calculated as the total length minus the condyle. (C) & (D) PCA of the Procrustes shape coordinates of the landmarks measured on mandibles of WT and *Fgfr3*$^{Y367C/+}$ mice treated with DMSO or NVP-BGJ398 and corresponding superimposition (n≥6 individuals for each genotype and treatment). Data shown as mean with SD; ***p<0.005.

Figure 6. **NVP-BGJ398 improves *in vivo* the chondrocyte differentiation in condyle of *Fgfr3*$^{Y367C/+}$ mice.** Histological staining (Safranin'O) (A) and immunostaining for

collagen X (B) of condylar cartilage of 16 days old WT and *Fgfr3*$^{Y367C/+}$ mice treated with DMSO or NVP-BGJ398 for 15 days since P01 (scale bar = 100μm).

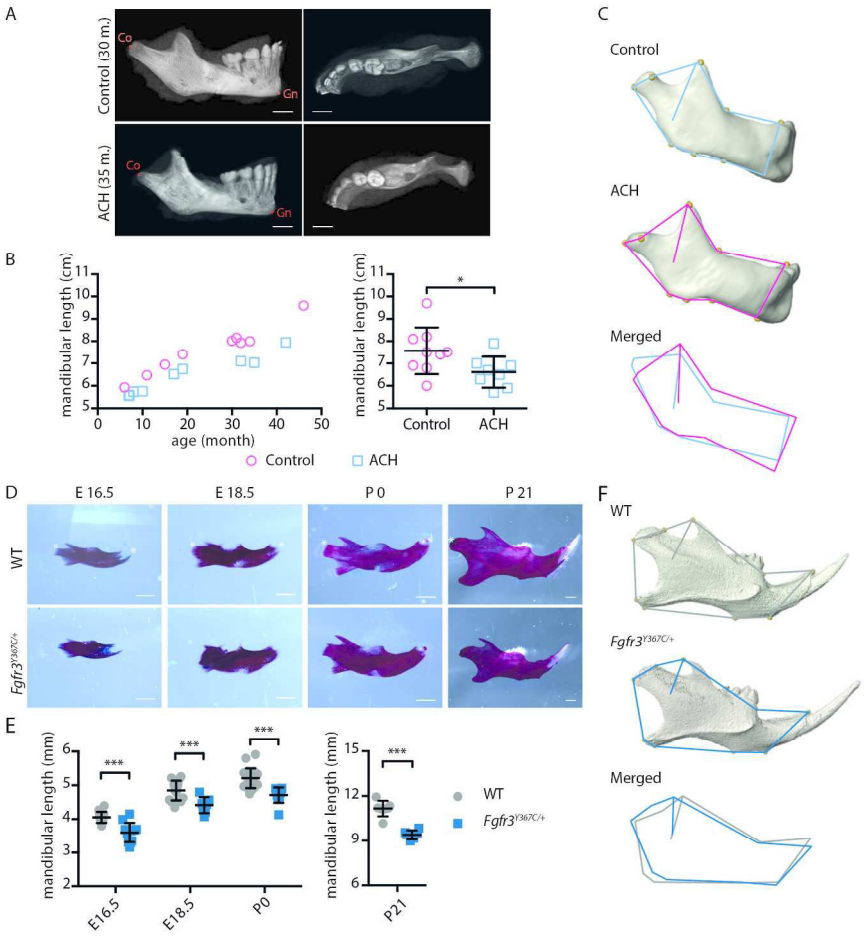

FGFR3 over activation in humans and mice results in mandibular hypoplasia and dysmorphogenesis. (A) 3D reconstructed CT images with volume rendering of a control and ACH patient (scale bar = 1cm). (B) Mandible length, measured as the distance between condylion (Co) and gnathion (Gn) on sagittal sections of 3D reconstructed CT images of controls (n= 9, mean age: 24.9 months) or ACH patients (n=8, mean age: 21.3 months) and plotted against the age of the children. (C) Landmarks and associated wireframes measured on the 3D reconstructed human mandibles and corresponding superimposition of the control and ACH wireframes computed on the basis of PC scores along PC1, the PC best separating the two groups and accounting for 47% of total shape variance. (D) & (E) Mandible length of embryos (E16.5 and E18.5), new born and 3 weeks-old WT and Fgfr3Y367C/+ mice (n≥6 individuals for each age and genotype), measured following alcian blue and alizarin red staining between the condylar and symphyseal ends (marked with *) (scale bar = 1mm). (F) Landmarks and associated wireframes measured on the 3D reconstructed mouse mandibles and corresponding superimposition of the control and Fgfr3Y367C/+ wireframes computed on the basis of PC scores along PC1, the PC best separating the two groups and accounting for 78% of total shape variance. Data shown as mean with SD; * p<0.05, ***p<0.005.
223x216mm (300 x 300 DPI)

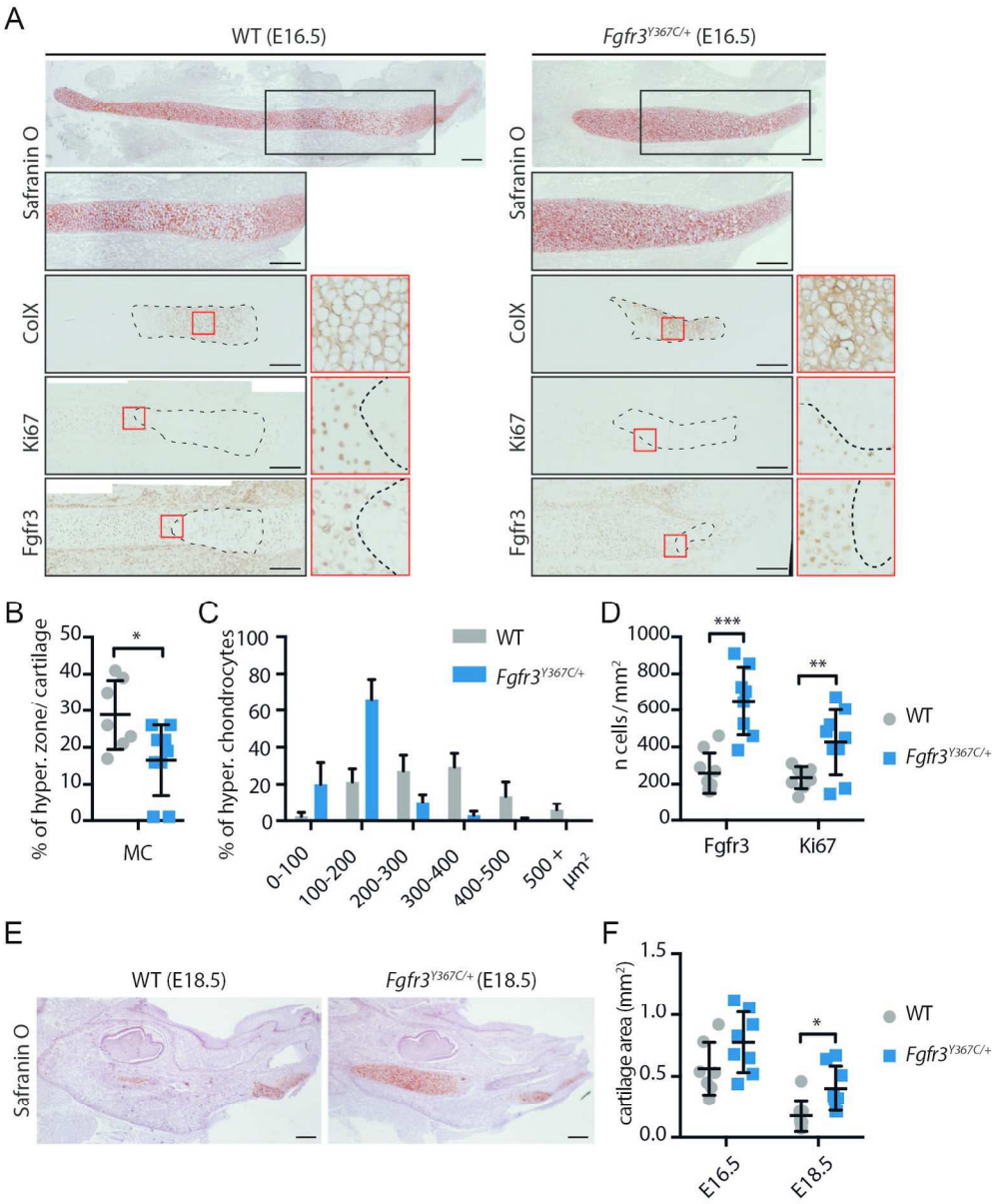

Chondrocytes homeostasis is disturbed in Meckel's cartilage of Fgfr3Y367C/+ mice. (A) Histological staining (Safranin'O) and immunostaining for Collagen X, Ki67 (proliferation marker) and Fgfr3 of MC of WT and Fgfr3Y367C/+ E16.5 embryos. An enlargement of the ColX immunostaining (red box) highlights the modification in the size of hypertrophic chondrocytes in Fgfr3Y367C/+ embryos (scale bar = 200µm). Area delimited with doted lines on the ColX panel corresponds to the hyperthrophic zone. Areas delimited with doted lines on the Ki67 and Fgfr3 panels correspond to immunonegative zones (respectively non-proliferative and Fgfr3-negative). Enlargements of the Ki67 and Fgfr3 immunostainings (red box) highlight the limits of the positive and negative zones. (B) Measurement of the ColX positive zone inside MC of WT and Fgfr3Y367C/+ E16.5 embryos (n≥7 individuals for each genotype). (C) Mean percentage of hypertrophic chondrocytes for different size categories (expressed in µm2) inside MC of WT and Fgfr3Y367C/+ E16.5 embryos (n≥50 cells from n≥6 individuals for each genotype). (D) Mean number of immuno-positive cells for Fgfr3 or Ki67 inside MC of WT and Fgfr3Y367C/+ E16.5 embryos (n≥7 individuals for each genotype). (E) Histological staining (Safranin'O) of WT and Fgfr3Y367C/+ E18.5 embryos (scale bar = 200µm). (F)

Mean cartilage area, measured on sagittal sections of MC in WT and Fgfr3Y367C/+ E16.5 and E18.5 embryos (n≥7 individuals for each age and genotype). Data shown as mean with SD; *p<0.05, **p<0.01, ***p<0.005.
160x194mm (300 x 300 DPI)

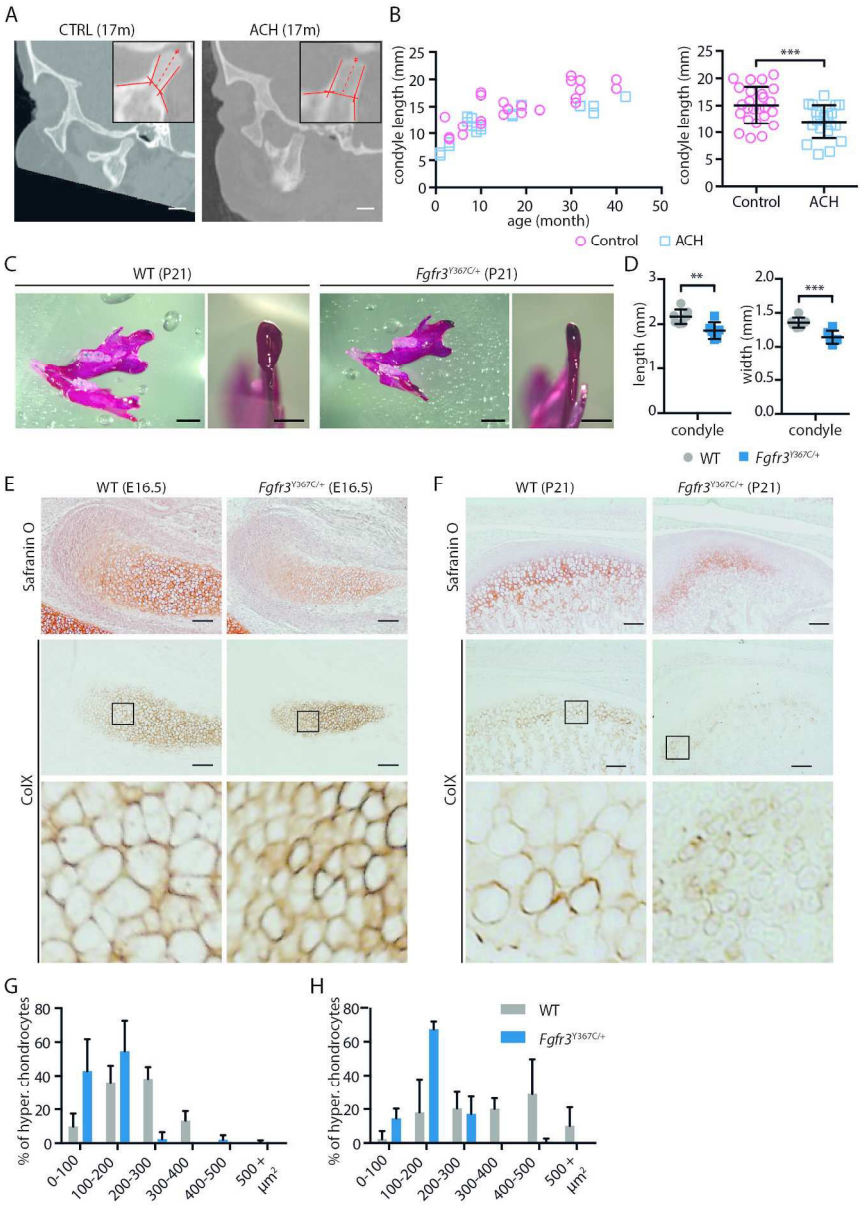

FGFR3 over activation in humans and mice results in condyle hypoplasia. (A) Representative sagittal sections of a control and ACH child, both 17 months of age, generated from the CT scans (scale bar = 1cm). (B) Condylar neck length, measured on CT scans sagittal sections of controls (n= 14, mean age= 32.4 months) or ACH patients (n= 12, mean age= 32.4 months) and plotted against the age of the children. (C) Representative macroscopic views of condyles of 3 weeks old WT and Fgfr3Y367C/+ mice, following alcian blue and alizarin red staining (scale bars = 2mm and 1mm). (D) Condylar neck length of 3 weeks-old WT and Fgfr3Y367C/+ mice, measured following alcian blue and alizarin red staining (n≥6 individuals for each genotype) (E) & (F) Histological staining (Safranin'O) and immunostaining for Collagen X of the condylar cartilage of WT and Fgfr3Y367C/+ E16.5 embryos (E) and 3 weeks old mice (F) (scale bar = 100µm). An enlargement of the ColX immunostaining (black box) highlights the modification in the size of hypertrophic chondrocytes in Fgfr3Y367C/+ embryos and P21 mice. (G) & (H) Mean percentage of hypertrophic chondrocytes for different size categories (expressed in µm2) inside the condylar cartilage of WT and Fgfr3Y367C/+ E16.5 embryos (G) and 3 weeks old mice (H) (n≥ 50 cells from n≥6 individuals for each age

and genotype). Data shown as mean with SD; **p<0.01, ***p<0.005.
189x265mm (300 x 300 DPI)

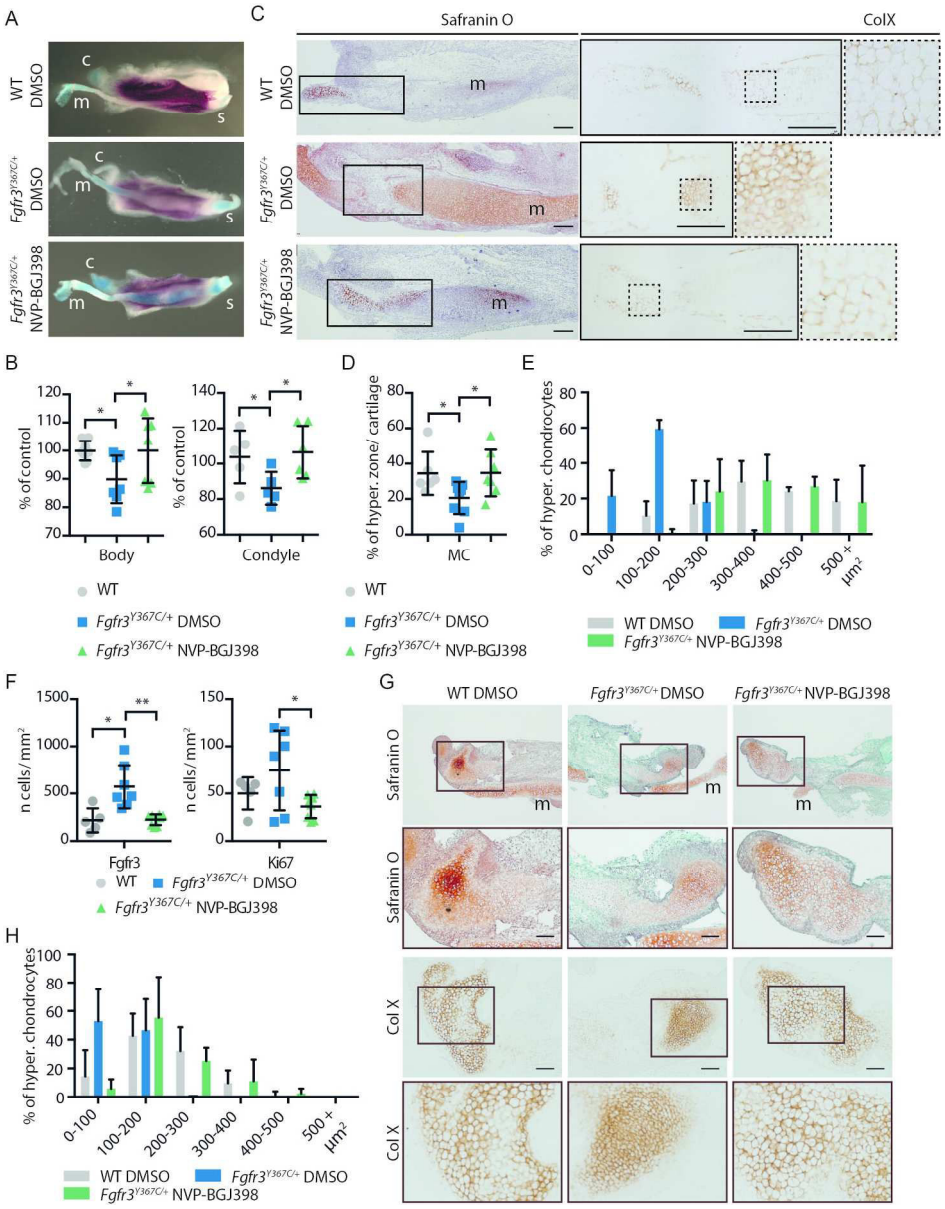

NVP-BGJ398 corrects primary and secondary cartilages defects in ex vivo cultures of mandibles from Fgfr3Y367C/+ embryos. (A) Representative macroscopic views of hemi mandibles from E16.5 WT or Fgfr3Y367C/+ embryos, treated with DMSO or NVP-BGJ398 and cultured for 6 days, following alcian blue and alizarin red staining. Symphyseal (s), condylar (c) and Meckel's (m) cartilages are indicated. (B) Mandibular body and condylar neck length of cultured hemi mandibles (n≥5 individuals for each genotype and treatment). Total length of the hemi-mandible was measured as well as the length of the condylar and symphyseal cartilages (identified with the alcian blue staining). The length of the body was calculated as the total length minus the condylar and symphyseal cartilages. (C) Histological staining (Safranin'O) and immunostaining for ColX of cultured hemi mandibles. An enlargement of the ColX immunostaining highlights the modification in the size of hypertrophic chondrocytes in MC of Fgfr3Y367C/+ embryos and the correction of the defect with NVP-BGJ398 (scale bar = 200µm). (D) Measurement of the ColX positive zone inside MC of cultured hemi mandibles (n≥6 individuals for each genotype and treatment). (E) Mean percentage of hypertrophic chondrocytes for different size categories (expressed in µm2) inside MC of cultured hemi

mandibles (n≥50 cells from n≥5 individuals for each genotype and treatment). (F) Mean number of immune positive cells for Fgfr3 or Ki67 inside MC of WT, Fgfr3Y367C/+ DMSO and Fgfr3Y367C/+ NVP-BGJ398 E16.5 embryos (n≥5 individuals for each genotype). (G) Histological staining (Safranin'O) and immunostaining for Collagen X of cultured hemi mandibles condylar cartilage (scale bar = 100μm). Meckel's cartilage (m) is indicated. (H) Mean percentage of hypertrophic chondrocytes for different size categories (expressed in μm2) inside condylar cartilage of cultured hemi mandibles (n≥50 cells from n≥5 individuals for each genotype and treatment). Data shown as mean with SD; *p<0.05, **p<0.01.
197x252mm (300 x 300 DPI)

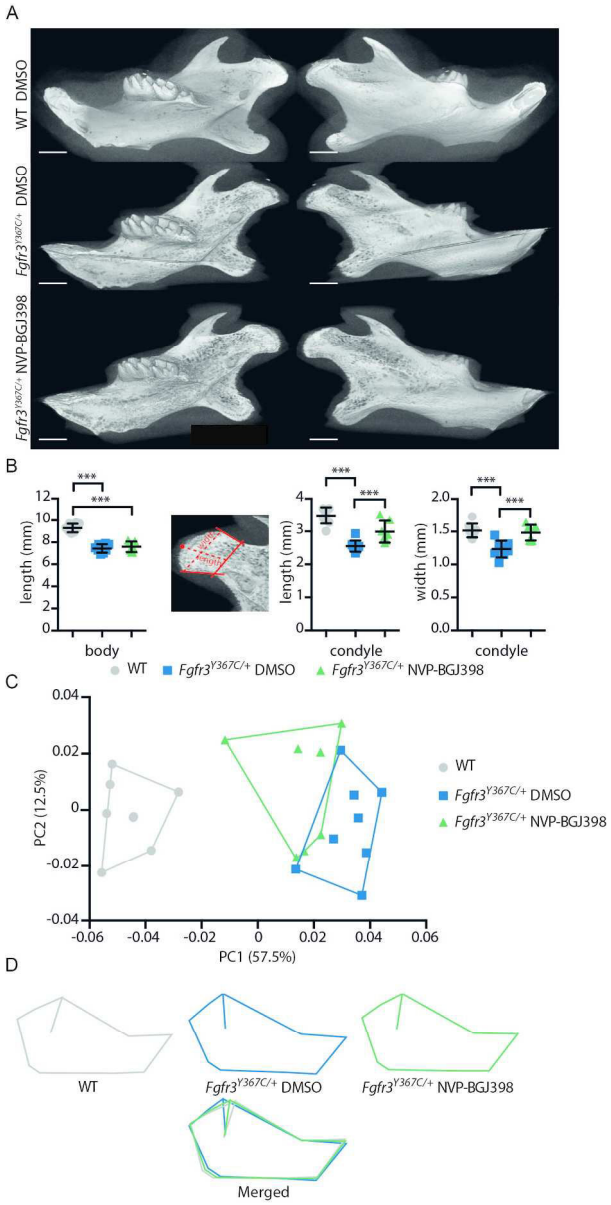

NVP-BGJ398 improves in vivo condyle growth of Fgfr3Y367C/+ mice. (A) Representative 3D reconstructions of 16 days old WT and Fgfr3Y367C/+ mice treated with DMSO or NVP-BGJ398 for 15 days since P01 (scale bar = 1mm). (B) Measurement of the mandible body and the condyle length and width of WT and Fgfr3Y367C/+ mice treated with DMSO or NVP-BGJ398 (n≥6 individuals for each genotype and treatment). Total length of the mandible was measured as well as the length of the condyle. The length of the body was calculated as the total length minus the condyle. (C) & (D) PCA of the Procrustes shape coordinates of the landmarks measured on mandibles of WT and Fgfr3Y367C/+ mice treated with DMSO or NVP-BGJ398 and corresponding superimposition (n≥6 individuals for each genotype and treatment). Data shown as mean with SD; ***p<0.005.
135x271mm (300 x 300 DPI)

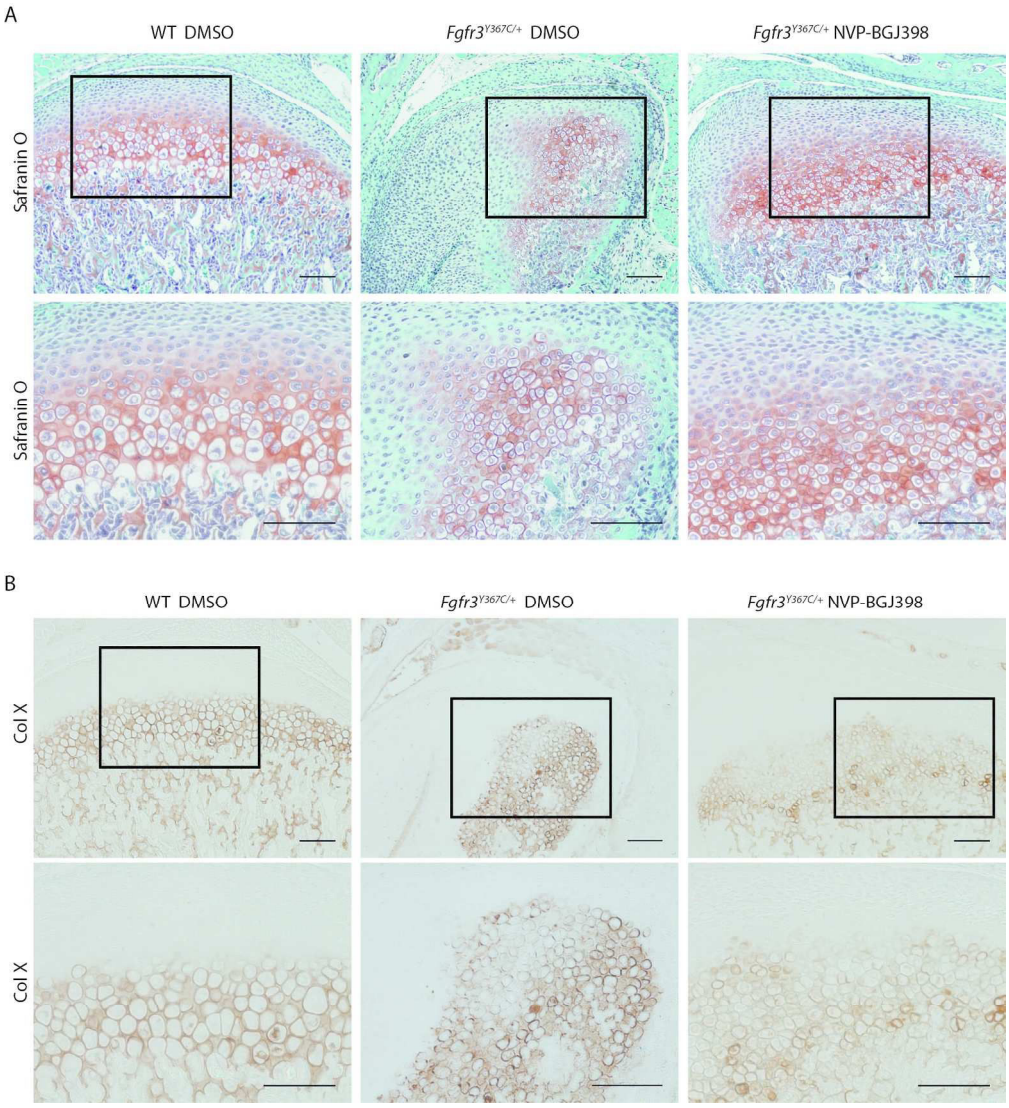

NVP-BGJ398 improves in vivo the chondrocyte differentiation in condyle of Fgfr3Y367C/+ mice. Histological staining (Safranin'O) (A) and immunostaining for collagen X (B) of condylar cartilage of 16 days old WT and Fgfr3Y367C/+ mice treated with DMSO or NVP-BGJ398 for 15 days since P01 (scale bar = 100µm).
189x207mm (300 x 300 DPI)

Preliminary data - Best understanding of structural and functional impact of FGFR3 mutations at the same position (K650N, K650M, K650E) leading to both mild and lethal dwarfism

Best understanding of structural and functional impact of FGFR3 mutations at the same position (K650N, K650M, K650E) leading to both mild and lethal dwarfism.

Davide KOMLA EBRI[1], Emilie DAMBROISE[1], Catherine BENOIST-LASSELIN[1], Nabil KACI[1], Patricia BUSCA[2], Florent BARBAULT[3], Laurence LEGEAI-MALLET[1]

[1]INSERM U1163, Université Paris Descartes, Sorbonne Paris Cité, Institut Imagine, 75015 Paris, France

[2]University Paris Descartes, UMR 8601 CNRS, Paris, France.

[3]University Paris Diderot, Sorbonne Paris Cité, ITODYS, UMR CNRS 7086, Paris, France

ABSTRACT

Three different missense mutations in the tyrosine kinase domain of Fibroblast Growth Factor Receptor 3 (FGFR3) affecting a lysine residue at position 650 lead to dwarfism with a spectrum of severity, hypochondroplasia (p.Lys650Asn), severe achondroplasia with developmental delay and acanthosis nigricans (p.Lys650Met), and thanatophoric dysplasia (p.Lys650Glu). Fgfr3 mutations induce a constitutive activation of the receptor characterized by a different sustained phosphorylation. To understand the severity of the clinical phenotype, we developed computational and biological studies. Computational studies were conducted to get an atomic description of the various phenotypes. The FGFR3K650M, FGFR3K650E and FGFRK650N were built using a validated structural model of the FGFR3 kinase domain. Structural analyses indicate that the salt bridge between R655 and E686 represents the FGFR3 kinase autoinhibitory molecular brake. This salt bridge is, significantly, disturbed with Lys650Glu mutation and is destroyed with Lys650Met and Lys650Asn mutants. There is a qualitative correlation with the severity of the clinical phenotype. We evaluated also the impact of the FGFR3 mutants on signaling pathways. Transient transfections of DNA mutants at position 650 in control human growth plate chondrocyte line show higher FGFR3 phosphorylation levels compared to FGFR3WT. The level of FGFR3 phosphorylation is correlated with the severity of the disease. Studying FGFR3 downstream signaling pathway, we observed the overactivation of the Mapkinase and PLCγ pathways in all mutants. Moreover different expressions of β-catenin and Adamts5 were observed in K650 mutants compared to WT. In conclusion, Lys650 mutation alters differently the conformation of the kinase domain thus leading to activate different signalling pathways. Various biological mechanisms seem to be responsible for moderate, severe and lethal dwarfism.

INTRODUCTION

In this study, we evaluated the changes in the FGFR3 molecular structure for Lys650N, Lys650Met and Lys650Glu mutants *in silico*. We observed protein conformational modifications that rationalize the mutant over-phosphorylation level. We then performed *in vitro* analyses using a human growth plate chondrocyte line transfected with the FGFR3 mutants to outline the outcome of the three activating mutations on signaling pathways. We confirmed the over-activation of FGFR3 canonical signaling pathways and we found interesting differences in β-catenin and "A disintegrin and metalloproteinase with thrombospondin motifs 5" (Adamts5) protein expression levels between the three mutants. The association of these data may provide clues on the molecular system behind the escalating severity of the pathological hallmarks. Activating mutations of Fibroblast Growth Factor Receptor 3 (FGFR3) are responsible for a family of chondrodysplasias marked by both endochondral and membranous bone defects (Vajo et al., 2000). Gain-of-function mutations in FGFR3 lead to the receptor over-activation determining alterations in the balance of chondrocyte proliferation and differentiation at the growth plate cartilage level (Legeai-Mallet et al., 2004). Different FGFR3 mutations lead to distinct pathologies such as chondrodysplasias and craniosynostoses affecting appendicular and axial skeleton or skull respectively (Ornitz and Marie, 2015). Nonetheless the effects due to the different mutations on the cartilage and bone signaling pathways are not well understood. In an effort to deepen our knowledge of the molecular pattern underlying the FGFR3 pathological activation we decided to study the molecular aspects of three FGFR3-related diseases: Hypochondroplasia (HCH), Severe Achondroplasia with Development Delay and Acanthosis Nigricans (SADDAN) and Thanatophoric Dysplasia type 2 (TDII).

HCH is the milder form of FGFR3-related chondrodysplasia, characterized by a rhizomelic dwarfism with short limbs, macrocephaly and lumbar lordosis (Bober et al., 1993). These pathological features are very similar to those observed in achondroplasia (ACH), but tend to be more moderate. SADDAN is a viable severe form of dwarfism due to the gain-of-function mutation in FGFR3. SADDAN patients develop a characteristic skin lesion named acanthosis nigricans (Bellus et al., 1999). TD is a dwarfism, that occurs with an estimated incidence closer to 1/20000 live

births, defined by its severity and perinatal lethality. Two types of TD are clinically diagnosed: TD type 1 (TDI) show prominently curved femurs, while TDII patients display typically straight femurs (Karczeski and Cutting, 1993; Maroteaux et al., 1967).

HCH, SADDAN and TDII present different phenotypic aspects. However, they share a particular common trait: the three chondrodysplasias are due to a missense mutation localized on the same Lys650 amino acid residue of FGFR3. In fact the substitution p.Lys650Asn has been detected in HCH patients, p.Lys650M mutation has been reported to be at the origin of SADDAN while all TDII individuals present the amino acid change p.Lys650Glu (Bellus et al., 1999, 2000; Leonard, 2016; Tavormina et al., 1999). Thus we decide to explore the substitution of Lys650 as a model to better understand the molecular pathways inducing such different disorders.

In this study, we evaluated the changes in the FGFR3 molecular structure for Lys650N, Lys650Met and Lys650Glu mutants in silico. We observed protein conformational modifications that rationalize the mutant over-phosphorylation level. We then performed in vitro analyses using a control human growth plate chondrocyte line transfected with the three FGFR3 mutants in order to study the FGFR3 downstream signaling pathways. We confirmed the over-activation of FGFR3 canonical Mpakinase and PLCγ signaling pathways and we found interesting differences in β-catenin and “A disintegrin and metalloproteinase with thrombospondin motifs 5” (Adamts5) protein expression levels between the three mutants. An inhibition of β-catenin has been detected in cell transfected with $FGFR3^{K650E}$ mutant whereas we observe a down-regulation of Adamts5 in cells tranfected with $FGFR3^{K650M}$ or $FGFR3^{K650E}$. The association of these data may provide clues on the molecular system behind the various severities of the pathological hallmarks.

RESULTS

Lys650 substitution modifies FGFR3 structure and alters transautophosporylation interactions

Computational studies were conducted to get an atomic description of the p.Lys650Met (SADDAN), p.Lys650Glu (TD) and p.Lys650Asn (HCH) built using a validated structural model of the FGFR3 kinase domain derived from the FGFR1 crystal structure (Jonquoy et al., 2012; Li et al., 2015; Tak-Tak et al., 2011). Monitoring of kinetic, potential, and overall energies along the 50 ns trajectories, as well as the density, pressure, and temperature, demonstrates the stability of the WT, K650E, K650M and K650N systems. For all systems, RMSD curves of the backbone atoms residues were produced, along the first 50 ns trajectories, to observe molecular movements and fluctuations. All curves reached a plateau after 5 ns. Comparison of the average protein structures in all complexes showed that the secondary structures and globular form of FGFR3 were retained during the simulations. AMD simulations were engaged for all systems in order to enhance their conformational sampling so that the ergodicity of systems may be considered. We performed AMD simulations of 100 ns which, broadly speaking, correspond to 1 µs of classical MD simulations. From these trajectories, we verify that the secondary structures of the 4 systems remain identical.

In non-mutant FGFRs the first step in the receptor activation process is the activation loop (A-loop) tyrosine phosphorylation ruled by the conformational modifications induced by the interaction of the extracellular domain with FGF ligands (Goetz and Mohammadi, 2013). Hence, in our FGFR3 model the two tyrosine residues involved in the receptor activation are Tyr647 and Tyr648 residing in the A-loop.

As for any chemical reaction, phosphorylation requires an access to the reactants. Therefore, the ability to phosphorylate Tyr647 or Tyr648 residues is proportional to their solvent accessibility. Structural analyses extracted from molecular dynamics trajectory indicate that a salt bridge between R655 and E686 is the cornerstone of the Tyr647/Tyr648 solvent exposition (Figure 1A). Thus this salt bridge constitutes the kinase autoinhibitory molecular brake (Chen et al., 2007). R655/E686 salt bridge is, significantly, disturbed with Lys650Asn (HCH) mutation and is totally absent in Lys650Met (SADDAN) and Lys650Glu (TDII) mutants. Moreover the effect on the salt

bridge leads to FGFR3 A-loop folding modifications. We observe a major change for $FGFR3^{K650M}$ (SADDAN) and $FGFR3^{K650E}$ (TDII) that take a hairpin conformation and a milder modification for $FGFR3^{K650N}$ (HCH) that slightly moves away the A-loop from the C-terminal domain (Fig. 1A).

A structural study was performed to evaluate the effect of these modifications during the transautophopshorylation process in a FGFR3 dimer (Figure 1B). Firstly we notice that in wild-type conformation a steric problem between the enzyme substrate helix harboring the tyrosine phosphorylatable residue Y648 and the enzyme kinase A-loop prevents the transautophosphorylation in FGFR3 dimers. This information suggests that the $FGFR3^{WT}$ needs a change in its structure to slightly move the A-loop and allow the interaction. This adjustment may be provided through the binding of a FGF ligand (Goetz and Mohammadi, 2013). Secondly, if we consider the FGFR3 mutants, we can observe the lack of steric hindrance previously detected in $FGFR3^{WT}$. This feature in mutant FGFR3 indicates the likely independence of the mutant proteins from the A-loop activation. Furthermore the A-loop hairpin structure displayed by both $FGFR3^{K650M}$ (SADDAN) and $FGFR3^{K650E}$ (TDII) allows an improved transautophosphorylation interaction compared to $FGFR3^{K650N}$ (HCH) structure. This exceptional interaction coincides with an increase of phosphorylation; thus $FGFR3^{K650M}$ (SADDAN) and $FGFR3^{K650E}$ (TDII) are over-phosphorylated compared to $FGFR3^{K650N}$ (HCH).

Quantification of the FGFR3s conformational modifications

To quantify the structural differences examined in our FGFR3 molecular models we determined two reference points representing the A-loop (backbone gravity center of 650-656 aa) and the C-terminal domain (backbone gravity center of 562-565 aa ; 620-623 aa) (Figure 2). The C-terminal domain is almost fixed in all FGFR3 reconstructions, the A-loop instead moves away. Thus we can measure the gap between these two points. We observe that the wider is the distance between the c-terminal domain and the A-loop and the more severe is the mutation (Table 1).

Mutant FGFR3s over-phosphorylation is transduced to downstream signaling pathways

We investigated the phosphorylation level of the three mutant FGFR3s in a human chondrocyte line derived from chondrocytes belonging to the growth plate. These cells have been transfected with suitable constructs to express the human

FGFR3 wild-type and mutant. Firstly we notice a different phosphorylation level of the mutant FGFR3 proteins. FGFR3^{K650M} (SADDAN) appears the most phosphorylated, followed by FGFR3^{K650E} (TDII) and ending with FGFR3^{K650N} (HCH) (Figure 3A). Secondly we analyzed the FGFR3 canonical pathways ERK and PLC-γ (Figure 3B). The FGFR3 mutations have triggered the activation of both ERK and PLC-γ. However it is not possible to determine with evidence if one mutation leads to a higher phosphorylation than the other ones.

Mutant FGFR3s modify β-catenin and Adamts5 expression

We decided to explore proteins belonging to non-canonical pathways to find the molecular reasons for the various phenotype of the three K650-FGFR3-related disorders. Wnt/β-catenin pathway is known to be involved in chondrocyte maturation at the growth plate level (Staines et al., 2012), thus we chose to investigate the presence of imbalances in this pathway. Interestingly, the analysis of β-catenin showed a decrease of the expression in FGFR3^{K650E} (TDII) compared to the wild-type form (Figure 4A).

In our quest for molecular differences among the Lys650 mutants we considered the putative impact of the activating mutations on the cartilage matrix. It is known that a large set of degrading enzymes play a major role in endochondral ossification and that the ADAMTS family is part of the group (Cawston and Wilson, 2006). For this reason we examined Adamts5 expression. Adamts5 provided different results among the FGFR3 variants (Figure 4B). While FGFR3^{K650N} (HCH) produces an Adamst5 expression equivalent to FGFR3^{WT}, FGFR3^{K650M} (SADDAN) and FGFR3^{K650E} (TDII) are characterized by a lower expression of the protein FGFR3^{K650M} (SADDAN) (~1/2 FGFR3^{WT} expression), with the lowest level attained by FGFR3^{K650E} (~1/3 FGFR3^{WT} expression).We decided to explore proteins belonging to non-canonical pathways to find the molecular reasons for the clinical appearance of the three mutations. The analysis of β-catenin showed an increase of its level in FGFR3^{K650N} (HCH) compared to FGFR3^{WT} and a decrease of the expression in FGFR3^{K650E} (TD) always compared to the wild-type form (Figure 4A). The study of another protein, Adamts5, provided different results among the FGFR3 variants (Figure 4B). While FGFR3^{K650N} (HCH) produces an Adamst5 expression equivalent to FGFR3^{WT}, FGFR3^{K650M} (SADDAN) (~1/2 FGFR3^{WT} expression) and FGFR3^{K650E}

(TD) are characterized by a lower expression of the protein, with the lowest level attained by $FGFR3^{K650E}$ (~1/3 $FGFR3^{WT}$ expression).

DISCUSSION

Gain-of-function mutations are responsible for the biological dysfunctions that characterize FGFR3-related chondrodysplasias and cranyosinostoses (Baujat et al., 2008; Karczeski and Cutting, 1993; Muenke et al., 1997; Tavormina et al., 1999). These mutations in FGFR3 determine an increase in the receptor phosphorylation as already been described in several studies (d'Avis et al., 1998; Bellus et al., 2000; Bonaventure et al., 2007; Gibbs and Legeai-Mallet, 2007; Naski et al., 1996). An absence of correlation between bone pathologies from which the FGFR3 mutations arise and the phosphorylation level of the receptor has also been described (Gibbs and Legeai-Mallet, 2007; Iwata et al., 2001). However, the biological processes between the various FGFR3 mutations and their effects on the receptor phosphorylation are still poorly understood. In an effort to shed light on these mechanisms we performed computational and biological studies of three FGFR3 mutations inducing three different chondrodysplasias: p.Lys650N (HCH), Lys650Met (SADDAN) and Lys650Glu (TDII).

The in silico analyses performed show that the phosphorylation of the receptor is linked with the conformational changes that the protein undergoes when mutated. In fact the salt bridge R655/E688, observed in $FGFR3^{WT}$ and $FGFR3^{K650N}$ (HCH), falls into a group of "molecular brake" mechanisms that regulate the activity of receptor tyrosine kinases already described (Chen et al., 2007). When the molecular brake is lost, as in the $FGFR3^{K650M}$ (SADDAN) and $FGFR3^{K650E}$ (TDII) salt bridge disruption, the kinase activity becomes independent from the phosphorylation of the A-loop residues. An almost identical event has been reported in the crystal structure of $FGFR3K^{K650E}$ validating our results (Huang et al., 2013). This peculiar A-loop insensitivity explains the elevated phosphorylation levels that we find in $FGFR3^{K650M}$ (SADDAN) and $FGFR3^{K650E}$ (TDII) (Figure 3A). Moreover, the absence of the molecular hindrance observed in all FGFR3 mutants in the transautophosphorylation interaction (Figure 2B) indicates that the three proteins will show a higher receptor activation compared to $FGFR3^{WT}$. These findings corroborate the thesis of the link between FGFR3 mutations and increased activity of the receptor. This abnormal receptor activation system, due to tyrosine kinase domain mutations, appears to be different from the molecular pattern regulating the mutations located in the

transmembrane domain that is based on greater stabilization of the FGFR3 dimer (Li et al., 2006; Placone and Hristova, 2012; Sarabipour and Hristova, 2016).

The steric hindrance observed in the $FGFR3^{WT}$ transautophosphorylation study, showing the necessity to move the A-loop to allow this interaction between two FGFR3 proteins, may indicate two potential non-mutant FGFR3 molecular behaviors. The first is that the interaction is still possible, but at a lower rate compared to the mutant FGFR3s. The second is that the binding with a FGF ligand could increase the transautophosphorylation rate in the $FGFR3^{WT}$ dimer inducing the A-loop movement necessary to allow the interaction between the enzyme kinase and the enzyme substrate (Goetz and Mohammadi, 2013; Hubbard, 2004). Furthermore, different FGF ligands may cause different FGFR3 conformations (Chen and Hristova, 2011) leading to the activation of different downstream proteins.

The FGFR3 deep structural modifications, illustrated through our computational investigations, could allow a change in the protein-protein interactions selectivity. This affinity alteration would lead to the activation / inhibition of molecular pathways that could result in the dramatically various clinical phenotypes of FGFR3-related disorders. The analyses of ERK and PLCγ pathways in human chondrocytes transiently expressing the FGFR3 mutants did not reveal any difference in the activation or expression of these proteins (Figure 3B). The equivalent ERK activation observed in $FGFR3^{K650M}$ (SADDAN) and $FGFR3^{K650E}$ (TDII) has already been reported in studies performed using RCS chondrocytes or HEK293 cells expressing the same mutants (Krejci et al., 2008; Lievens et al., 2006). However, we observed there that the ERK phosphorylation induced by $FGFR3^{K650N}$ (HCH), is comparable with the effects of the other two mutated proteins. Activation of MAPK pathway leads to chondrocyte differentiation defects (Ornitz and Marie, 2015), feature that we can observe among the three diseases (Krejci, 2014). By cons, PLCγ in chondrocytes is a signal transducer and activator of transcription of STAT1 (Harada et al., 2007; Ornitz and Itoh, 2015) whose activation inhibits cell proliferation (Sahni et al., 1999, 2001). The similar activation of PLCγ in the three conditions, seems to point to the presence of proliferation defects in the three mutants. However, there should be one or more molecular pathways responsible for the differences in HCH, SADDAN and TDII disorders.

Searching for alternative pathways we identified differences in the expression of β-catenin, protein belonging to the Wnt/β-catenin pathway. This pathway is strongly implicated in bone formation through osteoblasts regulation and growth plate chondrocytes differentiation as described in several studies (Akiyama et al., 2004; Day et al., 2005; Hu et al., 2005; Yuasa et al., 2009). We showed a downregulation of the expression of the protein in the presence of $FGFR3^{K650E}$ (TDII) (Figure 4A). A similar result have been obtained observing a decreased β-catenin expression level in the growth plate of mice expressing $Fgfr3^{K644E}$ under the promoter Prx1 (Shung et al., 2012). In addition the conditional knock-out of β-catenin under Prx1 promoter determined chondrocyte maturation defects (Hill et al., 2005) and its conditional inactivation under Col II promoter in mice caused endochondral ossification anomalies at the skull base level (Nagayama et al., 2008), thus confirming the importance of its correct expression. On the other hand recent studies on FGF2-stimulated RCS chondrocytes demonstrate an upregulation of β-catenin expression mediated by LRP6 phosphorylation (Buchtova et al., 2015). In our in vitro experiments we observed a strong inhibition of Adamts5 expression in $FGFR3^{K650M}$ (SADDAN) and $FGFR3^{K650E}$ (TDII). A decreased expression of Adamts5, one of the main proteinases responsible for aggrecan degradation in vivo (Malfait et al., 2002), may determine an accumulation of aggrecan in cartilage matrix. This larger quantity of aggrecan could lead to inhibition of mineralization (Marcus et al., 2013). It has been recently established that a conditional deletion of Fgfr3 leads to an increase of Adamts5 detected by RT-PCR in articular cartilage (Zhou et al., 2016). If the lower level of Adamts5 observed in our cells is due to the presence of activating mutations it is reasonable to think that a Fgfr3 knockout could induce an increase of the protein expression and vice versa. Adamts5 expression in growth plate cartilage seems to be negatively regulated by PI3K/Akt pathway since Adamts5 expression level analyzed by RT-PCR increases with the PI3K inhibition (Ulici et al., 2010). Nonetheless it has been reported that the response of RCS chondrocyte to FGF2 produced an increase in Adamts5 expression determined by RT-PCR (Buchtova et al., 2015). The different β-catenin and Adamts5 expressions reported in (Buchtova et al., 2015) may be due to differences between the response of $FGFR3^{WT}$ stimulated in RCS cells and FGFR3-mutants expressed in human chondrocytes from the growth plate. Interestingly, it has been reported that β-catenin overexpression is correlated with an increase of Adamts5 expression in cultured mouse mature chondrocytes (Tamamura

et al., 2005). All together our biological data seem to point out a pathogenic role for Wnt/β-catenin and PI3K/Akt pathways in growth cartilage.

In summary, we have decipher some of the molecular mechanisms by which the Lys650 mutations confer gain-of-function on FGFR3 kinase and we determined interesting imbalances in downstream signaling pathways due to these activating mutations.

These results may provide the rational to design new therapeutic strategies to counteract the effects of the hyperactivity of the pathogenic FGFR3 mutants.

MATERIAL AND METHODS

Molecular dynamics

The FGFR3 kinase domain and its three mutants, K650E, K650M and K650N were considered for computational studies. All simulations were performed by using the Amber software package (Case et al., 2010) with ff99SBildn force-field (Wickstrom et al., 2009). The FGFR3 kinase coordinates were taken from a previously validated model (Jonquoy et al., 2012; Tak-Tak et al., 2011), from which the K650X mutations were created with the Leap module of Amber. The four systems (wild-type and the three mutants) were then immersed in periodic boxes of water solvent. The simulations started with an energy optimization of the water solvent followed by a global minimization of the whole systems. The systems were firstly heated from 0 to 300 K and a molecular dynamics production were then performed in the NTP ensemble, leading to a trajectory of 50 ns. Other details about the computational procedure may be found elsewhere (Barbault and Maurel, 2012).

Accelerated molecular dynamics

Accelerated molecular dynamics (AMD) is a recent technique (Hamelberg et al., 2007), which aims to enhance the conformational sampling of a classical MD through the adjunction of a supplemental potential. The goal of this bias energy, called a boost, is to fill the minima of a protein potential energy hyper-surface in order to reduce the energy walls barriers. This modification intervenes only if the potential energy is lower than the average potential energy. The implication of this method on the Hamiltonian describing the protein appears in the following equations:

$$\begin{cases} \mathcal{H}(\vec{r},\vec{p}) = K(\vec{p}) + U(\vec{r}) & if\ U(\vec{r}) \leq E_{average} \\ \mathcal{H}(\vec{r},\vec{p}) = K(\vec{p}) + U(\vec{r}) + \Delta V(\vec{r}) & if\ U(\vec{r}) > E_{average} \end{cases}$$

The p and r vectors represent, respectively, the momenta and coordinates of all atoms. K is the kinetic energy of the system whereas U is the potential energy calculated through the amber force-field equations. When this last energy is greater than the average potential energy (Eaverage) a boost is applied (ΔV) through the following equation:

$$\Delta V(\vec{r},\phi) = \frac{\left(T_{pot} - U(\vec{r})\right)^2}{\alpha_{pot} + T_{pot} - U(\vec{r})} + \frac{(T_{tors} - E_{tors}(\phi))^2}{\alpha_{tors} + T_{tors} - E_{tors}(\phi)}$$

In this last equation the boost of AMD is implemented for the torsional and the whole potential energy. The threshold (T) term and α factor are easily determined using basic system information:

$$\alpha_{tors} = 0.7 \times N_{amino-acids} \qquad T_{tors} = \langle E_{tors}(\phi)\rangle + \alpha_{tors}$$

$$\alpha_{pot} = \frac{N_{atoms}}{5} \qquad T_{pot} = \langle U(\vec{r})\rangle + \alpha_{pot}$$

α and T values were determined by averaging the energies of the last 10ns extracted from the whole 50ns simulations of classical molecular dynamics. For all molecular systems, the accelerated molecular dynamics were launched for 100ns.

Computational analyses

To check the equilibration, root mean square deviations (RMSD) were recorded for all systems. The FGFR3 backbones atomic fluctuations were also recorded and mass-weighted for each residue. For each system, comparison of atomic fluctuations and RMSD between classical MD and AMD were performed to evaluate the impact of this last technique on the conformational sampling.

A distance between the centers of gravity of the activation loop (backbone atoms of residues 650 to 655) and the C-terminal domain (backbone atoms of residues 562 to 565 and 620 to 623) was recorded along the trajectory. This specific distance was chosen to decipher and quantify the opening process of the kinase activation loop. In all simulations a hydrogen bond was considered when the donor-acceptor distance was smaller than 3.5 Å and the donor-acceptor-H angle smaller than 60°. These weak criteria were chosen deliberately to count as much as possible hydrogen bonds.

Visualization and other analyses were performed with the help of VMD (Visual Molecular Dynamics) software (Humphrey et al., 1996).

Transient transfections of cDNA FGFR3 constructs

Human control chondrocyte lines (Benoist-Lasselin et al., 2007) at 80%–90% confluence were transiently transfected with FGFR3 human constructs ($FGFR3^{WT}$, $FGFR3^{K650N}$, $FGFR3^{K650M}$, $FGFR3^{K650E}$) obtained as previously reported (Gibbs and Legeai-Mallet, 2007) using JetPrime (Polyplus-transfection) following the manufacturer's instructions. Transfected cells were lysed in RIPA buffer (50 mM Tris-HCl pH 7.6, 150 mM NaCl, 0.5% NP40, and 0.25% sodium deoxycholate, supplemented with protease and phosphatase inhibitors; Roche). Immunoprecipitations were performed by incubating 3 µl rabbit anti-FGFR3 (SigmaAldrich F0425)/500 µg protein with protein A–agarose (Roche).

Immunoblotting

Whole-cell lysates and immunoprecipitated proteins were subjected to NuPAGE 4%–12% bis-tris acrylamide gels (Life Technologies). Blots were probed with antibodies using standard protocols: anti-FGFR3 polyclonal antibody (Sigma-Aldrich F0425; 1:1,000 dilution), anti–phospho-tyrosine P-Tyr-100 monoclonal antibody (Cell Signaling catalog 9411; 1:1,000 dilution), anti–phosphoERK1/2 monoclonal antibody (Cell Signaling catalog 4370; 1:1,000 dilution), anti-ERK1/2 polyclonal antibody (Sigma-Aldrich M5670; 1:1000 dilution), anti–phospho-PLCγ polyclonal antibody (Cell Signaling catalog 2821; 1:1,000 dilution), anti-PLCγ polyclonal antibody (Cell Signaling catalog 2822; 1:1,000 dilution), anti-β-catenin polyclonal antibody (Cell Signaling catalog 9562; 1:1,000 dilution), anti-ADAMTS5 polyclonal antibody (abcam ab41037, 1:1,000 dilution).

FIGURES

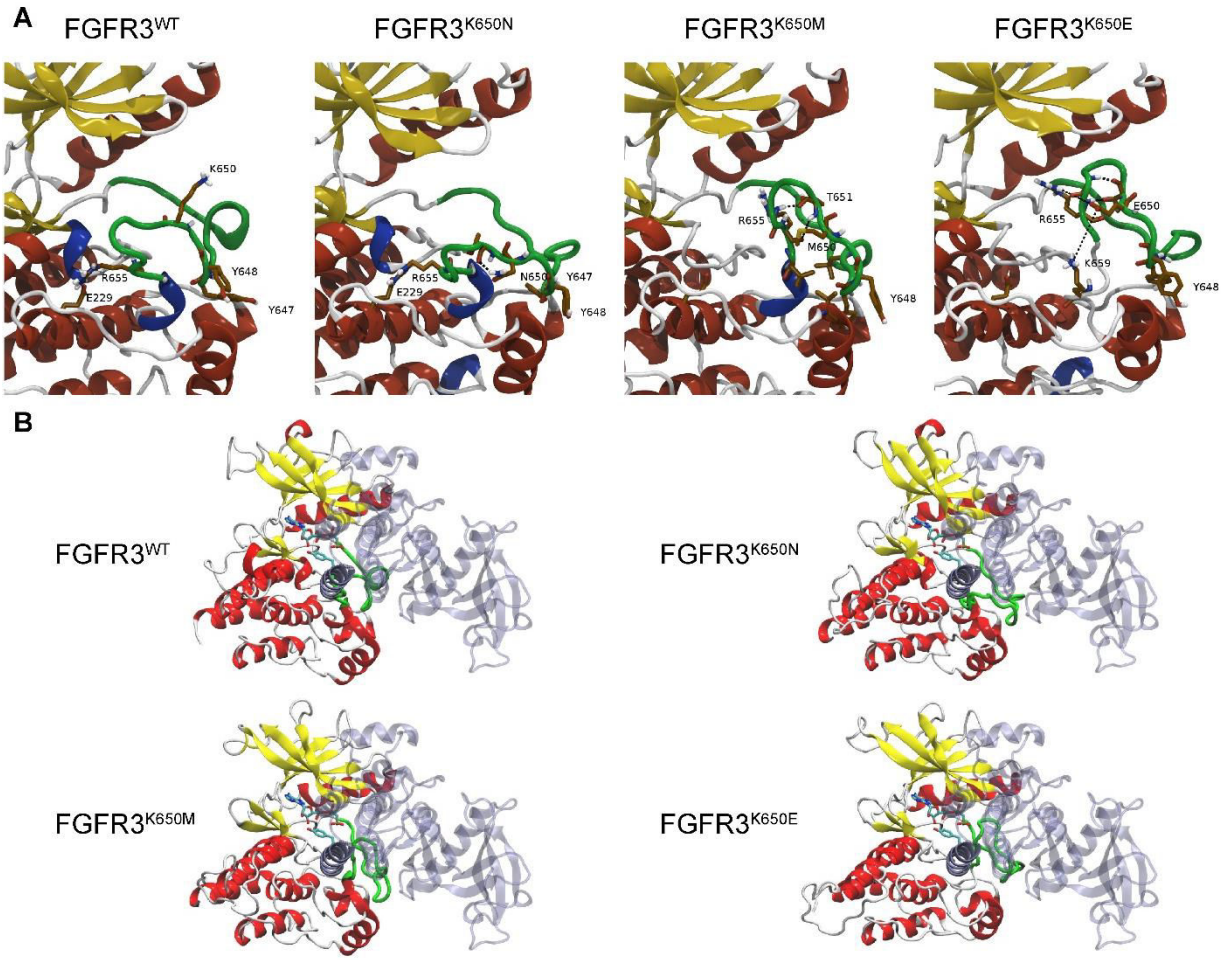

Figure 1. Wild-type and mutant FGFR3s modeling. (A) Predicted structures of $FGFR3^{WT}$ $FGFR3^{K650N}$ (HCH), $FGFR3^{K650M}$ (SADDAN), and $FGFR3^{K650E}$ (TDII). **(B)** Transphosphorylation model between a FGFR3 enzyme kinase (in different colors) and a FGFR3 enzyme substrate (transparent purple). $FGFR3^{WT}$ presents a molecular hindrance between the helix (opaque purple) carrying the phosphorylatable tyrosine (stick model) and the A-loop (green). ATP molecule is shown in stick model close to the phosphorylatable tyrosine.

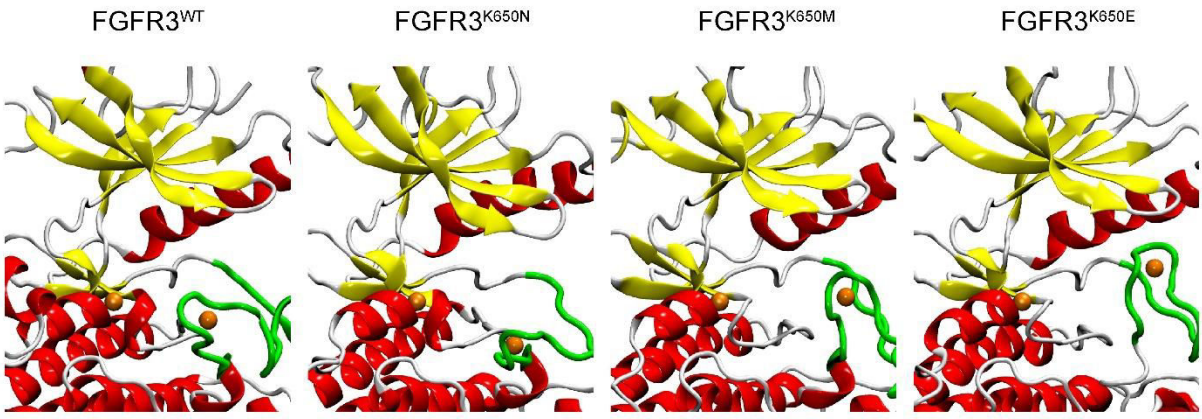

Figure 2. Representation of the points indicating the position of the activation loop and the C-terminal domain. The two points are indicated by the orange spheres. The activation loop (green) is defined by the backbone gravity center of 650-656 aa while the C-terminal domain is exemplified by the backbone gravity center of 562-565 aa ; 620-623 aa. This last point is almost fixed in all mutants and WT.

Table 1. Quantification of the distance between the activation loop and the C-terminal domain

System	Distance (Å)
$FGFR3^{WT}$	8.9
$FGFR3^{K650N}$	12.2
$FGFR3^{K650E}$	16.4
$FGFR3^{K650M}$	16.8

We measured the distance between the points illustrating the activation loop and the C-terminal domain (Figure 2). The more or less wide gap between the activation loop and the C-terminal domain correlates with the FGFR3 phosphorylation level.

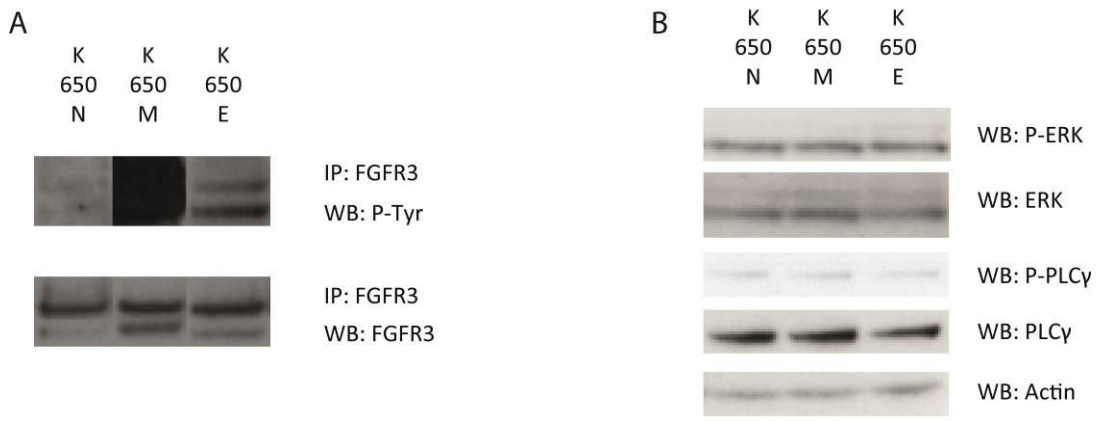

Figure 3. FGFR3 mutants display different FGFR3 phosphorylation levels and activation of the canonical FGFR3 downstream pathways. (A) Phosphorylated FGFR3 expression in transfected human chondrocytes with FGFR3^{K650N} (HCH), FGFR3^{K650M} (SADDAN), and FGFR3^{K650E} (TDII) constructs. **(B)** Phosphorylated ERK and PLC γ expression in transfected human chondrocytes with FGFR3^{K650N} (HCH), FGFR3^{K650M} (SADDAN), and FGFR3^{K650E} (TDII) constructs.

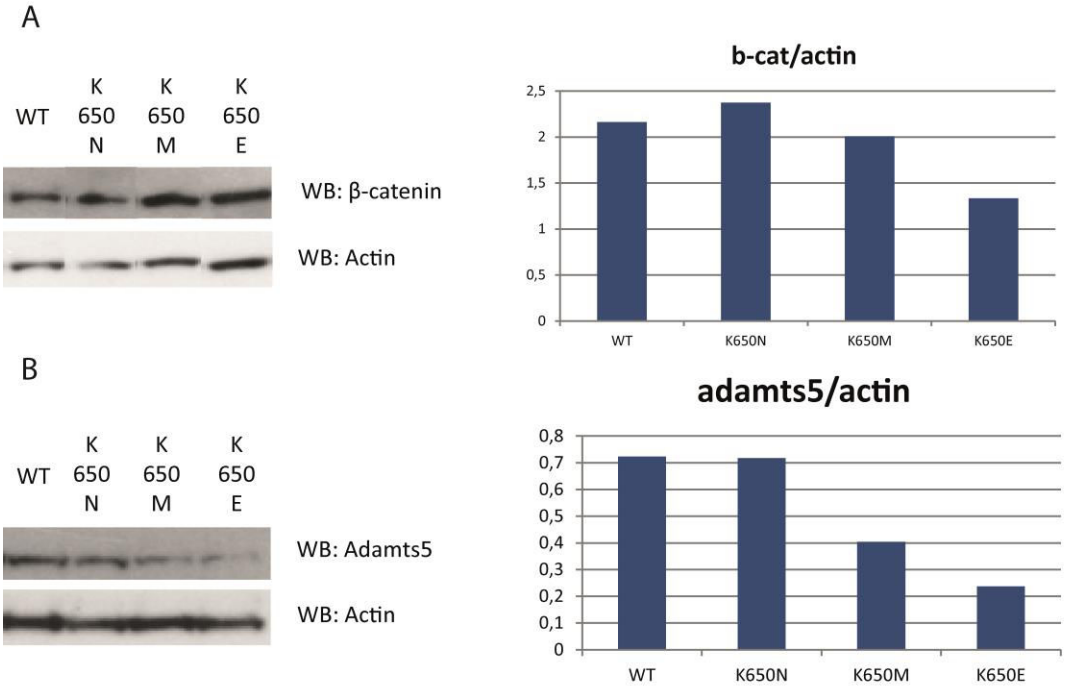

Figure 4. FGFR3 mutants have different β-catenin & Adamts5 protein expressions. (A) β-catenin expression level in transfected human chondrocytes with FGFR3^{K650N} (HCH), FGFR3^{K650M} (SADDAN), and FGFR3^{K650E} (TDII) constructs revealed by western blot and quantified with actin ratio. **(B)** Adamts5 expression level in transfected human chondrocytes with FGFR3^{K650N} (HCH), FGFR3^{K650M} (SADDAN), and FGFR3^{K650E} (TDII) constructs revealed by western blot and quantified with actin ratio.

REFERENCES

Akiyama, H., Lyons, J.P., Mori-Akiyama, Y., Yang, X., Zhang, R., Zhang, Z., Deng, J.M., Taketo, M.M., Nakamura, T., Behringer, R.R., et al. (2004). Interactions between Sox9 and beta-catenin control chondrocyte differentiation. Genes Dev. *18*, 1072–1087.

d'Avis, P.Y., Robertson, S.C., Meyer, A.N., Bardwell, W.M., Webster, M.K., and Donoghue, D.J. (1998). Constitutive activation of fibroblast growth factor receptor 3 by mutations responsible for the lethal skeletal dysplasia thanatophoric dysplasia type I. Cell Growth Differ. Mol. Biol. J. Am. Assoc. Cancer Res. *9*, 71–78.

Barbault, F., and Maurel, F. (2012). Is inhibition process better described with MD(QM/MM) simulations? The case of urokinase type plasminogen activator inhibitors. J. Comput. Chem. *33*, 607–616.

Baujat, G., Legeai-Mallet, L., Finidori, G., Cormier-Daire, V., and Le Merrer, M. (2008). Achondroplasia. Best Pract. Res. Clin. Rheumatol. *22*, 3–18.

Bellus, G.A., Bamshad, M.J., Przylepa, K.A., Dorst, J., Lee, R.R., Hurko, O., Jabs, E.W., Curry, C.J., Wilcox, W.R., Lachman, R.S., et al. (1999). Severe achondroplasia with developmental delay and acanthosis nigricans (SADDAN): phenotypic analysis of a new skeletal dysplasia caused by a Lys650Met mutation in fibroblast growth factor receptor 3. Am. J. Med. Genet. *85*, 53–65.

Bellus, G.A., Spector, E.B., Speiser, P.W., Weaver, C.A., Garber, A.T., Bryke, C.R., Israel, J., Rosengren, S.S., Webster, M.K., Donoghue, D.J., et al. (2000). Distinct missense mutations of the FGFR3 lys650 codon modulate receptor kinase activation and the severity of the skeletal dysplasia phenotype. Am. J. Hum. Genet. *67*, 1411–1421.

Benoist-Lasselin, C., Gibbs, L., Heuertz, S., Odent, T., Munnich, A., and Legeai-Mallet, L. (2007). Human immortalized chondrocytes carrying heterozygous FGFR3 mutations: an in vitro model to study chondrodysplasias. FEBS Lett. *581*, 2593–2598.

Bober, M.B., Bellus, G.A., Nikkel, S.M., and Tiller, G.E. (1993). Hypochondroplasia. In GeneReviews(®), R.A. Pagon, M.P. Adam, H.H. Ardinger, S.E. Wallace, A. Amemiya, L.J. Bean, T.D. Bird, C.-T. Fong, H.C. Mefford, R.J. Smith, et al., eds. (Seattle (WA): University of Washington, Seattle),.

Bonaventure, J., Gibbs, L., Horne, W.C., and Baron, R. (2007). The localization of FGFR3 mutations causing thanatophoric dysplasia type I differentially affects phosphorylation, processing and ubiquitylation of the receptor. FEBS J. *274*, 3078–3093.

Buchtova, M., Oralova, V., Aklian, A., Masek, J., Vesela, I., Ouyang, Z., Obadalova, T., Konecna, Z., Spoustova, T., Pospisilova, T., et al. (2015). Fibroblast growth factor and canonical WNT/β-catenin signaling cooperate in suppression of chondrocyte differentiation in experimental models of FGFR signaling in cartilage. Biochim. Biophys. Acta *1852*, 839–850.

Case, D., Darden, T., Cheatham, T., Simmerling, C., Wang, J., Duke, L., Luo, R., Crowley, M., Walker, R., Zhang, W., et al. (2010). AMBER v11.

Cawston, T.E., and Wilson, A.J. (2006). Understanding the role of tissue degrading enzymes and their inhibitors in development and disease. Best Pract. Res. Clin. Rheumatol. *20*, 983–1002.

Chen, F., and Hristova, K. (2011). The physical basis of FGFR3 response to fgf1 and fgf2. Biochemistry (Mosc.) *50*, 8576–8582.

Chen, H., Ma, J., Li, W., Eliseenkova, A.V., Xu, C., Neubert, T.A., Miller, W.T., and Mohammadi, M. (2007). A molecular brake in the kinase hinge region regulates the activity of receptor tyrosine kinases. Mol. Cell *27*, 717–730.

Day, T.F., Guo, X., Garrett-Beal, L., and Yang, Y. (2005). Wnt/beta-catenin signaling in mesenchymal progenitors controls osteoblast and chondrocyte differentiation during vertebrate skeletogenesis. Dev. Cell *8*, 739–750.

Gibbs, L., and Legeai-Mallet, L. (2007). FGFR3 intracellular mutations induce tyrosine phosphorylation in the Golgi and defective glycosylation. Biochim. Biophys. Acta *1773*, 502–512.

Goetz, R., and Mohammadi, M. (2013). Exploring mechanisms of FGF signalling through the lens of structural biology. Nat. Rev. Mol. Cell Biol. *14*, 166–180.

Hamelberg, D., de Oliveira, C.A.F., and McCammon, J.A. (2007). Sampling of slow diffusive conformational transitions with accelerated molecular dynamics. J. Chem. Phys. *127*, 155102.

Harada, D., Yamanaka, Y., Ueda, K., Nishimura, R., Morishima, T., Seino, Y., and Tanaka, H. (2007). Sustained phosphorylation of mutated FGFR3 is a crucial feature of genetic dwarfism and induces apoptosis in the ATDC5 chondrogenic cell line via PLCgamma-activated STAT1. Bone *41*, 273–281.

Hill, T.P., Später, D., Taketo, M.M., Birchmeier, W., and Hartmann, C. (2005). Canonical Wnt/β-Catenin Signaling Prevents Osteoblasts from Differentiating into Chondrocytes. Dev. Cell *8*, 727–738.

Hu, H., Hilton, M.J., Tu, X., Yu, K., Ornitz, D.M., and Long, F. (2005). Sequential roles of Hedgehog and Wnt signaling in osteoblast development. Dev. Camb. Engl. *132*, 49–60.

Huang, Z., Chen, H., Blais, S., Neubert, T.A., Li, X., and Mohammadi, M. (2013). Structural Mimicry of A-Loop Tyrosine Phosphorylation by a Pathogenic FGF Receptor 3 Mutation. Structure *21*, 1889–1896.

Hubbard, S.R. (2004). Juxtamembrane autoinhibition in receptor tyrosine kinases. Nat. Rev. Mol. Cell Biol. *5*, 464–471.

Humphrey, W., Dalke, A., and Schulten, K. (1996). VMD: visual molecular dynamics. J. Mol. Graph. *14*, 33–38.

Iwata, T., Li, C.L., Deng, C.X., and Francomano, C.A. (2001). Highly activated Fgfr3 with the K644M mutation causes prolonged survival in severe dwarf mice. Hum. Mol. Genet. *10*, 1255–1264.

Jonquoy, A., Mugniery, E., Benoist-Lasselin, C., Kaci, N., Le Corre, L., Barbault, F., Girard, A.-L., Le Merrer, Y., Busca, P., Schibler, L., et al. (2012). A novel tyrosine kinase inhibitor restores chondrocyte differentiation and promotes bone growth in a gain-of-function Fgfr3 mouse model. Hum. Mol. Genet. *21*, 841–851.

Karczeski, B., and Cutting, G.R. (1993). Thanatophoric Dysplasia. In GeneReviews(®), R.A. Pagon, M.P. Adam, H.H. Ardinger, S.E. Wallace, A. Amemiya, L.J. Bean, T.D. Bird,

C.-T. Fong, H.C. Mefford, R.J. Smith, et al., eds. (Seattle (WA): University of Washington, Seattle),.

Krejci, P. (2014). The paradox of FGFR3 signaling in skeletal dysplasia: Why chondrocytes growth arrest while other cells over proliferate. Mutat. Res. Mutat. Res. *759*, 40–48.

Krejci, P., Salazar, L., Kashiwada, T.A., Chlebova, K., Salasova, A., Thompson, L.M., Bryja, V., Kozubik, A., and Wilcox, W.R. (2008). Analysis of STAT1 activation by six FGFR3 mutants associated with skeletal dysplasia undermines dominant role of STAT1 in FGFR3 signaling in cartilage. PloS One *3*, e3961.

Legeai-Mallet, L., Benoist-Lasselin, C., Munnich, A., and Bonaventure, J. (2004). Overexpression of FGFR3, Stat1, Stat5 and p21Cip1 correlates with phenotypic severity and defective chondrocyte differentiation in FGFR3-related chondrodysplasias. Bone *34*, 26–36.

Leonard, D.G.B. (2016). Molecular Pathology in Clinical Practice (Cham: Springer International Publishing).

Li, E., You, M., and Hristova, K. (2006). FGFR3 dimer stabilization due to a single amino acid pathogenic mutation. J. Mol. Biol. *356*, 600–612.

Li, Y., Delamar, M., Busca, P., Prestat, G., Le Corre, L., Legeai-Mallet, L., Hu, R., Zhang, R., and Barbault, F. (2015). Molecular modeling study of the induced-fit effect on kinase inhibition: the case of fibroblast growth factor receptor 3 (FGFR3). J. Comput. Aided Mol. Des. *29*, 619–641.

Lievens, P.M.-J., Roncador, A., and Liboi, E. (2006). K644E/M FGFR3 mutants activate Erk1/2 from the endoplasmic reticulum through FRS2 alpha and PLC gamma-independent pathways. J. Mol. Biol. *357*, 783–792.

Malfait, A.-M., Liu, R.-Q., Ijiri, K., Komiya, S., and Tortorella, M.D. (2002). Inhibition of ADAM-TS4 and ADAM-TS5 prevents aggrecan degradation in osteoarthritic cartilage. J. Biol. Chem. *277*, 22201–22208.

Marcus, R., Feldman, D., Dempster, D.W., Luckey, M., and Cauley, J.A. (2013). Osteoporosis.

Maroteaux, P., Lamy, M., and Robert, J.M. (1967). [Thanatophoric dwarfism]. Presse Médicale *75*, 2519–2524.

Muenke, M., Gripp, K.W., McDonald-McGinn, D.M., Gaudenz, K., Whitaker, L.A., Bartlett, S.P., Markowitz, R.I., Robin, N.H., Nwokoro, N., Mulvihill, J.J., et al. (1997). A unique point mutation in the fibroblast growth factor receptor 3 gene (FGFR3) defines a new craniosynostosis syndrome. Am. J. Hum. Genet. *60*, 555–564.

Nagayama, M., Iwamoto, M., Hargett, A., Kamiya, N., Tamamura, Y., Young, B., Morrison, T., Takeuchi, H., Pacifici, M., Enomoto-Iwamoto, M., et al. (2008). Wnt/beta-catenin signaling regulates cranial base development and growth. J. Dent. Res. *87*, 244–249.

Naski, M.C., Wang, Q., Xu, J., and Ornitz, D.M. (1996). Graded activation of fibroblast growth factor receptor 3 by mutations causing achondroplasia and thanatophoric dysplasia. Nat. Genet. *13*, 233–237.

Ornitz, D.M., and Itoh, N. (2015). The Fibroblast Growth Factor signaling pathway. Wiley Interdiscip. Rev. Dev. Biol. *4*, 215–266.

Ornitz, D.M., and Marie, P.J. (2015). Fibroblast growth factor signaling in skeletal development and disease. Genes Dev. *29*, 1463–1486.

Placone, J., and Hristova, K. (2012). Direct Assessment of the Effect of the Gly380Arg Achondroplasia Mutation on FGFR3 Dimerization Using Quantitative Imaging FRET. PLOS ONE *7*, e46678.

Sahni, M., Ambrosetti, D.C., Mansukhani, A., Gertner, R., Levy, D., and Basilico, C. (1999). FGF signaling inhibits chondrocyte proliferation and regulates bone development through the STAT-1 pathway. Genes Dev. *13*, 1361–1366.

Sahni, M., Raz, R., Coffin, J.D., Levy, D., and Basilico, C. (2001). STAT1 mediates the increased apoptosis and reduced chondrocyte proliferation in mice overexpressing FGF2. Dev. Camb. Engl. *128*, 2119–2129.

Sarabipour, S., and Hristova, K. (2016). Mechanism of FGF receptor dimerization and activation. Nat. Commun. *7*, 10262.

Shung, C.-Y., Ota, S., Zhou, Z.-Q., Keene, D.R., and Hurlin, P.J. (2012). Disruption of a Sox9-β-catenin circuit by mutant Fgfr3 in thanatophoric dysplasia type II. Hum. Mol. Genet. *21*, 4628–4644.

Staines, K.A., Macrae, V.E., and Farquharson, C. (2012). Cartilage development and degeneration: a Wnt Wnt situation. Cell Biochem. Funct. *30*, 633–642.

Tak-Tak, L., Barbault, F., Maurel, F., Busca, P., and Le Merrer, Y. (2011). Synthesis of purin-2-yl and purin-6-yl-aminoglucitols as C-nucleosidic ATP mimics and biological evaluation as FGFR3 inhibitors. Eur. J. Med. Chem. *46*, 1254–1262.

Tamamura, Y., Otani, T., Kanatani, N., Koyama, E., Kitagaki, J., Komori, T., Yamada, Y., Costantini, F., Wakisaka, S., Pacifici, M., et al. (2005). Developmental Regulation of Wnt/β-Catenin Signals Is Required for Growth Plate Assembly, Cartilage Integrity, and Endochondral Ossification. J. Biol. Chem. *280*, 19185–19195.

Tavormina, P.L., Bellus, G.A., Webster, M.K., Bamshad, M.J., Fraley, A.E., McIntosh, I., Szabo, J., Jiang, W., Jabs, E.W., Wilcox, W.R., et al. (1999). A novel skeletal dysplasia with developmental delay and acanthosis nigricans is caused by a Lys650Met mutation in the fibroblast growth factor receptor 3 gene. Am. J. Hum. Genet. *64*, 722–731.

Ulici, V., James, C.G., Hoenselaar, K.D., and Beier, F. (2010). Regulation of gene expression by PI3K in mouse growth plate chondrocytes. PloS One *5*, e8866.

Vajo, Z., Francomano, C.A., and Wilkin, D.J. (2000). The Molecular and Genetic Basis of Fibroblast Growth Factor Receptor 3 Disorders: The Achondroplasia Family of Skeletal Dysplasias, Muenke Craniosynostosis, and Crouzon Syndrome with Acanthosis Nigricans. Endocr. Rev. *21*, 23–39.

Wickstrom, L., Okur, A., and Simmerling, C. (2009). Evaluating the performance of the ff99SB force field based on NMR scalar coupling data. Biophys. J. *97*, 853–856.

Yuasa, T., Kondo, N., Yasuhara, R., Shimono, K., Mackem, S., Pacifici, M., Iwamoto, M., and Enomoto-Iwamoto, M. (2009). Transient Activation of Wnt/β-Catenin Signaling Induces Abnormal Growth Plate Closure and Articular Cartilage Thickening in Postnatal Mice. Am. J. Pathol. *175*, 1993–2003.

Zhou, S., Xie, Y., Li, W., Huang, J., Wang, Z., Tang, J., Xu, W., Sun, X., Tan, Q., Huang, S., et al. (2016). Conditional Deletion of Fgfr3 in Chondrocytes leads to Osteoarthritis-like Defects in Temporomandibular Joint of Adult Mice. Sci. Rep. *6*, 24039.

Conclusions and Perspectives

1. TKIs as a potential therapeutic strategy for ACH

The FGFR3 abnormal activation triggers its downstream molecular cascade leading to several disorders as already thoroughly discussed (93). Numerous strategies have been developed to counteract the consequences of the mutant FGFR3 activity (159). Among them the one that seems the most effective consists in modulating the FGFR3 kinase, a strategy that can be performed by TKIs. FGFR3-TKIs have already demonstrated their therapeutic potential in the cancer field (160, 161, 205) however they have never been employed in skeletal disorders. In pre-clinical studies two FGFR3 selective inhibitors, one synthesized by Aviezer et al. and the other named A31, have been evaluated to restore bone growth (165, 167). Although these studies have revealed positive effects no assessment of those compounds in a living animal model has been reported.

To establish the TKIs efficacy for ACH we decided to evaluate one of these small molecules: NVP-BGJ398 (Article 1 – (206)). For the first time, using the ACH mouse model $Fgfr3^{Y367C/+}$, we demonstrated an *in vivo* beneficial effect on several pathological features. This work demonstrates the validity of the FGFR3-TKIs approach although it does not exclude the potential ineffectiveness of some of these small molecules or even toxicity if these compound are not highly selective for FGFR3 due to the inhibition of other tyrosine kinases as it has been recently described (169).

The improvements produced by the NVP-BGJ398 are evident, however one of the most frequently asked questions concerns the comparison with the effects induced by other approaches validated in fgfr3 mouse models. To address this issue I have limited the comparative analysis to the femur growth that has been reported in all these pre-clinical studies (176, 195, 200, 201, 204, 206). If we consider these data, the compound that determined the most important growth is the TKI NVP-BGJ398 (Table 5). However we have to note the presence of relevant discrepancies among these studies that could alter the comparative analysis here displayed.

	2012		2013	2014		2016
	Xie et al.	Lorget et al.	Garcia et al.	Yamashita et al.	Matsushita et al.	Komla-Ebri et al.
	PTH	BMN 111	sFGFR3	Statin	Meclozine	NVP-BGJ398
Femur increase	+ 10.3 %	+ 5.2 %	+ 5.2 %	+ 4.0 %	+ 6.4 %	+ 20.9 %
Mouse model	$Fgfr3^{G369C/+}$	$Fgfr3^{Y367C/+}$	$Fgfr3^{ach}$	$Fgfr3^{ach}$	$Fgfr3^{ach}$	$Fgfr3^{Y367C/+}$
Administration	SC	SC	SC	IP	Oral	SC
Period	D1-D28	D7-D17	D3-D21	D3-D14	D21-D42	D1-D16
Frequency	daily	daily	2 times per week	6 times per week	ad libitum	daily

Table 5. Comparison of ACH therapeutic approaches validated *in vivo*

Several parameters concerning the *in vivo* study design differ among the data reported in these 6 papers. Firstly, the experiments have been performed on 3 different mouse models: Ella-Cre $Fgfr3^{G369C/+}$ mice, transgenic human $Fgfr3^{G380R}$ under Col2a1 promoter mice named "$Fgfr3^{ach}$" and Cre-CMV $Fgfr3^{Y367C/+}$ mice (120, 166, 168). These mice share most of the dwarf features (short limbs, macrocephaly, growth plate anomalies) with the particularity that our $Fgfr3^{Y367C/+}$ mouse model presents a more severe phenotype than $Fgfr3^{G369C/+}$ and $Fgfr3^{ach}$.

Secondly, various routes of administration have been proposed. In most of the cases the pharmacological administration involves subcutaneous injections, but intraperitoneal injections and the oral route have also been proposed (Table 4). Our suggestion is that a change in the drug administration could improve or diminish the effect of the therapy.

Thirdly, mice have been treated at different ages, for disparate periods and with different frequencies. Drug administration frequency could have an impact in the prospect of patient care. In fact reducing dose frequency shows an effect on health outcomes and health care costs (207) thus meaning that a low frequency treatment would be more convenient. However the most crucial point consists in the beginning of the treatment. Since ACH is a disease detected prenatally (30) and considering that growth cartilage is replaced by bone in adulthood, we should administrate the treatment the earliest possible to reach the best phenotypic reversal. Overall, bone growth occurs progressively from the beginning of the ossification in embryo (E14.5 in mice, second month of development in humans) to 15-18 years old in humans

(208) equivalent to approximately 3 months in mice, nonetheless treatments for achondroplasia should be administrated in this period.

	2012	2016	
	Lorget et al.	Komla-Ebri et al.	
	BMN 111	**NVP-BGJ398**	
Femur increase	+ 5.2 %	+ 20.9 %	+ 12.1 %
Mouse model	*Fgfr3*$^{Y367C/+}$	*Fgfr3*$^{Y367C/+}$	*Fgfr3*$^{Y367C/+}$
Administration	SC	SC	SC
Period	D7-D17	D1-D16	D7-D17
Frequency	daily	daily	daily

Table 6. Comparison BMN 111 / NVP-BGJ398 (Protocol 1 & 2)

Thus, considering all the various differences observed among the design of the different studies, it is difficult to argue with certainty the effectiveness of NVP - BGJ398 over the other compounds proposed for ACH. We can just confirm that we have obtained a greater improvement with NVP-BGJ398 than BMN 111 as already reported (Article 1 – (206)). The comparison has been made possible modifying the period of treatment (Table 6). We observed a best improvement of the size of the femur with NVP-BGJ398 rather than BMN111 using the same protocol. The explanation behind this result probably reside in tyrosine kinase inhibitors direct action against the FGFR3 activation whereas BMN 111, CNP-analog, is more indirect antagonizing the FGFR3 downstream pathway through NPR-B stimulation. We observe that Protocol 1 is more effective than Protocol 2. However it is difficult to determine if the increased efficiency is due to the earlier therapy initiation, the longer time of treatment or a combination of both.

In future studies the treatment times should be carefully analysed to choose the perfect timing and correct duration to deliver the most impressive results. Evaluation of the potential effects of the drug *in utero* could revolutionize ACH treatment and for this reason we have some on going *in utero* experiments. Finally, it should not be excluded the simultaneous test of multiple drugs to assess possible additive effects.

In fact compounds stimulating growth through different pathways could determine a greater effect if used combined.

2. NVP-BGJ398 as an investigational tool for Fgfr3-related defects

We have determined the ability of NVP-BGJ398 in inhibiting the FGFR3 overactivity. Now this potential can be applied as a tool to analyze particular ACH features revealed in *Fgfr3*$^{Y367C/+}$ mouse model.

The experiments with NVP-BGJ398 allow us to understand IVD (Article 1 –(206)), Meckel's cartilage (MC) and condylar cartilage (Article 2) and foramen magnum (FM) (Article 1 –(206)) defects in achondroplasia.

We reported for the first time vertebrae and invertebral disc anomalies related to a FGFR3 activating mutation (Article 1 – (206)). In *Fgfr3*$^{Y367C/+}$ mice we observed a reduced size of vertebral bodies presenting short pedicles and an abnormal shape of Nuclei Pulposi (NP) in IVDs. These defects were all corrected with NVP-BGJ398 injections. These data revealed that vertebral body and IVD are severely affected in the mutant mice and confirm the impact of the activating FGFR3 mutation on the axial skeleton. These results are in agreement with clinical observations in ACH patients showing kyphosis, lordosis, platyspondyly, spinal stenosis and short pedicles.

We focused also our study on the craniofacial anomalies and the prognatism in ACH and mutant mice. Here, we reported a reduced size of the mandible in both ACH patients and mice (Article 2). In mandible development a major role is played by MC, as a consequence of FGFR3 overactivation, the MC is affected in ACH. While *in vivo* NVP-BGJ398 had no effect on the body length mandible, *ex vivo* cultures of *Fgfr3*$^{Y367C/+}$ embryos showed an improvement of the mandible length. If we consider that MC disappears before birth and *in vivo* experiments started from post-natal day 1 we obtain a threefold information: firstly MC is fundamental for the elongation of the mandible; secondly the FGFR3 inhibition in MC restore the mandible growth; thirdly mutant FGFR3 affects the MC. Likewise we observed defects on the hypertrophy of condylar cartilage and these anomalies were corrected both *ex vivo* and *in vivo* by the TKI NVP-BGJ398.

Some ACH patients suffer of cervicomedullary compression related to FM defects that are due to synchondroses loss (25). We observed the presence of the same skull base defects in *Fgfr3*$^{Y367C/+}$ mice (Appendix – (209)) and with the NVP-BGJ398 treatment we corrected them pointing out the importance of synchondroses in skull base (Article 1 – (206); Figure 21).

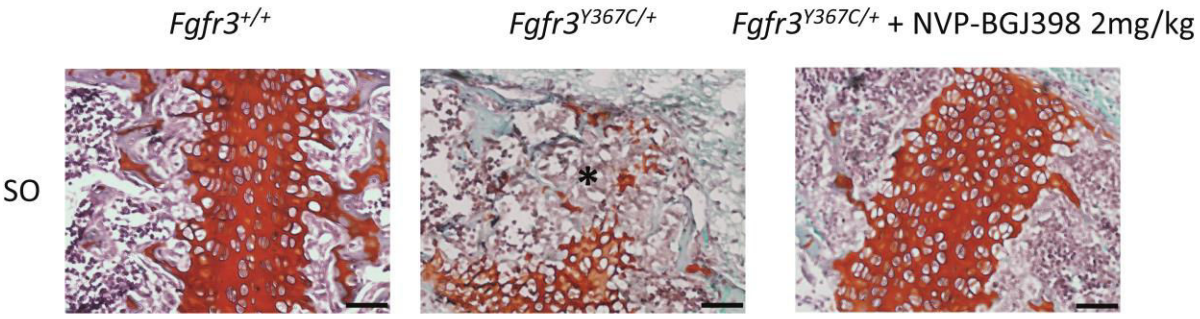

Figure 21. Interoccipital synchondroses. In *Fgfr3*$^{Y367C/+}$ mice we observe the presence of bone (asterisk). The treatment with NVP-BGJ398 prevent this abnormal ossification. Safranin-O staining, scale bar = 50 µm

In Di Rocco et al. we showed the appearance of membranous ossification defects in *Fgfr3*$^{Y367C/+}$ mice. In Article 1 (206) the treatment with NVP-BGJ398 ameliorated the membranous skull defect in organotypic cultures of calvaria. Thus similarly to the study of the previously discussed defects the use of NVP-BGJ398 was a valuable aid validating the role of FGFR3 in membranous ossification (Appendix – (209)).

3. Understanding of the pathological molecular patterns to determine new therapeutic approaches

Three different mutations localized in the same position of FGFR3 are responsible for 3 different pathologies: Lys650Asn leads to HCH, Lys650Met induces SADDAN and Lys650Glu causes TD (35). Lys650 is positioned on the FGFR3 kinase domain and its mutation determines an abnormal activation of the receptor. We conducted an investigation of the activation of FGFR3 downstream signaling pathways that involved experiments *in silico* and *in vitro* (Preliminary data)

The *in silico* works elucidated the FGFR3 kinase conformational modifications induced by the three mutants. The analysis of the mutant FGFR3 molecular behavior

has shedding light on the pathological molecular mechanisms, but it could also provide a basis for the development of new inhibitors based on these observations.

Biological studies have outlined some of the changes in the downstream pathways involved in the three diseases (Figure 22). The reduction in β-catenin and Adamts5 expression led by the mutations responsible for the severe form of dwarfism ($FGFR3^{K650M}$ (SADDAN), $FGFR3^{K650E}$ (TDII), confirmed the defects on chondrocyte maturation present in their clinical pathological features (210). These investigations have to be improved to understand the modifications involved in the signalling pathways concerned (Wnt/β-cat and PI3K/Akt). Understanding the differences in these downstream signalling pathways triggered by the three mutants could lead to the identification of a potential target for the development of a new therapeutic strategy as for the discovery of the role of CNP that led to the development of BMN 111.

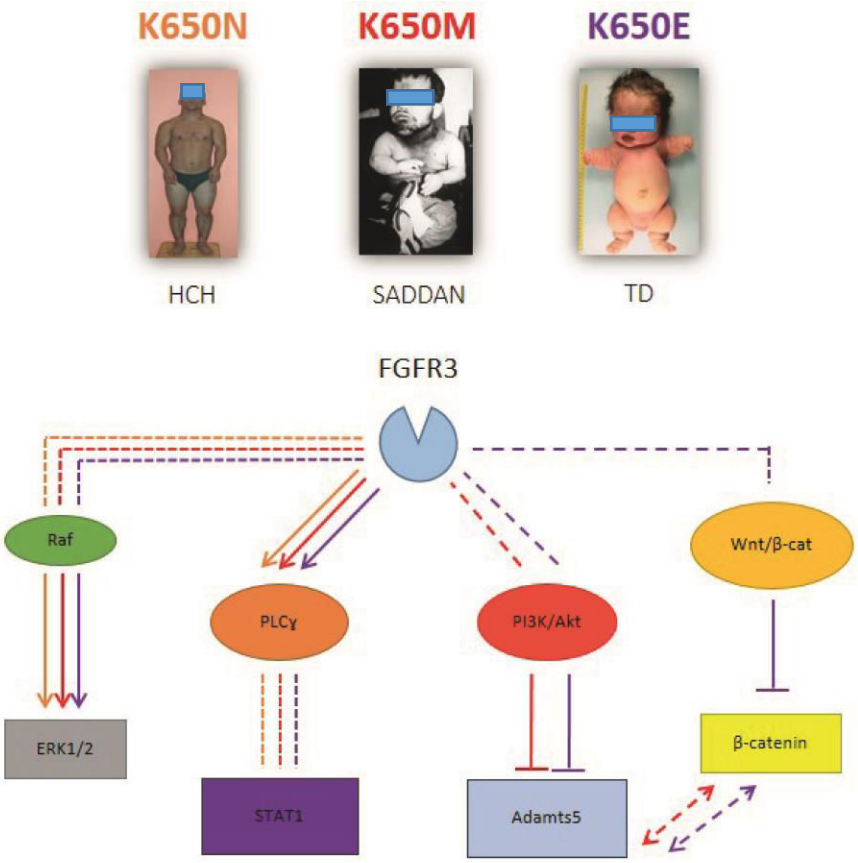

Figure 22. Scheme illustrating the signalling pathways involved in Lys650 mutation (Preliminary data). Dashed lines represent possible links, while full lines are used for data reported as Preliminary data.

Appendix

FGFR3 mutation causes abnormal membranous ossification in achondroplasia

Human Molecular Genetics, 2014, Vol. 23, No. 11 **2914–2925**
doi:10.1093/hmg/ddu004
Advance Access published on January 12, 2014

FGFR3 mutation causes abnormal membranous ossification in achondroplasia

Federico Di Rocco[1,2,†], Martin Biosse Duplan[1,3,†], Yann Heuzé[4], Nabil Kaci[1], Davide Komla-Ebri[1], Arnold Munnich[1], Emilie Mugniery[1], Catherine Benoist-Lasselin[1] and Laurence Legeai-Mallet[1,*]

[1]INSERM U781, Université Paris Descartes, Sorbonne Paris Cité, Institut Imagine, Hopital Necker-Enfants malades, Paris, France [2]Neurochirurgie Pédiatrique Hôpital Necker Enfants malades, Unité de chirurgie craniofaciale, Paris, France [3]Service d'Odontologie, Hôpital Bretonneau, HUPNVS, AP-HP, Paris, France [4]Department of Anthropology, The Pennsylvania State University, University Park, PA, USA

Received November 1, 2013; Revised and Accepted January 2, 2014

***FGFR3* gain-of-function mutations lead to both chondrodysplasias and craniosynostoses. Achondroplasia (ACH), the most frequent dwarfism, is due to an *FGFR3*-activating mutation which results in impaired endochondral ossification. The effects of the mutation on membranous ossification are unknown. *Fgfr3*$^{Y367C/+}$ mice mimicking ACH and craniofacial analysis of patients with ACH and FGFR3-related craniosynostoses provide an opportunity to address this issue. Studying the calvaria and skull base, we observed abnormal cartilage and premature fusion of the synchondroses leading to modifications of foramen magnum shape and size in *Fgfr3*$^{Y367C/+}$ mice, ACH and FGFR3-related craniosynostoses patients. Partial premature fusion of the coronal sutures and non-ossified gaps in frontal bones were also present in *Fgfr3*$^{Y367C/+}$ mice and ACH patients. Our data provide strong support that not only endochondral ossification but also membranous ossification is severely affected in ACH. Demonstration of the impact of FGFR3 mutations on craniofacial development should initiate novel pharmacological and surgical therapeutic approaches.**

INTRODUCTION

Fibroblast growth factor receptors (FGFRs) are known to be important receptor tyrosine kinase (RTK) involved in skeletal development. *FGFR3* gain-of-function mutations lead to both chondrodysplasias and craniosynostoses. Among chondrodysplasias, achondroplasia (ACH), the most frequent genetic dwarfism is due to one recurrent transmembrane (TM) activating *FGFR3* mutation (p.Gly380Arg) that causes a structural change which affects both the stability and activity of FGFR3 dimers in the absence of ligand (1–4). Thanatophoric dysplasia (TD) type I and II are a lethal form in which a point mutation localized either in the extracellular (EC) or intracellular domain of *FGFR3* induces a dimerization of FGFR3 in the absence of ligand (5). Muenke syndrome (MS), the most common craniosynostosis syndrome, is also due to a single *FGFR3* gain-of-function mutation (p.Pro250Arg) in EC domain leading to varying effects on ligand-binding specificity (6–8). Finally, a rare form of craniosynostosis with skin disorder, a Crouzon syndrome with acanthosis nigricans (CAN), results from another TM *FGFR3* point mutation (p. Ala391Glu) localized in the same functional domain as ACH (9). The CAN TM mutation enhances the activity of the receptor in the absence of ligand and facilitates the activation of the tyrosine located in the activating loop (9,10). *FGFR3* mutations disturb several signaling pathways in chondrocytes and osteoblasts such as MAPK, P38, PLCγ, STAT and PKC pathways thus inducing anomalies of cellular proliferation, differentiation and/or apoptosis (11).

In order to understand the FGFR3-skeletal diseases, several mouse models have been generated, but they do not always faithfully and comprehensively mimic the human diseases. Mouse models of MS syndrome (*Fgfr3*^{P244R}) inconstantly share some phenotypic traits with the human disorder such as hearing loss and facial dysmorphology (12–14). Interestingly, the murine *Fgfr3*^{P244R} mutation does not only affect the skull but can also disturb the long bones (13). Numerous *Fgfr3*-related chondrodysplasia mouse models have been generated as well (15–17). Among them, we generated and studied the *Fgfr3*$^{Y367C/+}$ mice (18). These mutant mice present a severe dwarfism phenotype with a reduction of the length of the appendicular and axial

*To whom correspondence should be addressed. Email: laurence.legeai-mallet@inserm.fr
†These authors contributed equally to this work.

skeleton, consequence of a disturbed endochondral ossification (18–21). In these mice, we also noted that the overall shape of the skull was affected, with a domed cranial vault and an inverted bite (18,21). ACH patients present a similar craniofacial phenotype that is considered an endochondral ossification defect leading to shorter cranial base (22). The following issue therefore remains to be elucidated: is membranous ossification primarily affected in ACH? The availability of *Fgfr3*$^{Y367C/+}$ mice mimicking ACH provides an opportunity to address this issue by studying specifically the calvaria and skull base. In addition, the analysis of cranial anomalies in ACH and craniosynostosis syndromes (MS, CAN) offers the opportunity to compare the skull phenotype of three FGFR3-related diseases.

Here, we first provide evidence obtained through analysis of both *Fgfr3*$^{Y367C/+}$ mice and children with ACH showing that disruption of endochondral ossification result in skull base anomalies with premature fusion of the basal synchondroses and reduction of the size of the foramen magnum (FM). Then, studying the skull vault, we highlight a defective membranous ossification in *Fgfr3*$^{Y367C/+}$ mice and children with ACH. We observed non-ossified gap in frontal bones and a partial and premature fusion of sutures in both mice and children with ACH. Together, these data expand the general concept of dwarfism by showing that FGFR3 mutations affect not only the skull base and facial skeleton but also induce anomalies of the skull vault. This study sheds new light on the impact of *FGFR3* mutations on membranous ossification and could explain clinical hallmarks of ACH such as the macrocephaly and frontal bossing.

RESULTS

Fgfr3$^{Y367C/+}$ mice exhibit skull dysmorphy that mimics the human pathology

To evaluate the impact of the activating *Fgfr3* mutation (p.Tyr367Cys) on the craniofacial phenotype, we analyzed the growth of the skull of *Fgfr3*$^{Y367C/+}$ mice (21) and their control littermates at three different time-points: embryonic period (E16.5), birth (P0) and 3 weeks of age (P21). We focused on bones of the skull formed either by endochondral (nasal, occipital) or membranous (frontal, parietal, interparietal) ossification, whose developmental anomalies can contribute to overall skull dysmorphy. The macroscopic analysis of the cranium showed that a rounder shape of the head and shorter snout were present in *Fgfr3*$^{Y367C/+}$ mice at E16.5 compared with control littermates (Fig. 1A).

The severity of the dysmorphy worsened as the mice developed and increased from birth (Fig. 1B) to 3 weeks of age (Fig. 1C). This is similar to alterations of the long bones in *Fgfr3*$^{Y367C/+}$ mice that worsen in the first week of life (18). At 3 weeks of age, we observed a significant reduction in the length of the skull (66% of the control size, $P < 0.007$) (Fig. 1D).

The measurements of the size of each calvarial bone showed that the different bones are not equally affected by the *Fgfr3* mutation. We found a severe decrease in size in nasal (54% $P < 0.001$) and occipital bones (47%, $P < 0.001$), which are in accordance with anomalies in endochondral ossification (18). Focusing on bones formed by membranous ossification, the size of the interparietal bone was increased (125%, $P < 0.001$) (Fig. 1E), which could be a compensation of the reduced size of the occipital bone. No anomaly was observed in parietal bones, whereas the frontal bones were significantly reduced in size (82%, $P < 0.01$). We also observed the presence of a non-ossified gap in the frontal bones in all *Fgfr3*$^{Y367C/+}$ mice. The cellular origin of these bones formed by membranous ossification is different; the frontal bones are derived from cranial neural crest cells, whereas the parietal bones are derived from mesodermal cells (23). Interestingly, the mice expressing the *Fgfr3* mutation constitutively in mesoderm-derived tissues (Prx1,*Fgfr3*$^{Y367C/+}$) did not display frontal bone anomalies (data not shown). Our results show that the expression of *Fgfr3*$^{Y367C/+}$ mutation in neural crest-derived tissues causes an abnormal membranous ossification. Overall, the anomalies of the cranial bones in *Fgfr3*$^{Y367C/+}$ mice indicate that activated *Fgfr3* disrupted both endochondral and membranous ossification and allow to conclude that FGFR3 also contribute to the cranial vault development.

Next we compared the consequences on the craniofacial phenotype of *Fgfr3*-activating mutations in mice and humans. Viscerocranium and neurocranium were analyzed using μ-computed tomography (μCT) and CT scans. As observed on macroscopic preparations of the skulls, *Fgfr3*$^{Y367C/+}$ mice exhibited a domed macrocephalic cranium with an alteration of the frontal bones, a shorter snout and malocclusion at P21 (Fig. 2A). In humans, *FGFR3*-activating mutations induced various skeletal anomalies of the skull. Comparative analysis of CT scans of ACH, CAN (one child), MS patients and controls showed that the various *FGFR3* mutations do not alter the morphology of the skull in the same way, but all of them altered the growth of the skull vault (Fig. 2B). Interestingly, we observed consistently a large non-ossified gap in the skull vault of ACH and CAN patients (Fig. 2B). Though macrocephaly was present in the three conditions, the coronal sutures were usually fused in MS and CAN patients inducing a typical turribrachycephaly. In both conditions, the craniosynostosis might be severe and result in a cloverleaf shaped skull. Conversely, the alterations of the midface are absent in MS (24), whereas prognathism with reduced size of maxilla and mandible were found in ACH patients and in the CAN patient with cloverleaf skull studied here and others CAN patients reported previously (9,25,26). Many of these features are observed in mice carrying the mutation responsible for MS syndrome (*Fgfr3*^{P244R}) such as abnormal skull shape, reduced snout and malocclusion (12,27).

To further characterize these defects, we performed morphometric analyses in *Fgfr3*$^{Y367C/+}$ mice and children with ACH and their respective controls. We analyzed μCT and CT scan images of the skull using anatomical landmarks and geometric morphometrics (28). The principal components analysis (PCA) of the mouse skull shape separates the *Fgfr3*$^{Y367C/+}$ mice and their control littermates. When compared with their control littermates, the *Fgfr3*$^{Y367C/+}$ mice were characterized by a domed cranial vault, more vertical interparietal and occipital bones, an anteriorly and inferiorly projected FM, a shorter basioccipital bone, a shorter palate mainly because of an anteriorly reduced premaxilla, and a shorter snout (Fig. 2C). The modification of the posterior vault and position of the posterior sutures found in the *Fgfr3*$^{Y367C/+}$ mice could be explained by differences in growth of the occipital and interparietal bones (Figs 1E and 2C). Importantly, total or partial premature fusion of coronal,

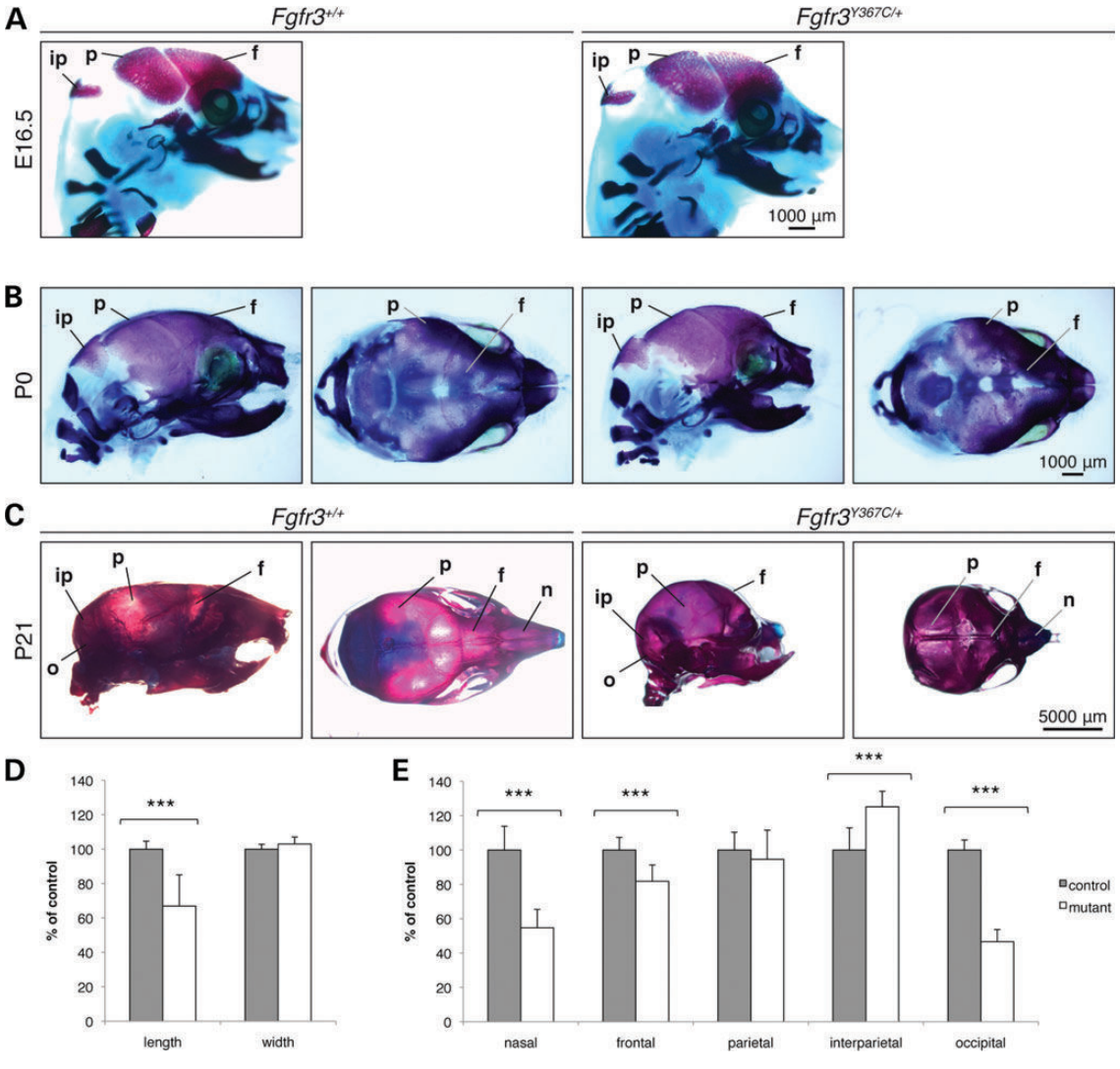

Figure 1. Macroscopic analysis of the skull of *Fgfr3*$^{Y367C/+}$ mice from antenatal to postnatal period. (**A**) Alizarin red and Alcian blue staining of the skull in *Fgfr3*$^{Y367C/+}$ ($n = 18$) compared with WT embryos ($n = 20$) at E16.5 of age showing the preliminary ongoing ossification. (**B**) Macroscopic analysis of the skull in *Fgfr3*$^{Y367C/+}$ ($n = 10$) compared with WT mice ($n = 11$) at birth (P0) showing a skull dysmorphy in mutant mice. (**C**) In P21 *Fgfr3*$^{Y367C/+}$ mice ($n = 41$) and WT mice ($n = 40$), a dramatic modification of the skull is present: the mutant mice display a turribrachycephaly with persistent defect of the medial skull vault at the level of frontal bone (non-ossified gap) with midface hypoplasia and inverted bite. (**D**) Measurements of the length and width of the skull of WT and *Fgfr3*$^{Y367C/+}$ mice at P21 showing a significant reduction of the length in mutant. (**E**) Measurements of the length of nasal, frontal, parietal, interparietal and occipital bones of *Fgfr3*$^{Y367C/+}$ mice versus WT, expressed as percentage of control. i.p. (interparietal), p (parietal), f (frontal) and o (occipital). $^{***}P < 0.001$.

frontonasal, squamous frontal and squamous parietal sutures were observed in all *Fgfr3*$^{Y367C/+}$ mice thus indicating that activated *Fgfr3* accelerated the closure of the sutures and disturbed osteogenesis in dwarf mice (Supplementary Material, Fig. S1).

In humans, the PCA of the human skull shape separated the ACH patients and the unaffected individuals. When compared with unaffected individuals, ACH patients were characterized by a domed cranial vault, an occipital bone more horizontally positioned but without a shorter posterior cranial fossa, a smaller FM, a shorter basioccipital bone, a shorter and flatter facial skeleton and a wider aspect of the most posterior facial skeleton (Fig. 2C). Focusing our analyses on sutures of the skull, we observed premature fusion of the sagittal and squamous sphenoidal sutures in ACH cases (3/6) (Supplementary Material, Fig. S1). This observation is consistent with recent papers reporting synostosis of multiple sutures in patients with ACH (29).

Our results revealed that the shape changes were highly similar in *Fgfr3*$^{Y367C/+}$ mice and ACH and that activated *FGFR3* disrupt membranous ossification in chondrodysplasia.

Fgfr3$^{Y367C/+}$ and human skull base anomalies appear during development

To evaluate the impact of activated *FGFR3* on the skull base, we focused our analyses on the spheno-occipital (SOS) and intra-occipital (IOS) synchondroses. At E16.5, macroscopic studies revealed no obvious abnormality (Fig. 3A). However, histological studies showed that in control mice, the cartilage

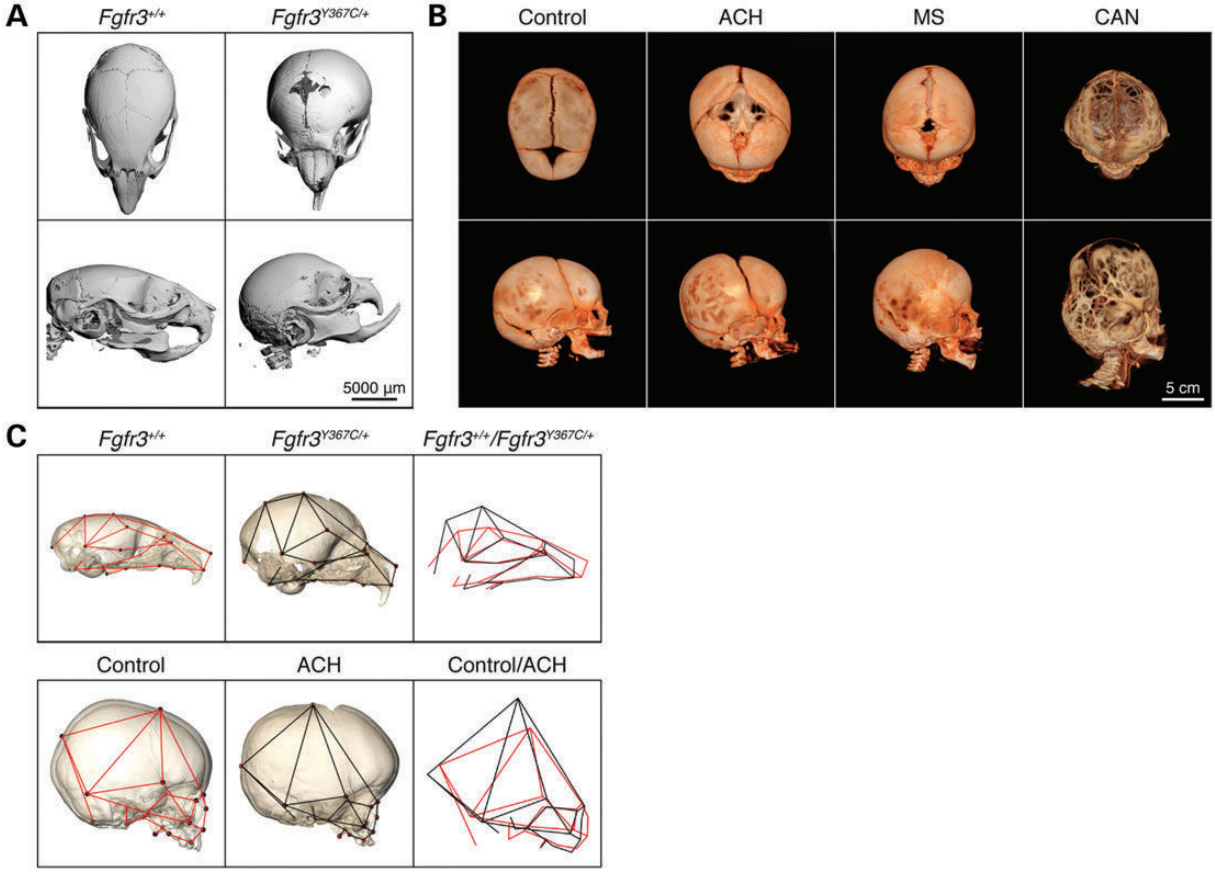

Figure 2. µCT of the head of *Fgfr3*$^{Y367C/+}$ mice and CT of ACH, MS, CAN patients with FGFR3-activating mutations. (**A**) µCT of *Fgfr3*$^{Y367C/+}$ ($n = 7$) and WT ($n = 7$) mice at P21 showing domed macrocephalic cranium with an impressive alteration of the vault and malocclusion in *Fgfr3*$^{Y367C/+}$ mice. (**B**) Representative CT of the skull at 3 months of age of control, ACH, MS and CAN patients. All FGFR3-related syndromes display macrocephaly and an altered shape of the skull. (**C**) Morphometric analyses of the *Fgfr3*$^{Y367C/+}$ mice ($n = 7$) versus their control littermates ($n = 7$), and ACH patients ($n = 6$) versus control patients of the same age ($n = 6$) showing the same modification of the skull vault and the midface. Superposition (Procrustes) of the consensus shape of the controls (red lines) and that of the mutants (black lines) showing similar anomalies.

was organized much like the growth plate cartilage of long bones, whereas in the *Fgfr3*$^{Y367C/+}$ mice, we observed a disorganized cartilage characterized by a smaller hypertrophic zone (Fig. 3B). At P0, the SOS anomaly was obvious with the sphenoid and occipital bones partially fused in most pups (6/7) (Fig. 3A). Both proliferative and hypertrophic zones were reduced, as was the size of the hypertrophic chondrocytes, revealed by Col X immunostaining (Fig. 3B). At P21, there was a total fusion of the SOS in all the mutants (Fig. 3A) and no hypertrophic chondrocytes were present (Fig. 3B). µCT scan analysis of the skull base confirmed this loss of SOS (Fig. 3C). Macroscopic and µCT analysis also showed that the IOS were fused in *Fgfr3*$^{Y367C/+}$ mice at P21 (Fig. 3C). The synchondroses defects are constant and severe compared with those reported in *Fgfr3*^{P244R} mice, where mild synchondroses anomalies are also present and lead to less premature closure of the IOS and SOS during development (12).

We next investigated the human cranial base in CT scans and observed a loss of SOS and IOS in ACH patients (Fig. 3D; Supplementary Material, Fig. S1) that was not found in MS or CAN (data not shown). The premature loss of the principal growth cartilage at the cranial base impaired postnatal growth of craniofacial bones and could explain some clinical hallmarks of ACH including hypoplasia of the midface and facial dysmorphy.

Fgfr3$^{Y367C/+}$ mice present an abnormal craniovertebral junction as in human pathology

To more firmly establish the extent of the anomalies at the craniovertebral junction in FGFR3-related disorders, we analyzed this region in both mouse model and human. µCT data of *Fgfr3*$^{Y367C/+}$ mice provided the opportunity to explore this area, in particular to look at the shape and size of the FM and atlas (C1). We observed a modification of FM in shape and size in *Fgfr3*$^{Y367C/+}$ mice at 3 weeks of age (Fig. 4A and B). The stenosis of the FM in *Fgfr3*$^{Y367C/+}$ mice affected the inner surface of the foramen with reduced sagittal (-20%; $P < 0.001$) and transverse (-40%; $P < 0.001$) diameters, modifying its shape. The inner transverse and sagittal diameters of the spinal canal at the level of C1 were also smaller in *Fgfr3*$^{Y367C/+}$ mice compared with controls (-25%; $P < 0.01$ and -10%; $P < 0.01$, respectively) (Fig. 4A and C). These alterations of craniovertebral junction are the consequence of both abnormal bone growth and premature fusion of cranial base synchondrosis.

In order to address the relevance to humans of these data, we measured in patients with FGFR3-related syndromes the size of the FM. It is established that the size of the FM in ACH patients is reduced (30). Here, we observed that the FM is not only reduced

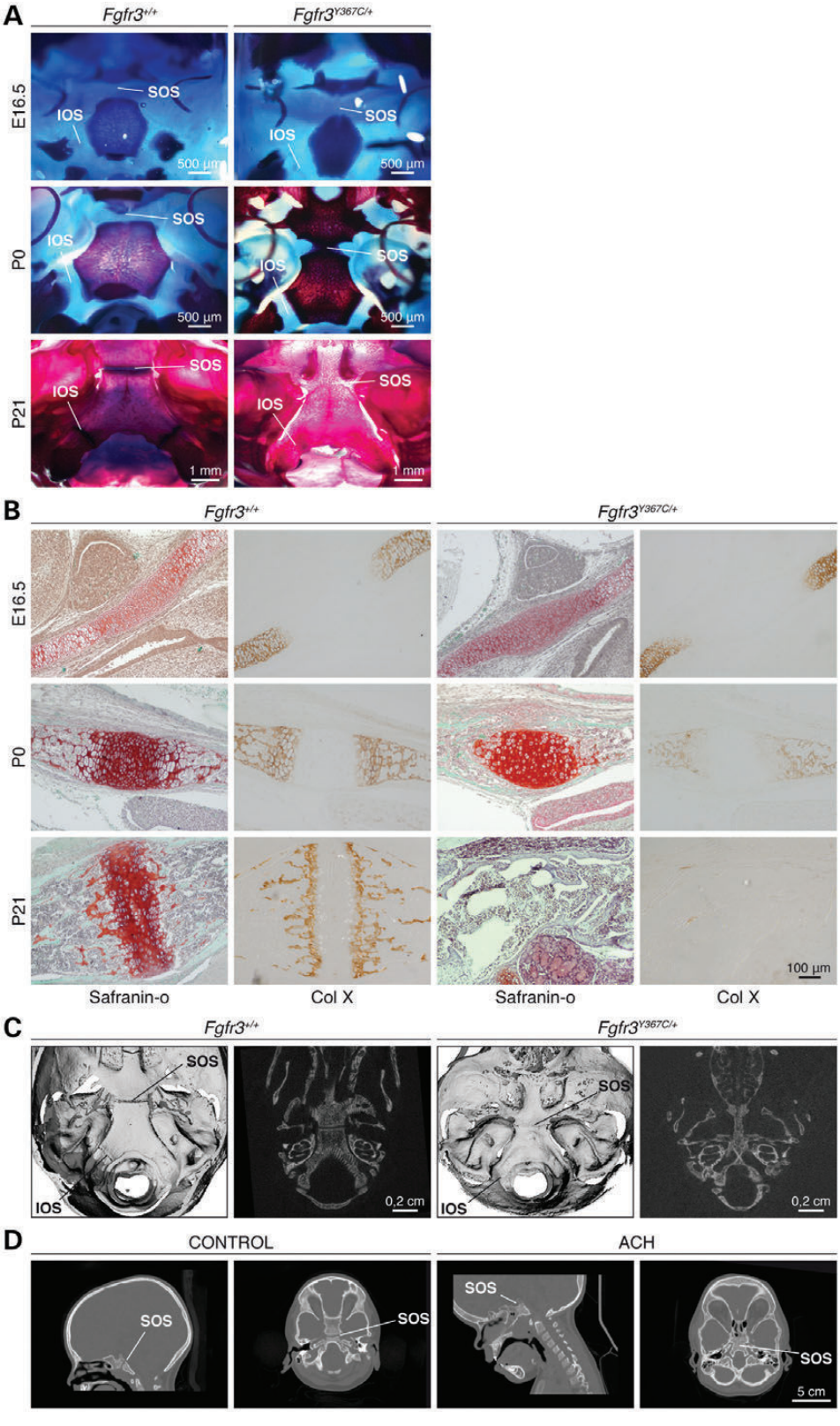

Figure 3. Analysis of the skull base of *Fgfr3*$^{Y367C/+}$ mice and ACH patients. (**A**) Macroscopic analysis of the skull base stained with Alizarin red and Alcian blue in control and mutant mice from E16.5 to 3 weeks of age (P21). Early fusion of the SOS and IOS during development in *Fgfr3*$^{Y367C/+}$ mice. (**B**) Histological analysis of SOS in E16.5 embryos, new born pups (P0) and 3-week-old mice (P21). The proliferative and hypertrophic zones of the cartilage are reduced in *Fgfr3*$^{Y367C/+}$ mice. An absence of SOS is observed at P21 in *Fgfr3*$^{Y367C/+}$ mice. (**C**) Representative µCT of WT ($n = 6$) and *Fgfr3*$^{Y367C/+}$ ($n = 6$) mice at P21 showing an absence of SOS and IOS in mutant. (**D**) Representative CT of ACH children (2 years old) and age-matched control showing the absence of SOS in ACH patient ($n = 6$) and its presence in controls ($n = 20$). SOS (spheno-occipital synchondrosis), IOS (intra-occipital synchondrosis).

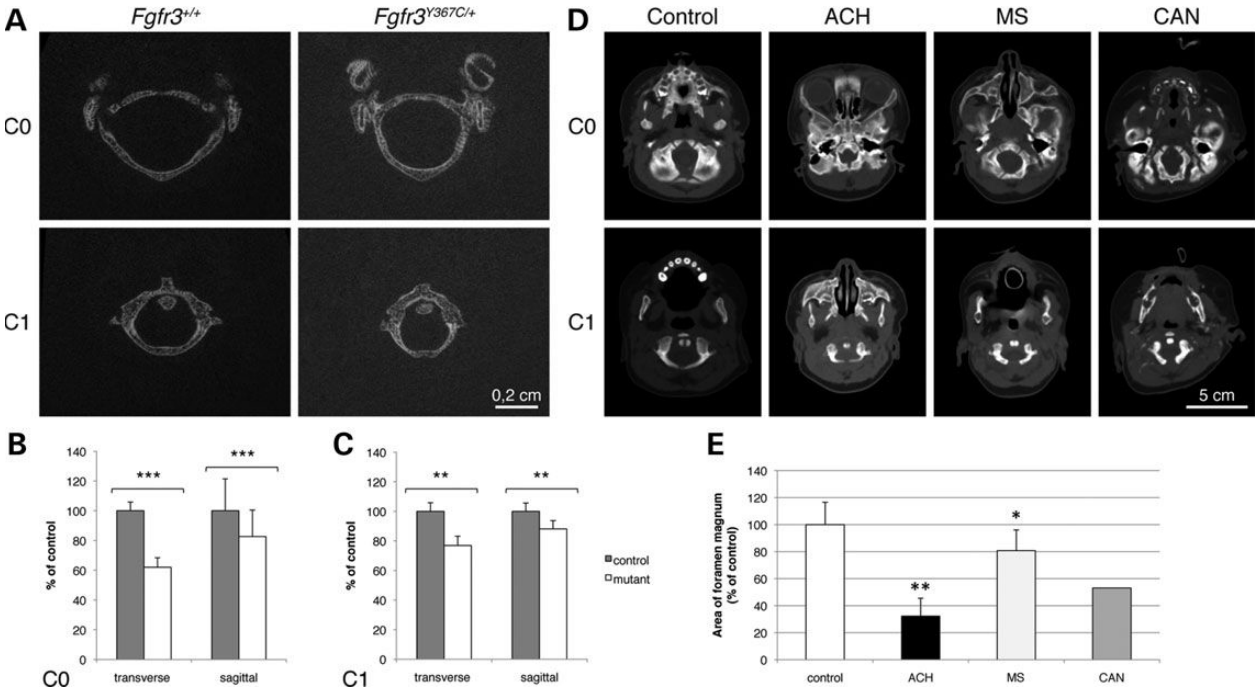

Figure 4. Reduction of the size of the FM in *Fgfr3*$^{Y367C/+}$ mice and ACH, MS, CAN patients with FGFR3-activating mutations. (**A**) Representative μCT of FM (C0) and atlas vertebra (C1) of *Fgfr3*$^{Y367C/+}$ mice and control littermate at 3 weeks of age. Modification of shape and size in mutant mice ($n = 7$). (**B**) Measurement of the transverse and sagittal length of C0 showing reduction of the size of C0 in *Fgfr3*$^{Y367C/+}$ mice ($n = 17$) compared with control ($n = 14$). (**C**) Measurement of the transverse and sagittal length of C1 showing reduction of the size of C1 in *Fgfr3*$^{Y367C/+}$ mice. (**D**) Representative CT of the FM at 3 months of age of control, ACH, MS and CAN patients. CT showing obvious reduction of the size of the FM in ACH and smaller reduction in MS and CAN. Measurement of the area of FM in control ($n = 20$, mean age 5.4 months), compared with ACH ($n = 6$, mean age 9.3 months), MS ($n = 8$, mean age 5.8 months) and CAN ($n = 1$, 3 months old) showing significant reduction of the size of ACH FM ($P < 0.001$) and MS ($P < 0.01$), $^{***}P < 0.001$, $^{**}P < 0.01$.

in ACH (32% of the size of controls; $P < 0.001$) but also in MS (81%; $P < 0.01$) and CAN patients (53%) (Fig. 4D and E). The degree of alteration of the FM is thus variable in FGFR3-related skeletal diseases and correlated to the severity of abnormal endochondral bone growth and the degree of fusion of the synchondroses.

Fgfr3$^{Y367C/+}$ mice exhibit cerebral alterations as in human pathology

To visualize the cervicomedullary junction at the level of the FM stenosis, we performed magnetic resonance imaging (MRI) of *Fgfr3*$^{Y367C/+}$ mice at 3 weeks of age. We observed severe brain alterations (Supplementary Material, Fig. S2A). The brain length was reduced by 20% ($P < 0.001$), and its height increased by 15% ($P < 0.01$) reflecting the skull modifications (Supplementary Material, Fig. S2B and C). When analyzing the posterior fossa, the neural structures in mutant mice appeared compressed and distorted when compared with controls. The cerebrospinal fluid (CSF) signal was reduced (Supplementary Material, Fig. S2D), especially at the level of the IV ventricle. No signs of hydrocephalus, ventricular dilation, nor increase of CSF subarachnoid spaces were found in mutant mice.

To address the relevance of these observations to human pathology, we used volumetric MRI analysis in humans identical to the methods used in *Fgfr3*$^{Y367C/+}$ mouse model. We found brain alterations in FGFR3-related diseases. In ACH, an enlargement of the subarachnoid spaces was commonly found (Supplementary Material, Fig. S2E) associated to a compression of the craniovertebral junction. These alterations were also present in another FGFR3-related chondrodysplasia, TD (data not shown) and in the CAN patient studied in this paper (Supplementary Material, Fig. S2E). In the great majority of MS patients, no compression of the craniovertebral junction and no hydrocephalus were found on MRI. Taken together, these results point toward the correlation between the size of FM and the significance of the cervicomedullary compression in FGFR3-related chondrodysplasia and craniosynostoses.

Fgfr3$^{Y367C/+}$ mice and human chondrodysplasia patients exhibit calvaria and coronal sutures defects

The skull vault consists mainly of flat bones formed by membranous ossification and separated by sutures. MS is characterized by uni or bilateral coronal suture synostosis (6,31). We tested here the hypothesis that activating Fgfr3 mutations disturb the suture development in dwarf mice and FGFR3-related chondrodysplasia. For that purpose, we analyzed coronal sutures of *Fgfr3*$^{Y367C/+}$ and control mice at E16.5, P0 and P21. We first confirmed that FGFR3 was present in the undifferentiated mesenchyme that separates the two fronts in *Fgfr3*$^{Y367C/+}$ coronal sutures at E16.5, P0 and P21 (data not shown) as in WT sutures (32). At P21, sagittal sections through the coronal sutures revealed that either (i) the two ossifications fronts, identified following Col I immunostaining, were fused or (ii) the overlap between the two

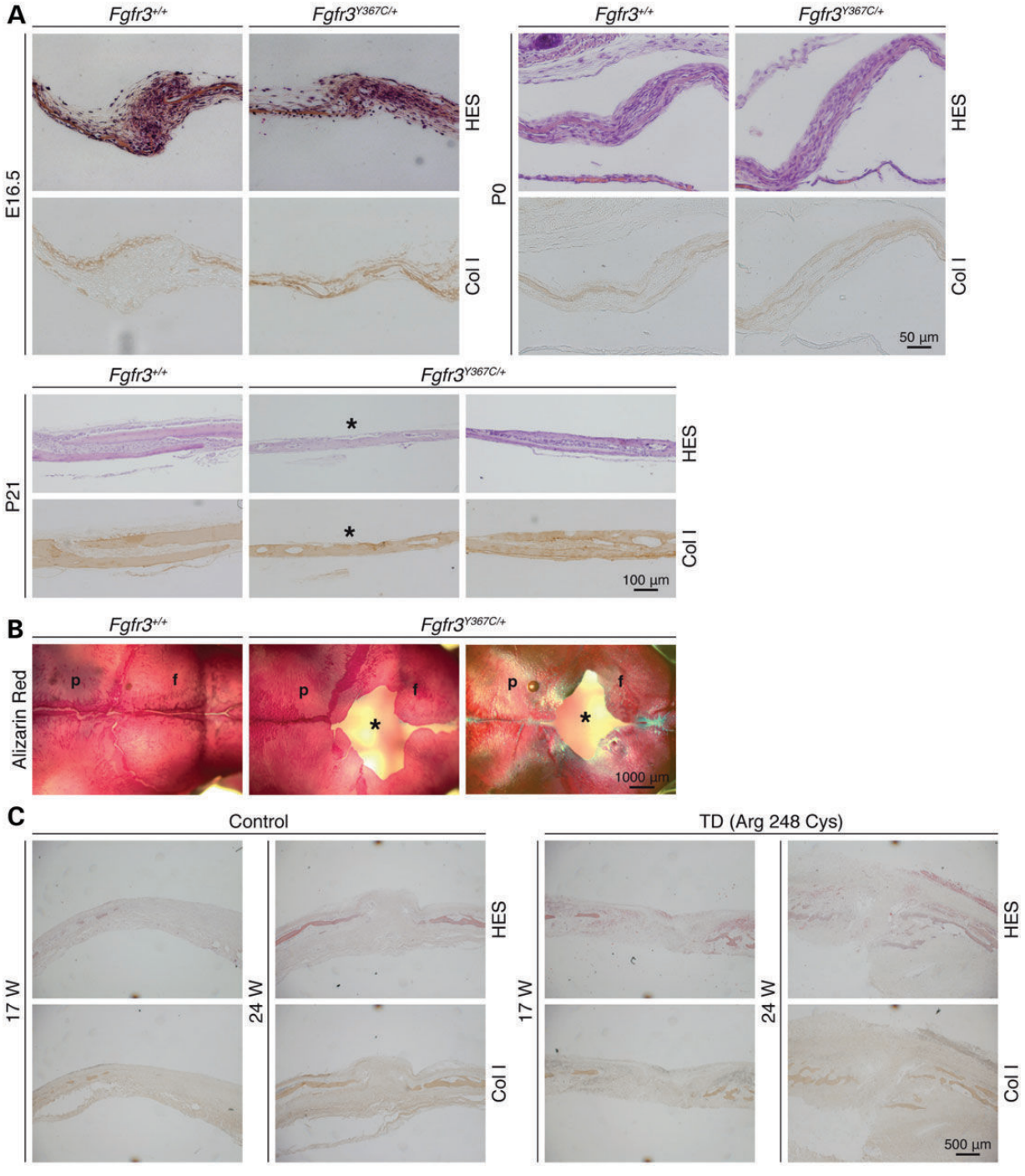

Figure 5. Partial fusion of the coronal suture in *Fgfr3*$^{Y367C/+}$ mice and TD patients. (**A**) Hematoxilin Eosin Safran (HES) staining of coronal sutures of E16.5, birth (P0), 3-week-old (P21) mutant and control mice. At P21, sutures are occasionally completely fused (*). Collagen type I (Col I) immunostaining of the coronal sutures, confirming the limits of the ossification fronts. (**B**) Macroscopic representation of the skull vault of *Fgfr3*$^{Y367C/+}$ mice and control littermates at 3 weeks of age stained with Alizarin red and Alcian blue. Impressive defect of the frontal bone (*) in mutant ($n = 13$) absent in control mice ($n = 14$). Sutures are occasionally completely fused and the overlap of the ossification fronts is increased. (**C**) Histological analysis of human coronal suture of TD ($n = 6$, aged 13–24 gestational weeks, mean age = 19.8) (TD) and age-matched control ($n = 6$, aged 16–26 gestational weeks, mean age = 21.5) fetuses. HES staining of coronal sutures and Col I immunostaining of the coronal sutures showing the premature fusion of TD suture compared with control at 17 and 24 gestational weeks. p (parietal), f (frontal).

fronts was increased (Fig. 5A). This is an important finding because in Muenke mouse model coronal suture fusion was a rare event (13).

Macroscopic examinations of P21 skull vaults confirmed the fusion or increased overlap of the ossifications fronts at the coronal suture, as well as an important medial non-ossified gap in *Fgfr3*$^{Y367C/+}$ affecting the two frontal bones anteriorly to the coronal suture (Fig. 5B). This defect was observed in >90% of the *Fgfr3*$^{Y367C/+}$ mice and was confirmed with µCT scans (Fig. 2A; Supplementary Material, Fig. S1).

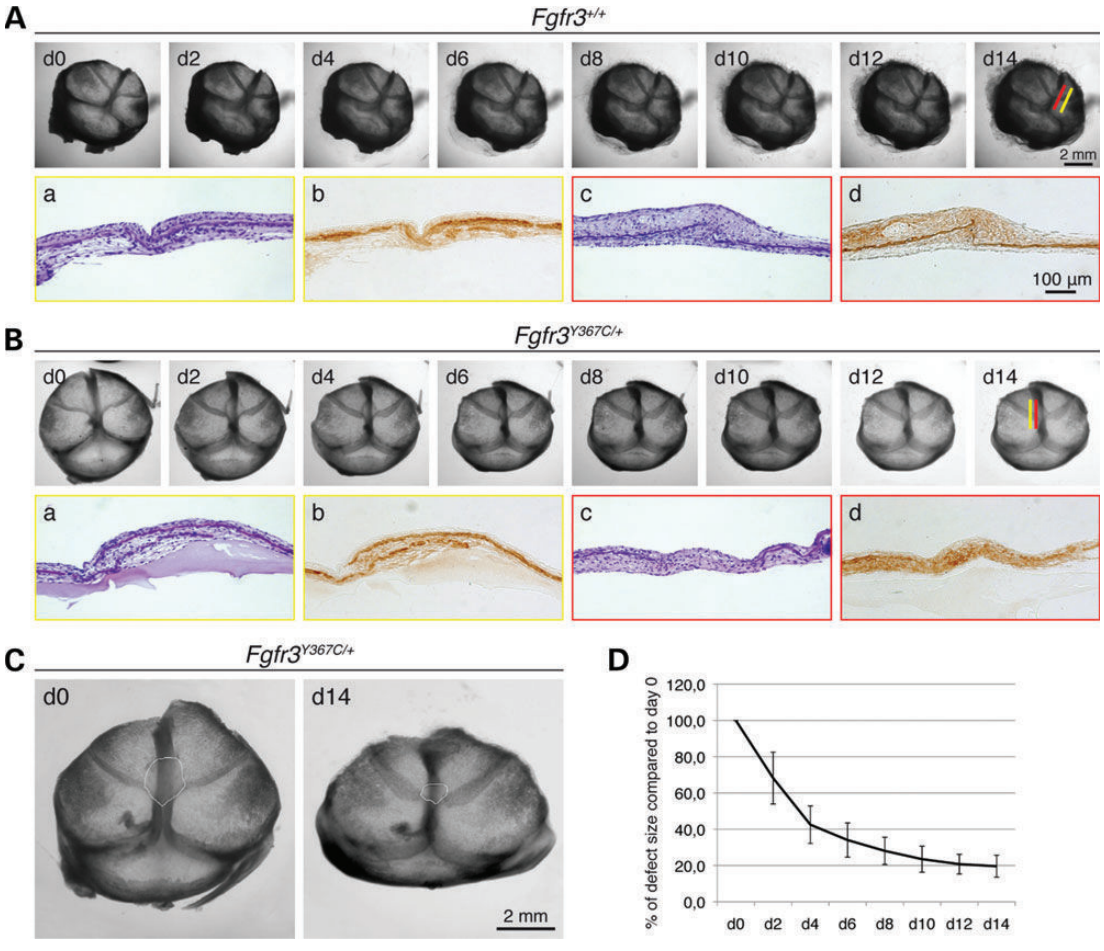

Figure 6. Culture of fetal calvaria isolated from *Fgfr3*$^{Y367C/+}$ mice and control littermate. (**A**) Representative images of the *ex vivo* culture of calvaria from control mice (*Fgfr3*$^{+/+}$) during 14 days ($n = 8$). HES staining and Col I immunostaining of the sutures revealed the absence of calvarial defect and limited overlap of ossifications fronts. Yellow line boxed images are representative images from sections of the coronal suture away from the sagittal midline, whereas red line boxed images are representative of sections closer to the midline. (**B**) Representative images of the *ex vivo* culture of calvaria from *Fgfr3*$^{Y367C/+}$ mice during 14 days ($n = 8$). HES staining and Col I immunostaining of the sutures revealed the presence of a large calvarial defect (red boxed) and increased overlap of ossifications fronts (yellow boxed). Yellow line boxed images are representative images from sections of the coronal suture away from the sagittal midline, whereas red line boxed images are representative of sections closer to the midline. (**C**) Higher magnification of the calvaria at Day 0 (d0) and Day 14 (d14) in *Fgfr3*$^{Y367C/+}$ mice. The calvarial defect is highlighted with a white line. (**D**) Evaluation of the reduction of the size of the calvaria defect during 14 days *ex vivo* culture in *Fgfr3*$^{Y367C/+}$ fetal mice ($n = 8$).

To parallel these analyses, we took opportunity of human coronal sutures isolated from TD, a severe and lethal form of chondrodysplasia associated with an *FGFR3*-activating mutation and age-matched control fetuses. At 17 weeks of gestational age, we observed an increased ossification of the coronal suture revealed by Col I immunostaining in TD when compared with age-matched controls (Fig. 5C). This premature fusion of the coronal suture in TD was even more pronounced at 24 weeks of age (Fig. 5C). These data, obtained in human coronal sutures, confirm the crucial role of FGFR3 in suture homeostasis during formation of the skull vault.

Fgfr3$^{Y367C/+}$ calvarial defects only partially resolve *ex vivo*

To add further support to the notion that *FGFR3* mutation disturbs skull vault, we next performed mouse calvarial *ex vivo* studies. Indeed, in ACH, it has been suggested that premature fusions of synchondrosis are responsible for the altered overall shape of the skull. It is therefore plausible that the observed defects of the cranial base may influence the fusion and growth of calvarial flat bones and contribute to the calvarial defect (foramina). In order to suppress any potential contribution of the cranial base to this defect, calvaria from *Fgfr3*$^{Y367C/+}$ and control embryos (E16.5) were dissected from the rest of the skull, separated from the influence of the brain and the cranial base and cultured *ex vivo* during 14 days (33). This strategy revealed that the cranial base and brain likely prevent the resolution of the defect since the size of the defect rapidly decreased when the calvaria was separated from the base (Fig. 6A and B). The defect regressed by >50% in 4 days (Fig. 6C and D). The defect however did not completely resolve and was still detected after 2 weeks of culture (Fig. 6B–D). Studying the coronal suture after 14 days of culture using Col I immunostaining, we observed anomalies characterized by an increase of the overlap between the two front of ossification (frontal and parietal bones). These data suggest that alterations of the underlying brain and skull base alone do not explain all the modifications we observed at the cranial vault and that activated *Fgfr3* induces an autonomous

membranous ossification delay of frontal bones. These results further confirm the role of FGFR3 in the vault formation and suture growth and fusion. Thus membranous ossification is disturbed by *FGFR3* mutations responsible for both chondrodysplasias and craniosynostoses.

DISCUSSION

This study arose from the observation that in humans, *FGFR3*-activating mutations result in ACH and MS where the bones predominantly affected are different: long bones formed by endochondral ossification in ACH and the parietal and frontal bones formed by membranous ossification in MS. It is usually considered that in ACH, endochondral ossification defects lead to reduced growth plate and fusion of synchondroses (22), while in MS membranous defects cause unilateral or bilateral premature fusion of coronal sutures (31). However, recent studies on patients and mouse models of FGFR3-related diseases, including this paper, draw a more complex picture. Here, we showed that in ACH patients and $Fgfr3^{Y367C/+}$ mice, the defective cranial phenotype is not the sole consequence of disturbed endochondral ossification but that membranous ossification is also affected.

In the developing skull base, we observed a severe defect of the endochondral ossification characterized by reduced size of the chondrocytes with a lack of organization, inducing synchondrosis premature fusion. This defect is similar to growth plate cartilage anomalies observed in $Fgfr3^{Y367C/+}$ mice, ACH and TD long bones (34) and confirms that activated FGFR3 disturbs all cartilages in the skeleton. Other reports on craniosynostosis and chondrodysplasia murine models support the evidence that FGFR3 and the Mapkinase pathway regulate synchondrosis closure (12,35,36). We also provided evidence that the synchondroses premature closure accounts for the FM stenosis and the cerebral alteration at posterior fossae in $Fgfr3^{Y367C/+}$ mice and ACH patients. These data correlate with clinical features of ACH (22,30). Interestingly, our study also demonstrated that in MS patients a significant reduction in the size of the FM was present suggesting that cranial base anomalies occur in craniosynostoses. The degree of reduction of FM area varied among FGFR3-related conditions with diverse clinical consequences; patients with ACH and CAN might need a surgical decompression of the craniovertebral junction, whereas in typical MS such surgical decompression is not needed. This spectrum of anomalies varying in FGFR3-related conditions may be due to the distinct impact of specific *FGFR3* mutations on chondrogenesis and osteogenesis during bone growth and highlight the complexity of RTK signaling in skeleton development. It was previously demonstrated that FGF signaling activates multiple downstream targets such as the mitogen-activated protein kinase pathway (21) and P38 (37) and synergizes with partners like transforming growth factor-β (38) and Wnt (39). The variable impact of FGFR3 mutations on endochondral ossification, limb and vertebral anomalies are reported not only in ACH but also in MS (40) and CAN syndromes (25). Interestingly, activating or loss-of-function mutations of FGFR1 and FGFR2, responsible for craniosynostosis, also induce defective long bone development (41).

The biological consequence of *FGFR3* mutations in craniosynostoses is a disruption of skeletal growth characterized by dysregulation of the intramembranous bone formation at the suture. The impairment of proliferation or accelerated differentiation of cranial osteoblasts leads to premature fusion of cranial sutures thus disturbing the expansion of the skull vault (42). Here, by investigating the skull vault of dwarf mice ($Fgfr3^{Y367C/+}$), we showed an alteration of membranous ossification with partial and premature fusion of the coronal sutures, and a reduced formation of the frontal bones, contrasting with the normal size of the parietal bones. To add further support to the notion that membranous ossification is affected in human pathology, we analyzed CT images of children with ACH and noted a delayed development of the frontal bones. Furthermore, we demonstrated that this ossification delay of the frontal bones was only partially rescued in calvaria cultured without skull base thus providing evidence that activated *FGFR3* affects specifically and autonomously membranous ossification. The high level of expression of *FGFR3* in the frontal bones compared with parietal bones (43) and this can also explain the difference in size (shorter frontals and normal parietals) due to the activating *FGFR3* mutation. We also analyzed ACH scans and TD coronal sutures by histology and we noted some degree of synostosis in coronal and sagittal sutures. Similar to our results, several cases of suture synostosis were reported in ACH patients (29,44,45), hypochondroplasia (MIM 146000) (46), mild dwarfism (47) and TD (48,49). Growth in the calvarial sutures is perpendicular to the orientation of the suture and is normally maintained throughout the period of growth of the brain. Synostosis of one or more sutures is accompanied by compensatory growth in other sutures and remodeling of other parts of the skull. Our data suggest thus that both synostosis and membranous ossification delay participate to the development of the prominent forehead observed in ACH. Here, we provide convincing data that abnormal FGF signaling leads to both synostoses and delay of membranous ossification.

This study highlights the impact of *FGFR3* mutations during cranial development in ACH and shows that both endochondral and intramembranous ossifications are primarily affected. The relevant hallmarks of ACH such as frontal bossing and macrocephaly might be the consequence of the disrupted membranous ossification. Demonstration of the impact of *FGFR3* mutations on craniofacial development should initiate novel pharmacological and surgical therapeutical approaches. $Fgfr3^{Y367C/+}$ mice will constitute a unique model to test these new strategies.

MATERIALS AND METHODS

Human subjects

All patients with craniosysnostoses and ACH were examined and followed at the Craniofacial Surgery Unit of Necker-Enfants Malades Hospital.

Children with MS ($n = 8$, mean age 5.8 months) and CAN ($n = 1$, 3 months old) presented with a brachycephaly due to a bicoronal synostosis and were operated on.

Coronal sutures were isolated from fetal skull derived from medically aborted control ($n = 6$) and TD ($n = 6$). Parents of all the subjects provided written, informed consent before recruitment into the study. Ethics approvals were obtained from the institutional review Board of Necker-Enfants Malades Hospital.

Mutational analysis of human FGFR3 gene

For the FGFR3 TM domain (ACH, CAN) and EC domain (MS), the primers used were described previously (2,6). Blood samples were obtained with the consents of the parents and were collected and processed in agreement with the French ethical committee guidelines.

Mouse models

WT and *Fgfr3*$^{Y367C/+}$ mice were generated by crossing *Fgfr3*^{neoY367C} mice (18) and Cmv-Cre mice (50). The mutant mice express the c.1100A > G (p.Tyr367Cys) mutation corresponding to the c.1118A > G (p.Tyr373Cys) in TD. All the mice were genotyped by PCR of tail DNA as described previously (18). All the experiments were conducted in *Fgfr3*$^{Y367C/+}$ mice, a mouse model that display parts of the clinical hallmarks of ACH (21). Experimental animal procedures and protocols were approved by the French Animal Care and Use Committee.

Whole-mount Alcian blue-Alizarin red staining

Calvariae of *Fgfr3*$^{Y367C/+}$ and their wild-type mice at E16.5, P0 and P21 were fixed in 95% ethanol and then stained with Alizarin red and Alcian blue, cleared by KOH treatment and stored in glycerol according to standard protocols (18). Size of the calvarial bones was measured on images captured with an Olympus PD70-IX2-UCB using cell sens software (Olympus).

Immunohistochemistry

Calvariae of *Fgfr3*$^{Y367C/+}$ and their wild-type littermates were fixed in 4% paraformaldehyde at 5°C, and decalcified in 0.5 M EDTA (pH 8.0) overnight or up to 1 week, depending on the age of the mice, and then dehydrated in graded series of ethanol, cleared in xylenes and embedded in paraffin. Five microns of sagittal sections were cut and stained with hematoxylin and eosin (H&E) and safrin-O and subjected to immunohistochemical staining using standard protocols using an antibody against FGFR3 (1:250 dilution; Sigma-Aldrich Co, St. Louis, MO, USA), anti-Col X (1:50 dilution; BIOCYC, Luckenwalde, Germany) and anti-Col I (1:500 for murine tissue, 1:1000 for human tissue, Novotec, Lyon, France) using the Dako Envision Kit (Dako North America, Inc, CA, USA). Same protocol was used for human coronal sutures. TD fetuses were obtained from legally terminated pregnancies according to the French ethical committee recommendations. The control group included spontaneously aborted fetuses showing no evidence of skeletal abnormalities. Images were captured with an Olympus PD70-IX2-UCB microscope (Olympus, Tokyo, Japan).

CT scanner of mouse and human

The head of the *Fgfr3*$^{Y367C/+}$ mice and their control littermates were imaged by μCT using a VivaCT40 microscanner (SCANCO Medical, Brüttisellen, Switzerland). All specimens from *Fgfr3*$^{+/+}$ and *Fgfr3*$^{Y367C/+}$ mice were scanned at the LBTO facility (INSERM U1059-IFR 143-IFRESIS St Etienne, France) using the following protocols (0.020 mm voxel resolution, 55 kV, Sigma 1.5/Support 2/Threshold 148, 150 μA).

Human scans were performed with a 64-slice CT system (LightSpeed VCT, General Electric Medical Systems, Milwaukee, WI, USA). The bone images were reconstructed in three dimensions using Carestream PACS v11.0 software (Carestream Health, Rochester, NY, USA).

Morphometric analysis

The samples consist of CT images of six patients diagnosed with ACH and six unaffected individuals matching on age the ACH patients (0.5–5 years), and of high-resolution CT images of seven P21 *Fgfr3*$^{Y367C/+}$ mice and seven control littermates. 3D coordinates of 31 landmarks were recorded on the reconstructed skulls of humans and mice and analyzed by geometric morphometric methods. Standardization for position, scale and orientation was obtained by Procrustes superimposition (51,52), and shape information (Procrustes coordinates) and size (centroid size; (52)) were extracted. Shape information was subsequently analyzed by PCA (for more information on geometric morphometrics applied to craniofacial birth defect, see, for example (28)). Wireframes are used to visualize the shape differences corresponding to the skull associated with specific scores on principal component 1 and 2.

Magnetic resonance imaging

All MRI were conducted on anesthetized (isoflurane) *Fgfr3*$^{+/+}$ and *Fgfr3*$^{Y367C/+}$ mice using a 4.7 T Bruker Biospec MR imager (Bruker BioSpin GmbH, Rheinstetten, Germany) at the Small Animal Imaging Facility of Paris Descartes University, INSERM, U970, Paris, France. The resolution was 0.0078 × 0.0078 cm/px × 625 μm/px for a matrix size of 256 × 256 × 32 with three averages and a repetition time of 1200 ms (echo time 80 ms) and two dummies scans. The total scan time was 30 min. Osirix software was used for postprocessing. For the quantification of CSF, after a midsagittal plane selection, a region of interest was drawn manually, delineating the posterior brain. The midsagittal slice (S) was normalized by subtracting S by Sm which was S filtered by a large median filter (5 × 5), resulting in a contrast image $C = S -$ Sm. The distribution of gray levels of C in brain tissue approximated a Gaussian behavior. Hence, bright CSF pixels corresponded to outliers for this Gaussian distribution. For CSF detection, we used one of the more current threshold (Th) used in 'box-and-whisker plots'. Th = Q75 + 1.5IQ, where Q75 and IQ are the 75 percentile and the interquartile range of C in the posterior brain, respectively. Then the fraction of pixels detected in the posterior brain (*FCSF*) was evaluated for each exam and *FCSF* values were compared between groups by a non-parametric Wilcoxon two-sample test. Difference between groups were considered significant for $P < 5\%$.

In human, MRI was performed with a 1.5T (Signa General Electric Medical Systems, Milwaukee, WI, USA) scanner using Carestream PACS v11.0 software (Carestream Health, Rochester, NY, USA). The MRI was performed without intravenous contrast enhancement.

Calvarial culture system

Ex vivo cultures were conducted as described previously (33) with slight modifications. E18.5 embryos were aseptically

dissected from the uterus of pregnant females and calvaria were separated from the rest of the skull after removal of the skin. The brain was detached form the calvaria and attention was paid not to remove the dura mater. Calvaria were then placed in 24-well plates, on top of 250 μl of Matrigel (BD Biosciences) previously placed at the bottom of the well. Calvaria were cultured in α-MEM (Gibco) supplemented with 10% fetal bovine serum (Gibco), 100 μg/ml ascorbic acid (Sigma) and 1% penicillin/streptomycin (Gibco). After 2 weeks, calvaria were separated from the gel, fixed in 4% paraformaldehyde at 4°C and embedded in paraffin. Serial sections of 5 mm were stained with H&E using standard protocols for histological analysis and submitted to immunohistological protocol. Images were captured with an Olympus PD70-IX2-UCB microscope. The size of the calvaria defect was measured using ImageJ software (NIH).

SUPPLEMENTARY MATERIAL

Supplementary Material is available at *HMG* online.

AUTHORS' CONTRIBUTIONS

F.D.R., M.B.D. and L.L.M. designed the mouse experiments, F.D.R. and A.M. implemented the clinical data, Y.H. generated CT data, M.D.B., N.K., D.K.E., E.M. and C.B.L. generated the data, F.D.R., M.B.D., Y.H. and L.L.M. analyzed the data; and F.D.R., M.B.D. and L.L.M. wrote the paper.

ACKNOWLEDGEMENTS

We thank Prof. Nathalie Boddaert for providing panel of control MRI (Hôpital Necker, Paris). We thank Dr Chiara Villa for her anatomopathological advices. We thank Gwennhael Autret and Daniel Balvay for MRI analyses (PIPA-ParisDescartes University) and Dr Laurence Vico and Norbert Laroche for μCT scanner analyses (LBTO INSERM U1059). We thank Dr Anne-Lise Delezoide, Dr B. Bessières and Dr J. Martinovic for providing the human suture samples. We thank Rachid Zoubairi for his work at the animal facility and Eric Le Gall for the artwork. We are grateful to the Association des Personnes de Petites Tailles and the Fondation des Gueules Cassées for supporting this work.

Conflicts of Interest statement. None declared.

WEB RESOURCE

www.omim.org.

REFERENCES

1. Naski, M.C., Wang, Q., Xu, J. and Ornitz, D.M. (1996) Graded activation of fibroblast growth factor receptor 3 by mutations causing achondroplasia and thanatophoric dysplasia. *Nat. Genet.*, **13**, 233–237.
2. Rousseau, F., Bonaventure, J., Legeai-Mallet, L., Pelet, A., Rozet, J.M., Maroteaux, P., Le Merrer, M. and Munnich, A. (1994) Mutations in the gene encoding fibroblast growth factor receptor-3 in achondroplasia. *Nature*, **371**, 252–254.
3. Shiang, R., Thompson, L.M., Zhu, Y.Z., Church, D.M., Fielder, T.J., Bocian, M., Winokur, S.T. and Wasmuth, J.J. (1994) Mutations in the transmembrane domain of FGFR3 cause the most common genetic form of dwarfism, achondroplasia. *Cell*, **78**, 335–342.
4. Placone, J. and Hristova, K. (2012) Direct assessment of the effect of the Gly380Arg achondroplasia mutation on FGFR3 dimerization using quantitative imaging FRET. *PLoS ONE*, **7**, e46678.
5. Rousseau, F., el Ghouzzi, V., Delezoide, A.L., Legeai-Mallet, L., Le Merrer, M., Munnich, A. and Bonaventure, J. (1996) Missense FGFR3 mutations create cysteine residues in thanatophoric dwarfism type I (TD1). *Hum. Mol. Genet.*, **5**, 509–512.
6. Muenke, M., Gripp, K.W., McDonald-McGinn, D.M., Gaudenz, K., Whitaker, L.A., Bartlett, S.P., Markowitz, R.I., Robin, N.H., Nwokoro, N., Mulvihill, J.J. *et al.* (1997) A unique point mutation in the fibroblast growth factor receptor 3 gene (FGFR3) defines a new craniosynostosis syndrome. *Am. J. Hum. Genet.*, **60**, 555–564.
7. Ibrahimi, O.A., Zhang, F., Eliseenkova, A.V., Linhardt, R.J. and Mohammadi, M. (2004) Proline to arginine mutations in FGF receptors 1 and 3 result in Pfeiffer and Muenke craniosynostosis syndromes through enhancement of FGF binding affinity. *Hum. Mol. Genet.*, **13**, 69–78.
8. Lajeunie, E., El Ghouzzi, V., Le Merrer, M., Munnich, A., Bonaventure, J. and Renier, D. (1999) Sex related expressivity of the phenotype in coronal craniosynostosis caused by the recurrent P250R FGFR3 mutation. *J. Med. Genet.*, **36**, 9–13.
9. Meyers, G.A., Orlow, S.J., Munro, I.R., Przylepa, K.A. and Jabs, E.W. (1995) Fibroblast growth factor receptor 3 (FGFR3) transmembrane mutation in Crouzon syndrome with acanthosis nigricans. *Nat. Genet.*, **11**, 462–464.
10. Chen, F., Sarabipour, S. and Hristova, K. (2013) Multiple consequences of a single amino acid pathogenic RTK mutation: the A391E mutation in FGFR3. *PLoS ONE*, **8**, e56521.
11. Marie, P.J., Miraoui, H. and Severe, N. (2012) FGF/FGFR signaling in bone formation: progress and perspectives. *Growth Factors (Chur, Switzerland)*, **30**, 117–123.
12. Laurita, J., Koyama, E., Chin, B., Taylor, J.A., Lakin, G.E., Hankenson, K.D., Bartlett, S.P. and Nah, H.D. (2011) The Muenke syndrome mutation (FgfR3(P244R)) causes cranial base shortening associated with growth plate dysfunction and premature perichondrial ossification in murine basicranial synchondroses. *Dev. Dyn.*, **240**, 2584–2596.
13. Twigg, S.R., Healy, C., Babbs, C., Sharpe, J.A., Wood, W.G., Sharpe, P.T., Morriss-Kay, G.M. and Wilkie, A.O. (2009) Skeletal analysis of the Fgfr3(P244R) mouse, a genetic model for the Muenke craniosynostosis syndrome. *Dev. Dyn.*, **238**, 331–342.
14. Mansour, S.L., Twigg, S.R., Freeland, R.M., Wall, S.A., Li, C. and Wilkie, A.O. (2009) Hearing loss in a mouse model of Muenke syndrome. *Hum. Mol. Genet.*, **18**, 43–50.
15. Naski, M.C., Colvin, J.S., Coffin, J.D. and Ornitz, D.M. (1998) Repression of hedgehog signaling and BMP4 expression in growth plate cartilage by fibroblast growth factor receptor 3. *Development*, **125**, 4977–4988.
16. Iwata, T., Chen, L., Li, C., Ovchinnikov, D.A., Behringer, R.R., Francomano, C.A. and Deng, C.X. (2000) A neonatal lethal mutation in FGFR3 uncouples proliferation and differentiation of growth plate chondrocytes in embryos. *Hum. Mol. Genet.*, **9**, 1603–1613.
17. Segev, O., Chumakov, I., Nevo, Z., Givol, D., Madar-Shapiro, L., Sheinin, Y., Weinreb, M. and Yayon, A. (2000) Restrained chondrocyte proliferation and maturation with abnormal growth plate vascularization and ossification in human FGFR-3(G380R) transgenic mice. *Hum. Mol. Genet.*, **9**, 249–258.
18. Pannier, S., Couloigner, V., Messaddeq, N., Elmaleh-Berges, M., Munnich, A., Romand, R. and Legeai-Mallet, L. (2009) Activating Fgfr3 Y367C mutation causes hearing loss and inner ear defect in a mouse model of chondrodysplasia. *Biochim. Biophys. Acta*, **1792**, 140–147.
19. Jonquoy, A., Mugniery, E., Benoist-Lasselin, C., Kaci, N., Le Corre, L., Barbault, F., Girard, A.L., Le Merrer, Y., Busca, P., Schibler, L. *et al.* (2012) A novel tyrosine kinase inhibitor restores chondrocyte differentiation and promotes bone growth in a gain of function Fgfr3 mouse model. *Hum. Mol. Genet.*, **21**, 841–851.
20. Mugniery, E., Dacquin, R., Marty, C., Benoist-Lasselin, C., de Vernejoul, M.C., Jurdic, P., Munnich, A., Geoffroy, V. and Legeai-Mallet, L. (2012) An activating Fgfr3 mutation affects trabecular bone formation via a paracrine mechanism during growth. *Hum. Mol. Genet.*, **21**, 2503–2513.
21. Lorget, F., Kaci, N., Peng, J., Benoist-Lasselin, C., Mugniery, E., Oppeneer, T., Wendt, D.J., Bell, S.M., Bullens, S., Bunting, S. *et al.* (2012) Evaluation of the therapeutic potential of a CNP analog in a Fgfr3 mouse model recapitulating achondroplasia. *Am. J. Hum. Genet.*, **91**, 1108–1114.
22. Horton, W.A., Hall, J.G. and Hecht, J.T. (2007) Achondroplasia. *Lancet*, **370**, 162–172.

23. Morriss-Kay, G.M. (2001) Derivation of the mammalian skull vault. *J. Anat.*, **199**, 143–151.
24. Ridgway, E.B., Wu, J.K., Sullivan, S.R., Vasudavan, S., Padwa, B.L., Rogers, G.F. and Mulliken, J.B. (2011) Craniofacial growth in patients with FGFR3Pro250Arg mutation after fronto-orbital advancement in infancy. *J. Craniofac. Surg.*, **22**, 455–461.
25. Arnaud-Lopez, L., Fragoso, R., Mantilla-Capacho, J. and Barros-Nunez, P. (2007) Crouzon with acanthosis nigricans. Further delineation of the syndrome. *Clin. Genet.*, **72**, 405–410.
26. Di Rocco, F., Collet, C., Legeai-Mallet, L., Arnaud, E., Le Merrer, M., Hadj-Rabia, S. and Renier, D. (2011) Crouzon syndrome with acanthosis nigricans: a case-based update. *Childs Nerv. Syst.*, **27**, 349–354.
27. Nah, H.D., Koyama, E., Agochukwu, N.B., Bartlett, S.P. and Muenke, M. (2012) Phenotype profile of a genetic mouse model for Muenke syndrome. *Childs Nerv. Syst.*, **28**, 1483–1493.
28. Heuze, Y., Boyadjiev, S.A., Marsh, J.L., Kane, A.A., Cherkez, E., Boggan, J.E. and Richtsmeier, J.T. (2010) New insights into the relationship between suture closure and craniofacial dysmorphology in sagittal nonsyndromic craniosynostosis. *J. Anat.*, **217**, 85–96.
29. Bessenyei, B., Nagy, A., Balogh, E., Novak, L., Bognar, L., Knegt, A.C. and Olah, E. (2013) Achondroplasia with multiple-suture craniosynostosis: a report of a new case of this rare association. *Am. J. Med. Genet. A*, **161**, 2641–2644.
30. Hecht, J.T., Horton, W.A., Reid, C.S., Pyeritz, R.E. and Chakraborty, R. (1989) Growth of the foramen magnum in achondroplasia. *Am. J. Med. Genet.*, **32**, 528–535.
31. Doherty, E.S., Lacbawan, F., Hadley, D.W., Brewer, C., Zalewski, C., Kim, H.J., Solomon, B., Rosenbaum, K., Domingo, D.L., Hart, T.C. *et al.* (2007) Muenke syndrome (FGFR3-related craniosynostosis): expansion of the phenotype and review of the literature. *Am. J. Med. Genet. A*, **143A**, 3204–3215.
32. Rice, D.P., Rice, R. and Thesleff, I. (2003) FGFR mRNA isoforms in craniofacial bone development. *Bone*, **33**, 14–27.
33. Perlyn, C.A., Morriss-Kay, G., Darvann, T., Tenenbaum, M. and Ornitz, D.M. (2006) A model for the pharmacological treatment of crouzon syndrome. *Neurosurgery*, **59**, 210–215; discussion 210–215.
34. Legeai-Mallet, L., Benoist-Lasselin, C., Munnich, A. and Bonaventure, J. (2004) Overexpression of FGFR3, Stat1, Stat5 and p21Cip1 correlates with phenotypic severity and defective chondrocyte differentiation in FGFR3-related chondrodysplasias. *Bone*, **34**, 26–36.
35. Sebastian, A., Matsushita, T., Kawanami, A., Mackem, S., Landreth, G.E. and Murakami, S. (2011) Genetic inactivation of ERK1 and ERK2 in chondrocytes promotes bone growth and enlarges the spinal canal. *J. Orthop. Res.*, **29**, 375–379.
36. Matsushita, T., Wilcox, W.R., Chan, Y.Y., Kawanami, A., Bukulmez, H., Balmes, G., Krejci, P., Mekikian, P.B., Otani, K., Yamaura, I. *et al.* (2009) FGFR3 promotes synchondrosis closure and fusion of ossification centers through the MAPK pathway. *Hum. Mol. Genet.*, **18**, 227–240.
37. Su, N., Sun, Q., Li, C., Lu, X., Qi, H., Chen, S., Yang, J., Du, X., Zhao, L., He, Q. *et al.* (2010) Gain-of-function mutation in FGFR3 in mice leads to decreased bone mass by affecting both osteoblastogenesis and osteoclastogenesis. *Hum. Mol. Genet.*, **19**, 1199–1210.
38. Chim, H., Manjila, S., Cohen, A.R. and Gosain, A.K. (2011) Molecular signaling in pathogenesis of craniosynostosis: the role of fibroblast growth factor and transforming growth factor-beta. *Neurosurg. Focus*, **31**, E7.
39. Krejci, P., Aklian, A., Kaucka, M., Sevcikova, E., Prochazkova, J., Masek, J.K., Mikolka, P., Pospisilova, T., Spoustova, T., Weis, M. *et al.* (2012) Receptor tyrosine kinases activate canonical WNT/beta-catenin signaling via MAP kinase/LRP6 pathway and direct beta-catenin phosphorylation. *PLoS ONE*, **7**, e35826.
40. Agochukwu, N.B., Solomon, B.D., Benson, L.J. and Muenke, M. (2013) Talocalcaneal coalition in Muenke syndrome: report of a patient, review of the literature in FGFR-related craniosynostoses, and consideration of mechanism. *Am. J. Med. Genet. A*, **161A**, 453–460.
41. Hatch, N.E. (2010) FGF signaling in craniofacial biological control and pathological craniofacial development. *Crit. Rev. Eukaryotic Gene Expression*, **20**, 295–311.
42. Wilkie, A.O. (1997) Craniosynostosis: genes and mechanisms. *Hum. Mol. Genet.*, **6**, 1647–1656.
43. Quarto, N., Behr, B., Li, S. and Longaker, M.T. (2009) Differential FGF ligands and FGF receptors expression pattern in frontal and parietal calvarial bones. *Cells Tissues Organs*, **190**, 158–169.
44. Georgoulis, G., Alexiou, G. and Prodromou, N. (2011) Achondroplasia with synostosis of multiple sutures. *Am. J. Med. Genet. A*, **155A**, 1969–1971.
45. Karadimas, C., Trouvas, D., Haritatos, G., Makatsoris, C., Dedoulis, E., Velissariou, V., Antoniadi, T., Hatzaki, A. and Petersen, M.B. (2006) Prenatal diagnosis of achondroplasia presenting with multiple-suture synostosis: a novel association. *Prenat. Diagn.*, **26**, 258–261.
46. Angle, B., Hersh, J.H. and Christensen, K.M. (1998) Molecularly proven hypochondroplasia with cloverleaf skull deformity: a novel association. *Clin. Genet.*, **54**, 417–420.
47. Bellus, G.A., McIntosh, I., Smith, E.A., Aylsworth, A.S., Kaitila, I., Horton, W.A., Greenhaw, G.A., Hecht, J.T. and Francomano, C.A. (1995) A recurrent mutation in the tyrosine kinase domain of fibroblast growth factor receptor 3 causes hypochondroplasia. *Nat. Genet.*, **10**, 357–359.
48. Tavormina, P.L., Shiang, R., Thompson, L.M., Zhu, Y.Z., Wilkin, D.J., Lachman, R.S., Wilcox, W.R., Rimoin, D.L., Cohn, D.H. and Wasmuth, J.J. (1995) Thanatophoric dysplasia (types I and II) caused by distinct mutations in fibroblast growth factor receptor 3. *Nat. Genet.*, **9**, 321–328.
49. Barroso, E., Perez-Carrizosa, V., Garcia-Recuero, I., Glucksman, M.J., Wilkie, A.O., Garcia-Minaur, S. and Heath, K.E. (2011) Mild isolated craniosynostosis due to a novel FGFR3 mutation, p.Ala334Thr. *Am. J. Med. Genet. A*, **155A**, 3050–3053.
50. Metzger, D., Clifford, J., Chiba, H. and Chambon, P. (1995) Conditional site-specific recombination in mammalian cells using a ligand-dependent chimeric Cre recombinase. *Proc. Natl. Acad. Sci. USA*, **92**, 6991–6995.
51. Rohlf, F.S.D. (1990) Extensions of the Procrustes method for the optimal superimposition of landmarks. *Syst. Zool.*, **39**, 40–59.
52. Dryden, I.L. and Mardia, K.V. (1998) *Statistical Shape Analysis*. Wiley, Chichester, UK.

Supplemental Data

Supplementary Figure S1

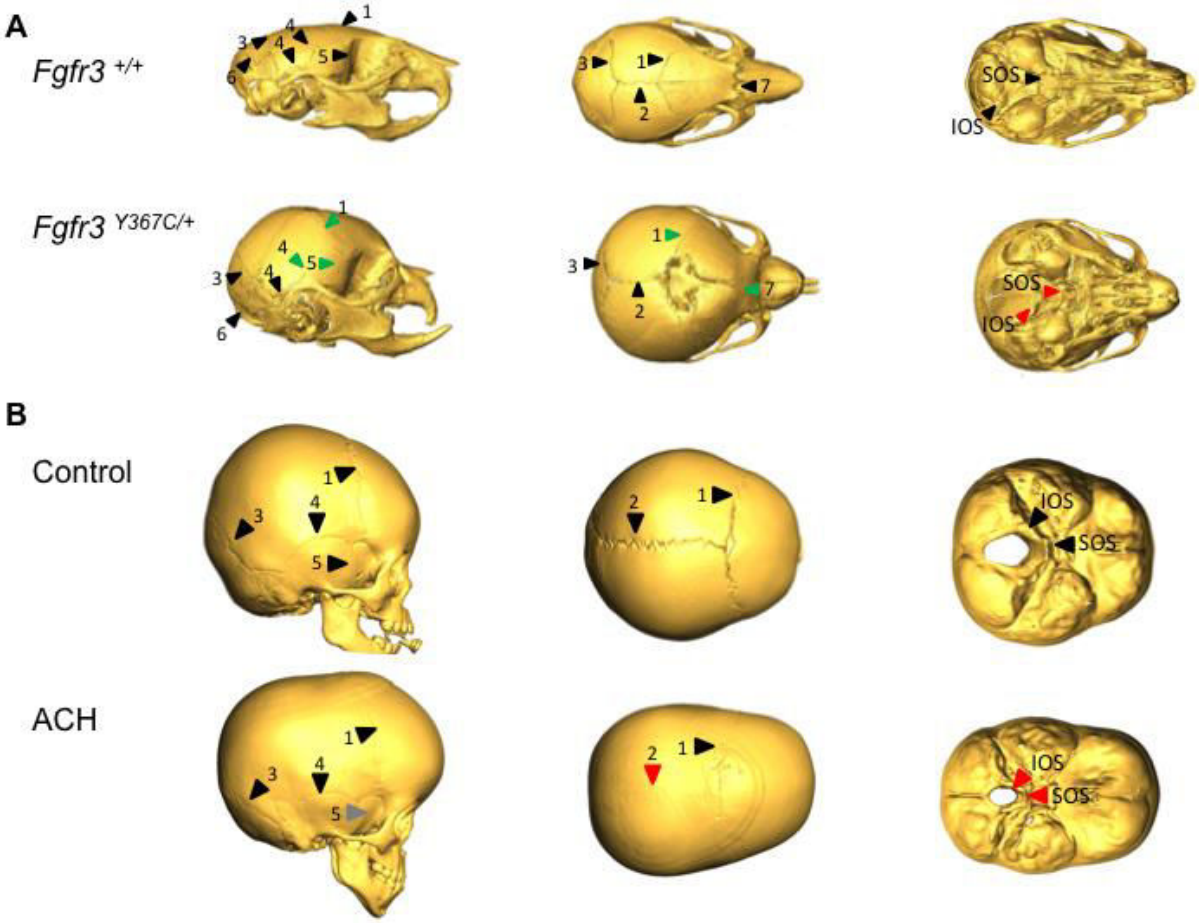

Computed Tomography of the head of *Fgfr3*$^{Y367C/+}$ mice (µCT) and ACH patients (CT). (**A**) µCT images of vault and skull base of *Fgfr3*$^{Y367C/+}$ (n=7) and WT (n=7) mice at P21 showing in mutant mice partially fused suture (green arrow) and absence of SOS (spheno occipital synchondrosis (SOS) and intra occipital synchondrosis (IOS)(red arrows). The patent sutures are indicated with a black arrow. (**B**) CT of patients with ACH (n=6) and age matched control (n=6). CT images of vault and skull base (endocranial view) of ACH (2 years old) and control (1.5 years old) showing in ACH patient fused sagittal sutures (red arrow) and partially fused squamous sphenoidal suture (green arrow) and absence of SOS (spheno occipital synchondrosis (SOS) and intra occipital synchondrosis (IOS)(red arrows). Each suture is numbered, coronal suture (1), sagittal suture (2), lambdoid suture (3), squamous parietal suture (4), squamous sphenoidal suture (5), interparietal supraoccipital suture (6), fronto-nasal suture (7).

Supplementary Figure S2

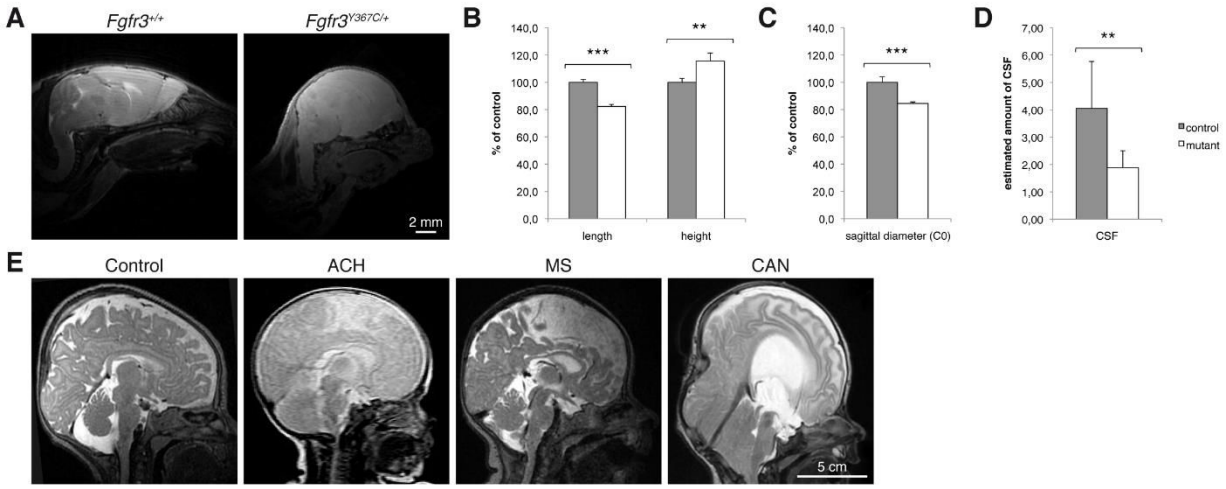

Magnetic Resonance Imaging (MRI) of the head of *Fgfr3*$^{Y367C/+}$ mice and ACH, MS, CAN patients. (**A**) Representative image of MRI of *Fgfr3*$^{Y367C/+}$ mice and control littermates. Severe brain alteration in shape and size in mutant (n=5) compared with control (n=6) at 3 weeks of age. (**B**) Measurement of length and height of the brain showing a decrease of the length and an increase of the height. (**C**) Measurement of sagittal diameter of the neural canal at the level of the foramen magnum showing a decrease of the size in *Fgfr3*$^{Y367C/+}$ mice. (**D**) Evaluation of the quantity of cerebrospinal fluid in *Fgfr3*$^{Y367C/+}$ mice (n=5) and control (n=6) showing strong reduction in mutant mice similar to FGFR3-related disorders (**E**) Representative MRI images at 2 months of age of control showing the severe alterations of the posterior fossa and foramen magnum. ***P<0,001, **P<0,01.

References

1. Ornitz,D.M. and Itoh,N. (2015) The Fibroblast Growth Factor signaling pathway. *Wiley Interdiscip. Rev. Dev. Biol.*, **4**, 215–266.

2. Armelin,H.A. (1973) Pituitary Extracts and Steroid Hormones in the Control of 3T3 Cell Growth. *Proc. Natl. Acad. Sci.*, **70**, 2702–2706.

3. Gospodarowicz,D. (1974) Localisation of a fibroblast growth factor and its effect alone and with hydrocortisone on 3T3 cell growth. *Nature*, **249**, 123–127.

4. Li,X., Wang,C., Xiao,J., McKeehan,W.L. and Wang,F. (2016) Fibroblast growth factors, old kids on the new block. *Semin. Cell Dev. Biol.*, 10.1016/j.semcdb.2015.12.014.

5. Kalinina,J., Dutta,K., Ilghari,D., Beenken,A., Goetz,R., Eliseenkova,A.V., Cowburn,D. and Mohammadi,M. (2012) The alternatively spliced acid box region plays a key role in FGF receptor autoinhibition. *Struct. Lond. Engl. 1993*, **20**, 77–88.

6. Mohammadi,M., Olsen,S.K. and Ibrahimi,O.A. (2005) Structural basis for fibroblast growth factor receptor activation. *Cytokine Growth Factor Rev.*, **16**, 107–137.

7. Jacob,A.L., Smith,C., Partanen,J. and Ornitz,D.M. (2006) Fibroblast growth factor receptor 1 signaling in the osteo-chondrogenic cell lineage regulates sequential steps of osteoblast maturation. *Dev. Biol.*, **296**, 315–328.

8. Verheyden,J.M., Lewandoski,M., Deng,C., Harfe,B.D. and Sun,X. (2005) Conditional inactivation of Fgfr1 in mouse defines its role in limb bud establishment, outgrowth and digit patterning. *Dev. Camb. Engl.*, **132**, 4235–4245.

9. Xu,X., Weinstein,M., Li,C., Naski,M., Cohen,R.I., Ornitz,D.M., Leder,P. and Deng,C. (1998) Fibroblast growth factor receptor 2 (FGFR2)-mediated reciprocal regulation loop between FGF8 and FGF10 is essential for limb induction. *Dev. Camb. Engl.*, **125**, 753–765.

10. Yu,K., Xu,J., Liu,Z., Sosic,D., Shao,J., Olson,E.N., Towler,D.A. and Ornitz,D.M. (2003) Conditional inactivation of FGF receptor 2 reveals an essential role for FGF signaling in the regulation of osteoblast function and bone growth. *Dev. Camb. Engl.*, **130**, 3063–3074.

11. Weinstein,M., Xu,X., Ohyama,K. and Deng,C.X. (1998) FGFR-3 and FGFR-4 function cooperatively to direct alveogenesis in the murine lung. *Development*, **125**, 3615–3623.

12. Baertschi,S., Zhuang,L. and Trueb,B. (2007) Mice with a targeted disruption of the Fgfrl1 gene die at birth due to alterations in the diaphragm. *FEBS J.*, **274**, 6241–6253.

13. Catela,C., Bilbao-Cortes,D., Slonimsky,E., Kratsios,P., Rosenthal,N. and Te Welscher,P. (2009) Multiple congenital malformations of Wolf-Hirschhorn syndrome are recapitulated in Fgfrl1 null mice. *Dis. Model. Mech.*, **2**, 283–294.

14. Fantl,W.J., Johnson,D.E. and Williams,L.T. (1993) Signalling by receptor tyrosine kinases. *Annu. Rev. Biochem.*, **62**, 453–481.

15. Sarabipour,S. and Hristova,K. (2016) Mechanism of FGF receptor dimerization and activation. *Nat. Commun.*, **7**, 10262.

16. Yin,L., Du,X., Li,C., Xu,X., Chen,Z., Su,N., Zhao,L., Qi,H., Li,F., Xue,J., *et al.* (2008) A Pro253Arg mutation in fibroblast growth factor receptor 2 (Fgfr2) causes skeleton malformation

mimicking human Apert syndrome by affecting both chondrogenesis and osteogenesis. *Bone*, **42**, 631–643.

17. Boulet,S.L., Rasmussen,S.A. and Honein,M.A. (2008) A population-based study of craniosynostosis in metropolitan Atlanta, 1989-2003. *Am. J. Med. Genet. A.*, **146A**, 984–991.

18. Wilkie,A.O. (2000) Epidemiology and genetics of craniosynostosis. *Am. J. Med. Genet.*, **90**, 82–84.

19. Wilkie,A.O. (1997) Craniosynostosis: genes and mechanisms. *Hum. Mol. Genet.*, **6**, 1647–1656.

20. L'Hôte,C.G.M. and Knowles,M.A. (2005) Cell responses to FGFR3 signalling: growth, differentiation and apoptosis. *Exp. Cell Res.*, **304**, 417–431.

21. Baujat,G., Legeai-Mallet,L., Finidori,G., Cormier-Daire,V. and Le Merrer,M. (2008) Achondroplasia. *Best Pract. Res. Clin. Rheumatol.*, **22**, 3–18.

22. Horton,W.A., Hall,J.G. and Hecht,J.T. (2007) Achondroplasia. *The Lancet*, **370**, 162–172.

23. Horton,W.A. (1997) Fibroblast growth factor receptor 3 and the human chondrodysplasias. *Curr. Opin. Pediatr.*, **9**, 437–442.

24. Tolo,V.T. (1990) Spinal deformity in short-stature syndromes. *Instr. Course Lect.*, **39**, 399–405.

25. Matsushita,T., Wilcox,W.R., Chan,Y.Y., Kawanami,A., Bukulmez,H., Balmes,G., Krejci,P., Mekikian,P.B., Otani,K., Yamaura,I., *et al.* (2008) FGFR3 promotes synchondrosis closure and fusion of ossification centers through the MAPK pathway. *Hum. Mol. Genet.*, **18**, 227–240.

26. Goriely,A. and Wilkie,A.O.M. (2012) Paternal age effect mutations and selfish spermatogonial selection: causes and consequences for human disease. *Am. J. Hum. Genet.*, **90**, 175–200.

27. Rousseau,F., Bonaventure,J., Legeai-Mallet,L., Pelet,A., Rozet,J.-M., Maroteaux,P., Merrer,M.L. and Munnich,A. (1994) Mutations in the gene encoding fibroblast growth factor receptor-3 in achondroplasia. *Nature*, **371**, 252–254.

28. Shiang,R., Thompson,L.M., Zhu,Y.Z., Church,D.M., Fielder,T.J., Bocian,M., Winokur,S.T. and Wasmuth,J.J. (1994) Mutations in the transmembrane domain of FGFR3 cause the most common genetic form of dwarfism, achondroplasia. *Cell*, **78**, 335–342.

29. Szendröi,M. and Sim,F.H. (2009) Color Atlas of Clinical Orthopedics Springer Berlin Heidelberg, Berlin, Heidelberg.

30. Chitty,L.S., Griffin,D.R., Meaney,C., Barrett,A., Khalil,A., Pajkrt,E. and Cole,T.J. (2011) New aids for the non-invasive prenatal diagnosis of achondroplasia: dysmorphic features, charts of fetal size and molecular confirmation using cell-free fetal DNA in maternal plasma. *Ultrasound Obstet. Gynecol. Off. J. Int. Soc. Ultrasound Obstet. Gynecol.*, **37**, 283–289.

31. Yang,P.-Y., Liao,H.-G., Yeh,G.-P. and Tsung-Che Hsieh,C. (2012) Prenatal Diagnosis of Achondroplasia with Ultrasound, Three-Dimensional Computed Tomography and Molecular Methods. *J. Med. Ultrasound*, **20**, 176–179.

32. Wynn,J., King,T.M., Gambello,M.J., Waller,D.K. and Hecht,J.T. (2007) Mortality in achondroplasia study: a 42-year follow-up. *Am. J. Med. Genet. A.*, **143A**, 2502–2511.

33. Bober,M.B., Bellus,G.A., Nikkel,S.M. and Tiller,G.E. (1993) Hypochondroplasia. In Pagon,R.A., Adam,M.P., Ardinger,H.H., Wallace,S.E., Amemiya,A., Bean,L.J., Bird,T.D., Fong,C.-T., Mefford,H.C., Smith,R.J., et al. (eds), *GeneReviews(®)*. University of Washington, Seattle, Seattle (WA).

34. Maroteaux,P., Lamy,M. and Robert,J.M. (1967) [Thanatophoric dwarfism]. *Presse Médicale*, **75**, 2519–2524.

35. Leonard,D.G.B. (2016) Molecular Pathology in Clinical Practice Springer International Publishing, Cham.

36. Tavormina,P.L., Bellus,G.A., Webster,M.K., Bamshad,M.J., Fraley,A.E., McIntosh,I., Szabo,J., Jiang,W., Jabs,E.W., Wilcox,W.R., *et al.* (1999) A novel skeletal dysplasia with developmental delay and acanthosis nigricans is caused by a Lys650Met mutation in the fibroblast growth factor receptor 3 gene. *Am. J. Hum. Genet.*, **64**, 722–731.

37. Bellus,G.A., Bamshad,M.J., Przylepa,K.A., Dorst,J., Lee,R.R., Hurko,O., Jabs,E.W., Curry,C.J., Wilcox,W.R., Lachman,R.S., *et al.* (1999) Severe achondroplasia with developmental delay and acanthosis nigricans (SADDAN): phenotypic analysis of a new skeletal dysplasia caused by a Lys650Met mutation in fibroblast growth factor receptor 3. *Am. J. Med. Genet.*, **85**, 53–65.

38. Farmakis,S.G., Shinawi,M., Miller-Thomas,M., Radmanesh,A. and Herman,T.E. (2015) FGFR3-related condition: a skeletal dysplasia with similarities to thanatophoric dysplasia and SADDAN due to Lys650Met. *Skeletal Radiol.*, **44**, 441–445.

39. Bellus,G.A., Spector,E.B., Speiser,P.W., Weaver,C.A., Garber,A.T., Bryke,C.R., Israel,J., Rosengren,S.S., Webster,M.K., Donoghue,D.J., *et al.* (2000) Distinct missense mutations of the FGFR3 lys650 codon modulate receptor kinase activation and the severity of the skeletal dysplasia phenotype. *Am. J. Hum. Genet.*, **67**, 1411–1421.

40. Cossiez Cacard,M.A., Coulombe,J., Bernard,P., Kaci,N., Bressieux,J.M., Souchon,P.F., Motte,J., Legeai-Mallet,L., Hadj-Rabia,S. and Eschard,C. (2016) Familial hypochondroplasia and acanthosis nigricans with FGFR3 K650T mutation. *J. Eur. Acad. Dermatol. Venereol. JEADV*, **30**, 897–898.

41. Kruszka,P., Addissie,Y.A., Yarnell,C.M.P., Hadley,D.W., Guillen Sacoto,M.J., Platte,P., Paelecke,Y., Collmann,H., Snow,N., Schweitzer,T., *et al.* (2016) Muenke syndrome: An international multicenter natural history study. *Am. J. Med. Genet. A.*, **170**, 918–929.

42. Muenke,M., Gripp,K.W., McDonald-McGinn,D.M., Gaudenz,K., Whitaker,L.A., Bartlett,S.P., Markowitz,R.I., Robin,N.H., Nwokoro,N., Mulvihill,J.J., *et al.* (1997) A unique point mutation in the fibroblast growth factor receptor 3 gene (FGFR3) defines a new craniosynostosis syndrome. *Am. J. Hum. Genet.*, **60**, 555–564.

43. Rannan-Eliya,S.V., Taylor,I.B., De Heer,I.M., Van Den Ouweland,A.M.W., Wall,S.A. and Wilkie,A.O.M. (2004) Paternal origin of FGFR3 mutations in Muenke-type craniosynostosis. *Hum. Genet.*, **115**, 200–207.

44. Arnaud-López,L., Fragoso,R., Mantilla-Capacho,J. and Barros-Núñez,P. (2007) Crouzon with acanthosis nigricans. Further delineation of the syndrome. *Clin. Genet.*, **72**, 405–410.

45. Wilkes,D., Rutland,P., Pulleyn,L.J., Reardon,W., Moss,C., Ellis,J.P., Winter,R.M. and Malcolm,S. (1996) A recurrent mutation, ala391glu, in the transmembrane region of FGFR3 causes Crouzon syndrome and acanthosis nigricans. *J. Med. Genet.*, **33**, 744–748.

46. Toydemir,R.M., Brassington,A.E., Bayrak-Toydemir,P., Krakowiak,P.A., Jorde,L.B., Whitby,F.G., Longo,N., Viskochil,D.H., Carey,J.C. and Bamshad,M.J. (2006) A novel mutation in FGFR3 causes camptodactyly, tall stature, and hearing loss (CATSHL) syndrome. *Am. J. Hum. Genet.*, **79**, 935–941.

47. Makrythanasis,P., Temtamy,S., Aglan,M.S., Otaify,G.A., Hamamy,H. and Antonarakis,S.E. (2014) A novel homozygous mutation in FGFR3 causes tall stature, severe lateral tibial deviation, scoliosis, hearing impairment, camptodactyly, and arachnodactyly. *Hum. Mutat.*, **35**, 959–963.

48. Turner,N. and Grose,R. (2010) Fibroblast growth factor signalling: from development to cancer. *Nat. Rev. Cancer*, **10**, 116–129.

49. Iida,S. and Ueda,R. (2003) Multistep tumorigenesis of multiple myeloma: its molecular delineation. *Int. J. Hematol.*, **77**, 207–212.

50. Pouessel,D., Neuzillet,Y., Mertens,L.S., van der Heijden,M.S., de Jong,J., Sanders,J., Peters,D., Leroy,K., Manceau,A., Maille,P., *et al.* (2016) Tumor Heterogeneity of Fibroblast Growth Factor Receptor 3 (FGFR3) Mutations in Invasive Bladder Cancer: Implications for Peri-Operative anti-FGFR3 Treatment. *Ann. Oncol. Off. J. Eur. Soc. Med. Oncol. ESMO*, 10.1093/annonc/mdw170.

51. Sjödahl,G., Lauss,M., Lövgren,K., Chebil,G., Gudjonsson,S., Veerla,S., Patschan,O., Aine,M., Fernö,M., Ringnér,M., *et al.* (2012) A molecular taxonomy for urothelial carcinoma. *Clin. Cancer Res. Off. J. Am. Assoc. Cancer Res.*, **18**, 3377–3386.

52. van Tilborg,A.A., de Vries,A., de Bont,M., Groenfeld,L.E., van der Kwast,T.H. and Zwarthoff,E.C. (2000) Molecular evolution of multiple recurrent cancers of the bladder. *Hum. Mol. Genet.*, **9**, 2973–2980.

53. Hernández,S., de Muga,S., Agell,L., Juanpere,N., Esgueva,R., Lorente,J.A., Mojal,S., Serrano,S. and Lloreta,J. (2009) FGFR3 mutations in prostate cancer: association with low-grade tumors. *Mod. Pathol. Off. J. U. S. Can. Acad. Pathol. Inc*, **22**, 848–856.

54. Goriely,A., Hansen,R.M.S., Taylor,I.B., Olesen,I.A., Jacobsen,G.K., McGowan,S.J., Pfeifer,S.P., McVean,G.A.T., Rajpert-De Meyts,E. and Wilkie,A.O.M. (2009) Activating mutations in FGFR3 and HRAS reveal a shared genetic origin for congenital disorders and testicular tumors. *Nat. Genet.*, **41**, 1247–1252.

55. Cappellen,D., De Oliveira,C., Ricol,D., de Medina,S., Bourdin,J., Sastre-Garau,X., Chopin,D., Thiery,J.P. and Radvanyi,F. (1999) Frequent activating mutations of FGFR3 in human bladder and cervix carcinomas. *Nat. Genet.*, **23**, 18–20.

56. Wu,R., Connolly,D., Ngelangel,C., Bosch,F.X., Muñoz,N. and Cho,K.R. (2000) Somatic mutations of fibroblast growth factor receptor 3 (FGFR3) are uncommon in carcinomas of the uterine cervix. *Oncogene*, **19**, 5543–5546.

57. Hafner,C., van Oers,J.M.M., Hartmann,A., Landthaler,M., Stoehr,R., Blaszyk,H., Hofstaedter,F., Zwarthoff,E.C. and Vogt,T. (2006) High frequency of FGFR3 mutations in adenoid seborrheic keratoses. *J. Invest. Dermatol.*, **126**, 2404–2407.

58. Hafner,C., van Oers,J.M.M., Vogt,T., Landthaler,M., Stoehr,R., Blaszyk,H., Hofstaedter,F., Zwarthoff,E.C. and Hartmann,A. (2006) Mosaicism of activating FGFR3 mutations in human skin causes epidermal nevi. *J. Clin. Invest.*, **116**, 2201–2207.

59. Hafner,C., Stoehr,R., van Oers,J.M.M., Zwarthoff,E.C., Hofstaedter,F., Landthaler,M., Hartmann,A. and Vogt,T. (2009) FGFR3 and PIK3CA mutations are involved in the molecular pathogenesis of solar lentigo. *Br. J. Dermatol.*, **160**, 546–551.

60. Groesser,L., Herschberger,E., Landthaler,M. and Hafner,C. (2012) FGFR3, PIK3CA and RAS mutations in benign lichenoid keratosis. *Br. J. Dermatol.*, **166**, 784–788.

61. Gibbs,L. and Legeai-Mallet,L. (2007) FGFR3 intracellular mutations induce tyrosine phosphorylation in the Golgi and defective glycosylation. *Biochim. Biophys. Acta*, **1773**, 502–512.

62. Iwata,T., Li,C.L., Deng,C.X. and Francomano,C.A. (2001) Highly activated Fgfr3 with the K644M mutation causes prolonged survival in severe dwarf mice. *Hum. Mol. Genet.*, **10**, 1255–1264.

63. Chen,F., Degnin,C., Laederich,M., Horton,W.A. and Hristova,K. (2011) The A391E mutation enhances FGFR3 activation in the absence of ligand. *Biochim. Biophys. Acta*, **1808**, 2045–2050.

64. Webster,M.K. and Donoghue,D.J. (1996) Constitutive activation of fibroblast growth factor receptor 3 by the transmembrane domain point mutation found in achondroplasia. *EMBO J.*, **15**, 520–527.

65. Cho,J.Y., Guo,C., Torello,M., Lunstrum,G.P., Iwata,T., Deng,C. and Horton,W.A. (2004) Defective lysosomal targeting of activated fibroblast growth factor receptor 3 in achondroplasia. *Proc. Natl. Acad. Sci. U. S. A.*, **101**, 609–614.

66. Lefebvre,V. and Bhattaram,P. (2010) Vertebrate skeletogenesis. *Curr. Top. Dev. Biol.*, **90**, 291–317.

67. Iimura,T., Denans,N. and Pourquié,O. (2009) Establishment of Hox vertebral identities in the embryonic spine precursors. *Curr. Top. Dev. Biol.*, **88**, 201–234.

68. Li,Y., Toole,B.P., Dealy,C.N. and Kosher,R.A. (2007) Hyaluronan in limb morphogenesis. *Dev. Biol.*, **305**, 411–420.

69. Lim,J., Tu,X., Choi,K., Akiyama,H., Mishina,Y. and Long,F. (2015) BMP-Smad4 signaling is required for precartilaginous mesenchymal condensation independent of Sox9 in the mouse. *Dev. Biol.*, **400**, 132–138.

70. Kosher,R.A., Kulyk,W.M. and Gay,S.W. (1986) Collagen gene expression during limb cartilage differentiation. *J. Cell Biol.*, **102**, 1151–1156.

71. Dy,P., Wang,W., Bhattaram,P., Wang,Q., Wang,L., Ballock,R.T. and Lefebvre,V. (2012) Sox9 directs hypertrophic maturation and blocks osteoblast differentiation of growth plate chondrocytes. *Dev. Cell*, **22**, 597–609.

72. Ikegami,D., Akiyama,H., Suzuki,A., Nakamura,T., Nakano,T., Yoshikawa,H. and Tsumaki,N. (2011) Sox9 sustains chondrocyte survival and hypertrophy in part through Pik3ca-Akt pathways. *Dev. Camb. Engl.*, **138**, 1507–1519.

73. Yoshida,C.A., Yamamoto,H., Fujita,T., Furuichi,T., Ito,K., Inoue,K., Yamana,K., Zanma,A., Takada,K., Ito,Y., *et al.* (2004) Runx2 and Runx3 are essential for chondrocyte maturation, and Runx2 regulates limb growth through induction of Indian hedgehog. *Genes Dev.*, **18**, 952–963.

74. Kozhemyakina,E., Lassar,A.B. and Zelzer,E. (2015) A pathway to bone: signaling molecules and transcription factors involved in chondrocyte development and maturation. *Dev. Camb. Engl.*, **142**, 817–831.

75. Li,Y., Ahrens,M.J., Wu,A., Liu,J. and Dudley,A.T. (2011) Calcium/calmodulin-dependent protein kinase II activity regulates the proliferative potential of growth plate chondrocytes. *Dev. Camb. Engl.*, **138**, 359–370.

76. Behonick,D.J. and Werb,Z. (2003) A bit of give and take: the relationship between the extracellular matrix and the developing chondrocyte. *Mech. Dev.*, **120**, 1327–1336.

77. Yang,G., Zhu,L., Hou,N., Lan,Y., Wu,X.-M., Zhou,B., Teng,Y. and Yang,X. (2014) Osteogenic fate of hypertrophic chondrocytes. *Cell Res.*, **24**, 1266–1269.

78. Zhou,X., von der Mark,K., Henry,S., Norton,W., Adams,H. and de Crombrugghe,B. (2014) Chondrocytes transdifferentiate into osteoblasts in endochondral bone during development, postnatal growth and fracture healing in mice. *PLoS Genet.*, **10**, e1004820.

79. Kaufman,M.H. and Bard,J.B.L. (1999) The anatomical basis of mouse development Academic Press, San Diego.

80. Maes,C., Kobayashi,T., Selig,M.K., Torrekens,S., Roth,S.I., Mackem,S., Carmeliet,G. and Kronenberg,H.M. (2010) Osteoblast precursors, but not mature osteoblasts, move into developing and fractured bones along with invading blood vessels. *Dev. Cell*, **19**, 329–344.

81. Liu,Y. and Olsen,B.R. (2014) Distinct VEGF functions during bone development and homeostasis. *Arch. Immunol. Ther. Exp. (Warsz.)*, **62**, 363–368.

82. Ortega,N., Behonick,D.J. and Werb,Z. (2004) Matrix remodeling during endochondral ossification. *Trends Cell Biol.*, **14**, 86–93.

83. Nakashima,K. and de Crombrugghe,B. (2003) Transcriptional mechanisms in osteoblast differentiation and bone formation. *Trends Genet. TIG*, **19**, 458–466.

84. Hall,B.K. and Miyake,T. (2000) All for one and one for all: condensations and the initiation of skeletal development. *BioEssays News Rev. Mol. Cell. Dev. Biol.*, **22**, 138–147.

85. Opperman,L.A. (2000) Cranial sutures as intramembranous bone growth sites. *Dev. Dyn. Off. Publ. Am. Assoc. Anat.*, **219**, 472–485.

86. Rice,D.P., Kim,H.J. and Thesleff,I. (1999) Apoptosis in murine calvarial bone and suture development. *Eur. J. Oral Sci.*, **107**, 265–275.

87. Fujita,T., Azuma,Y., Fukuyama,R., Hattori,Y., Yoshida,C., Koida,M., Ogita,K. and Komori,T. (2004) Runx2 induces osteoblast and chondrocyte differentiation and enhances their migration by coupling with PI3K-Akt signaling. *J. Cell Biol.*, **166**, 85–95.

88. Marie,P.J. (2008) Transcription factors controlling osteoblastogenesis. *Arch. Biochem. Biophys.*, **473**, 98–105.

89. Rice,D.P. and Rice,R. (2008) Locate, condense, differentiate, grow and confront: developmental mechanisms controlling intramembranous bone and suture formation and function. *Front. Oral Biol.*, **12**, 22–40.

90. Zeller,R., López-Ríos,J. and Zuniga,A. (2009) Vertebrate limb bud development: moving towards integrative analysis of organogenesis. *Nat. Rev. Genet.*, **10**, 845–858.

91. Orr-Urtreger,A., Givol,D., Yayon,A., Yarden,Y. and Lonai,P. (1991) Developmental expression of two murine fibroblast growth factor receptors, flg and bek. *Dev. Camb. Engl.*, **113**, 1419–1434.

92. Sheeba,C.J., Andrade,R.P., Duprez,D. and Palmeirim,I. (2010) Comprehensive analysis of fibroblast growth factor receptor expression patterns during chick forelimb development. *Int. J. Dev. Biol.*, **54**, 1517–1526.

93. Ornitz,D.M. and Marie,P.J. (2015) Fibroblast growth factor signaling in skeletal development and disease. *Genes Dev.*, **29**, 1463–1486.

94. Yu,K. and Ornitz,D.M. (2008) FGF signaling regulates mesenchymal differentiation and skeletal patterning along the limb bud proximodistal axis. *Dev. Camb. Engl.*, **135**, 483–491.

95. Coumoul,X., Shukla,V., Li,C., Wang,R.-H. and Deng,C.-X. (2005) Conditional knockdown of Fgfr2 in mice using Cre-LoxP induced RNA interference. *Nucleic Acids Res.*, **33**, e102.

96. Li,C., Xu,X., Nelson,D.K., Williams,T., Kuehn,M.R. and Deng,C.-X. (2005) FGFR1 function at the earliest stages of mouse limb development plays an indispensable role in subsequent autopod morphogenesis. *Dev. Camb. Engl.*, **132**, 4755–4764.

97. Eswarakumar,V.P., Monsonego-Ornan,E., Pines,M., Antonopoulou,I., Morriss-Kay,G.M. and Lonai,P. (2002) The IIIc alternative of Fgfr2 is a positive regulator of bone formation. *Dev. Camb. Engl.*, **129**, 3783–3793.

98. Purcell,P., Joo,B.W., Hu,J.K., Tran,P.V., Calicchio,M.L., O'Connell,D.J., Maas,R.L. and Tabin,C.J. (2009) Temporomandibular joint formation requires two distinct hedgehog-dependent steps. *Proc. Natl. Acad. Sci. U. S. A.*, **106**, 18297–18302.

99. Karolak,M.R., Yang,X. and Elefteriou,F. (2015) FGFR1 signaling in hypertrophic chondrocytes is attenuated by the Ras-GAP neurofibromin during endochondral bone formation. *Hum. Mol. Genet.*, **24**, 2552–2564.

100. Kumar,D. and Lassar,A.B. (2014) Fibroblast growth factor maintains chondrogenic potential of limb bud mesenchymal cells by modulating DNMT3A recruitment. *Cell Rep.*, **8**, 1419–1431.

101. Murakami,S., Kan,M., McKeehan,W.L. and de Crombrugghe,B. (2000) Up-regulation of the chondrogenic Sox9 gene by fibroblast growth factors is mediated by the mitogen-activated protein kinase pathway. *Proc. Natl. Acad. Sci. U. S. A.*, **97**, 1113–1118.

102. Shung,C.-Y., Ota,S., Zhou,Z.-Q., Keene,D.R. and Hurlin,P.J. (2012) Disruption of a Sox9-β-catenin circuit by mutant Fgfr3 in thanatophoric dysplasia type II. *Hum. Mol. Genet.*, **21**, 4628–4644.

103. Oh,C., Lu,Y., Liang,S., Mori-Akiyama,Y., Chen,D., de Crombrugghe,B. and Yasuda,H. (2014) SOX9 regulates multiple genes in chondrocytes, including genes encoding ECM proteins, ECM modification enzymes, receptors, and transporters. *PloS One*, **9**, e107577.

104. Havens,B.A., Velonis,D., Kronenberg,M.S., Lichtler,A.C., Oliver,B. and Mina,M. (2008) Roles of FGFR3 during morphogenesis of Meckel's cartilage and mandibular bones. *Dev. Biol.*, **316**, 336–349.

105. Hung,I.H., Yu,K., Lavine,K.J. and Ornitz,D.M. (2007) FGF9 regulates early hypertrophic chondrocyte differentiation and skeletal vascularization in the developing stylopod. *Dev. Biol.*, **307**, 300–313.

106. Coutu,D.L., François,M. and Galipeau,J. (2011) Inhibition of cellular senescence by developmentally regulated FGF receptors in mesenchymal stem cells. *Blood*, **117**, 6801–6812.

107. Weng,T., Yi,L., Huang,J., Luo,F., Wen,X., Du,X., Chen,Q., Deng,C., Chen,D. and Chen,L. (2012) Genetic inhibition of fibroblast growth factor receptor 1 in knee cartilage attenuates the degeneration of articular cartilage in adult mice. *Arthritis Rheum.*, **64**, 3982–3992.

108. Yan,D., Chen,D., Cool,S.M., van Wijnen,A.J., Mikecz,K., Murphy,G. and Im,H.-J. (2011) Fibroblast growth factor receptor 1 is principally responsible for fibroblast growth factor 2-induced catabolic activities in human articular chondrocytes. *Arthritis Res. Ther.*, **13**, R130.

109. Rice,D.P.C., Rice,R. and Thesleff,I. (2003) Fgfr mRNA isoforms in craniofacial bone development. *Bone*, **33**, 14–27.

110. Ohbayashi,N., Shibayama,M., Kurotaki,Y., Imanishi,M., Fujimori,T., Itoh,N. and Takada,S. (2002) FGF18 is required for normal cell proliferation and differentiation during osteogenesis and chondrogenesis. *Genes Dev.*, **16**, 870–879.

111. Quarto,N., Behr,B., Li,S. and Longaker,M.T. (2009) Differential FGF ligands and FGF receptors expression pattern in frontal and parietal calvarial bones. *Cells Tissues Organs*, **190**, 158–169.

112. Reinhold,M.I. and Naski,M.C. (2007) Direct interactions of Runx2 and canonical Wnt signaling induce FGF18. *J. Biol. Chem.*, **282**, 3653–3663.

113. Kim,H.J., Rice,D.P., Kettunen,P.J. and Thesleff,I. (1998) FGF-, BMP- and Shh-mediated signalling pathways in the regulation of cranial suture morphogenesis and calvarial bone development. *Dev. Camb. Engl.*, **125**, 1241–1251.

114. Hung,I.H., Schoenwolf,G.C., Lewandoski,M. and Ornitz,D.M. (2016) A combined series of Fgf9 and Fgf18 mutant alleles identifies unique and redundant roles in skeletal development. *Dev. Biol.*, **411**, 72–84.

115. Ornitz,D.M. and Marie,P.J. (2002) FGF signaling pathways in endochondral and intramembranous bone development and human genetic disease. *Genes Dev.*, **16**, 1446–1465.

116. Lazarus,J.E., Hegde,A., Andrade,A.C., Nilsson,O. and Baron,J. (2007) Fibroblast growth factor expression in the postnatal growth plate. *Bone*, **40**, 577–586.

117. Colvin,J.S., Bohne,B.A., Harding,G.W., McEwen,D.G. and Ornitz,D.M. (1996) Skeletal overgrowth and deafness in mice lacking fibroblast growth factor receptor 3. *Nat. Genet.*, **12**, 390–397.

118. Deng,C., Wynshaw-Boris,A., Zhou,F., Kuo,A. and Leder,P. (1996) Fibroblast growth factor receptor 3 is a negative regulator of bone growth. *Cell*, **84**, 911–921.

119. Naski,M.C., Wang,Q., Xu,J. and Ornitz,D.M. (1996) Graded activation of fibroblast growth factor receptor 3 by mutations causing achondroplasia and thanatophoric dysplasia. *Nat. Genet.*, **13**, 233–237.

120. Naski,M.C., Colvin,J.S., Coffin,J.D. and Ornitz,D.M. (1998) Repression of hedgehog signaling and BMP4 expression in growth plate cartilage by fibroblast growth factor receptor 3. *Dev. Camb. Engl.*, **125**, 4977–4988.

121. Kolupaeva,V., Laplantine,E. and Basilico,C. (2008) PP2A-mediated dephosphorylation of p107 plays a critical role in chondrocyte cell cycle arrest by FGF. *PloS One*, **3**, e3447.

122. Kurimchak,A., Haines,D.S., Garriga,J., Wu,S., De Luca,F., Sweredoski,M.J., Deshaies,R.J., Hess,S. and Graña,X. (2013) Activation of p107 by fibroblast growth factor, which is essential for chondrocyte cell cycle exit, is mediated by the protein phosphatase 2A/B55α holoenzyme. *Mol. Cell. Biol.*, **33**, 3330–3342.

123. Legeai-Mallet,L., Benoist-Lasselin,C., Munnich,A. and Bonaventure,J. (2004) Overexpression of FGFR3, Stat1, Stat5 and p21Cip1 correlates with phenotypic severity and defective chondrocyte differentiation in FGFR3-related chondrodysplasias. *Bone*, **34**, 26–36.

124. de Frutos,C.A., Vega,S., Manzanares,M., Flores,J.M., Huertas,H., Martínez-Frías,M.L. and Nieto,M.A. (2007) Snail1 is a transcriptional effector of FGFR3 signaling during chondrogenesis and achondroplasias. *Dev. Cell*, **13**, 872–883.

125. Smith,B.N., Burton,L.J., Henderson,V., Randle,D.D., Morton,D.J., Smith,B.A., Taliaferro-Smith,L., Nagappan,P., Yates,C., Zayzafoon,M., *et al.* (2014) Snail promotes epithelial mesenchymal transition in breast cancer cells in part via activation of nuclear ERK2. *PloS One*, **9**, e104987.

126. Zhang,K., Corsa,C.A., Ponik,S.M., Prior,J.L., Piwnica-Worms,D., Eliceiri,K.W., Keely,P.J. and Longmore,G.D. (2013) The collagen receptor discoidin domain receptor 2 stabilizes SNAIL1 to facilitate breast cancer metastasis. *Nat. Cell Biol.*, **15**, 677–687.

127. Chen,Y. and Gridley,T. (2013) Compensatory regulation of the *Snai1* and *Snai2* genes during chondrogenesis. *J. Bone Miner. Res.*, **28**, 1412–1421.

128. Murakami,S., Balmes,G., McKinney,S., Zhang,Z., Givol,D. and de Crombrugghe,B. (2004) Constitutive activation of MEK1 in chondrocytes causes Stat1-independent achondroplasia-like dwarfism and rescues the Fgfr3-deficient mouse phenotype. *Genes Dev.*, **18**, 290–305.

129. Zhou,Z.-Q., Ota,S., Deng,C., Akiyama,H. and Hurlin,P.J. (2015) Mutant activated FGFR3 impairs endochondral bone growth by preventing SOX9 downregulation in differentiating chondrocytes. *Hum. Mol. Genet.*, **24**, 1764–1773.

130. Yasoda,A., Komatsu,Y., Chusho,H., Miyazawa,T., Ozasa,A., Miura,M., Kurihara,T., Rogi,T., Tanaka,S., Suda,M., *et al.* (2004) Overexpression of CNP in chondrocytes rescues achondroplasia through a MAPK-dependent pathway. *Nat. Med.*, **10**, 80–86.

131. Krejci,P., Salazar,L., Goodridge,H.S., Kashiwada,T.A., Schibler,M.J., Jelinkova,P., Thompson,L.M. and Wilcox,W.R. (2008) STAT1 and STAT3 do not participate in FGF-mediated growth arrest in chondrocytes. *J. Cell Sci.*, **121**, 272–281.

132. Raucci,A., Laplantine,E., Mansukhani,A. and Basilico,C. (2004) Activation of the ERK1/2 and p38 mitogen-activated protein kinase pathways mediates fibroblast growth factor-induced growth arrest of chondrocytes. *J. Biol. Chem.*, **279**, 1747–1756.

133. Matsushita,T., Chan,Y.Y., Kawanami,A., Balmes,G., Landreth,G.E. and Murakami,S. (2009) Extracellular signal-regulated kinase 1 (ERK1) and ERK2 play essential roles in osteoblast differentiation and in supporting osteoclastogenesis. *Mol. Cell. Biol.*, **29**, 5843–5857.

134. Sebastian,A., Matsushita,T., Kawanami,A., Mackem,S., Landreth,G.E. and Murakami,S. (2011) Genetic inactivation of ERK1 and ERK2 in chondrocytes promotes bone growth and enlarges the spinal canal. *J. Orthop. Res. Off. Publ. Orthop. Res. Soc.*, **29**, 375–379.

135. Chen,L., Li,C., Qiao,W., Xu,X. and Deng,C. (2001) A Ser(365)-->Cys mutation of fibroblast growth factor receptor 3 in mouse downregulates Ihh/PTHrP signals and causes severe achondroplasia. *Hum. Mol. Genet.*, **10**, 457–465.

136. Qi,H., Jin,M., Duan,Y., Du,X., Zhang,Y., Ren,F., Wang,Y., Tian,Q., Wang,X., Wang,Q., *et al.* (2014) FGFR3 induces degradation of BMP type I receptor to regulate skeletal development. *Biochim. Biophys. Acta*, **1843**, 1237–1247.

137. Li,M., Seki,Y., Freitas,P.H.L., Nagata,M., Kojima,T., Sultana,S., Ubaidus,S., Maeda,T., Shimomura,J., Henderson,J.E., *et al.* (2010) FGFR3 down-regulates PTH/PTHrP receptor gene expression by mediating JAK/STAT signaling in chondrocytic cell line. *J. Electron Microsc. (Tokyo)*, **59**, 227–236.

138. Buchtova,M., Oralova,V., Aklian,A., Masek,J., Vesela,I., Ouyang,Z., Obadalova,T., Konecna,Z., Spoustova,T., Pospisilova,T., *et al.* (2015) Fibroblast growth factor and canonical WNT/β-catenin signaling cooperate in suppression of chondrocyte differentiation in experimental models of FGFR signaling in cartilage. *Biochim. Biophys. Acta*, **1852**, 839–850.

139. Krejci,P., Aklian,A., Kaucka,M., Sevcikova,E., Prochazkova,J., Masek,J.K., Mikolka,P., Pospisilova,T., Spoustova,T., Weis,M., *et al.* (2012) Receptor tyrosine kinases activate canonical WNT/β-catenin signaling via MAP kinase/LRP6 pathway and direct β-catenin phosphorylation. *PloS One*, **7**, e35826.

140. McEwen,D.G., Green,R.P., Naski,M.C., Towler,D.A. and Ornitz,D.M. (1999) Fibroblast growth factor receptor 3 gene transcription is suppressed by cyclic adenosine 3',5'-monophosphate. Identification of a chondrocytic regulatory element. *J. Biol. Chem.*, **274**, 30934–30942.

141. Liu,Z., Lavine,K.J., Hung,I.H. and Ornitz,D.M. (2007) FGF18 is required for early chondrocyte proliferation, hypertrophy and vascular invasion of the growth plate. *Dev. Biol.*, **302**, 80–91.

142. Jilka,R.L. (2003) Biology of the basic multicellular unit and the pathophysiology of osteoporosis. *Med. Pediatr. Oncol.*, **41**, 182–185.

143. Siddiqui,J.A. and Partridge,N.C. (2016) Physiological Bone Remodeling: Systemic Regulation and Growth Factor Involvement. *Physiol. Bethesda Md*, **31**, 233–245.

144. Wang,Y., Nishida,S., Boudignon,B.M., Burghardt,A., Elalieh,H.Z., Hamilton,M.M., Majumdar,S., Halloran,B.P., Clemens,T.L. and Bikle,D.D. (2007) IGF-I Receptor Is Required for the Anabolic Actions of Parathyroid Hormone on Bone. *J. Bone Miner. Res.*, **22**, 1329–1337.

145. Wang,B.L., Dai,C.L., Quan,J.X., Zhu,Z.F., Zheng,F., Zhang,H.X., Guo,S.Y., Guo,G., Zhang,J.Y. and Qiu,M.C. (2006) Parathyroid hormone regulates osterix and Runx2 mRNA expression predominantly through protein kinase A signaling in osteoblast-like cells. *J. Endocrinol. Invest.*, **29**, 101–108.

146. Kousteni,S. and Bilezikian,J.P. (2008) The cell biology of parathyroid hormone in osteoblasts. *Curr. Osteoporos. Rep.*, **6**, 72–76.

147. Trouvin,A.-P. and Goëb,V. (2010) Receptor activator of nuclear factor-κB ligand and osteoprotegerin: maintaining the balance to prevent bone loss. *Clin. Interv. Aging*, **5**, 345–354.

148. Bellido,T., Saini,V. and Pajevic,P.D. (2013) Effects of PTH on osteocyte function. *Bone*, **54**, 250–257.

149. van Driel,M. and van Leeuwen,J.P.T.M. (2014) Vitamin D endocrine system and osteoblasts. *BoneKEy Rep.*, **3**, 493.

150. Chambers,T.J. and Magnus,C.J. (1982) Calcitonin alters behaviour of isolated osteoclasts. *J. Pathol.*, **136**, 27–39.

151. Kameda,T., Mano,H., Yuasa,T., Mori,Y., Miyazawa,K., Shiokawa,M., Nakamaru,Y., Hiroi,E., Hiura,K., Kameda,A., *et al.* (1997) Estrogen inhibits bone resorption by directly inducing apoptosis of the bone-resorbing osteoclasts. *J. Exp. Med.*, **186**, 489–495.

152. Frenkel,B., Hong,A., Baniwal,S.K., Coetzee,G.A., Ohlsson,C., Khalid,O. and Gabet,Y. (2010) Regulation of adult bone turnover by sex steroids. *J. Cell. Physiol.*, **224**, 305–310.

153. Liu,W. and Zhang,X. (2015) Receptor activator of nuclear factor-κB ligand (RANKL)/RANK/osteoprotegerin system in bone and other tissues (Review). *Mol. Med. Rep.*, 10.3892/mmr.2015.3152.

154. Baca,K.E., Abdullah,M.A., Ting,B.L., Schkrohowsky,J.G., Hoernschemeyer,D.G., Carson,B.S. and Ain,M.C. (2010) Surgical decompression for lumbar stenosis in pediatric achondroplasia. *J. Pediatr. Orthop.*, **30**, 449–454.

155. White,K.K., Bompadre,V., Goldberg,M.J., Bober,M.B., Campbell,J.W., Cho,T.-J., Hoover-Fong,J., Mackenzie,W., Parnell,S.E., Raggio,C., *et al.* (2016) Best practices in the evaluation and treatment of foramen magnum stenosis in achondroplasia during infancy. *Am. J. Med. Genet. A.*, **170**, 42–51.

156. Bouali,H. and Latrech,H. (2015) Achondroplasia: Current Options and Future Perspective. *Pediatr. Endocrinol. Rev. PER*, **12**, 388–395.

157. Nagy,L. and Demke,J.C. (2014) Craniofacial anomalies. *Facial Plast. Surg. Clin. N. Am.*, **22**, 523–548.

158. Seino,Y., Yamanaka,Y., Shinohara,M., Ikegami,S., Koike,M., Miyazawa,M., Inoue,M., Moriwake,T. and Tanaka,H. (2000) Growth hormone therapy in achondroplasia. *Horm. Res.*, **53 Suppl 3**, 53–56.

159. Laederich,M.B. and Horton,W.A. (2012) FGFR3 targeting strategies for achondroplasia. *Expert Rev. Mol. Med.*, **14**, e11.

160. Trudel,S., Li,Z.H., Wei,E., Wiesmann,M., Chang,H., Chen,C., Reece,D., Heise,C. and Stewart,A.K. (2005) CHIR-258, a novel, multitargeted tyrosine kinase inhibitor for the potential treatment of t(4;14) multiple myeloma. *Blood*, **105**, 2941–2948.

161. de Brito,L.R., Batey,M.A., Zhao,Y., Squires,M.S., Maitland,H., Leung,H.Y., Hall,A.G., Jackson,G., Newell,D.R. and Irving,J.A.E. (2011) Comparative pre-clinical evaluation of receptor tyrosine kinase inhibitors for the treatment of multiple myeloma. *Leuk. Res.*, **35**, 1233–1240.

162. Mohammadi,M., Froum,S., Hamby,J.M., Schroeder,M.C., Panek,R.L., Lu,G.H., Eliseenkova,A.V., Green,D., Schlessinger,J. and Hubbard,S.R. (1998) Crystal structure of an angiogenesis inhibitor bound to the FGF receptor tyrosine kinase domain. *EMBO J.*, **17**, 5896–5904.

163. Pardo,O.E., Latigo,J., Jeffery,R.E., Nye,E., Poulsom,R., Spencer-Dene,B., Lemoine,N.R., Stamp,G.W., Aboagye,E.O. and Seckl,M.J. (2009) The fibroblast growth factor receptor inhibitor PD173074 blocks small cell lung cancer growth in vitro and in vivo. *Cancer Res.*, **69**, 8645–8651.

164. Shaw,A.T., Hsu,P.P., Awad,M.M. and Engelman,J.A. (2013) Tyrosine kinase gene rearrangements in epithelial malignancies. *Nat. Rev. Cancer*, **13**, 772–787.

165. Aviezer,D., Golembo,M. and Yayon,A. (2003) Fibroblast growth factor receptor-3 as a therapeutic target for Achondroplasia--genetic short limbed dwarfism. *Curr. Drug Targets*, **4**, 353–365.

166. Chen,L., Adar,R., Yang,X., Monsonego,E.O., Li,C., Hauschka,P.V., Yayon,A. and Deng,C.X. (1999) Gly369Cys mutation in mouse FGFR3 causes achondroplasia by affecting both chondrogenesis and osteogenesis. *J. Clin. Invest.*, **104**, 1517–1525.

167. Jonquoy,A., Mugniery,E., Benoist-Lasselin,C., Kaci,N., Le Corre,L., Barbault,F., Girard,A.-L., Le Merrer,Y., Busca,P., Schibler,L., *et al.* (2012) A novel tyrosine kinase inhibitor restores chondrocyte differentiation and promotes bone growth in a gain-of-function Fgfr3 mouse model. *Hum. Mol. Genet.*, **21**, 841–851.

168. Pannier,S., Couloigner,V., Messaddeq,N., Elmaleh-Bergès,M., Munnich,A., Romand,R. and Legeai-Mallet,L. (2009) Activating Fgfr3 Y367C mutation causes hearing loss and inner ear defect in a mouse model of chondrodysplasia. *Biochim. Biophys. Acta*, **1792**, 140–147.

169. Gudernova,I., Vesela,I., Balek,L., Buchtova,M., Dosedelova,H., Kunova,M., Pivnicka,J., Jelinkova,I., Roubalova,L., Kozubik,A., *et al.* (2016) Multikinase activity of fibroblast growth factor receptor (FGFR) inhibitors SU5402, PD173074, AZD1480, AZD4547 and BGJ398 compromises the use of small chemicals targeting FGFR catalytic activity for therapy of short-stature syndromes. *Hum. Mol. Genet.*, **25**, 9–23.

170. Qing,J., Du,X., Chen,Y., Chan,P., Li,H., Wu,P., Marsters,S., Stawicki,S., Tien,J., Totpal,K., *et al.* (2009) Antibody-based targeting of FGFR3 in bladder carcinoma and t(4;14)-positive multiple myeloma in mice. *J. Clin. Invest.*, **119**, 1216–1229.

171. Yin,Y., Ren,X., Smith,C., Guo,Q., Malabunga,M., Guernah,I., Zhang,Y., Shen,J., Sun,H., Chehab,N., *et al.* (2016) Inhibition of FGF Receptor 3-dependent lung adenocarcinoma with a human monoclonal antibody. *Dis. Model. Mech.*, 10.1242/dmm.024760.

172. Chusho,H., Tamura,N., Ogawa,Y., Yasoda,A., Suda,M., Miyazawa,T., Nakamura,K., Nakao,K., Kurihara,T., Komatsu,Y., *et al.* (2001) Dwarfism and early death in mice lacking C-type natriuretic peptide. *Proc. Natl. Acad. Sci. U. S. A.*, **98**, 4016–4021.

173. Hunt,P.J. (1994) Bioactivity and metabolism of C-type natriuretic peptide in normal man. *J. Clin. Endocrinol. Metab.*, **78**, 1428–1435.

174. Yasoda,A., Kitamura,H., Fujii,T., Kondo,E., Murao,N., Miura,M., Kanamoto,N., Komatsu,Y., Arai,H. and Nakao,K. (2009) Systemic administration of C-type natriuretic peptide as a novel therapeutic strategy for skeletal dysplasias. *Endocrinology*, **150**, 3138–3144.

175. Wendt,D.J., Dvorak-Ewell,M., Bullens,S., Lorget,F., Bell,S.M., Peng,J., Castillo,S., Aoyagi-Scharber,M., O'Neill,C.A., Krejci,P., *et al.* (2015) Neutral endopeptidase-resistant C-type natriuretic peptide variant represents a new therapeutic approach for treatment of fibroblast growth factor receptor 3-related dwarfism. *J. Pharmacol. Exp. Ther.*, **353**, 132–149.

176. Lorget,F., Kaci,N., Peng,J., Benoist-Lasselin,C., Mugniery,E., Oppeneer,T., Wendt,D.J., Bell,S.M., Bullens,S., Bunting,S., *et al.* (2012) Evaluation of the therapeutic potential of a CNP analog in a Fgfr3 mouse model recapitulating achondroplasia. *Am. J. Hum. Genet.*, **91**, 1108–1114.

177. Del Ry,S., Cabiati,M., Vozzi,F., Battolla,B., Caselli,C., Forini,F., Segnani,C., Prescimone,T., Giannessi,D. and Mattii,L. (2011) Expression of C-type natriuretic peptide and its receptor NPR-B in cardiomyocytes. *Peptides*, **32**, 1713–1718.

178. Legeai-Mallet,L. (2016) C-Type Natriuretic Peptide Analog as Therapy for Achondroplasia. *Endocr. Dev.*, **30**, 98–105.

179. Charlesworth,D. (2016) BioMarin Provides Program Update on Vosoritide in Achondroplasia - http://investors.bmrn.com/releasedetail.cfm?ReleaseID=966001.

180. Davidson,B.L. and McCray,P.B. (2011) Current prospects for RNA interference-based therapies. *Nat. Rev. Genet.*, **12**, 329–340.

181. Boudreau,R.L., Rodríguez-Lebrón,E. and Davidson,B.L. (2011) RNAi medicine for the brain: progresses and challenges. *Hum. Mol. Genet.*, **20**, R21–27.

182. Michigami,T. (2013) Regulatory mechanisms for the development of growth plate cartilage. *Cell. Mol. Life Sci. CMLS*, **70**, 4213–4221.

183. Miyaki,S., Sato,T., Inoue,A., Otsuki,S., Ito,Y., Yokoyama,S., Kato,Y., Takemoto,F., Nakasa,T., Yamashita,S., *et al.* (2010) MicroRNA-140 plays dual roles in both cartilage development and homeostasis. *Genes Dev.*, **24**, 1173–1185.

184. Bi,Y., Jing,Y. and Cao,Y. (2015) Overexpression of miR-100 inhibits growth of osteosarcoma through FGFR3. *Tumour Biol. J. Int. Soc. Oncodevelopmental Biol. Med.*, **36**, 8405–8411.

185. Shukla,V., Coumoul,X., Wang,R.-H., Kim,H.-S. and Deng,C.-X. (2007) RNA interference and inhibition of MEK-ERK signaling prevent abnormal skeletal phenotypes in a mouse model of craniosynostosis. *Nat. Genet.*, **39**, 1145–1150.

186. Guzmán-Aránguez,A., Legeai-Mallet,L. and Pintor,J. (2011) Fibroblast growth factor receptor 3 inhibition by small interfering RNAs in achondroplasia. *An. Real Acad. Nac. Farm.*, **77**, 4–11.

187. Hartl,F.U., Bracher,A. and Hayer-Hartl,M. (2011) Molecular chaperones in protein folding and proteostasis. *Nature*, **475**, 324–332.

188. Laederich,M.B., Degnin,C.R., Lunstrum,G.P., Holden,P. and Horton,W.A. (2011) Fibroblast growth factor receptor 3 (FGFR3) is a strong heat shock protein 90 (Hsp90) client: implications for therapeutic manipulation. *J. Biol. Chem.*, **286**, 19597–19604.

189. Trepel,J., Mollapour,M., Giaccone,G. and Neckers,L. (2010) Targeting the dynamic HSP90 complex in cancer. *Nat. Rev. Cancer*, **10**, 537–549.

190. Gaykema,S.B.M., Schröder,C.P., Vitfell-Rasmussen,J., Chua,S., Oude Munnink,T.H., Brouwers,A.H., Bongaerts,A.H.H., Akimov,M., Fernandez-Ibarra,C., Lub-de Hooge,M.N., *et al.* (2014) 89Zr-trastuzumab and 89Zr-bevacizumab PET to evaluate the effect of the HSP90 inhibitor NVP-AUY922 in metastatic breast cancer patients. *Clin. Cancer Res. Off. J. Am. Assoc. Cancer Res.*, **20**, 3945–3954.

191. Hendrickson,A.E.W., Oberg,A.L., Glaser,G., Camoriano,J.K., Peethambaram,P.P., Colon-Otero,G., Erlichman,C., Ivy,S.P., Kaufmann,S.H., Karnitz,L.M., *et al.* (2012) A phase II study of gemcitabine in combination with tanespimycin in advanced epithelial ovarian and primary peritoneal carcinoma. *Gynecol. Oncol.*, **124**, 210–215.

192. Johnson,M.L., Yu,H.A., Hart,E.M., Weitner,B.B., Rademaker,A.W., Patel,J.D., Kris,M.G. and Riely,G.J. (2015) Phase I/II Study of HSP90 Inhibitor AUY922 and Erlotinib for EGFR-Mutant Lung Cancer With Acquired Resistance to Epidermal Growth Factor Receptor Tyrosine Kinase Inhibitors. *J. Clin. Oncol. Off. J. Am. Soc. Clin. Oncol.*, **33**, 1666–1673.

193. Degnin,C.R., Laederich,M.B. and Horton,W.A. (2011) Ligand activation leads to regulated intramembrane proteolysis of fibroblast growth factor receptor 3. *Mol. Biol. Cell*, **22**, 3861–3873.

194. Wolfe,M.S. (2009) gamma-Secretase in biology and medicine. *Semin. Cell Dev. Biol.*, **20**, 219–224.

195. Garcia,S., Dirat,B., Tognacci,T., Rochet,N., Mouska,X., Bonnafous,S., Patouraux,S., Tran,A., Gual,P., Le Marchand-Brustel,Y., *et al.* (2013) Postnatal soluble FGFR3 therapy rescues achondroplasia symptoms and restores bone growth in mice. *Sci. Transl. Med.*, **5**, 203ra124.

196. Martz,L. (2013) sFGFR for achondroplasia. *SciBX Sci.-Bus. Exch.*, **6**.

197. Grande,M.T., Sánchez-Laorden,B., López-Blau,C., De Frutos,C.A., Boutet,A., Arévalo,M., Rowe,R.G., Weiss,S.J., López-Novoa,J.M. and Nieto,M.A. (2015) Snail1-induced partial epithelial-to-mesenchymal transition drives renal fibrosis in mice and can be targeted to reverse established disease. *Nat. Med.*, **21**, 989–997.

198. Moulton,J.D. and Yan,Y.-L. (2008) Using Morpholinos to control gene expression. *Curr. Protoc. Mol. Biol. Ed. Frederick M Ausubel Al*, **Chapter 26**, Unit 26.8.

199. Su,N., Jin,M. and Chen,L. (2014) Role of FGF/FGFR signaling in skeletal development and homeostasis: learning from mouse models. *Bone Res.*, **2**, 14003.

200. Xie,Y., Su,N., Jin,M., Qi,H., Yang,J., Li,C., Du,X., Luo,F., Chen,B., Shen,Y., *et al.* (2012) Intermittent PTH (1-34) injection rescues the retarded skeletal development and postnatal lethality of mice mimicking human achondroplasia and thanatophoric dysplasia. *Hum. Mol. Genet.*, **21**, 3941–3955.

201. Yamashita,A., Morioka,M., Kishi,H., Kimura,T., Yahara,Y., Okada,M., Fujita,K., Sawai,H., Ikegawa,S. and Tsumaki,N. (2014) Statin treatment rescues FGFR3 skeletal dysplasia phenotypes. *Nature*, **513**, 507–511.

202. Bush,J.R., Bérubé,N.G. and Beier,F. (2015) A new prescription for growth? Statins, cholesterol and cartilage homeostasis. *Osteoarthr. Cartil. OARS Osteoarthr. Res. Soc.*, **23**, 503–506.

203. Matsushita,M., Kitoh,H., Ohkawara,B., Mishima,K., Kaneko,H., Ito,M., Masuda,A., Ishiguro,N. and Ohno,K. (2013) Meclozine facilitates proliferation and differentiation of chondrocytes by attenuating abnormally activated FGFR3 signaling in achondroplasia. *PloS One*, **8**, e81569.

204. Matsushita,M., Hasegawa,S., Kitoh,H., Mori,K., Ohkawara,B., Yasoda,A., Masuda,A., Ishiguro,N. and Ohno,K. (2015) Meclozine promotes longitudinal skeletal growth in transgenic mice with achondroplasia carrying a gain-of-function mutation in the FGFR3 gene. *Endocrinology*, **156**, 548–554.

205. Grand,E.K., Chase,A.J., Heath,C., Rahemtulla,A. and Cross,N.C.P. (2004) Targeting FGFR3 in multiple myeloma: inhibition of t(4;14)-positive cells by SU5402 and PD173074. *Leukemia*, **18**, 962–966.

206. Komla-Ebri,D., Dambroise,E., Kramer,I., Benoist-Lasselin,C., Kaci,N., Le Gall,C., Martin,L., Busca,P., Barbault,F., Graus-Porta,D., *et al.* (2016) Tyrosine kinase inhibitor NVP-BGJ398 functionally improves FGFR3-related dwarfism in mouse model. *J. Clin. Invest.*, 10.1172/JCI83926.

207. Richter,A., Anton,S.F., Anton,S.E., Koch,P. and Dennett,S.L. (2003) The impact of reducing dose frequency on health outcomes. *Clin. Ther.*, **25**, 2307–2335; discussion 2306.

208. Lorget,F. and Legeai-Mallet,L. (2015) Key challenges in the treatment of rare pediatric skeletal genetic disorders: from bench to bedside. *Drug Discov. Today*, **20**, 781–783.

209. Di Rocco,F., Biosse Duplan,M., Heuze,Y., Kaci,N., Komla-Ebri,D., Munnich,A., Mugniery,E., Benoist-Lasselin,C. and Legeai-Mallet,L. (2014) FGFR3 mutation causes abnormal membranous ossification in achondroplasia. *Hum. Mol. Genet.*, **23**, 2914–2925.

210. Krejci,P. (2014) The paradox of FGFR3 signaling in skeletal dysplasia: Why chondrocytes growth arrest while other cells over proliferate. *Mutat. Res. Mutat. Res.*, **759**, 40–48.

Curriculum vitae

Davide Selom Komi KOMLA-EBRI

4yr PhD student (Genetics & Development)

57 boulevard de la Villette, 75010 Paris (France)
+33 6 68 19 09 01
davide-selom-kom.komla-ebri@inserm.fr
born January 16, 1988
Italian nationality

CAREER

2012-2016 **PhD student** (dissertation defence 04/07/2016) enrolled in BioSPC graduate school

Fellowships: Université Paris Descartes 3 years PhD fellowship (since October 2012); Fondation pour la Recherche Médicale 6 months PhD fellowship (since October 2015); Imagine Institute 4 months PhD fellowship (since April 2016)

Lab: "INSERM U781 - Génétique et épigénétique des maladies métaboliques, neurosensorielles et du développement"; Team: "Molecular and Physiopathological bases of osteochondrodysplasia" - Hôpital Necker - Enfants Malades - Paris (France) (October 2012 – January 2014)

Lab: "INSERM U1163 – Imagine Institute"; Team: "Molecular and Physiopathological bases of osteochondrodysplasia" **-** Paris (France) (Febraury 2014 – present)

Supervisor: Dr. Laurence LEGEAI-MALLET

Thesis: "*New therapeutic approaches for achondroplasia*"

2014 **Animal Experiment Agreement, Level 1** – Université Paris Descartes (Paris 5)

ECTS (European Calcified Tissue Society) **PhD Training Course** - St Catherine's College - Oxford (UK)

2012 **Double Degree**

Cell Molecular Biology MS (Master 2) - "Università degli Studi di Milano (UNIMI)"

Graduation: with honors (110 cum laude/110)

Genetics MS (Master 2) – "Université Paris Diderot (Paris 7)"

Graduation: with honors (mention bien)

Graduation thesis: "*In vitro and ex vivo evaluation of inhibitors targeting the FGFR3 kinase domain in cell and mouse chondrodysplasia models*"

Stage at: "INSERM U781 - Génétique et épigénétique des maladies métaboliques, neurosensorielles et du développement"; Team: "Molecular and Physiopathological bases of osteochondrodysplasia" Hôpital Necker - Enfants Malades - Paris (France)

Supervisor: Dr. Laurence LEGEAI-MALLET

2011 **Cell Molecular Biology (Master 1)** - "Università degli Studi di Milano (UNIMI)"

2010 **Bachelor's degree in Biological Sciences** - "Università degli Studi di Milano (UNIMI)"

Graduation thesis: "Molecular characterization by array-CGH of subtelomeric rearrangements associated with 22q13 microdeletion syndrome"

Stage at: “Cytogenetics lab” IRCSS Eugenio Medea – Bosisio Parini (Italy)

Supervisor: Dr. Maria Clara BONAGLIA

Graduation: 102/110

PUBLICATIONS

- Biosse Duplan M, **KOMLA-EBRI D**, Heuzé Y, Estibal V, Gaudas E, Kaci N, Benoist-Lasselin C, Kneissel M, Kramer I, Graus Porta D, Di Rocco F, Legeai-Mallet L. *Meckel’s and condylar cartilages anomalies in achondroplasia result in defective development and growth of the mandible*. Hum Mol Genet. 2016 Jun 3. pii: ddw153. [Epub ahead of print].

- **KOMLA-EBRI D**, Dambroise E, Kramer I, Benoist-Lasselin C, Kaci N, Le Gall C, Martin L, Busca P, Barbault F, Graus-Porta D, Munnich A, Kneissel M, Di Rocco F, Biosse-Duplan M, Legeai-Mallet L. *Tyrosine-kinase inhibitor NVP-BGJ398 functionally improves FGFR3-related dwarfism in mouse model.* J Clin Invest. 2016 Apr 11. pii: 83926. doi: 10.1172/JCI83926.

- Di Rocco F, Biosse-Duplan M, Heuzé Y, Kaci N, **KOMLA-EBRI D**, Munnich A, Mugniery E, Benoist-Lasselin C, Legeai-Mallet L. *FGFR3 mutation causes abnormal membranous ossification in achondroplasia.* Hum Mol Genet. 2014 Jun 1;23(11):2914-25. doi: 10.1093/hmg/ddu004. Epub 2014 Jan 12.

ORAL COMMUNICATIONS

National meetings

1. Busca P, Le Corre L, Tak-Tak L, Barbault F, **KOMLA-EBRI D**, Benoist-Lasselin C, Kaci N, Legeai-Mallet L, Prestat G, Gravier-Pelletier C. *Design, synthesis and biological evaluation of pyrazole-based kinase inhibitors.* 26th JFBP (Journées Franco-Belges de Pharmacochimie), May 2012 24-25, Orléans, France.

2. **KOMLA-EBRI D**, Benoist-Lasselin C, Kaci N, Busca P, Prestat G, Munnich A, Barbault F, Legeai-Mallet L. *In silico and in vitro analyses of three FGFR3 mutants (K650N, K650M, K650E) associated with different chondrodysplasias.* 15th JFBTM (Journées Françaises de Biologie des Tissus Minéralisés) – May 30-31 and July 01, 2013, Poitiers, France.

3. **KOMLA-EBRI D**, Dambroise E, Benoist-Lasselin C, Kaci N, Graus-Porta D, Biosse-Duplan M, Di Rocco F, Legeai-Mallet L. *A new therapeutic approach for achondroplasia and hypochondroplasia: tyrosine kinase inhibitor “BN016”* 17th JFBTM (Journées Françaises de Biologie des Tissus Minéralisés) - February 04-06, 2015, Super Besse, France.

4. **KOMLA-EBRI D**, Dambroise E, Benoist-Lasselin C, Kaci N, Graus-Porta D, Biosse-Duplan M, Di Rocco F, Legeai-Mallet L. *A new therapeutic approach for achondroplasia: tyrosine kinase inhibitor “BN016”*. 1st YR2I (Young Researchers of Imagine Institute) congress - May 06, 2015, Paris, France

5. **KOMLA-EBRI D**, Dambroise E, Kramer I, Benoist-Lasselin C, Kaci N, Busca P, Prestat G, Barbault F, Graus-Porta D, Munnich A, Kneissel M, Di Rocco F, Biosse-Duplan M, Legeai-Mallet L. *Treatment with FGFR inhibitor NVP-BGJ398 corrects all skeletal anomalies in achondroplasia mice.* 8èmes Assises de Génétique Humaine et Médicale – February 03-05, 2016, Lyon, France

International meetings

1. **KOMLA-EBRI D**, Benoist-Lasselin C, Kaci N, Busca P, Prestat G, Munnich A, Barbault F, Legeai-Mallet L. *Best understanding of structural and functional impact of FGFR3 mutations at the same position (K650N, K650M, K650E) leading to both mild and lethal dwarfism.* American Society of Human Genetics (ASHG)-Annual meeting-October 22-26, 2013, Boston, USA

2. Biosse-Duplan M, Di Rocco F, Heuzé Y, Gaudas E, **KOMLA-EBRI D**, Kaci N, Benoist-Lasselin C, Legeai-Mallet L. *Disturbed cartilages of the mandible in achondroplasia are associated with defective mandible shape and position*. European Calcified Tissue Society-May 17-20, 2014, Prague, Czech Republic

3. **KOMLA-EBRI D**, Benoist-Lasselin C, Kaci N, Martin L, Barbault F, Prestat G, Munnich A, Patricia B, Legeai-Mallet L. *Evaluation of tyrosine kinase inhibitors: a potential therapeutic approach for achondroplasia.* ECTS (European Calcified Tissue Society) PhD training course - June 27-30, 2014, Oxford, UK

4. **KOMLA-EBRI D**, Dambroise E, Kramer I, Benoist-Lasselin C, Kaci N, Le Gall C, Busca P, Martin L, Barbault F, Graus Porta D, Munnich A, Kneissel M, Di Rocco F, Biosse-Duplan M, Legeai-Mallet L. *The pan-FGFR tyrosine kinase inhibitor NVP-BGJ398 corrects skull anomalies in a mouse model of achondroplasia*. Society for Craniofacial Genetics and Developmental Biology –Annual meeting-October 05-06, 2015, Baltimore, USA

5. **KOMLA-EBRI D**, Dambroise E, Kramer I, Benoist-Lasselin C, Kaci N, Busca P, Prestat G, Barbault F, Graus-Porta D, Munnich A, Kneissel M, Di Rocco F, Biosse-Duplan M, Legeai-Mallet L. *Functional correction of dwarfism in a mouse model of achondroplasia using the tyrosine kinase inhibitor NVP-BGJ398*. American Society of Human Genetics (ASHG)-Annual meeting-October 06-08, 2015, Baltimore, USA

6. **KOMLA-EBRI D**, Dambroise E, Benoist-Lasselin C, Kaci N, Barbault F, Legeai-Mallet L *Analyses of structural and functional impact of FGFR3 mutations at the same position (K650) leading to both mild and lethal dwarfism.* 43rd European Calcified Tissue Society Congress – May 14-17 2016, Rome, Italy

AWARDS & HONORS

1. The image of a Safranin-O staining of mouse intervertebral disc (excerpt from J Clin Invest. 2016 Apr 11. pii: 83926. doi: 10.1172/JCI83926) is the **JCI and JCI This Month cover** of May 2016.

2. **SFBTM award** (Société Française de Biologie des Tissus Minéralisés) for oral communication 17th JFBTM (Journées Françaises de Biologie des Tissus Minéralisés) at Super Besse (04-06 February 2015).

3. **SFBTM award** (Société Française de Biologie des Tissus Minéralisés) for oral communication at 15th JFBTM (Journées Françaises de Biologie des Tissus Minéralisés) at Poitiers (30-31 May, 1st July 2013).

RESEARCH INTERESTS AND CAREER GOALS

Since the beginning of my university studies I was interested in genetic diseases and biomedical research.

For this reason in Italy I have found an internship in a laboratory of cytogenetics where I had my first encounter with the world of research. Later to achieve a double master degree between the universities of Milan (UNIMI) and Paris Diderot (Paris 7) I had the opportunity to work with Dr. Laurence Legeai-Mallet. Following this experience I decided to stay in her lab enrolled as a PhD student.

I have been working for four years in the field of skeletal diseases (achondroplasia and other FGFR3-related pathologies) performing fundamental and translational research. During my experience at Legeai-Mallet's lab, I had the opportunity to develop valuable skills in cell culture, molecular biology techniques, immunohistological methods, X-rays and µCT scans analyses and expertise in working with mouse models with skeletal disorders. I consider my most important success the experimental work carried out with the tyrosine-kinase inhibitor NVP-BGJ398 that could lead to the development of a therapy for achondroplasia based on this strategy. This study (published on J Clin Invest) shows the beneficial effects of this compound *in vitro*, *ex vivo* and *in vivo*.

In this sense I would like to keep working on the research of therapeutic approaches for rare genetic diseases. I would also be glad to pursue skeletal biology studies because I could start from the already acquired familiarity with the subject to then deepen my knowledge in this field. My short term objective is to live a stimulating work experience in a new country and environment, to learn new techniques and to be able to enrich my scientific background while in the long term I would like to reach a research position.

LANGUAGE SKILLS

English: *Fluent*

Italian: *Mother Tongue*

French: *Fluent*

REFERENCES

Dr Maria Clara BONAGLIA, PhD - Staff Scientist and Coordinator of Diagnostic Laboratory of Cytogenetics, E. Medea Scientific Institute, Bosisio Parini, Italy (clara.bonaglia@bp.lnf.it / 00 39 031 877 913)

Dr Laurence LEGEAI-MALLET, PhD – Director of Research INSERM and Team leader of "Molecular basis and pharmacological approaches of FGFR3-related chondrodysplasias" at Imagine Institute, Paris, France (laurence.legeai-mallet@inserm.fr / 00 33 142 754 302)

Dr Federico DI ROCCO, MD PhD – Former surgeon at Neurosurgery Department of Necker-Enfants Malades Hospital (Paris, France), currently at Pediatric Neurosurgery Department of Femme Mère Enfant Hospital, Lyon, France (federicodirocco@gmail.com / 00 33 142 754 429)

Prof Arnold MUNNICH, **MD PhD** – Former Director of INSERM U781 laboratory, Present Head of Clinical Genetics Service at Necker-Enfants Malades Hospital, Paris, France (arnold.munnich@inserm.fr / 00 33 142 754 242)

Abstract

Missense mutations in the tyrosine kinase receptor FGFR3 (Fibroblast Growth Factor Receptor 3) lead to its overactivation causing biological dysfunctions in several diseases. Achondroplasia, the most common Fgfr3-related chondrodysplasia, is a rare genetic disorder, affecting 1 in 20000 live births, characterized by particular clinical features: rhizomelic dwarfism, short limbs, macrocephaly, midface hypoplasia, cervicomedullary compression. The abnormal activity of the receptor induces endochondral ossification defects that are responsible for the pathological phenotype. For a long time the only treatment for this disease was the limb lengthening surgery, however in recent years several researchers have developed potential therapeutic strategies based on molecular studies. The objective of my thesis was to evaluate a novel therapeutic approach for achondroplasia.

A promising therapeutic strategy involved the use of small chemical inhibitors, known as tyrosine kinase inhibitors, that are able to arrest the FGFR3 activity. I have assessed the effects of one of these compounds, NVP-BGJ398, in a mouse model mimicking the acondroplastic dwarfism ($Fgfr3^{Y367C/+}$). The experiments performed showed an improvement of all pathological hallmarks in NVP-BGJ398 treated mice.

We have also inspected the impact of the activating FGFR3 mutation on the mandibular development. The study established a defect in mandibular growth in both affected patients and mice. Furthermore we could investigate the mandibular bone growth and correct the pathological defect with NVP-BGJ398.

Finally I have participated in molecular analyses to describe how three FGFR3 mutations at the same position could lead to three different dwarfisms with increasing severity. The results provided a better understanding of FGFR3 pathological molecular mechanisms and could lead to new targets for therapeutic approaches.

Résumé

Des mutations faux-sens au niveau du récepteur à activité tyrosine kinase FGFR3 (Fibroblast Growth Factor Receptor 3) entrainent sa suractivation qui apporte des dysfonctions biologiques dans plusieurs maladies. L'achondroplasie, la forme la plus commune de chondrodysplasie liée à Fgfr3, est une maladie génétique rare, touchant 1 nouveau-né sur 20 000, caractérisée par des signes cliniques spécifiques : nanisme rhizomélique, membres courts, macrocéphalie, hypoplasie de l'étage moyen de la face, compression cervico-médullaire. L'activité anormale du récepteur induit des défauts de l'ossification endochondrale responsables du phénotype pathologique. Pendant longtemps le seul traitement pour cette maladie a été l'allongement chirurgical des membres, cependant au cours des dernières années de nombreux chercheurs ont développé des potentielles stratégies thérapeutiques basées sur des études moléculaires. L'objectif de ma thèse était d'évaluer une nouvelle approche thérapeutique pour l'achondroplasie.

Une stratégie thérapeutique prometteuse prévoit l'utilisation de petits inhibiteurs chimiques, connus sous le nom d'inhibiteurs de tyrosine kinases, qui sont capables d'arrêter l'activité de FGFR3. J'ai estimé les effets d'un de ces composés, NVP-BGJ398, dans un modèle murin mimant le nanisme achondroplase (*Fgfr3*$^{Y367C/+}$). Des expérimentations effectuées ont montré une amélioration des caractéristiques pathologiques dans les souris traitées avec NVP-BGJ398.

Nous avons également examiné l'impact de la mutation activatrice de FGFR3 sur le développement mandibulaire. L'étude a reconnu un défaut dans la croissance mandibulaire chez l'homme et la souris atteints. En outre nous avons pu investiguer la croissance osseuse de la mandibule et corriger le défaut pathologique avec NVP-BGJ398.

Enfin j'ai participé à des analyses moléculaires pour décrire comment trois mutations de FGFR3 localisées à la même position (Lys650) peuvent induire trois différents nanismes avec sévérité croissante. Les résultats ont fourni une meilleure compréhension des mécanismes moléculaires pathologiques et pourront mener à des nouvelles cibles pour des approches thérapeutiques.